

ISBN 978-2-87355-033-2

Proceedings of the International Meteor Conference

Bollmannsruh, Germany, 2019

October 3 – 6



Published by the International Meteor Organization

Edited by Urška Pajer, Jürgen Rendtel,
Marc Gyssens and Cis Verbeeck

Copyright notices:

© 2020 The International Meteor Organization.

The copyright of papers submitted to the IMC Proceedings remains with the authors.

It is the aim of the IMO to increase the spread of scientific information, not to restrict it. When material is submitted to the IMO for publication, this is taken as indicating that the author(s) grant(s) permission for the IMO to publish this material any number of times, in any format(s), without payment. This permission is taken as covering rights to reproduce both the content of the material and its form and appearance, including images and typesetting. Formats may include paper and electronically readable storage media. Other than these conditions, all rights remain with the author(s). When material is submitted for publication, this is also taken as indicating that the author(s) claim(s) the right to grant the permissions described above. The reader is granted permission to make unaltered copies of any part of the document for personal use, as well as for non-commercial and unpaid sharing of the information with third parties, provided the source and publisher are mentioned. For any other type of copying or distribution, prior written permission from the publisher is mandatory.

Editing and printing:

Front cover picture: Logo of the IMC 2019, by Felice Meer.

Publisher: The International Meteor Organization

Printed: The International Meteor Organization

Editors: Urška Pajer, Jürgen Rendtel, Marc Gyssens, Cis Verbeeck

Bibliographic records: all papers are listed with the SAO/NASA Astrophysics Data System (ADS)

<http://adsabs.harvard.edu> with publication code 2019pimo.conf.

Distribution:

Further copies of this publication may be ordered from the International Meteor Organization, through the IMO website (<http://www.imo.net>). Legal address: International Meteor Organization, Mattheessensstraat 60, 2540 Hove, Belgium.

ISBN 978-2-87355-033-2

Proceedings of the International Meteor Conference

Bollmannsruh, Germany, 2019

October 3 – 6



Published by the International Meteor Organization

Edited by Urška Pajer, Jürgen Rendtel,
Marc Gyssens and Cis Verbeeck

The IMC 2019 was supported by:



Some impressions from the conference:



Opening and registration



Talks and excursion with cake buffet.



Early morning silence at the lake.

Table of contents

Editors' notes	4
Organizer's notes	5
Program of the IMC 2019	7
List of participants	10

Video (FRIPON and AllSky6)

NEMO Vol 3. – Status of the NEar real-time MOnitoring system <i>T. Ott, E. Drolshagen, D. Koschny, G. Drolshagen, C. Pilger, P. Mialle, J. Vaubaillon, and B. Poppe</i> ..	11
FRIPON vs. AllSky6: a practical comparison <i>S. Molau</i>	17
The AllSky6 and Video Meteor Program of the AMS Ltd. <i>M. Hankey, V. Perlerin and D. Meisel</i>	21
FRIPON first results after 3 years of observations <i>F. Colas, B. Zanda, S. Jeanne, M. Birlan, S. Bouley, P. Vernazza, J.L. Rault and J. Gattacceca</i>	26

Radio observations

BRAMS forward scatter observations of major meteor showers in 2016–2019 <i>C. Verbeeck, H. Lamy, S. Calders, A. Martínez Picar, A. Calegaro</i>	27
The Radio Meteor Zoo: identifying meteor echoes using artificial intelligence <i>S. Calders, S. Draulans, T. Calders, H. Lamy</i>	32
Calibration of the BRAMS interferometer <i>H. Lamy, M. Anciaux, S. Ranvier, A. Martínez Picar, S. Calders, A. Calegaro, C. Verbeeck</i>	33
The BRAMS receiving station v2.0 <i>M. Anciaux, H. Lamy, A. Martínez Picar, S. Ranvier, S. Calders, A. Calegaro, C. Verbeeck</i>	39

Meteoroid properties

Mass determination of iron meteoroids <i>D. Čapek, P. Koten, J. Borovička, V. Vojáček, P. Spurný, R. Štork</i>	43
The study of meteoroid parameters with multi-techniques data <i>A. Kartashova, Y. Rybnov, O. Popova, D. Glazachev, G. Bolgova, V. Efremov</i>	45
Simulation of meteors by TC-LIBS: advantages, limits and challenges <i>M. Ferus, A. Křivková, L. Petera, V. Laitl, L. Lenža, J. Koukal, A. Knížek, J. Srba, N. Schmidt, P. Boháček, S. Čiviš, M. Krůs, J. Kubát, L. Paloušová, E. Chatzitheodoridis, P. Kubelík</i>	47
A spectral mystery <i>B. Ward</i>	55

Video and visual

MeteorFlux reloaded <i>S. Molau</i>	57
Double and triple meteor detections <i>I. Fernini, M. Talafha, A. Al-Owais, Y. Eisa Yousef Doostkam, M. Sharif, M. Al-Naser, S. Zarafshan, H. Al-Naimiy, A. Hassan Harriri, I. Abu-Jami1, S. Subhi, Y. Al-Nahdi, R. Fernini, A. Omar Adwan</i>	60
Minor meteor shower anomalies: predictions and observations <i>J. Rendtel</i>	63
School of Meteor Astronomy at Petnica Science Center <i>D. Pavlović, V. Lukić</i>	69

Table of contents (contd.)

Parent bodies, showers, sporadics

Meteor pairs among Geminids

<i>P. Koten, D. Čapek, P. Spurný, R. Štork, V. Vojaček, J. Bednář</i>	70
---	----

Analysis of a boulder in the surroundings of 67P

<i>J. Marin-Yaseli de la Parra, M. Kueppers and the OSIRIS-Team</i>	74
---	----

Parent bodies of some minor meteor showers

<i>L. Neslušan, M. Hajduková</i>	76
--	----

Modelling and analysis

Where are the missing fireballs?

<i>Á. Keresztsuri and V. Steinmann</i>	80
--	----

Impact fluxes on the Columbus module of the ISS: survey and predictions

<i>G. Drolshagen, M. Klaß, R. Putzar, D. Koschny, B. Poppe</i>	86
--	----

De-biasing of meteor radiant distributions obtained by the Canary Island Long-Baseline Observatory (CILBO)

<i>A. Rietze, D. Koschny, G. Drolshagen, B. Poppe</i>	90
---	----

How to test whether the magnitude distribution of the meteors is exponential

<i>J. Richter</i>	95
-------------------------	----

Video observation networks and campaigns

3414–2018: a Perseid fireball with exceptional light effects

<i>P.C. Slansky</i>	98
---------------------------	----

Results of the Polish Fireball Network in 2018

<i>M. Wiśniewski, P. Żoładek, A. Olech, A. Raj, Z. Tymiński, M. Maciejewski, K. Fietkiewicz,</i>
--

<i>M. Myszkiewicz, M.P. Gawroński, T. Suchodolski, M. Stolarz and M. Gozdalski</i>	102
--	-----

Beta Taurids video campaign

<i>P. Żoładek, A. Olech, M. Wiśniewski, M. Bęben, H. Dróżdż, M. Gawroński, K. Fietkiewicz,</i>
--

<i>A. Jaśkiewicz, M. Krasnowski, H. Krygiel, T. Krzyżanowski, M. Kwinta, J. Laskowski, Z. Laskowski,</i>
--

<i>T. Lojek, M. Maciejewski, M. Myszkiewicz, P. Nowak, P. Onyszczuk, K. Polak, K. Polakowski,</i>

<i>A. Raj, A. Skoczewski, M. Szlagor, Z. Tymiński, J. Twardowski, W. Węgrzyk, P. Zaręba</i>	106
---	-----

AMOS and interesting fireballs

<i>J. Tóth, P. Matlovič, L. Kornoš, P. Zigo, D. Kalmanček, J. Šimon, J. Šilha, J. Világí, B. Baláž, P. Vereš</i> 109
--

Instruments, software

A little tour across the wonderful realm of meteor radiometry

<i>J.-L. Rault, F. Colas</i>	112
------------------------------------	-----

FRIPON Network internal structure

<i>A. Malgoyre Adrien, F. Colas</i>	118
---	-----

Optimizing the scientific output of satellite formation for a stereoscopic meteor observation

<i>J. Petri, J. Zink, S. Klinkner</i>	119
---	-----

Investigation of meteor properties using a numerical simulation

<i>M. Baláž, J. Tóth, P. Vereš</i>	126
--	-----

The Bridge of Spies

<i>P.C. Slansky</i>	133
---------------------------	-----

Table of contents (contd.)

Fireballs and meteorites

Daytime fireball capturing	
<i>F. Bettonvil</i>	135
The daylight fireball of September 12, 2019	
<i>S. Molau, J. Strunk, M. Hankey, A. Knöfel, A. Möller, W. Hamburg</i>	140
ESA's activities on fireballs in Planetary Defence	
<i>R. Rudawska, N. Artemieva, J. L. Cano, R. Cennamo, L. Faggioli, R. Jehn, D. Koschny,</i> <i>R. Luther, J. Martín-Ávila, M. Micheli, K. Wünnemann</i>	143
Provision of European Network Fireball Data	
<i>A. Margonis, S. Elgner, D. Heinlein, D. Koschny, R. Rudawska, L. Faggioli, J. Oberst</i>	147
Evidence of shock metamorphism in Bursa L6 chondrite: Raman and infrared spectroscopic approach	
<i>O. Unsalan, C. Altunayar-Unsalan</i>	150

Observations

Optimisation of double-station balloon flights for meteor observation	
<i>J. Vaubaillon, A. Caillou, P. Deverchere, D. Zilkova, A. Christou, J. Laskar, M. Birlan, B. Carry,</i> <i>F. Colas, S. Bouley, L. Maquet, P. Beck, P. Vernazza</i>	151
Polarization of the night sky in Chile 2019	
<i>B. Gährken</i>	155
The ESA Leonids 2002 expedition	
<i>D. Koschny, R. Trautner, J. Zender, A. Knöfel, J. Diaz del Rio, R. Jehn</i>	157
Conference summary	
<i>F. Bettonvil</i>	158

Poster contributions

Python ablation and dark flight calculator	
<i>D. Bettonvil</i>	164
My first visual observation	
<i>U. Bettonvil</i>	166
Comparison of radio meteor observations during the period from 1. to 17. August 2019	
<i>P. Dolinsky, A. Necas, J. Karlovsky</i>	168
Deep Learning Applied to Post-Detection Meteor Classification	
<i>P. Gural</i>	171
Application of high power lasers for a laboratory simulation of meteor plasma	
<i>A. Křivková, L. Petera, M. Ferus</i>	172
Numerical model of flight and scattering of meteor body fragments in the Earth's atmosphere	
<i>V. Lukashenko, F. Maksimov</i>	173
Nachtlicht-Bühne: a citizen science project for the development of a mobile app for night light phenomena	
<i>M. Hauenschild, A. Margonis, S. Elgner, J. Flohrer, J. Oberst, F. Klan, C. Kyba, H. Kuechly</i>	177
Automated determination of dust particles trajectories in the coma of comet 67P	
<i>J. Marin-Yaseli de la Parra, M. Kueppers and the OSIRIS-Team</i>	180
Elemental composition, mineralogy and orbital parameters of the Porangaba meteorite	
<i>L. Petera, L. Lenža, J. Koukal, J. Haloda, B. Drtinová, D. Matýsek, M. Ferus and S. Civiš</i>	182
Geminids 2018	
<i>J. Rendtel</i>	183
Meteor candidate observations from automated sampling of weather cameras in VBA	
<i>T. Stenborg</i>	189
Photo and poster contest	191

Editors' Notes

Cis Verbeeck

The 38th International Meteor Conference (IMC) took place from October 3 to 6, 2019, in Bollmannsruh, Germany, in the same place as the great IMC of 2003. It was organized by the Arbeitskreis Meteore, the German meteor observers' group, 16 years after the previous IMC at this location.

The conference brought together 99 participants from 32 countries (Australia, Belgium, Czech Republic, Denmark, France, Germany, Greece, Hungary, Israel, Japan, The Netherlands, Poland, Russia, Serbia, Slovakia, Slovenia, Spain, Sweden, Turkey, United Arab Emirates, United Kingdom, and United States). The varied schedule of events comprised 54 presentations (42 lectures and 12 posters), as well as an excursion to "Telegraph hill", hosting the historical buildings of the Astrophysical Observatory of Potsdam, and several long-lasting socializing evenings. These are just numbers, and in no way can they evoke the very nice atmosphere during the conference and the many offline discussions and collaboration plans. This was a great IMC in all aspects: very well-organized, a great venue, a very interesting program, a good atmosphere, and a very cosy camp fire on Saturday evening.

Organizing an IMC is a major effort. Especially the last few weeks before the conference are very intense for the Local Organizing Committee (LOC) and the Scientific Organizing Committee (SOC). The IMC 2019 was organized by the Arbeitskreis Meteore, one of the major cornerstones of IMO since its foundation in 1988. Apart from their exceptional proficiency in meteor observations, the members of this group also have performed major tasks in our organization, for a long time. This is exemplified by the fact that during the final weeks before the IMC, they also took care, as always, of printing and assembling both the IMC 2018 Proceedings and WGN. The smooth organization of the IMC showed that they have a lot of experience in organizing IMCs (this was the fourth IMC organized by the Arbeitskreis Meteore). In name of IMO, I want to thank the LOC: Rainer Arlt, André Knöfel, Sirkko Molau, Ina Rendtel, Jürgen Rendtel, Roland Winkler, and all other LOC members.

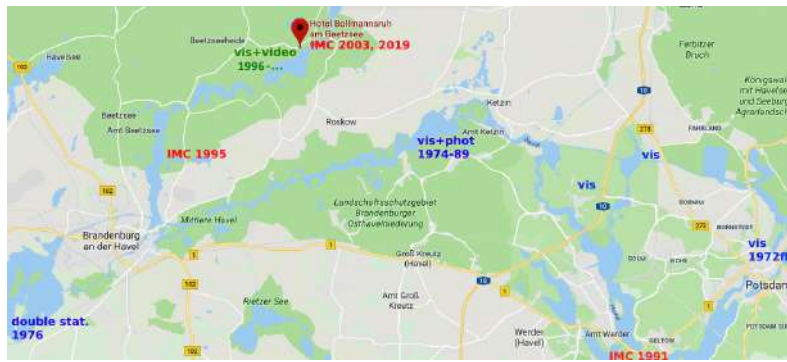
Also many thanks to SOC Co-Chairs David Asher, Theresa Ott and Esther Drolshagen, to all SOC members (Marc Gyssens, Jean-Louis Rault, Jürgen Rendtel, Juraj Töth, and Jérémie Vaubaillon), to Mike Hankey and Vincent Perlerin for developing the IMC website and registration form, and to Marc Gyssens for his nonrelenting assistance to the LOC and SOC.

The annual IMCs are a unique opportunity for amateurs and professionals interested in meteors to meet each other. However, the publication and distribution of the IMC Proceedings that bring together all the papers prepared by the contributors is also an important aspect, to make sure that results of the Conference are documented and can be relied on for future meteor work. At the General Assembly Meeting during the IMC 2018 in Pezinok-Modra, the challenges of timely publication of IMC Proceedings was discussed. Several persons voiced that they have a strong preference for Proceedings to be published a few months after the conference. In order to meet this need, the IMO Board decided to appoint a guest editor (Urška Pajer) and observe an early deadline. We were happy to see that many authors had submitted their manuscript before the deadline, and are proud to present the IMC 2019 Proceedings just a few months after the conference. This was only possible thanks to the efforts made by Urška Pajer (editor), Jürgen Rendtel (cover, front matter and technical arrangements), Marc Gyssens (contacting the authors) and Cis Verbeeck (coordination).

We are looking forward to hearing about your new results at the IMC 2020 in Hortobágy, Hungary, and to read about it in the IMC 2020 Proceedings! We intend to have them produced a few months after the conference, just like the Proceedings of the IMC 2019 you are now reading. Meanwhile, enjoy reading this representative overview of the IMC 2019.

Organizer's notes

When looking at the geographical distribution of IMC locations, some “hot spots” appear. Some of these are connected to the centres of meteor astronomy at the time of the IMO foundation. At the 1989 IMC in Balatonföldvár – in a way the first IMO meteor conference – it was decided to have the next two in the (at that time) two parts of Germany. So we met in Violau near Munich in 1990 and a year later in Petzow near Potsdam. The meteor group of Potsdam had several centres in the region, comprising observing locations (indeed, the sky is reasonably dark so close to Berlin and Potsdam) as well as meeting venues. So also the German Arbeitskreis Meteore (AKM) had its headquarter here for many years. Later IMC venues along the Havel river were in Mötzow (Brandenburg, 1995) and Bollmannsruh (2003).



Meteor hot spots along the Havel river between Potsdam and Brandenburg, showing observing sites (blue for visual, green for visual + video) and the four IMC locations (red).

Participants had not the possibility to attend two meteor conferences in a year, which left flexibility with the rooms and meals.

The late date led to the situation that by the end of the early registration deadline the number of participants seemed to be smaller compared to previous IMCs. We had to adjust our reservations at the IMC venue and re-assure the IMC is well-resourced, since the finances were originally made on a 100–120 people basis. However, in the late phase many registrations followed until we reached about 100 – the last one coming in at the evening before the opening. The situation with the contributions seemed similar and thus resembling the “old IMCs” to some extent. In the 1990s the registration desk had a place where the arriving participants told what they brought with them to present. Only after this, the program of an IMC was established. Nowadays, the participants find the program with abstracts in their welcome package – credit of the Scientific Organizing Committee (SOC), led by David Asher, Esther Drolshagen and Theresa Ott. They also took care about the awards (best poster, best photo). The winners got a fine piece of space rock donated via the LOC from the registration fees, and special prices were rewarded to the youngsters for their creative poster presentations (see elsewhere in this Proceedings).

Preparing an IMC takes some time and requires to coordinate the LOC activities for about a year. We had regular LOC meetings on a monthly basis plus a few more in September. It was amazing to see how the team acted together, both during the preparations as well as during the IMC. We also had wonderful support from our

Traditionally an IMC is organized in conjunction with the professional “Meteorooids” conference (every three years) if possible. That worked out many times, but in 2019, combining the two conferences turned out to be difficult. Hence our Local Organizing Committee (LOC) team of six – Rainer Arlt, André Knöfel, Sirk Molau, Ina Rendtel, Jürgen Rendtel and Roland Winkler of the *Arbeitskreis Meteore e. V.* – offered to organize the IMC in Bollmannsruh again. The earliest weekend we were able to book the venue was in October, certainly quite late as we learned because the university semester starts at the same time. Another restriction came from the fact that many potential IMC participants had not the possibility to attend two meteor conferences in a year, which left flexibility with the rooms and meals.



Preparing the IMC was eventually indicated in the sky.

families – helping during the registration, baking cakes for the excursion, running shuttle service to Brandenburg station, arranging the barbecue and so on. The many happy faces during the IMC were a compensation for all the efforts. We also had a good relationship with the administration and kitchen staff of the KiEZ which was helpful to get many apparently minor things going. The heating failure in the first night was an uncomfortable incident, but the bonfire – a tradition which connected the Havel IMCs since 1995 – under clear dark skies allowed to keep everyone warm enough until well after midnight.

At this point, we want to thank the German *Vereinigung der Sternfreunde (VdS)* for their great support of the conference. Last but not least we also want to thank the people of the *Förderverein Großer Refraktor Potsdam* for their tours during the excursion.

Sixteen years after the previous Bollmannsruh IMC it was another conference of the long series which approaches the number 40 soon. So we look forward to seeing you at one of the next IMCs. Meanwhile, good luck with all your meteor projects and keep the old and new contacts alive!



Your LOC of the IMC 2019 at the end of the conference: Roland Winkler, Rainer Arlt, André Knöfel, Ina Rendtel, Sirko Molau, Jürgen Rendtel (left to right; photo Bernd Klemt).



...and consider that meteor observers being outside at unknown places in the dark may be in danger from various beasts (photo: Jürgen Rendtel).

Program of the IMC 2019

Thursday, 3 October 2019

14:00–18:00	Arrival of participants
18:00–19:30	Dinner
20:00–20:10	<i>Cis Verbeeck</i> : Opening of the IMC 2019
20:10–20:20	<i>LOC</i> : Practical hints for Conference
20:20–20:40	<i>Jürgen Rendtel</i> : Recollections from the past IMCs in Brandenburg

Friday, 4 October 2019

SESSION 1: Video (FRIPON and Allsky6) Chair: <i>Detlef Koschny</i>	
09:00–09:15	<i>Theresa Ott, Esther Drolshagen</i> : NEMO Vol 3. – Status of the NEar real-time MOnitoring system
09:15–09:35	<i>Sirko Molau</i> : FRIPON vs. Allsky6 : A Practical Comparison
09:35–09:55	<i>Mike Hankey</i> : The Allsky6 and Video Meteor Program of the AMS Ltd.
09:55–10:10	<i>François Colas</i> : FRIPON first results after 3 years of observations
10:10–10:25	Poster Pitches Chairs: <i>Esther Drolshagen, Theresa Ott</i>
	<i>Dušan Bettonvil</i> : Python Ablation and Dark Flight Calculator
	<i>Uroš Bettonvil</i> : My first visual observation
	<i>Peter Dolinsky</i> : Comparison of radio meteor observations during the period from 1. to 17. August 2019
	<i>Pete Gural</i> : Deep Learning Applied to Post-Detection Meteor Classification
	<i>Mike Hankey</i> : The Allsky6 and Video Meteor Program of the AMS Ltd.
	<i>Anna Křivková, Lukáš Petera, Martin Ferus</i> : Application of High Power Lasers for a Laboratory Simulation of Meteor Plasma
	<i>Vladislav Lukashenko</i> : Numerical model of flight and scattering of meteor body fragments in the Earth's atmosphere
	<i>Anastasios Margonis</i> : Nachtlicht-BÜHNE: a citizen science project for the development of a mobile app for night light phenomena
	<i>Julia Marin-Yaseli de la Parra</i> : Automated determination of dust particles trajectories in the coma of comet 67P
	<i>Lukáš Petera</i> : Elemental Composition, Mineralogy and Orbital Parameters of the Porangaba Meteorite
	<i>Jürgen Rendtel</i> : Geminids 2018
	<i>Travis Stenborg</i> : Meteor Candidate Observations from Automated Sampling of Weather Cameras in VBA
10:25–10:45	Coffee break and poster session
SESSION 2: Radio Chair: <i>Jean-Louis Rault</i>	
10:45–10:55	<i>Cis Verbeeck</i> : BRAMS forward scatter observations of major meteor showers in 2016–2019
10:55–11:10	<i>Stijn Calders</i> : The Radio Meteor Zoo: identifying meteor echoes using artificial intelligence
11:10–11:30	<i>Hervé Lamy</i> : Calibration of the BRAMS interferometer
11:30–11:45	<i>Antonio Martínez Picar</i> : The BRAMS receiving station v2.0
11:45–12:00	Group photograph
12:00–13:00	Lunch

Friday, 4 October 2019 (contd.)

SESSION 3: Meteoroid properties Chair: *Travis Stenborg*

- 13:30–13:40 *David Čapek*: Mass determination of iron meteoroids
 13:40–13:55 *Anna Kartashova*: The study of meteoroid parameters with multi-techniques data
 13:55–14:10 *Martin Ferus*: Simulation of meteors by TW-class high power laser – advantages, limits and future challenges
 14:10–14:25 *Bill Ward*: A spectral mystery

SESSION 4: Video and visual Chair: *Ella Ratz*

- 14:25–14:45 *Sirko Molau*: MeteorFlux reloaded
 14:45–15:05 *Mohammed Talafha*: Double and triple meteor detections
 15:05–15:25 *Jürgen Rendtel*: Minor meteor shower anomalies: predictions and observations
 15:25–15:35 *Dušan Pavlović*: School of Meteor Astronomy at Petnica Science Center
 15:35–16:05 Coffee break and poster session

SESSION 5: Parent bodies, showers, sporadics Chair: *Martin Baláž*

- 16:05–16:20 *Pavel Koten*: Meteor pairs among Geminids
 16:20–16:35 *Julia Marin-Yaseli de la Parra*: Analysis of a boulder in the surroundings of 67P
 16:35–16:50 *Mária Hajduková*: Parent bodies of some minor meteor showers
 16:50–17:00 *Roman Piffl*: How many “sporadics” are sporadic meteors?

SESSION 6: Modelling and analysis Chair: *Regina Rudawska*

- 17:00–17:10 *Ákos Keresztfuri*: Where are the missing fireballs?
 17:10–17:25 *Maximilian Klaß*: Impact fluxes on the Columbus module of the ISS: survey and predictions
 17:25–17:40 *Athleen Rietze*: De-Biasing of meteor radiant distributions obtained by the Canary Island Long-Baseline Observatory (CILBO)
 17:40–18:00 *Janko Richter*: How to test whether the magnitude distribution of the meteors is exponential
 18:00–19:00 Dinner
 20:00–21:00 **IMO General Assembly** (all IMC participants welcome)
-

Saturday, 5 October 2019

SESSION 7: Video observation networks and campaigns Chair: *Dušan Pavlović*

- 09:00–09:25 *Peter C. Slansky*: 3414-2018: A Perseid Fireball with exceptional Light Effects
 09:25–09:35 *Mariusz Wiśniewski*: Results of Polish Fireball Network in 2018
 09:35–09:55 *Przemysław Żołądek*: Beta Taurids video campaign
 09:55–10:15 *Juraj Tóth*: AMOS and interesting fireballs
 10:15–10:35 Coffee break and poster session

SESSION 8: Instruments, software Chair: *Mária Hajduková*

- 10:35–10:50 *Jean-Louis Rault*: A little tour across the wonderful realm of meteor radiometry
 10:50–11:05 *François Colas*: FRIPON Network internal structure
 11:05–11:25 *Jona Petri*: Optimizing the scientific output of satellite formation for a stereoscopic meteor observation
 11:25–11:40 *Martin Baláž*: Investigation of meteor properties using a numerical simulation
 11:40–12:00 *Peter C. Slansky*: The Bridge of Spies
 12:00–13:00 Lunch
 13:00–19:00 **Saturday afternoon excursion**
 19:00–21:00 Saturday evening BBQ
 21:00 Bonfire at the lake
-

Sunday, 6 October 2019

SESSION 9: Fireballs and meteorites Chair: *Antal Igaz*

- 09:00–09:15 *Felix Bettonvil*: Daytime fireball capturing
09:15–09:30 *Sirko Molau*: The daylight fireball of September 12, 2019
09:30–09:45 *Regina Rudawska*: ESA's activities on fireballs in Planetary Defence
09:45–09:55 *Anastasios Margonis*: Service Level Agreement (SLA) for European Network Fireball Data Provision
09:55–10:20 *Ozan Unsalan*: Evidence of shock metamorphism in Bursa L6 chondrite: Raman and Infrared Spectroscopic Approach
10:20–10:25 Announcement of poster and photo competition winners
10:25–10:40 Coffee break and poster session

SESSION 10: Observations Chair: *Mike Hankey*

- 10:40–10:50 *Jeremie Vaubaillon*: Update on the MALBEC project
10:50–11:15 *Bernd Gährken*: Polarization of the night sky in Chile 2019
11:15–11:35 *Detlef Koschny*: The ESA Leonids 2002 Expedition
11:35–11:50 *Felix Bettonvil*: Conference summary
11:50–12:00 **Closing of the 38th IMC**
-



The “official group photo” of the IMC 2019 taken on Friday before lunch in the amphitheatre of the conference venue.

List of participants

Australia:

Travis Stenborg

Belgium:

Stijn Calders, Antoine Calegaro, Marc Gyssens, Hervé Lamy, Antonio Martínez Picar, Tom Roelandts, Cis Verbeeck

Czech Republic:

David Čapek, Martin Ferus, Pavel Koten, Anna Křivková, Lukas Petera

Denmark:

Frank Rasmussen

France:

François Colas, Vincent Perlerin, Jean-Louis Rault, Jérémie Vaubaillon

Germany:

Rainer Arlt, Stela Arlt, Tom Daniel Arlt, Szilárd Csizmadia, Esther Drolshagen, Gerhard Drolshagen, Ridwan Fernini, Bernd Gährken, Wolfgang Hamburg, Anna Kartashova, Wolfgang Kinzel, Maximilian Klaß, Bernd Klemt, André Knöfel, Anastasios Margonis, Sirko Molau, Theresa Ott, Jona Petri, Ina Rendtel, Jürgen Rendtel, Janko Richter, Athleen Rietze, Peter C. Slansky, Petra Strunk, Jörg Strunk, Hans Wilschut, Roland Winkler

Greece:

Vagelis Tsamis

Hungary:

Antal Igaz, Ákos Kereszturi, Nándor Opitz, Márton Rózsahegyi, Krisztián Sárneczky

Israel:

Ella Ratz, Tamara Tchenak, Yakov Tchenak, Ariel Westfried

Japan:

Nagatoshi Nogami

Netherlands:

Dušan Bettonvil, Felix Bettonvil, Uroš Bettonvil, Ben Kokkeler, Detlef Koschny, Gabi Koschny, Marc Neijts, Dragana Okolic, Regina Rudawska, Joe Zender

Poland:

Maciej Maciejewski, Arkadiusz Raj, Walburga Węgrzyk, Mariusz Wiśniewski, Paweł Zgrzebnicki, Przemysław Żoładek

Russia:

Anna Kartashova, Vladislav Lukashenko

Serbia:

Milica Marčetić, Ana Nikolić, Dušan Pavlović

Slovakia:

Martin Baláž, Peter Dolinsky, Mária Hajduková, Matej Korec, Roman Piffl, Juraj Toth

Slovenia:

Javor Kac, Kristina Veljković

Spain:

Julia Marin Yaseli de la Parra, Suyin Perret-Gentil R.

Sweden:

Stefan Björk, James Gage, Mats Wretborn

Turkey:

Cisem Altunayar-Unsalan, Ozan Unsalan

United Arab Emirates:

Mohammad Fadel Ali Talafha

United Kingdom:

Malcolm Currie, Michael German, James Rowe, Alan Shuttleworth, Peter Stewart, Bill Ward

United States:

Mike Hankey

NEMO Vol 3. – Status of the NEar real-time MOnitoring system

Theresa Ott^{1*}, Esther Drolshagen^{1*}, Detlef Koschny^{2,3}, Gerhard Drolshagen¹, Christoph Pilger⁴, Pierrick Mialle⁵, Jeremie Vaubaillon⁶, and Björn Poppe¹

¹ University of Oldenburg, Germany,

Theresa.ott@uol.de, esther.drolshagen@uol.de

²ESA/ESTEC, Noordwijk, The Netherlands,

³Chair of Astronautics, TU Munich, Germany,

⁴BGR, Hannover, Germany,

⁵CTBTO PTS/IDC, Vienna International Center, Austria,

⁶Observatoire de Paris, France.

*These authors contributed equally to this work

NEMO, our NEar real-time MOnitoring system for bright fireballs, has been under development for about two years now. We have added and incorporated an increasing number of different data sources to the system. By combination, further information could already be obtained with the system which might otherwise have been lost. An example is the size determination of the impacting NEO (near-Earth object) that caused a fireball. The size is of particular interest to us and can be found by combination of data sources from seemingly unrelated fields. We are systematically checking infrasound data of the IMS (International Monitoring System) operated by the CTBTO (Comprehensive Nuclear-Test-Ban Treaty Organisation). The network monitors the whole Earth during day and night in search for nuclear explosions. However, the technique is also applicable to bolides. If an event is detected via this method, the total deposited energy in the atmosphere can be determined from the data. In addition to the energy we can use the data in NASA's (National Aeronautics and Space Administration) CNEOS (Center for near-Earth object Studies) JPL (Jet Propulsion Laboratory) fireball database that contain information on the velocity and deposited energy. Connecting both information leads to a size and mass estimation.

On a more local scale, the established collaboration with the FRIPON (Fireball Recovery and InterPlanetary Observation Network) system is a fast source of scientific information for objects that entered the Earth atmosphere above Europe which can be compared to other sources.

The alarm system will be further improved but already ensures that we are informed within a few hours about almost all fireballs that attract public attention in the western hemisphere. The system will be moved in the next months to ESA's Near-Earth Object Coordination Centre (NEOCC) to be operated from there. The NEMO events will be included in the NEOCC's Fireball Information System. All collected data from public sources will be made available online. For especially interesting fireballs IMO (International Meteor Organisation) summaries are written on a more regular basis and hence the information and results derived from NEMO are already being distributed.

In this work we will give an overview about the current status of NEMO and the next planned steps.

1 Introduction

Bright fireballs appear in our atmosphere on a regular basis. Since they are often seen by observers from distances up to hundreds of kilometres they spark public interest, not only locally but also worldwide. These events usually start an online discussion on origin and validity right after the event occurred. To inform people, one of the main goals of NEMO, the NEar real-time MOnitoring system, is to gather information and provide additional data in near-real time. This is achieved with an alert system that is mainly based on Twitter, yielding very fast information.

By collecting, analysing, and combining as much available data of the event as possible often more information about the fireball and the corresponding meteoroid or asteroid can be derived. Doing so and publishing the results is the second objective of NEMO.

The different data sources cover the complete spectrum of possible observations. They range from rather conventional meteor and fireball networks, designed for meteor research, to the infrasound data of the IMS (International Monitoring System). This system is operated by the CTBTO (Comprehensive Nuclear-Test-Ban Treaty Organisation) to detect nuclear explosions.

NEMO focuses only on bright events. To be operational in near-real time and to cover the whole world is part of our ongoing work.

A more detailed description of the NEMO system and its goals can be found in Drolshagen et al. (2018) and Drolshagen et al. (2019).

In Section 2 some of the different data sources utilized by NEMO are briefly described. Section 3 presents summaries of four different fireballs which occurred in

2019, caused a lot of public attention, and for which summaries were written and published. A short conclusion is given in Section 4.

2 Data Sources

For NEMO diverse data sources are accessed and the gathered information combined. Some of them will be presented here in greater detail.

Social Media

Bright fireball are often very prominent in social media. Witness reports, origin theories, and calls for further information are shared via Twitter, Facebook, and others. The NEMO alert system is mainly based on Twitter and the Google Alert System. Twitter yields very fast information and informs us that something has happened. In many cases a picture or even a video is tweeted. The more attention an event has caused the more tweets are available and the more information we can collect from these. The most common details are the date, time, and location of the fireball. Then we start with further investigations. The events computed from witness reports on the AMS/IMO (American Meteor Society/International Meteor Organisation) webpage are very helpful for fast confirmation of the first information or even the first information source. For information on the AMS/IMO see e.g. Hankey and Perlerin (2014).

From the Google Alert System further information is collected. Online newspapers and articles are found very fast which can include further details e.g. from interviews of local researchers.

The alert system has been in test-operational mode since August 2017. It sends alerts for almost all fireballs that cause public attention. The most problematic part of finding valid events is the reduction of wrong detections and spam. Moreover, investigating which tweets correspond to which fireball event is a manual process.

Meteor and Fireball Networks

Networks designed for meteor and fireball monitoring are spread all over the world. If a fireball was detected by such a network in most cases high quality scientific information is available in the network's data. Nonetheless, most of them only cover a small part of the atmosphere. If we know when an event has happened as well as the rough location of the entry of the impacting object, we check if it could have been detected by one of these networks. Thanks to various collaborations with those networks we can include their derived scientific information in our summaries or even in further computations.

FRIPON (Fireball Recovery and InterPlanetary Observation Network) covers the sky over France, and large parts of the neighbouring countries. Its extension into different countries is in progress. The cooperation of NEMO with FRIPON is well established; we are informed about detected events on a daily basis. For more

information about the FRIPON network see e.g. Colas et al. (2014).

Infrasound Data

The CTBTO (Comprehensive Nuclear-Test-Ban Treaty Organisation) operates the IMS (International Monitoring System). This system contains a network of seismic, infrasound, hydroacoustic, and radionuclide stations all over the world. It is designed for the detection of nuclear explosions monitoring the whole world during day and night.

The infrasound data can contain signals of the fireball if the entering object deposited enough energy into the atmosphere as the infrasound sensors can detect the energy released by meteoroids or asteroids into the atmosphere as pressure changes. For more information about meteor generated infrasound see e.g. the recently published review paper by Silber et al. (2018).

For an event with a promising large enough entering body the infrasound data are requested and analysed. Our well established cooperation with the BGR (Bundesanstalt für Geowissenschaften und Rohstoffe) the German National Data Center for the verification of the CTBT allows us to investigate the infrasound data. If a fireball related signal is found in the data, a source energy of the entering meteoroid or asteroid can be computed. This enables us to compute an estimated size and mass for the object.

The infrasound generated by meteoroids and asteroids itself is a very interesting topic and part of current research. In the course of the NEMO project further work in this field is planned. Due to its strategy of combining different data of fireball events, this is an obvious next step; see Ott et al. (2019, in press).

Additional Sources

For larger events different publicly available databases are checked.

One example is the fireball database of CNEOS/JPL (NASA/CNEOS - Center for NEO Studies and JPL - Jet Propulsion Laboratory) which is based on US Govt. satellites data. They publish information about large fireball events, including a location and a velocity of the fireball as well as the corresponding source energy of the entering object. Unfortunately, their database is not complete and new events are often added with some delay. Additionally, there is not much known about the analysis process (CNEOS/JPL, 2019).

Based on online articles we are often informed about further data sources that have information about the fireball. These can be of a large variety, ranging from meteorological satellites (see e.g. Borovička and Charvát (2009), or Miller et al. (2013)) to lightning detectors (see e.g. Jenniskens et al. (2018)).

Reports about recovered meteorites that can be related to a fireball event are rather rare. But, if available, these

extra-terrestrial stones can yield a lot of further information.

Re-entering space debris can also cause bright and especially very long lasting fireballs. To investigate if the fireball might be caused by a man-made object is also part of NEMO's goal. ESA's re-entry predictions as well as the re-entry database published by Aerospace are regularly checked.

Combination of all these data sources can yield or significantly improve fireball information.

3 Event summaries

For events that raised more public interest than usual, e.g. if they were seen by a high number of observers based on AMS/IMO reports, we publish an IMO summary. In the following some of these fireballs will be presented.

Fireball over Germany

On September 12, 2019, around 12:50 UT (14:50 CEST) a very bright fireball occurred over northern Germany, reported mainly from the Netherlands and Germany, but also from Belgium, England, and Denmark. Till today there are 583 witness reports collected (status as of October 17, 2019). The fireball was accidentally recorded on video by a windsurfer who was unaware of it at the moment. The video was uploaded to YouTube and started trending (Ott and Drolshagen, 2019d).

Figure 1 presents a map of the reports with computed ground trajectory of the event. The trajectory is based on only those reports that were submitted very soon after the event. The limit was set to two hours. This was done by Mike Hankey since it is expected that these fast submitted reports are the most accurate. Following the computed trajectory the fireball was traveling above Schleswig-Holstein in Germany towards the north-west, with its end close to the border of Denmark (Perlerin, 2019).

Furthermore, the fireball was detected with one camera of the AllSky6 network operated by Jörg Strunk. Further information about this camera system can be found in Hankey and Perlerin (2017). Additionally, the fireball is

listed in the fireball database of CNEOS/JPL. They published coordinates of the fireball of 54.5° N and 9.2° E as well as an energy of 0.48 kt TNT and a velocity of 18.5 km/s for the entering asteroid (CNEOS/JPL, 2019). With an assumed density of 3000 kg/m³ this corresponds to a mass of the entering object of about 12 t and a size of roughly 2 m.

Witnesses also reported a sonic boom, but an analysis of the IMS infrasound data did not show any significant signature of the fireball. The closest station was I26DE (Germany) with an estimated distance to the fireball of about 680 km (Ott and Drolshagen, 2019d).

Fireball over Alberta

The fireball over Alberta, Canada, happened on September 1, 2019 at 04:28 UT (August 31, 2019 at 22:28 MDT). It was reported mainly from Edmond, Canada, and there are 203 AMS reports so far (status as of October 17, 2019). It was captured by different video cameras, from dash cams to doorbell surveillance cameras. With these interesting visual aids it started trending on social media and various news outlets. Figure 2 shows a picture of the fireball. For this event there was also a sonic boom reported but an investigation of the IMS infrasound data did not show a significant signature of the fireball. The event is also not listed in the CNEOS/JPL database (Ott and Drolshagen, 2019c).

Mediterranean sea Asteroid

Over the western-central Mediterranean Sea a widely visible fireball occurred on August 16, 2019 at 20:44 UT (22:44 CEST). AMS/IMO witness reports were collected from France, Italy, Spain, Switzerland, and Tunisia.

The entering asteroid that caused the fireball was detected by at least two IMS infrasound stations: I48TN (Tunisia) and I42PT (Azores, Portugal). Based on these data we computed an energy of about 0.1 kt TNT (Ott and Drolshagen, 2019b).

Later the fireball also appeared on the CNEOS/JPL database. They list a location of 38.9° N and 7.0° E, a velocity of 14.9 km/s, and an energy of 89 t TNT for the event (CNEOS/JPL, 2019).

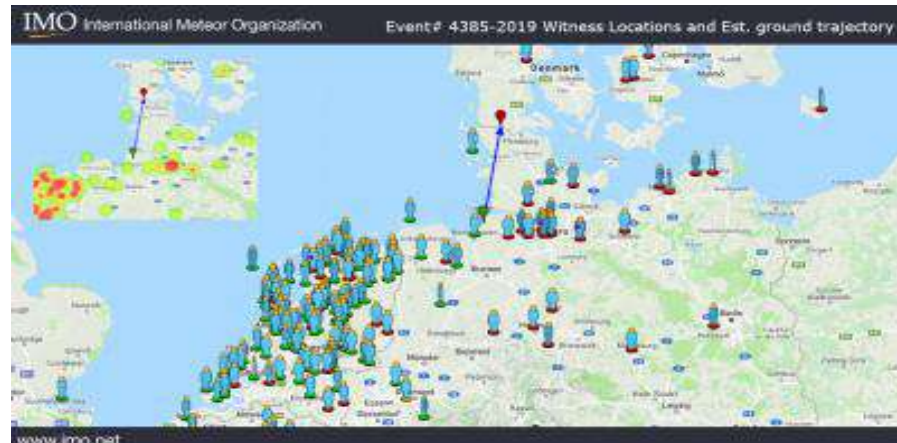


Figure 1 – The IMO reports of the German fireball from September 12, 2019 with computed trajectory (Ott and Drolshagen (2019d) based on Perlerin (2019)).



Figure 2 – Picture of the fireball over Alberta from September 1, 2019. Image credit: Robert M.

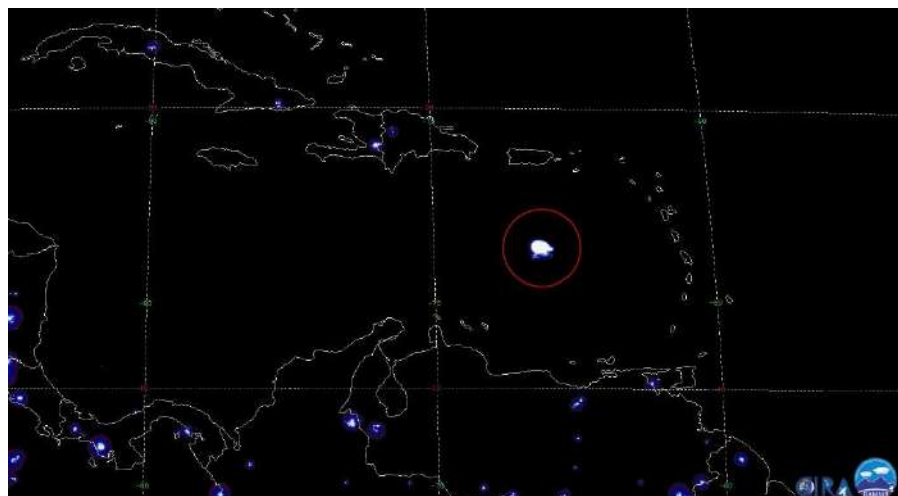


Figure 3 – Picture of the fireball over the Caribbean as seen with the Geostationary Lightning Mapper. Image credit: NASA/GOES-16/GLM

A combination of the velocity value based on the satellite data with the energy based on infrasound data and an assumed density of 3000 kg/m^3 yields a size of roughly 1.3 m and a mass of about 3.8 t for the entering asteroid.

Fireball over the Caribbean

On June 22, 2019 at 21:25 UT (17:35 AST) there was a bright fireball over the Caribbean, south of Puerto Rico.

This event was observed with a large number of different types of instruments. This is the cause for the high amount of attention the event received from the public, even though the fireball occurred over the sea and has no known eye witnesses.

The entry was detected with the IMS infrasound arrays and the Geostationary Lightning Mapper on board of the GOES-16 satellite. An image of the asteroid as seen by the lightning mapper is presented in Figure 3. The signature of the fireball could be identified in the data of three infrasound stations for which a source energy of the

entering asteroid of around 2.5 kt TNT could be derived. This would correspond to a size of about 4.5 m (Ott and Drolshagen, 2019a).

The CNEOS/JPL database lists a location of 14.9° N and 66.2° W , a velocity of 14.9 km/s, and an energy of 6 kt TNT for the event (CNEOS/JPL, 2019).

The asteroid was even detected by a ground-based telescope before it entered the Earth's atmosphere. After the asteroids (2008) TC3 (Jenniskens et al. 2009), (2014) AA (de la Fuente Marcos et al. 2016), and (2018) LA (de la Fuente Marcos, C., and de la Fuente Marcos, R., 2018), this was the fourth time an asteroid has been detected before its entry.

After detection with the Atlas Project Survey the object was provisionally named A10eoM1 and recommended for follow-up observations. This was successfully done with the PanSTARRS system. Later the asteroid received the designation 2019 MO. Following a press release of

the University of Hawaii (University of Hawaii, 2019), the Pan-STARRS 2 team found data of the sky region where the asteroid should have been two hours prior to the detection by the ATLAS system. A detailed analysis of this data yielded even earlier data of the asteroid. For further information about this the reader is referred to the mentioned press release (University of Hawaii, 2019).

NEMO has caught the fireball based on very early information about this event that was posted e.g. by Peter Brown on Twitter (Brown, 2019). After his post a lot of information was tweeted, e.g. about the Geostationary Lightning Mapper detection (Lucena, 2019). Even first orbit parameters were shared (Smolić, 2019). This way the asteroid generated a lot of public interest.

4 Conclusion

NEMO, the NEar real-time MOnitoring system, collects information for bright fireballs. One of its goals is to combine as much information for a fireball from different data sources as possible. This way the amount of knowledge about an event can be maximized. NEMO includes an alert system which is based on social media to achieve information for events in near-real time.

The alarm system already ensures that we are informed of almost all fireballs that cause a lot of public attention within a few hours.

Including more social media platforms is one of the next planned steps. This internet-based information is very fast and world-wide. However, it is biased towards densely populated areas and the western hemisphere.

For more and more events IMO summaries are published on the IMO homepage and this way the collected information is made publicly available.

Since autumn 2017 NEMO has been in test operation mode. In January 2020 the system will be installed at ESA's Near-Earth Object Coordination Centre (NEOCC) and further operated from there. The NEMO events will be included in the NEOCC's Fireball Information System and made publicly available online.

Acknowledgement

We thank the European Space Agency and the University of Oldenburg for funding this project. We are also grateful to all networks and projects that have already agreed to cooperate with this endeavour. A special gratitude goes to the CTBTO for the help with this work and for providing us with data and software. CTBTO is providing access to vDEC (<https://www.ctbto.org/specials/vdec/>) for research related to NEMO.

References

- Borovička, J., and Charvát, Z (2009). "Meteosat observation of the atmospheric entry of 2008 TC over Sudan and the associated dust cloud." *A&A*, Volume 507, Number 2, pp. 1015 - 1022
- Brown, P. G., Assink, J. D., Astiz, L., Blaauw, R., Boslough, M. B., Borovička, J., Brachet, N., Brown, D., Campbell-Brown, M., Ceranna, L., Cooke, W., de Groot-Hedlin, C., Drobm D. P., Edwards, W., Evers, L. G., Garces, M., Gill, J., Hedlin, M., Kingery, A., Laske, G., Le Pichon, A., Mialle, P., Moser, D. E., Saffer, A., Silber, E., Smets, P., Spalding, R. E., Spurný, P., Tagliaferri, E., Uren, D., Weryk, R. J., Whitaker, R., Krzeminski, Z., (2013). "A 500-kiloton airburst over Chelyabinsk and an enhanced hazard from small impactors." *Nature*. 2013 Nov 14;503(7475):238-41
- Brown, P., (2019), Tweet [online], Available at: <https://twitter.com/pgbrown/status/1143264346837082112> [Accessed: 17 Oct. 2019].
- CNEOS/JPL, NASA (2019), "Fireballs" [online], Available at: <https://cneos.jpl.nasa.gov/fireballs/> [Accessed: 17 Oct. 2019].
- Colas, F., Zanda, B., Bouley, S., Vaubaillon, J., Vernazza, P., Gattaccea, J., Marmo, C., Audureau, Y., Kwon, Min K., Maquet, L., Rault, J.-L., Birlan, M., Egal, A., Rotaru, M., Birnbaum, C., Cochard, F., Thizy, O. (2014). "The FRIPON and Vigie-Ciel networks." *Proceedings of the International Meteor Conference*, Giron, France, 18-21 September 2014 Eds.: Rault, J.-L.; Roggemans, P. International Meteor Organization
- de la Fuente Marcos, C., de la Fuente Marcos, R., Mialle, P. (2016). "Homing in for New Year: impact parameters and pre-impact orbital evolution of meteoroid 2014 AA." *Astrophysics and Space Science*, Vol. 361, p. 358 (33 pp.), <https://arxiv.org/pdf/1610.01055.pdf>.
- de la Fuente Marcos, C., de la Fuente Marcos, R. (2018). "On the Pre-impact Orbital Evolution of 2018 LA, Parent Body of the Bright Fireball Observed Over Botswana on 2018 June ." *Research Notes of the AAS*, Vol. 2, Number 2.
- Drolshagen, E., Ott, T., Koschny, D., Drolshagen, G., Poppe, B. (2018). "NEMO – Near real-time Monitoring system." *Proceedings of the International Meteor Conference*, Petnica, Serbia, 21-24 September 2017, pp. 38 - 41
- Drolshagen, E., Ott, T., Koschny, D., Drolshagen, G., Mialle, P., Vaubaillon, Poppe, B. (2019). „NEMO Vol 2 – Near real-time Monitoring system.” *Proceedings of the International Meteor Conference*, Pezinok-Modra, Slovakia, 30 August - 2 September 2018.
- Hankey, M. and Perlerin, V., (2014). "IMO Fireball Reports" *Proceedings of the International Meteor*

- Conference*, Giron, France, 18-21 September 2014
Eds.: Rault, J.-L.; Roggemans, P. International Meteor Organization, pp. 160-161
- Hankey, M. and Perlerin, V., (2018). "American Meteor Society fireball camera." *Proceedings of the International Meteor Conference*, Petnica, Serbia, 21-24 September 2017, pp. 177 - 180
- Jenniskens, P., Shaddad, M. H., Numan, D., Elsir, S., Kudoda, A. M., Zolensky, M. E., Le, L.; Robinson, G. A., Friedrich, J. M., Rumble, D., Steele, A., Chesley, S. R., Fitzsimmons, A., Duddy, S., Hsieh, H. H., Ramsay, G., Brown, P. G., Edwards, W. N., Tagliaferri, E., Boslough, M. B., Spalding, R. E., Dantowitz, R., Kozubal, M., Pravec, P., Borovicka, J., Charvat, Z., Vaubaillon, J., Kuiper, J., Albers, J., Bishop, J. L., Mancinelli, R. L., Sandford, S. A., Milam, S. N., Nuevo, M., Worden, S. P. (2009), "The impact and recovery of asteroid 2008 TC3." *Nature* 458(7237):485–488.
- Jenniskens, P., Albers, J., Tillier, C. E., Edgington, S. F., Longenbaugh, R. S., Goodman, S. J., Rudlosky, S. D., Hildebrand, A. R., Hanton, L., Ciceri, F., Nowell, R., Lyytinen, E., Hladiuk, D., Free, D., Moskovitz, N., Bright, L., Johnston, C. O., Stern, E. (2018). "Detection of meteoroid impacts by the Geostationary Lightning Mapper on the GOES-16 satellite." *Meteoritics & Planetary Science* 1–25 (2018), doi: 10.1111/maps.13137
- Lucena, F., (2019), Tweet [online], Available at: <https://twitter.com/frankie57pr/status/114469831292844416> [Accessed: 17 Oct. 2019].
- Miller, S. D., Straka, W. C., Bachmeier, A. S., Schmit, T. J., Partain, P. T., Noh, Y.-J., (2013). „Earth-viewing satellite perspectives on the Chelyabinsk meteor event.” *PNAS*, vol. 110 no. 45, 18092–18097
- Ott, T. and Drolshagen, E. (2019a). "Fireball over the Caribbean (South of Puerto Rico) detected before it entered!" [online] Available at: <https://www.imo.net/fireball-over-the-caribbean-detected-before-it-entered/> [Accessed 17 Oct. 2019].
- Ott, T. and Drolshagen, E. (2019b). "Bright fireball over Alberta" [online] Available at: <https://www.imo.net/bright-fireball-over-alberta/> [Accessed 17 Oct. 2019].
- Ott, T. and Drolshagen, E. (2019c). "Mediterranean Sea Asteroid" [online] Available at: <https://www.imo.net/mediterranean-sea-asteroid/> [Accessed 17 Oct. 2019].
- Ott, T. and Drolshagen, E. (2019d). "Bright fireball over Northern Germany!" [online] Available at: <https://www.imo.net/bright-fireball-over-northern-germany/> [Accessed 17 Oct. 2019].
- Ott, T., Drolshagen, E., Koschny, D., Mialle, P., Pilger, C., Vaubaillon, J., Drolshagen, G., Poppe, B. (2019, in press), "Combination of infrasound signals and complementary data for the analysis of bright fireballs", in press, *PSS*
- Perlerin, V. (2019). "Daytime Bright Fireball over danish border on Sept. 12th 2019" [online] Available at: <https://www.amsmeteors.org/2019/09/daytime-fireball-over-north-sea-on-sept-12th-2019/> [Accessed 17 Oct. 2019].
- Pilger, C., Ceranna, L., Ross, J.O., Le Pichon, A., Mialle, P., Garces, M.A. (2013). "CTBT infrasound network performance to detect the 2013 Russian fireball event." *Geophysical Research Letters* 42(7), 2523—2531
- Silber, E.A., Le Pichon, A., Brown, P.G. (2011) "Infrasonic detection of a near-Earth object impact over Indonesia on 8 October 2009". *Geophysical Research Letters* 38(12)
- Silber, E. A., Boslough, M., Hocking W. K., Gritsevich, M., Whitaker, R. W., (2018) "Physics of meteor generated shock waves in the Earth's atmosphere – A review." *Advances in Space Research*, in press.
- Smolić, I., (2019), Tweet [online], Available at: <https://twitter.com/pseudotrabant/status/1143481102188916737> [Accessed 17 Oct. 2019].
- University of Hawaii (2019), Press release, "Breakthrough: UH team successfully locates incoming asteroid", [online] Available at: http://www.ifa.hawaii.edu/info/press-releases/ATLAS_2019MO/ [Accessed 17 Oct. 2019].

FRIPOON vs. AllSky6 – a Practical Comparison

Sirko Molau¹

¹Arbeitskreis Meteore e.V, Germany

sirko@molau.de

In recent years, there have been a number of projects to establish video networks for fireball observation using standardized video cameras. One if not the largest is the FRIPOON network in central Europe, which consist of over 150 stations. Each camera is equipped with a fish-eye lens that covers the whole hemisphere. Recently another camera type dubbed AllSky6 has been presented, which follows a different approach. It consists of six individual cameras with 80x40 degree field of view each, which together cover almost the full sky.

Since November 2018, the author has been operating a FRIPOON and an AllSky6 camera side-by-side. This paper reflects the experience made with these systems. It does not only compare technical parameters, but also practical aspects like software, data access, monitoring capabilities, costs and support for each of these cameras.

1 Introduction

After the FRIPOON network¹ was introduced at the 2017 IMC, I decided to install two FRIPOON cameras for testing at my own premises. DEBY02 was deployed in December 2017 in Seysdorf, DEBB01 in February 2018 in Ketzür, Germany (Figure 1). The systems have been in operation ever since.



Figure 1 – Location of the FRIPOON cameras DEBB01 and DEBY02 in Germany.

At the following IMC, Mike Hankey introduced a new fireball camera named AllSky6². I found the design highly interesting and bought the demo system straight away. The camera was temporarily installed at my house in Seysdorf, and since November 2018, AMS16 has been operating for comparison right beside DEBB01 in Ketzür (Figure 2).

In this paper I will share first experiences with these cameras systems and their frameworks.



Figure 2 – DEBB01 and AMS16 mounted side-by-side at a roof-top in Ketzür.

2 Comparison

Concept

FRIPOON is a single, monolithic CMOS camera with a field of views of >180°. The camera has a Power-over-Ethernet (PoE) supply, which means there is just one cable from the camera to the computer. The system comes with a small, pre-configured Mini-PC that requires internet access.

FRIPOON is prepared for day&night operation. Data processing and upload to the FRIPOON network is automated. The focus of FRIPOON camera is on simplicity and robustness – it's a real plug&play system (Figure 3). The price for a whole system is about 2,000€.

AllSky6 consists of six highly sensitive NetSurveillance NVT CMOS cameras with 4 mm f/1.0 lens. Five of them are pointing in horizontal directions, one towards zenith (Figure 4). Each camera provides two data streams, one in standard (SD) and one in high definition (HD). The cameras do not cover the whole hemisphere, however, but there are small gaps between the zenith and the horizontal fields of view (Figure 5).

¹ <https://www.fripo.org/>

² <https://allskycams.com/>



Figure 3 – Unboxing a FRIPON camera.



Figure 4 – AllSky6 camera without the dome.



Figure 5 – Composite image of the different cameras of an AllSky6 system showing the gaps between them.

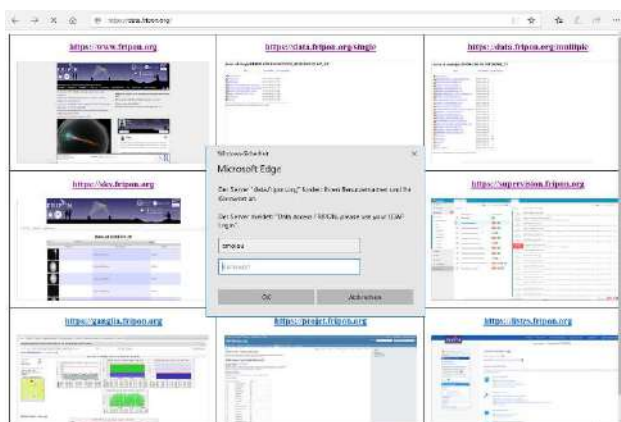


Figure 6 – FRIPON Web portal (access restricted).

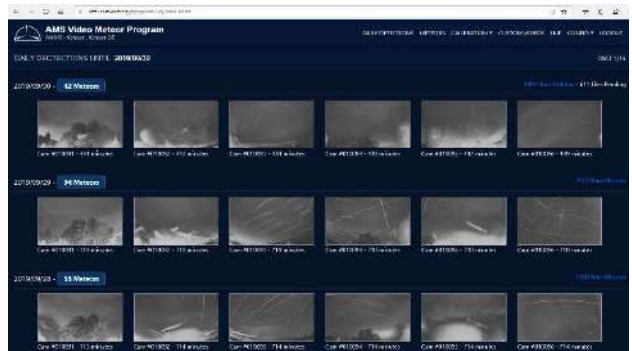


Figure 7 – AllSky6 Web user interface.

AllSky6 has a PoE power supply and is prepared for day&night operation, too. It comes with a small, pre-configured Mini-PC, which records and processes all six video data streams.

The focus of AllSky6 is on high resolution, high sensitivity and low costs. In fact, due to the high sensitivity, it is a kind of hybrid camera that can be used for ordinary meteor and for fireball observation (Table 1). The price for a complete system varies between 800 and 1,100€.

Table 1 – Technical parameters of the two camera systems.

	FRIPON	AllSky6
Sensor	1280x960 pix	SD: 6x640x480 pix HD: 6x1920x1080 pix
Field of view	>180°	6x80x40°
Resolution	ca. 5 pix/°	ca. 25 pix/°
Lim. mag.	ca. -4 mag	ca. +4 mag
Efficiency	ca. 50 met p.a.	Ca. 5,000 met p.a.

Software and Data Access

FRIPON is using the open-source FreeTure pipeline for data processing. There are typically a small number of false detections in twilight. Daytime operation is currently not possible because the number of false detections would be too high.

All data are uploaded to a FRIPON server and matched with the data of other stations in the FRIPON network. If data quality is sufficient, fireball trajectories are computed automatically.

You do not have access to the FRIPON Mini PC and to the recordings. A web portal which provides access to the data has been promised for years, but is still not available (Figure 6). An interface to the IMO Fireball Database is currently tested.

AllSky6 is using an own meteor detection and processing software. The number of false detections depends on cloudiness and airplane traffic and ranges typically between 0 and 30 per night. Data upload to the Internet and matching of data from different stations is still under development.

You have root access to the AllSky6 Mini PC running Ubuntu and therefore full access to all data, which are stored on a local hard drive. The software comes with a

Web user interface that grants access to the data. It is used to delete false detections and refine fireballs measures (Figure 7).

Monitoring and Support

The camera operator receives an email alert when a FRIPON system is down. There is a monitoring portal with detailed health data, and a live view image from all cameras every five minutes.

FRIPON has a dedicated support hotline which can be contacted by e-mail. Some requests are answered immediately, for other requests you have to wait forever.

The AllSky6 software provides a live image for all six cameras every five minutes, too. An monitoring email alert is currently in implementation.

You can reach Mike Hankey for support topics virtually at any time and feedback is provided typically within 24 hours. Most of the software has been implemented in 2019, i.e. the development cycles are very short. Your feedback has direct influence on hardware and software design improvements.

Rollout and Maturity

A FRIPON camera has a mature commercial design. It is hermetically sealed, so modifications are not possible (black box).

There is a large network with over 150 FRIPON stations in Europe today. Local sub-networks are established in France, Italy, Romania and the Netherlands.

AllSky6 is a system which is still growing up and has some child diseases (e.g. thermal and stability problems, which had to be fixed in 2019). The hardware design is open and upgradeable. All six cameras of my system were replaced with a new model in February 2019, for example, that is significantly more sensitive. An upgrade to AllSky7, which will contain two zenith cameras to remove the gap between the cameras, is expected for the end of 2019.

At this time, there are about 25 AllSky6 stations deployed world-wide, and sub-networks in the US and Germany are about to be established.

3 Fireball Examples

Here are the two most spectacular fireballs that were recorded in the testing phase.

2019/04/16, 21:51:27 UT

In mid of April, a bright fireball occurred over northern Germany, for which AMS/IMO received 74 visual reports.

Figure 8 shows the fireball as recorded by DEBB01 in western direction, Figure 9 the same fireball recorded by camera 5 of AMS16.

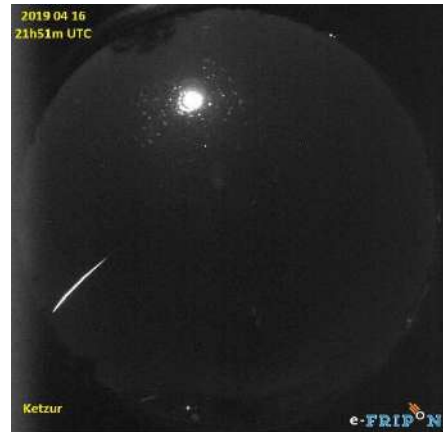


Figure 8 – Fireball of April 16, 2019, as recorded by DEBB01.



Figure 9 – Fireball of April 16, 2019, as recorded by camera 5 of AMS16.

2019/09/27, 17:29:30 UT

In a late September evening, in bright twilight right after a rain shower, another bright fireball occurred over northern Germany. AMS/IMO received 157 visual reports from that event to date.

Figure 10 shows the fireball as recorded by DEBB01 low in the north-eastern horizon, Figure 11 and 12 the same fireball recorded by camera 2 and 1 of AMS16, respectively.

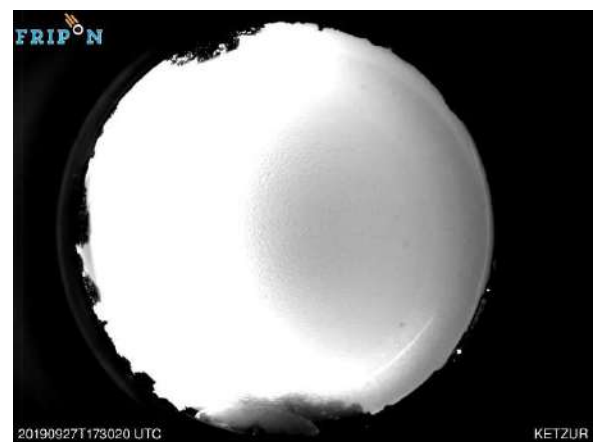


Figure 10 – Fireball of September 27, 2019, as recorded by DEBB01.



Figure 11 – Fireball of September 27, 2019, as recorded by camera 2 of AMS16.



Figure 12 – Close-up view from the HD video stream by camera 1 of AMS16 that shows the disintegration of the meteoroid.

4 Summary and Conclusion

The FRIPON system has been developed for many years and is more mature than AllSky6 with respect to hardware, software, monitoring and portals. At this time, there are far more FRIPON than AllSky6 stations deployed.

FRIPON is state-funded and supported by a team of French professional astronomers. The camera has a closed design and data access is severely restricted. Software development is very slow.

AllSky6 is privately funded and the project of a single, enthusiastic amateur. Still it is much more agile with respect to hardware and software development. Both the design and the data access are open. AllSky6 is less expensive and in most technical parameters superior to FRIPON.

For observers who just want to become part of a large, international fireball network and who are not interested in the hardware, software and data, FRIPON may be the first choice.

For observers who want to take part in the development of a new system, who are keen on their data and who would like to record more than a few dozen fireballs per year, AllSky6 is the better choice.

The All-Sky-6 and Video Meteor Archive System of the AMS Ltd.

Mike Hankey¹, David Meisel², Vincent Perlerin¹

¹ American Meteor Society and International Meteor Organization
mike.hankey@gmail.com, vperlerin@gmail.com

² State University of New York College at Geneseo | SUNY Geneseo · Department of Physics and Astronomy
ddmmeteor@frontier.com

In this paper, we present the current status of the All Sky 6 (AS6) camera project and future vision for the American Meteor Society (AMS) Video Meteor Program. We have presented the first AS6 prototype at the International Meteor Conference 2016. Since then, the hardware has evolved into a robust and feature rich, offering including an aluminum heat-proof structure, 6 generic IMX291 cameras and custom PCB boards that enable power and communications over a single wire. On the software side, programs have been built and integrated to automate the recording, detection, reduction, sharing and solving of meteor captures. Operators can review and manage the captures and associated information through an easy to use web-based interface installed on the host computer.

1 Introduction

While the All Sky 6 has been actively developed for the last 3 years, our desires to create a meteor camera system and network in the United States dates back 10 years and our first camera prototype was briefly presented at the IMC in 2013 (Hankey et al., 2013). Since then, our knowledge and capabilities have grown exponentially and this would not have been possible without the information, support and knowledge we obtained through the International Meteor Organization (IMO), many of their members and the annual International Meteor Conference (IMC) – see.

Acknowledgement for details.

In this paper, we highlight some of the most important technical aspects that helped bring this project into fruition. We particularly choose to highlight the items useful to anybody wanting to build custom cameras or networks.

2 Hardware

IMX-IP-Based Cameras (IMX291)

Over the last several years, Sony has developed a low-light CMOS camera chip technology called Starvis (*aka* Starlight), that has revolutionized the low-light camera industry. The IMX291 camera allows 25 fps full real-time monitoring, using H.264 video compression technology, low bit rate and high definition image.

The main advantage of the IMX291 camera is its superior low-light sensitivity capable of capturing magnitude 5 stars (and meteors) from a 4 mm lens while recording at 25 frames per second at an extremely low cost. Additionally, IP based digital cameras are much easier to work with as communications from multiple devices can travel over the same wire. Furthermore, H.264 compressed video (while suffering from some artifacts) is considerably smaller in storage size than raw video. This

allows us to save 24 hours of continuous video with just a few 10s of Gigabytes. As a result, AS6 operators can have access to more than 2 weeks of continuous recordings. This continuous recording feature enables the capture of daytime fireballs and other atypical events of public interest that would have otherwise gone undetected.



Figure 1 – Early AllSky6 Prototype (2018)

Power Over Ethernet (POE)

POE is a technique for delivering power and Ethernet over a single wire. Cat 6 cables have 4 pairs of wires (8 total wires). In a POE setup, 4 of these wires are used for communications (TX+, TX-, RX+, RX-) while the other 4 wires are used for low-voltage DC power (2 positive and 2 negative). One end of the wire terminates at the camera device, while the other end terminates at a POE Injector (which feeds power into the wire), and then at the computer (which feeds the wire Ethernet). This setup greatly simplifies the work needed to setup and manage multi-camera applications.

CAD Software and CNC Cutting Machines

Many open source CAD (Computer Aided Design) programs exist that can be downloaded and installed for free. For this project, we are using a program called OpenSCAD to design the All Sky 6 enclosure and

mounts. These designs are then transferred to CNC (Computer Numerical Control) cutting machines that can fabricate the raw materials exactly as designed. We first started with acrylic materials for prototyping and then moved to aluminum for its durability and thermal benefits. Most of the hardware parts of the project have been prototyped, refined and fabricated at a local “Maker Space” (or *Fab lab*), that provides access to many CNC and other fabricating machines.

Printed Circuit Board (PCB) - EasyEDA.com

One of the challenges in developing the All Sky 6 was the need for a custom PCB that could split the power and Ethernet out of the incoming POE cable, and then transfer each to a network and power bus, so that all devices inside the enclosure could be powered and communicate over a single wire. This process started with proto-boards and lots of wires but was quickly upgraded thanks to EasyEDA.com. With this website, we easily designed our own custom circuit boards online. When completed, the boards are ordered with a click of a button and relatively low cost. The result is your very own, custom PCB that is professional manufactured and shipped in less than 1-week time. The All Sky 6 hardware would not have been possible without our own custom designed PCB that was created with EasyEDA.com. We recommend this website for anyone designing custom tools or electronics for meteor work (for example radiometers).

Custom parts and cheap but reliable components

Aliexpress.com and Alibaba.com provide direct access to manufacturers and suppliers in China. These sites are among the most convenient places to acquire cameras, lenses or other materials needed for meteor camera work. Aliexpress.com is consumer driven and provides instant purchasing of goods, while Alibaba is a business-to-business model designed for wholesalers. Orders on Alibaba are not instant but rather negotiated and usually vendors expect larger quantity orders. However, these orders come with better prices and often customizations if needed.

There are many vendors and service providers on Alibaba.com who can be hired for custom jobs. For the All Sky 6 project, we have contracted vendors through Alibaba.com for fabrication of aluminum parts, fabrication of custom wires and fabrication of custom acrylic domes. We have also secured vendors through Alibaba for: cameras, lenses, wire connectors, common wires, screws / hardware, power supplies and computers.

3 Software

Operating System and Programming Language

The All Sky 6 software runs on the free and open-source Linux operating system and while currently configured to work with Ubuntu, the software can easily run on any flavor of Linux (Mint, Debian, Fedora, etc.). The core functionalities have been implemented in Python, as this is easy to use, popular with astronomers and provides a huge repository of scientific libraries for astronomy and

other fields. Some features of the web-based interface installed on the host computer have been implemented in Javascript.

Video processing tools

All Sky 6 utilizes FFmpeg for many video related processes. FFmpeg is a video processing tool that can be used to accomplish many video tasks. With just 1 FFmpeg line, we can continuously record streams from cameras into time stamped marked files. We use FFmpeg to re-format videos, cut videos, merge videos, extract frames from videos, add overlays to videos, live stream videos and many other things. Based on our experience, FFmpeg is the fastest way to read and process videos.

Computer Vision (CV) is a field of computer science relating to image and video processing such that objects in images can be identified, tracked and analyzed through computer programs. These tasks have been greatly simplified with the OpenCV library. This software library provides routines that allow for quick and easy implementation of many types of CV applications. For example, a simple motion detection program can be written in less than 20 lines of code. The All Sky 6 programs rely heavily on OpenCV in Python.

Astrometry Engine

Astrometry.net is an open source software program that enables blind plate solving of images containing enough stars. (Lang et al., 2010). When successful, the program will report back the fields needed to calibrate and identify stars and astrometric positions in the image, specifically: the image’s center right accession and declination, the position angle and the pixel scale (arc seconds to pixel relationship). While designed for use with mostly narrow field telescopic images, while challenging, it is possible to get successful results with wide field (80-90 degree) images.

Astrometry.net is an extremely powerful program, can be installed locally and customized. We have successfully implemented Astrometry.net software as the first step in the calibration process of the All Sky 6. Astrometry.net however does not take lens distortion into consideration and as such, there is inaccuracy throughout the image but especially at the edges. Without lens distortion correction, this error can be as much as 10 degrees in the corners.

Lens distortion polynomial fitting and astrometry

Denis Vida has created a lens distortion polynomial fitting and astrometry routine inside his Raspberry Pi Meteor Station (RMS) (Vida et al., 2016) open source project, based in part on the work of Jiří Borovicka (Borovička, 1995). We have slightly adapted Denis’s lens distortion and astrometry routines into the AS6 calibration and reduction processes. By using Astrometry.net as a first step, we can jump-start the calibration, greatly simplifying the steps and minimizing user intervention. Once a first calibration has been completed, “follow-up” calibrations are run multiple

times each night and on every meteor capture as long as it has enough stars.

This per-meteor refinement process utilizes a Python minimization function that changes each rigid Astrometry.net variable (center Ra, Dec, position angle and pixel scale) over and over, until the residual error between the star's image location (x, y) is minimized with the expected star catalog position (x, y). As temperatures change through the night, small shifts occur with the mounts and optical fixtures that introduce astrometric errors. This means, a calibration that was taken the night before, or even a few hours earlier, will have more error, than a calibration taken at an exact moment. For these reasons, we re-calibrate every meteor in the system (when possible) and with this technique we can achieve astrometric accuracy with error of less than .05 degrees.

We have also slightly modified the RMS lens distortion polynomial routines to accept stars registered across many images spanning an entire night or many nights. The more stars that can be used in the lens distortion fitting process, the better the model will be. Ideally 50 or more stars would be required. Sometimes in light polluted areas it is difficult to get more than 10 stars in a single image. By combining registered star positions across images, it is possible to create a lens distortion model that uses hundreds or even thousands of stars.

When this master lens distortion model is created, the astrometric accuracy even at the corners is near perfect and at least significantly better, then a model constructed from a single image's stars.

It is also important to note that once the polynomial variables for the lens distortion are properly defined, they do not change over long periods of time. For example, we have tested lens distortion models up to 1 year after they were initially created and they can still be valid to .05 degree accuracy as long as the center Ra, Dec position angle and pixel scale error has been minimized first.

Denis Vida's WMPL

While we are currently not at the point where we are automatically solving multi-station meteors in real-time, we have implemented Denis Vida's Western Meteor Python Library (WMPL) (Vida et al., 2019) and started working with it. This open source project provides trajectory, velocity and orbit calculating routines that can be programmatically called. Event data inside the All Sky 6 is structured such that multiple solutions can be run for each event, for example, multiple solvers inside WMPL (Intersecting Planes, Monte Carlo etc), or even multiple slightly different input variables. Events in the AS6 have a one to many relationships with event solutions. WMPL is currently our only implemented solver; however, we do have plans to support more than a single solving process. Custom solvers can also be added.

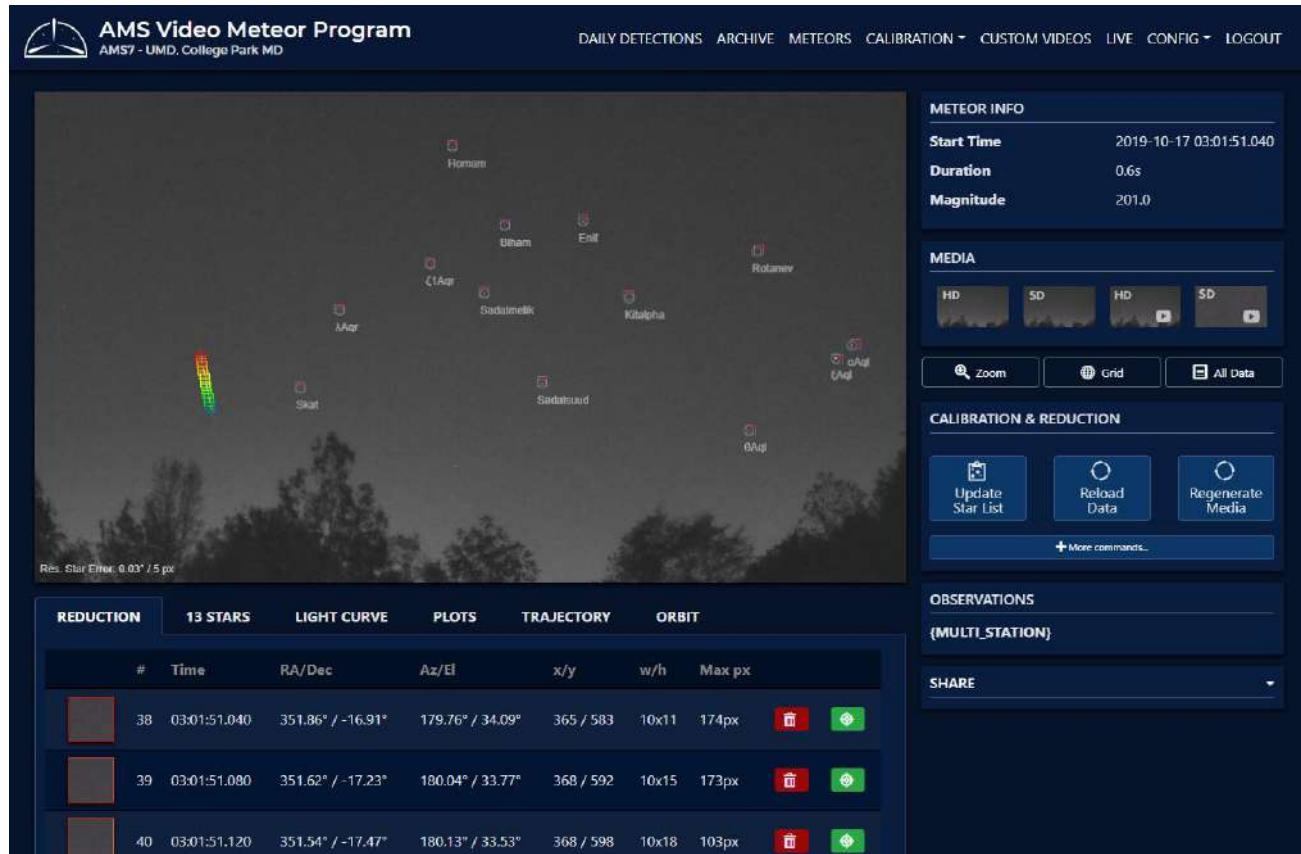


Figure 2 – All Sky 6 web-based interface: meteor detail Screen showing stars and meteor reduction values

Web-based interface

All Sky 6 operators can review and manage the captures and associated information through an easy to use web-

based interface installed on the host computer and implemented in Python CGI and JavaScript (Figure 2).

Through this interface, the operator can browse all his detections, semi-automatically redefine the reduction data when necessary, check the quality of the calibration for

each camera, create custom time-lapse videos and monitor the health of the system among other tasks.

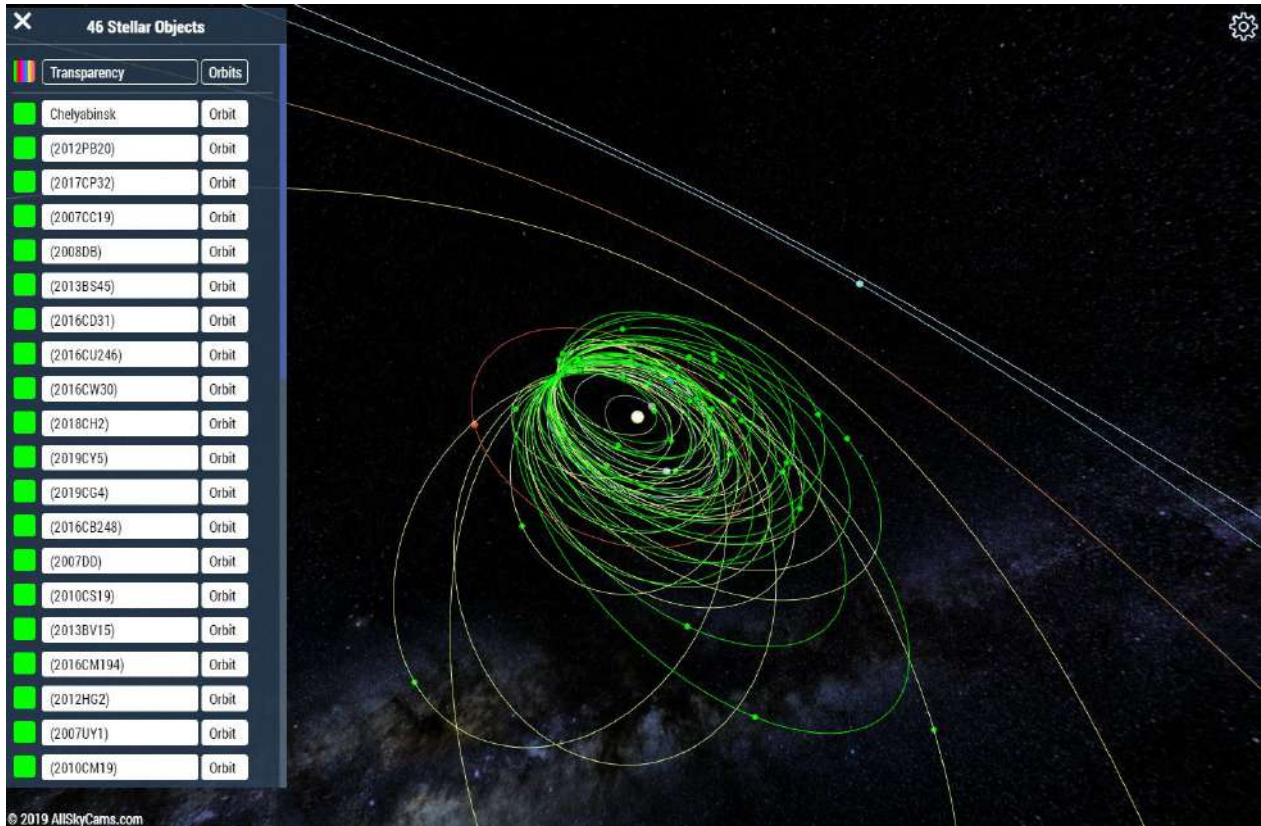


Figure 3 – New AMS Online 3D Orbit Viewer

4 Current Status and prospect

There are currently 20 All Sky 6 stations operational in the United States and Europe comprising a total of 120 deployed cameras. Over the last 3 years, we have been developing and refining the hardware and software and have limited the flow of new systems. We are now at the point where we are shifting from a development focus to a manufacturing and operational focus. We still have some development milestones we hope to accomplish soon, including:

- Virtually perfect event reduction
- Real time cloud synchronization and event solving with WMPL and other methods
- Implementation of the public facing Video Meteor Archive

Once these last pieces are in place, our resources will shift to manufacturing and placing more units in the field. We are also working on a few alternative All Sky products including the All Sky 7, an off-grid version (solar and cellular data), a spectroscopic version, a single camera part sky version, a PTZ version and a mega-camera (16 or more) camera version.

One of the primary goals of the All Sky 6 from the beginning was to create an open and easy starting point for any multi-camera computer vision project. The All Sky 6 is a complete 360 video camera product, but it can also serve as a starting place and computer vision

development kit for something new. Many future or alternative versions are possible.

While our efforts are still under development, the long-term plan is to share all videos, images and reduction data to an online archive hosted by the AMS. The archive will include tools to browse the captures, examine specific events and aggregate multiple events across stations or times of year. Meteor orbits and groups of orbits can be visualized in a feature rich 3D orbit viewer or exported for analysis (Figure 3).

While still operating in a beta capacity, All Sky 6 systems and kits are available for purchase at www.allskycams.com.

Acknowledgement

Since attending our first IMC in 2013, our knowledge and capabilities have grown exponentially and this would not have been possible without the information, support and knowledge we obtained through the International Meteor Organization (IMO), many of their members and the annual International Meteor Conference (IMC). Everyone who has operated a meteor network or built a meteor camera has helped inspire and create the All Sky 6 and we have great respect and appreciation for all these contributions. We specifically thank and recognize Denis Vida of the University of Western Ontario (UWO) for his work with the RMS and WMPL, Peter Gural (Gural

Software and Analysis LLC) and Peter Jenniskens (SETI) for CAMS¹, Sirko Molau for METREC, Peter Brown (University of Western Ontario), Bill Cooke (NASA Meteoroid Environment Office) for ASGARD, François Colas (CNRS, Observatoire de Paris) and Jeremie Vaubaillon (IMCCE, Observatoire de Paris) for FRIPON, Ellie Sansom, Hadrien Devillepoix and Phil Bland (Curtin University) for the Desert Fireball Network, Mariusz Wiśniewski for the Polish Fireball Network, Juraj Toth for AMOS, Jiří Borovicka and Pavel Spurný for the European Fireball Network, and everyone else who has operated a Watec or UFO Capture system and has shared their work in the field at a conference. We listened and learned from you and would not have been able to build the All Sky 6 without your help. We also have great appreciation for the help, support and work of AMS Executive David Meisel (AMS), who has been very supportive of this effort and overseen, reviewed and advised on the development.

References

- Hankey, M., Perlerin, V., (2013). “AMS fireball program, community website, mobile app and all sky camera program”, In Gyssens M., Roggemans P., Żoładek, P. editors, Proceedings of the International Meteor Conference 2013, Poznan, Poland, 2013. IMO, pages 93-97
- Lang, D., Hogg, D. W., Mierle, K., Blanton, M., & Roweis, S., (2010), “Astrometry.net: Blind astrometric calibration of arbitrary astronomical images”, *The Astronomical Journal* 139, 1782–1800
- Borovička J., Spurný P., and Keclíková J. (1995). “A new positional astrometric method for all-sky cameras”. *Astronomy and Astrophysics Supplement*, 112, 173–178
- Vida D., Zubović D., Segon D, Gural P. and Cupec R. (2016). “Open-source meteor detection software for low-cost single-board computers”, In Roggemans A., Roggemans P., editors, Proceedings of the International Meteor Conference 2016, Egmond, the Netherlands, 2-5 June 2016. IMO, pages 307-318
- Vida, D., Gural, P., Brown, P., Campbell-Brown, M., Wiegert, P. (2019). *Estimating trajectories of meteors: an observational Monte Carlo approach.* MNRAS, submitted

¹ <http://cams.seti.org/>

Fripón first results after 3 years of observations

François Colas¹, Brigitte Zanda², Simon Jeanne¹, Mirel Burlan¹, S. Bouley³, P. Vernazza⁴, J. L. Rault⁵, and J. Gattacceca⁶

¹Institut de Mécanique Céleste et de Calcul des Ephémérides (IMCCE), Observatoire de Paris, 75014 Paris,
France

francois.colas@obspm.fr
simon.jeanne@obspm.fr
mirel.burlan@obspm.fr

²Muséum National d'Histoire Naturelle, 75005 Paris, France
brigitte.zanda@mnhn.fr

³Géosciences Paris Sud (GEOPS), Université Paris Sud, CNRS, Université Paris-Saclay, 91405 Orsay
sylvain.bouley@gmail.com

⁴Laboratoire d'Astrophysique de Marseille, Université d'Aix-Marseille, 13007 Marseille, France
pierre.vernazza@lam.fr

⁵International Meteor Organization (IMO), Radio Commission, 91360 Epinay sur Orge, France
f6agr@orange.fr

⁶Centre Européen de Recherche et d'Enseignement des Géosciences de l'Environnement (CEREGE), CNRS, Aix-en-Provence, France
gattacceca@cerege.fr

We presented the first results of the Fripón network after 3 years of observations. We focused our presentation on the more than 2000 orbits obtained.

BRAMS forward scatter observations of major meteor showers in 2016–2019

Cis Verbeeck¹, Hervé Lamy², Stijn Calders², Antonio Martínez Picar¹, and Antoine Calegaro²

¹ Royal Observatory of Belgium, Ringlaan 3, 1180 Brussels, Belgium

cis.verbeeck@oma.be and antonio.martinez@oma.be

² Royal Belgian Institute of Space Aeronomy, Ringlaan 3, 1180 Brussels, Belgium

herve.lamy@aeronomie.be, stijn.calders@aeronomie.be and antoine.calegaro@aeronomie.be

The BRAMS network consists of a dedicated forward scatter beacon and about 25 forward scatter receiving stations located in or near Belgium. Though these stations perform observations all year round, we still need the help of citizen scientists from the Radio Meteor Zoo for accurate detection of complex overdense meteor echoes observed during meteor showers. From 2016 onwards, we organized Radio Meteor Zoo campaigns for the major showers. Here, we present and compare activity curves from BRAMS forward scatter observations of major showers in the years 2016–2019. The estimated shower component is obtained after subtracting an estimate of the sporadic background. It is obvious that the obtained shower rates require further analysis, as they still have to be corrected for the diurnal sensitivity of the setup as a function of the radiant position (the Observability Function).

1 Introduction

BRAMS (Belgian RAdio Meteor Stations) is a radio network located in Belgium using forward scatter measurements to detect and characterize meteoroids. It consists of one dedicated transmitter located in Dourbes in the south of Belgium and approximately 25 receiving stations spread all over the Belgian territory. The transmitter emits a circularly polarized continuous wave (CW) at a frequency of 49.97 MHz and with a power of 150 W. All receiving stations use the same material (including a 3 elements Yagi antenna) and are synchronized using GPS clocks. More details can be found in, e.g., (Lamy et al., 2015).

Each BRAMS receiving station is recording continuously, producing each day 288 WAV files and detecting about 1500–2000 meteors. Though significant advances in automatic detection of meteor reflections in the BRAMS spectrograms has been made, the best detector is still the human eye. In August 2016, the Radio Meteor Zoo¹ was launched. This citizen science project, hosted on the Zooniverse platform (Lintott, 2008), exploits the (trained) human eye of many volunteers for classifying meteor reflections during certain observing campaigns. This enabled the BRAMS team to publish the present shower activity results. More information about the Radio Meteor Zoo can be found in (Calders, 2016) and (Calders, 2017).

In the current paper, we present meteor shower activity profiles from BRAMS observations of the Geminids between 2016 and 2018 and the Perseids between 2016 and 2019. All observations pertain to the BRAMS receiving station in Humain. In order to estimate the sporadic background during shower observations, a sine

curve is fitted to the average diurnal hourly rates of meteor echoes on a few days well outside the main shower activity. This sine curve is then subtracted from the hourly total number of meteor reflections to yield an estimate of the hourly number of shower meteors. This approach was described in detail in (Verbeeck et al., 2017). The hourly total duration of meteor reflections (i.e., the sum of all durations of the meteor reflections during that hour) is often a more robust measure of meteor activity than the hourly number of reflections. We present both the results for hourly number of reflections and hourly total duration of meteor reflections.

Sections 2 and 3 present the BRAMS activity curves near the maximum period of the Perseids between 2016 and 2019, and the Geminids between 2016 and 2018, respectively. Conclusions and future plans are outlined in Section 4.

2 Perseids 2016–2019

The BRAMS station in Humain observed the Perseids near their maximum period in 2016, 2017, 2018, and 2019.

Since we know that the hourly total number of meteor reflections is dominated by the large number of reflections by faint underdense meteors (Verbeeck et al., 2017), we focus exclusively on the meteor reflections lasting at least 10 seconds, which are dominated by shower meteor reflections. Figures 1, 2, 3, and 4 show an estimate of the Perseid activity as observed from Humain in 2019, 2018, 2017, and 2016, respectively. All these plots pertain to meteor reflections lasting at least 10 seconds.

The hourly total number of meteor reflections is shown in the top left plot (red curve). As a proxy for the di-

¹<http://www.radiometeorzoo.org>

urnal variation of the sporadic background, the average hourly number of meteor reflections observed away from the shower maximum is plotted (black circles for the average and black sine curve for its weighted sine fit), as explained in (Verbeeck et al., 2017). An estimate of the number of Perseid reflections per hour (blue curve) is obtained by subtracting the modeled sporadic background (the black weighted sine fit) from the hourly total number of reflections. The Perseid radiant elevation is featured in the bottom left plot. The plots on the right show the same curves, but for the total duration of meteor reflections rather than the number of meteor reflections.

When we compare the Perseid plots from year to year, we observe a very similar shape every year, at fixed local time. For instance, there are peaks around 4h and 8h UT and near zero values around 18h UT on every day. We do see that these specific profiles can be a bit higher or lower from year to year or especially from day to day; this is an indication of a higher or lower meteor shower activity on that day and year. This is well-understood: it is the effect of the diurnal variation of the sensitivity of the forward scatter setup as the radiant crosses the sky. The sensitivity of the forward scatter setup as a function of radiant position is called the Observability Function and was modeled in (Verbeeck, 1997).

3 Geminids 2016–2018

The BRAMS station in Humain observed the Geminids near their maximum period in 2016, 2017, and 2018. Figures 5, 6, and 7 show the sporadic and shower activity plots for the Geminids in 2018, 2017, and 2016, respectively, for meteor reflections lasting at least 10 seconds.

Also for the Geminids, we observe a very similar shape every year, at a fixed local time. For instance, there is a peak around 2h UT and there are near zero values around 14h UT on every day. This shows once more that raw meteor reflection rates — even when corrected for the sporadic background — are dominated by the effect of the Observability Function, and one cannot determine from raw rates the exact time of maximum, only the day of maximum or two days nearest to the maximum. In order to estimate the exact time of maximum and the activity profile more precisely, one must divide the raw rates by the Observability Function.

4 Discussion and future outlook

Employing the Radio Meteor Zoo detections of meteor reflections from forward scatter observations from the BRAMS receiving station at Humain, we have estimated the sporadic background and subtracted it from the total radio meteor activity to obtain an estimate of the shower activity around the maximum of the Perseids 2016–2019 and the Geminids 2016–2018.

From the observations of both showers it is very clear

that raw forward scatter reflection rates do not represent the pure shower meteor activity, but are dominated by the diurnal sensitivity of the setup as the radiant crosses the sky. Indeed, there is a clear diurnal pattern in the shower observations, which is the same over different years and is just dependent on the relative position of the radiant with respect to the transmitter and receiver. This sensitivity is called the Observability Function, and was described in (Verbeeck, 1997). In order to obtain shower rates that represent the pure shower meteor activity, the obtained shower rates have to be divided by the Observability Function, which is highly dependent on radiant-setup geometry and antenna gains. Calculation of the Observability Function is under development.

Since the true shower activity is convoluted with the Observability Function in our observations (repeating every 24 hours), the time of shower maximum can only be estimated up to 24 hours. Taking this into account, the observations above are consistent with video and visual results.

Acknowledgements

The BRAMS network is a project from the Royal Belgian Institute for Space Aeronomy and funded by the Solar-Terrestrial Center of Excellence (STCE). The authors thank all volunteers who helped us with the classification of the spectrograms. These volunteers make the success of the Radio Meteor Zoo. We also thank the Zooniverse team, who are hosting the Radio Meteor Zoo and who are always very enthusiastic in supporting us. Last but not least, we want to thank all volunteers who host a BRAMS receiving station. Their assistance is of course essential to the BRAMS project. The authors are grateful for their constant support.

References

- Calders S., Verbeeck C., Lamy H., and Martínez Picar A. (2016). “The Radio Meteor Zoo: a citizen science project”. In Roggemans A. and Roggemans P., editors, *Proceedings of the International Meteor Conference*, Egmond, The Netherlands, 2–5 June 2016. IMO, 46–49.
- Calders S., Lamy H., Martínez Picar A., Tétard C., Verbeeck C., and Gamby E. (2017). “The Radio Meteor Zoo: involving citizen scientists in radio meteor research”. In Gyssens M., Pavlović D., and Rault J.-L., editors, *Proceedings of the International Meteor Conference*, Petnica, Serbia, 21–24 September 2017. IMO, 13–15.
- Lamy H., Anciaux M., Ravier S., Calders S., Gamby E., Martínez Picar A., and Verbeeck C. (2015). “Recent advances in the BRAMS network”. In Rault J.-L. and Roggemans P., editors, *Proceedings of the International Meteor Conference*, Mis-

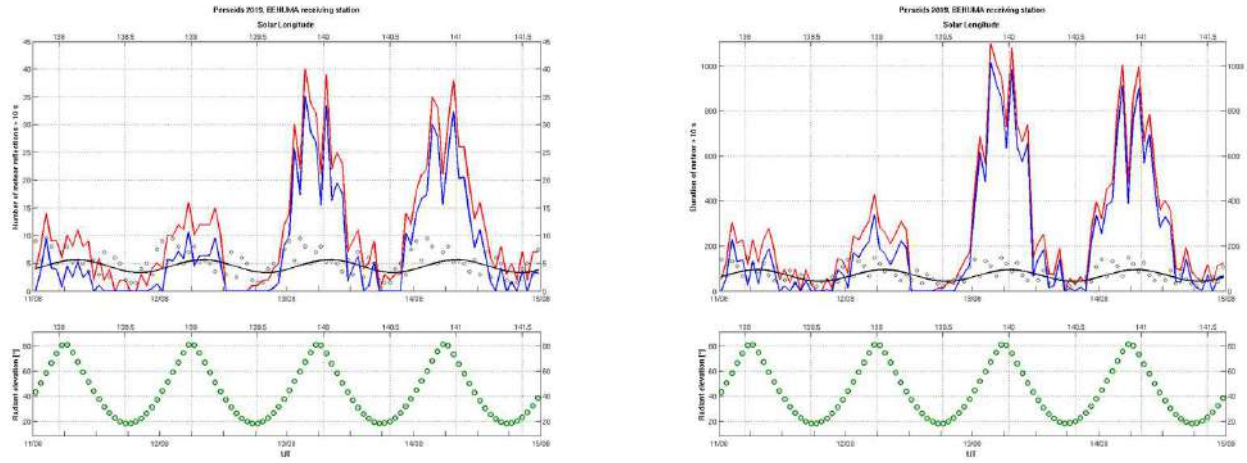


Figure 1 – Estimate of Perseids 2019 activity (BRAMS receiving station: Humain). *Top left:* Hourly number of meteor reflections lasting at least 10 seconds (upper red curve: total observed; black circles and curve: estimation of diurnal variation of sporadic background and its weighted sine fit; lower blue curve: estimated hourly number of Perseid reflections). *Bottom left:* Radiant elevation. *Top right:* Hourly total duration (s) of meteor reflections lasting at least 10 seconds (upper red curve: total observed; black circles and curve: estimation of diurnal variation of sporadic background and its weighted sine fit; lower blue curve: estimated hourly total duration of Perseid reflections). *Bottom right:* Radiant elevation. Times are in UT and durations in seconds.

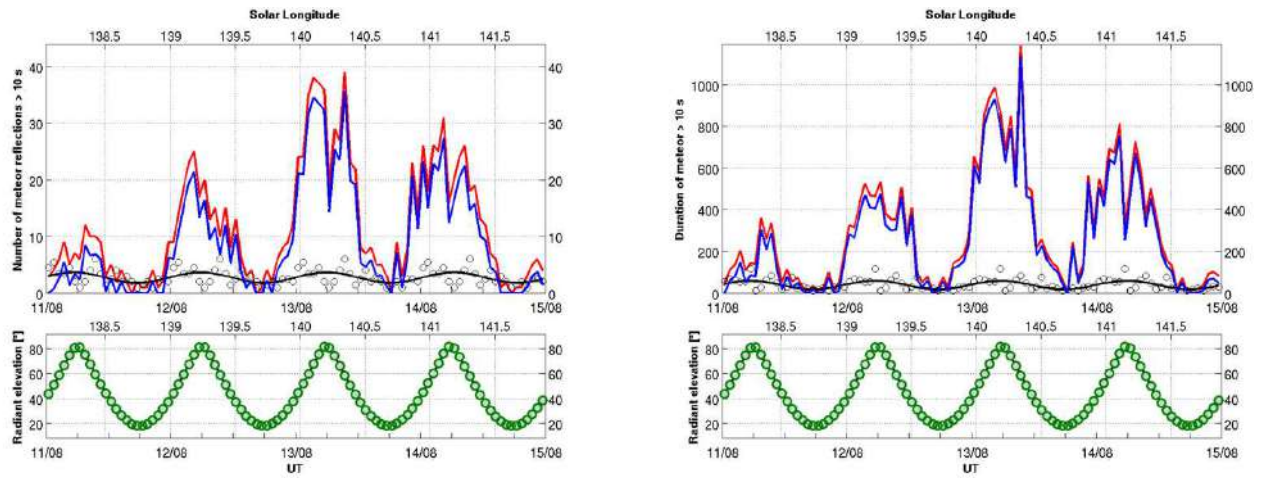


Figure 2 – Estimate of Perseids 2018 activity (BRAMS receiving station: Humain). Description of the plots: see Figure 1.

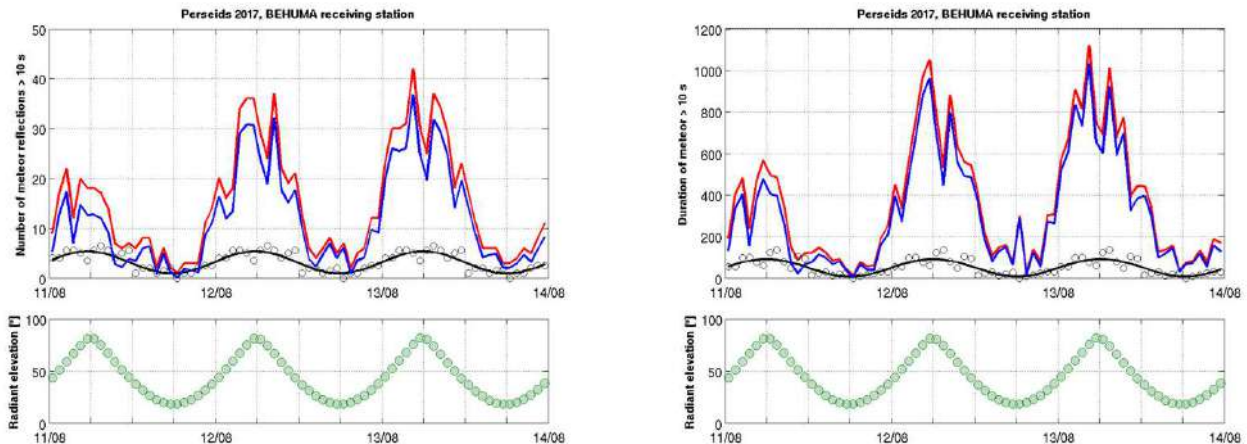


Figure 3 – Estimate of Perseids 2017 activity (BRAMS receiving station: Humain). Description of the plots: see Figure 1.

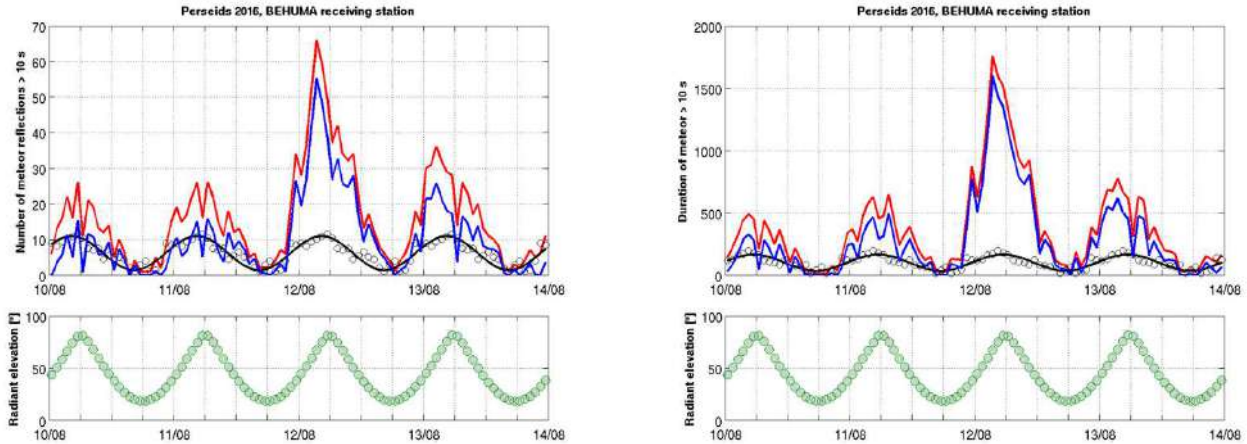


Figure 4 – Estimate of Perseids 2016 activity (BRAMS receiving station: Humain). Description of the plots: see Figure 1.

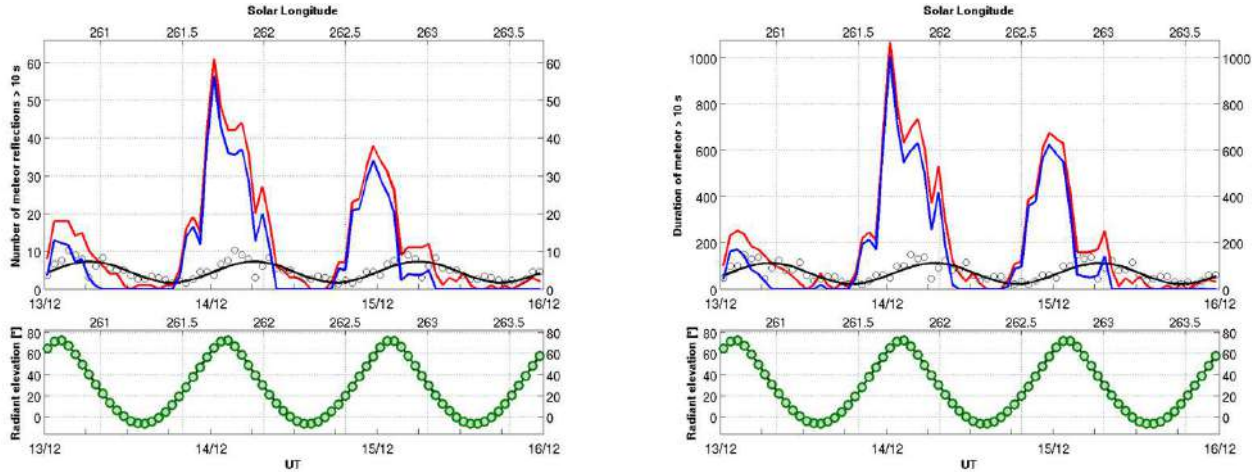


Figure 5 – Estimate of Geminids 2018 activity (BRAMS receiving station: Humain). Description of the plots: see Figure 1.

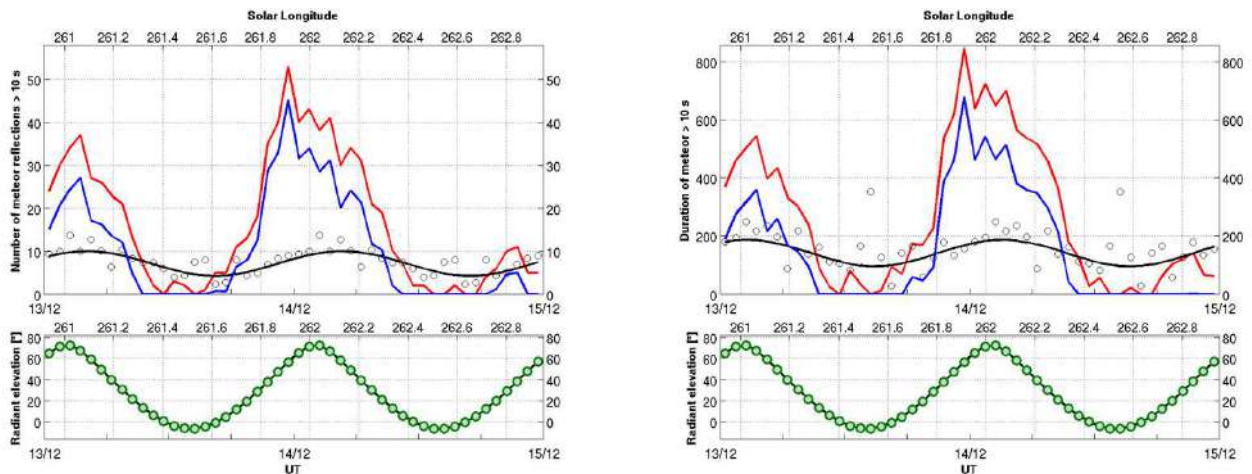


Figure 6 – Estimate of Geminids 2017 activity (BRAMS receiving station: Humain). Description of the plots: see Figure 1.

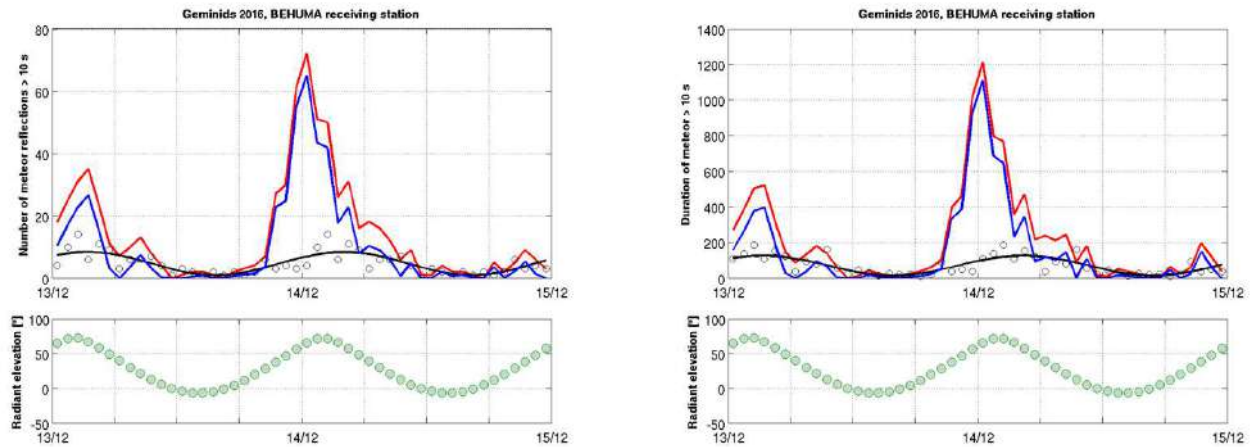


Figure 7 – Estimate of Geminids 2016 activity (BRAMS receiving station: Humain). Description of the plots: see Figure 1.

telbach, Austria, 27–30 August 2015. IMO, 171–175.

Lintott C. J., Schawinski K., Slosar A., Land K., Bamford S., Thomas D., Raddick M. J., Nichol R. C., Szalay A., Andreescu D., Murray P., and Vandenberg J. (2008). “Galaxy Zoo: Morphologies derived from visual inspection of galaxies from the Sloan Digital Sky Survey”. *Monthly Notices of the Royal Astronomical Society*, **389**, 1179–1189.

Molau S., Crivello S., Goncalves R., Saraiva C., Stomeo E., Strunk J., and Kac J. (2018). “Results of the IMO Video Meteor Network — December 2017”. *WGN, Journal of the IMO*, **46:5**, 166–172.

Molau S., Crivello S., Goncalves R., Saraiva C., Stomeo E., Strunk J., and Kac J. (2018). “Results of the IMO Video Meteor Network — January 2018”. *WGN, Journal of the IMO*, **46:6**, 205–209.

Rendtel J., Veljković K., Weiland T., Verbeeck C., and Knöfel A. (2019). “Perseids 2018 — Analysis of Global Visual Data”. *WGN, Journal of the IMO*, **47:X**, XX–XX.

Verbeeck C. (1997). “Calculating the sensitivity of a forward scatter setup for underdense shower meteors”. In Knöfel A. and Roggeman P., editors, *Proceedings of the International Meteor Conference*, Apeldoorn, The Netherlands, 19–22 September 1997. IMO, 122–132.

Verbeeck C., Lamy H., Calders S., Tétard C., and Martínez Picar A. (2017). “Overview of major shower observations 2016–2017 by the BRAMS network”. In Gyssens M., Pavlović D., and Rault J.-L., editors, *Proceedings of the International Meteor Conference*, Petnica, Serbia, 21–24 September 2017. IMO, 138–144.

The Radio Meteor Zoo: identifying meteor echoes using artificial intelligence

Stijn Calders¹, Stan Draulans², Toon Calders², Hervé Lamy¹

¹ BIRA-IASB

stijn.calders@aeronomie.be

²Universiteit Antwerpen

BRAMS (Belgian RAdio Meteor Stations) is a Belgian network using forward scatter radio techniques to detect and study meteoroids entering the Earth's atmosphere. It consists of one beacon and 26 identical receiving stations, and it generates a huge amount of data with thousands of meteor echoes detected every day. With such large amounts of data, it is impossible to process it all ourselves.

The automatic detection of meteor echoes in the BRAMS data has proven to be a difficult problem to solve. Therefore the BRAMS researchers, in collaboration with Zooniverse team, have launched a citizen science project called the Radio Meteor Zoo (RMZ) in August 2016.

Since the beginning of the RMZ, more than 8500 volunteers have identified thousands of meteors. Using this data set, a new way to set up an automatic detection algorithm is being explored: a convolutional neural network (CNN, a special class of deep neural networks designed to analyze images) has been trained to identify meteors in new spectrograms. During this talk we will present the CNN model and discuss how its performance is evaluated. We will also discuss how to improve this algorithm in the future.

In order to allow publication of the Proceedings in January, the handling editor imposed a strict deadline which could not be met by the authors of this paper. Hence, only the abstract is published here. It became clear later that other editors allowed more relaxed deadlines. A full paper about the subject will be submitted to WGN.

Calibration of the BRAMS interferometer

H. Lamy¹, M. Anciaux¹, S. Ravnier¹, A. Martínez Picar², S. Calders¹, A. Calegaro¹, C. Verbeeck²

¹ Royal Belgian Institute for Space Aeronomy, Avenue Circulaire 3,
1180 Brussels, Belgium

herve.lamy@aeronomie.be and michel.anciaux@aeronomie.be

² Royal Observatory of Belgium, Avenue Circulaire 3
1180 Brussels, Belgium

antonio.martinez@observatory.be

BRAMS is a Belgian network using forward scatter radio techniques to detect and study meteoroids entering the Earth's atmosphere. One of the 26 receiving stations is located in Humain and is a radio interferometer using phase difference measurements between five antennas to accurately retrieve the direction of arrival of a meteor echo.

The direction of arrival of a meteor echo is not known a priori and so the meteor echoes cannot be used to calibrate the interferometer, i.e. to check that the retrieved direction of arrival is consistent with the position of the source. In this paper, three methods to calibrate the interferometer are presented using 3 sources at known positions:

- 1) the signal from the BRAMS calibrator flying on a UAV in the far-field of the interferometer,
- 2) the signal reflected off an airplane whose position is known by decoding ADS-B signals recorded with a specific antenna and receiver,
- 3) meteor echoes corresponding to trajectories reconstructed from CAMS-BeNeLux optical observations for which the direction of the first Fresnel zone can be calculated.

Preliminary results are shown. Advantages and limitations of each method are highlighted.

1 Introduction

BRAMS (Belgian RAdio Meteor Stations) is a Belgian network using forward scatter radio techniques to detect and study meteoroids entering the Earth's atmosphere. One dedicated transmitter, located in the south of Belgium, transmits a pure sine wave at a frequency of 49.97 MHz ($\lambda \sim 6$ m) with a power of 150 watts. The transmitter is a crossed dipole antenna with a 8m \times 8m metallic grid which ensures that most of the power is emitted towards the zenith but with a wide radiation pattern in order to cover a large portion of the sky. The radio wave can then be reflected off the ionized trail formed along the meteoroid path and recorded by one or several of the 26 receiving stations spread all around Belgium. The recorded signal is usually called a meteor echo. 25 of the receiving stations are identical, using the same material provided by the Royal Belgian Institute for Space Aeronomy (BIRA-IASB). In particular, a 3-element Yagi antenna is used with the goal to cover a large portion of the sky since the signals reflected off the meteor trails can come from a wide range of directions.

One of the receiving stations located in Humain in the south-east of Belgium is a radio interferometer and can determine the direction of arrival of meteor echoes. It is made of five 3-element Yagi antennas placed along 2 orthogonal axes with the central antenna being common to both legs (Figure 1). The axes are roughly aligned along the North-South and East-West directions.

The phase difference between signals recorded at two antennas depends on the additional path the front wave



Figure 1 – Picture of the BRAMS radio interferometer in Humain. The five Yagi antennas are visible along the two orthogonal axes.

has to travel, which itself depends on the distance between the antennas and the angle of arrival. For each leg, the separations between the central antenna and the two other antennas are of 2.5λ and 2λ (Figure 2).

Following the classical work of (Jones et al., 1998), for each axis, the phase differences between the central antenna 0 and the other two antennas, 1 and 2, are combined to provide a very accurate ($\sim 1^\circ$) and unambiguous estimate of the projection of the angle of arrival of the meteor echo in the plane of the 3 antennas (see Figure 3). The process is repeated for each axis and the combination of the two results allows us to determine the elevation and azimuth angle of the meteor echo. More details about the interferometer, Jones method and an example of result can be found in (Lamy et al., 2017).

Since the direction of a meteor echo is not known a priori, a source at a known position has to be used in order to calibrate the radio interferometer, i.e. to check

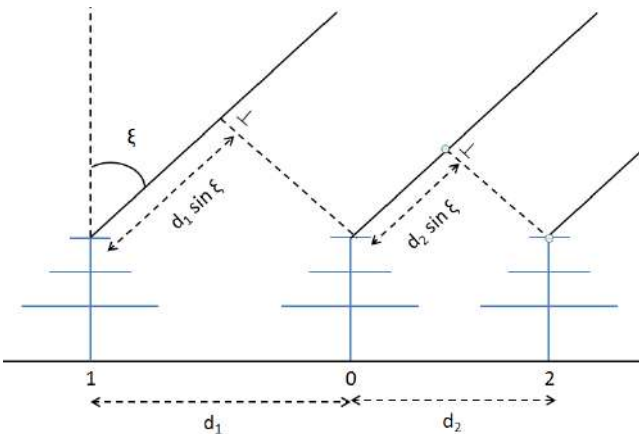


Figure 2 – A linear array of 3 antennas with the central antenna 0 being the phase reference. For the BRAMS interferometer, $d_1 = 2.5\lambda$ and $d_2 = 2\lambda$

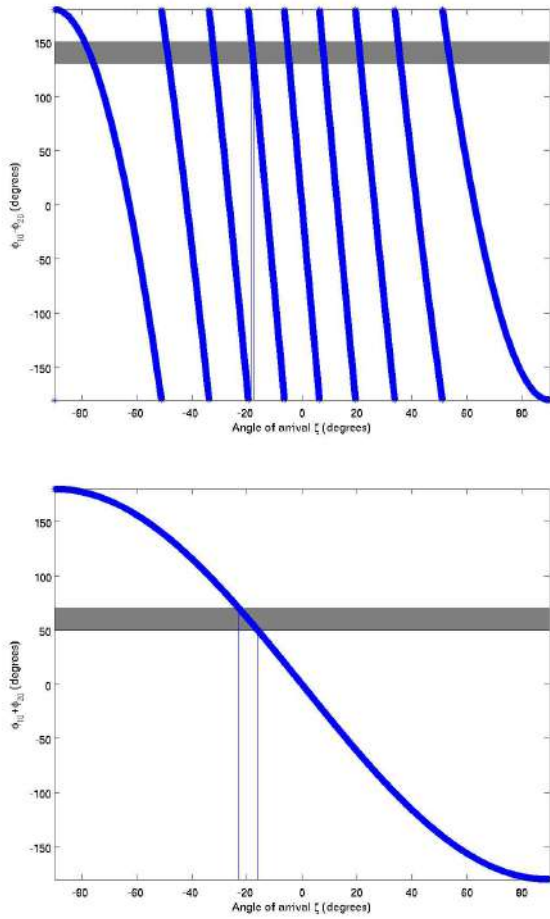


Figure 3 – Relationship between the sum and the difference of the phase differences, $\phi_{10} + \phi_{20}$ and $\phi_{10} - \phi_{20}$, as a function of the angle of arrival ζ . The gray shaded bands illustrate an uncertainty of $\pm 10^\circ$. The sum provides a single unambiguous solution for ζ but with a poor accuracy, while the difference provides 9 possible solutions with an accuracy of $\sim 1^\circ$. The combination of both graphs allows to select the correct accurate value for ζ .

that the retrieved direction of arrival of the signal is within approximately 1° of the position of the source. In this paper, we present preliminary results using signals from 3 sources:

1. the signal coming from a transmitter flying on a UAV,
2. the radio signal reflected off an airplane flying nearby the BRAMS transmitter,
3. a meteor echo corresponding to a meteoroid observed with the CAMS-BeNeLux optical network.

2 Calibration with the signal from a transmitter flying on a UAV

In 2016, the BRAMS calibrator (Lamy et al., 2015) connected to a simple dipole antenna was added as payload on a UAV (an OktoXL ARF-Mikrokopter, (Martínez Picar et al., 2015)). The BRAMS calibrator, designed at BIRA-IASB, emits a signal of known frequency and amplitude. The amplitude can be controlled by software with steps of 3dB and was chosen at a level ensuring no saturation of the receivers. The frequency was chosen to appear in a region of the receiver band where no meteor echo or reflection off the airplanes occurs. The internal frequency reference using a Temperature-controlled Crystal Oscillator ensures a frequency stability of a few Hz. The UAV was flying in the far-field of the interferometer which is the region located at a distance equal to or larger than $2D^2/\lambda$, where λ is the wavelength ($\sim 6\text{m}$) and D is the largest dimension of the interferometer ($= 4.5\lambda \sim 27\text{m}$). The far-field of the BRAMS interferometer is located at a distance of $\sim 243\text{ m}$ from the central antenna.

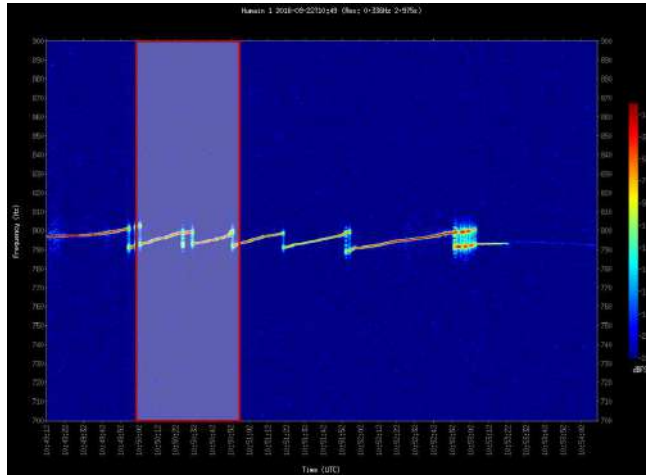


Figure 4 – Spectrogram recorded at one of the antennas of the BRAMS interferometer during the second flight of the UAV and showing the signal from the BRAMS calibrator. The UAV was stable during the time interval corresponding to the red rectangle.

Several flights with the UAV were carried out. The results of the second flight are presented here but the conclusions are similar for all the flights. The position of the drone was stable within a few meters at a distance of $\sim 400\text{ m}$ from the central antenna during approximately 50 seconds. The position of the UAV during the flight is given by at least 5 GPS satellites, and the height of the UAV is controlled by a barometric altimeter. The accuracy on the position is usually within a

meter. The signal from the BRAMS calibrator can be seen in the spectrogram shown in Figure 4. The stable part of the flight corresponds to the red rectangle.

Figure 5 shows the phase differences between the north, south, east and west antennas with the central one, computed for the frequency of the BRAMS calibrator signal with the highest signal-to-noise ratio in Figure 4. The stable part of the flight is again highlighted with the red rectangles.

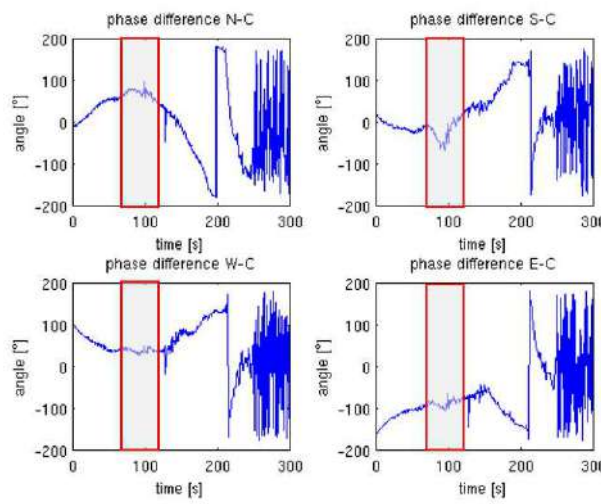


Figure 5 – Phase differences between north (top left), south (top right), east (bottom left), west (bottom right) antennas and the central one recorded during the second flight of the UAV. The stable part of the flight is highlighted.

Unfortunately, the direction of the drone could not be retrieved correctly when applying the Jones method to these data. The reasons are not yet fully understood but we list below several likely origins for this problem. First, the central antenna of the interferometer was tilted by 45° in azimuth compared to the other ones. Therefore its phase diagram is modified in a way that we did not take into account yet. Second, the position of the UAV in the horizontal plane was stable only to within a few meters in order to not empty the battery too quickly while fighting against the wind. This is a non-negligible part of the wavelength and therefore there might also be an uncertainty about selecting the correct solution. Finally, the phase diagram of the transmitter could also be affected by the fact that the UAV is not completely stable while fighting against the wind to stay in position and the transmitting antenna might be tilted in regard to its theoretical vertical orientation. The impact of these parameters must be studied in more detail. However, since flying the UAV proves to become more and more difficult (due e.g. to wind and weather conditions, regulations, etc.), this might not be the best solution to calibrate regularly the BRAMS interferometer.

3 Calibration with the radio signal reflected off an airplane

Reflections of the radio wave on airplanes flying nearby the BRAMS transmitter produce the typical long-lasting curves in BRAMS spectrograms that usually complicate the analysis of data (e.g. for automatic detection of meteor echoes or computation of meteor echo power profiles). However, in Humain, a bright signal coming from an airplane can be used for calibration of the interferometer. Indeed, the airplane location can be recorded using Automatic Dependent Surveillance – Broadcast (ADS-B) signals sent automatically and periodically by airplanes for traffic control. Among other information, airplanes send their positions determined via satellite navigation, their speed and their identification. ADS-B signals are sent at a frequency of 1.09 GHz and can be easily recorded using specific ADS-B antenna and receiver which can be purchased commercially.

On 15 April 2019, ADS-B signals were recorded in Uccle. These data were used to identify the airplane at the origin of the bright signal visible in the spectrogram recorded at Humain at 22:30 UT and shown in Figure 6. This spectrogram was selected because the reflection of the airplane is very bright and with no overlap with meteor echoes. In the following, the Jones method is applied to data during the ~ 40 seconds time interval corresponding to the yellow rectangle in Figure 6. During that time interval, the position of the plane (elevation and azimuth as seen from Humain) was computed using positions recorded in ADS-B signals.

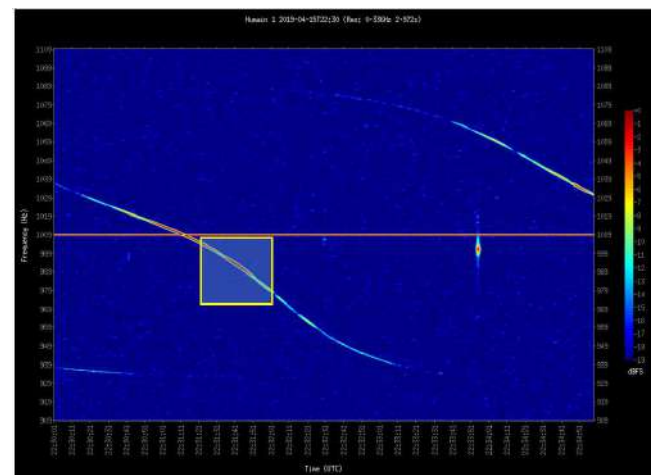


Figure 6 – Spectrogram obtained in Humain on 15 April 2019 at 22:30 UT. The yellow rectangle highlights the part of the airplane reflection that is used to retrieve the direction of the plane.

The phase differences between the various antennas are computed for each time interval at the frequency of the airplane reflection with the highest signal-to-noise ratio. The results are presented in Figure 7. The phase differences are extremely coherent with very small scatter. The sudden jumps correspond to a variation of 360° and are purely artificial.

In Figure 8, the elevation and azimuth of the plane, computed using Jones method, are compared to the

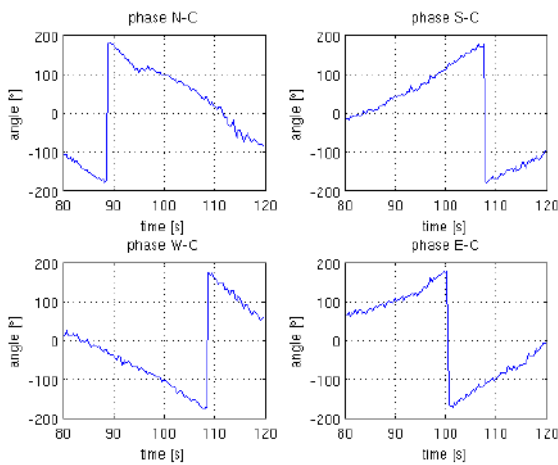


Figure 7 – Phase differences between North (top left), South (top right), West (bottom left), and the central antenna for the airplane reflection during the time interval corresponding to the yellow rectangle in Figure 6

ones calculated using the real position of the plane recorded with ADS-B signals. The two angles are more or less in the right directions, which gives confidence in the method. Nevertheless, the accuracy of the results using Jones method is still rather poor, with computed angles being only within $10 - 20^\circ$ of the correct ones. The sudden variations on the computed elevation and azimuth are due to changes of branches in Jones method related to uncertainties in the phase measurements (see Figure 3). They will be accounted for in a next version of the code.

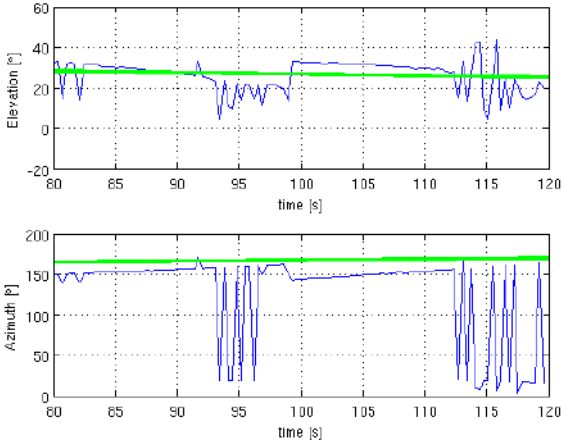


Figure 8 – Elevation and azimuth of the plane during the time interval corresponding to the yellow rectangle in Figure 6. The blue curves are obtained using Jones method applied to the signals recorded in Humain. The green lines are computed using positions of the plane sent with ADS-B signals.

4 Calibration using data from the CAMS-Benelux optical network

CAMS or Cameras for All Sky Meteor Surveillance is a project funded by NASA, coordinated by Peter Jenniskens (Jenniskens et al., 2010). The purpose of the

project is to validate the IAU Working List of Meteor Showers. CAMS uses small field of view optics covering the complete sky at around 90 km altitude. Each portion of the sky is covered by at least 2 cameras. The CAMS-BeNeLux network uses the same concept and is run mostly by amateurs (Roggemans et al., 2016). BIRA-IASB contributes to the network by providing images from 4 cameras located in Uccle, Dourbes and Humain.

CAMS provides very accurate trajectories of meteoroids in the Earth's atmosphere down to magnitude of $\sim +5$. When the trajectory of a given meteoroid is known, finding the location of the specular reflection point for the radio wave for a given configuration Transmitter-Receiver is a very straightforward analytical problem (Lamy & Tétard, 2016). The theoretical time of appearance of the meteor echo in the corresponding BRAMS data is the time when the meteoroid passes through the specular reflection point (see Figure 9). It can also be accurately computed using the speed measurement provided by the CAMS data and the begin time of the visual trajectory observed by the CAMS cameras.

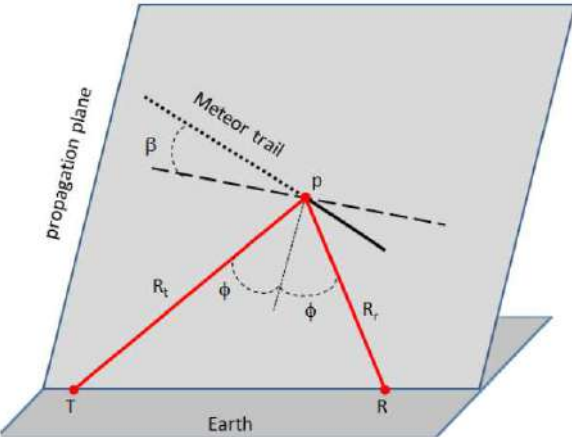


Figure 9 – Geometrical parameters of a radio forward scatter set-up

As an example, we consider a meteor detected by CAMS cameras on 4 October 2018 at around 23H44m43s UT. The spectrogram obtained at Humain from 23H40m to 23H45m is shown in Figure 10 and the corresponding meteor echo is surrounded by a red rectangle centered on the theoretical time of appearance. Note that the temporal resolution in the spectrogram is only of ~ 3 seconds since the Fourier transform is carried out on 16384 consecutive samples and the sampling frequency of the raw BRAMS data is of 5512 Hz. So this red rectangle is only an indication that a meteor echo occurs approximately at the correct expected time. To obtain a more accurate comparison, a study of the power profile in the raw data is needed but this is beyond the scope of this paper.

Since the position of the specular reflection point is known, the corresponding azimuth and elevation, as seen from Humain, can be computed. The Jones method was applied to the data corresponding to this meteor

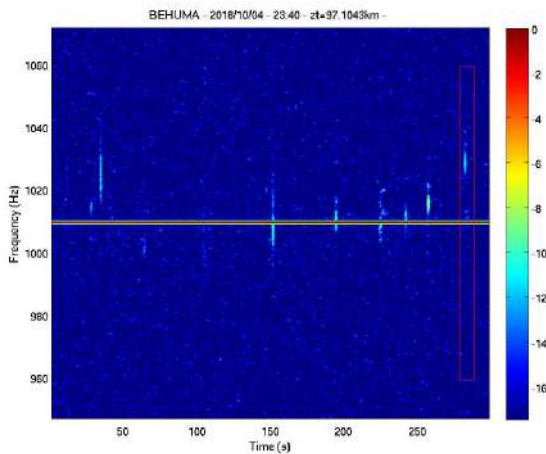


Figure 10 – Spectrogram obtained at the Humain station at 23H40 UT on 4 October 2018. The red rectangle is centered on the theoretical time of appearance for a meteor observed by CAMS cameras at around 23H44m43s.

echo and a direction of arrival was also obtained. In Figure 11, a comparison between the two methods is provided for both angles in a polar diagram. Again, the results are encouraging but not accurate enough. The elevation angles are within a few degrees of each other but the azimuth angles are separated by $\sim 15^\circ$.

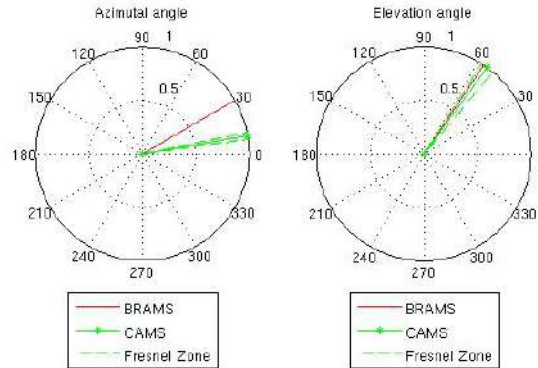


Figure 11 – Comparison between the direction (given as azimuth and elevation angles) of the specular reflection point along the CAMS trajectory as seen from Humain (green lines) and the direction of the specular reflection point as retrieved using BRAMS data from the interferometer (red lines). Also shown are the directions of the extremities of the first Fresnel zone (dotted green lines).

The meteor echo studied here is underdense with a duration of the order of 0.2 second. Therefore, since the Fourier transform is carried out on nearly 3 seconds, a contribution is expected not only from the specular reflection point itself but also from the entire so-called first Fresnel zone which is the region along the meteoroid path where the reflection of the radio wave adds up coherently to the main signal coming from the reflection point (Wislez, 2006). The length of the first Fresnel zone (see Figure 12) can be computed analytically and is equal to

$$FZ = \sqrt{\frac{\lambda R_T R_R}{(R_T + R_R)(1 - (\sin \phi)^2)(\cos \beta)^2}} \quad (1)$$

where λ is the wavelength (~ 6 m), R_T and R_R are the distances between the specular reflection point and respectively the transmitter and the receiver, ϕ is half the scattering angle, and β is the inclination of the meteoroid path with respect to the propagation plane of the wave (see Figure 9). The retrieved elevation using BRAMS data falls exactly within the size of the first Fresnel zone but there is still an offset of $\sim 20^\circ$ for the azimuth angle.

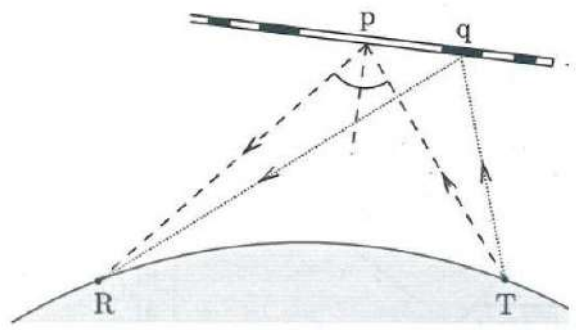


Figure 12 – Example illustrating the various Fresnel zones along a meteoroid path. The white zone centered on the specular reflection point p is the first Fresnel zone whose size is computed in Figure 11. Reflections from the dark zone called q are destructive with the main signal coming from p . Adapted from (Wislez, 2006).

5 Conclusions and additional remarks

In this article, we have proposed 3 methods to calibrate the BRAMS interferometer using signals coming from a source with a known position. The first one using the BRAMS calibrator as transmitter flying on a UAV did not provide good results. There are a number of issues to solve first before we can conclude anything about this method. The other two methods (using reflection of the radio wave off an aircraft and using a meteor echo coming from a trajectory computed from CAMS-BeNeLux observations) give more promising results but are still far from being accurate enough. The whole procedure must be double-checked and possible remaining systematic errors must be identified and taken into account. These preliminary results are nevertheless encouraging. The last 2 methods have the advantage that they can be used regularly to calibrate the BRAMS interferometer, while the method using the UAV is more complex to set-up.

Acknowledgements and disclaimer

The BRAMS network is a project of the Royal Belgian Institute for Space Aeronomy (BIRA-IASB) and funded by the Solar-Terrestrial Center of Excellence (STCE).

The authors would like to thank Ms. Léa Plancquart, student from the University of Brussels, who helped developing the MATLAB codes during her internship at BIRA-IASB during the summer of 2019, and Mr. Justin Botton, student from EPHEC Louvain-La-Neuve, who helped developing the acquisition software of ADS-B signals during his internship at BIRA-IASB in spring 2019.

Finally the authors would like to thank Mr. Carl Johannink, who kindly provided us with the CAMS data.

References

Jenniskens P., Gural P., Dynneson C., Grisgby B., Newman K., Borden M., Koop M., and Holman D. (2010). “Cams: Cameras for allsky meteor surveillance to establish minor meteor showers”. **33**, 55–65.

Jones J., Webster A., and Hocking W. (1998). “An improved interferometer design for use with meteor radars”. *Radio Science*, **33**, 55–65.

Lamy H., Anciaux M., Ravnier S., Calders S., Gamby E., Martínez Picar A., and Verbeeck C. (2015). “Recent advances in the brams network”. In Rault J.-L. and Roggemans P., editors, *Proceedings of the International Meteor Conference*, Mistelbach, Austria, 27–30 August 2015. IMO, pages 171–175.

Lamy H. and Tétard C. (2016). “Retrieving meteoroids trajectories using brams data: preliminary simulations”. In Roggemans A. and Roggemans P., editors, *Proceedings of the International Meteor Conference*, Egmond, the Netherlands, 2–5 June 2016. IMO, pages 143–147.

Lamy H., Tétard C., Anciaux M., Ravnier S., Martínez Picar A., Calders S., and Verbeeck C. (2017). “First observations with the brams radio interferometer”. In Gyssens M. and Rault J., editors, *Proceedings of the International Meteor Conference*, Petnica, Serbia, 15–18 September 2017. IMO, pages 19–21.

Martínez Picar A., Marqué C., Anciaux M., and Lamy H. (2015). “Directional pattern measurement of the brams beacon antenna system”. In Rault J.-L. and Roggemans P., editors, *Proceedings of the International Meteor Conference*, Mistelbach, Austria, 27–30 August 2015. IMO, pages 177–179.

Roggemans P., Johannink C., and Breukers M. (2016). “Status of the cams-benelux network”. In Roggemans A. and Roggemans P., editors, *Proceedings of the International Meteor Conference*, Egmond, the Netherlands, 2–5 June 2016. IMO, pages 254–260.

Wislez J.-M. (2006). “Meteor astronomy using a forward scatter set-up”. In Verbeeck C. and Wislez J.-M., editors, *Proceedings of the Radio Meteor School*, Oostmalle, Belgium, 10–14 September 2005. IMO, pages 85–107.

The BRAMS receiving station v2.0

Michel Anciaux¹, Hervé Lamy¹, Antonio Martínez Picar², Sylvain Ranzier¹, Stijn Calders¹, Antoine Calegaro¹, and Cis Verbeeck²

¹ Royal Belgian Institute for Space Aeronomy,
Bruxelles, Belgium

michel.anciaux@aeronomie.be and herve.lamy@aeronomie.be

² Royal Observatory of Belgium,
Bruxelles, Belgium
antonio.martinez@observatory.be

BRAMS is a Belgian network using forward scatter radio techniques to detect and study meteoroids entering the Earth's atmosphere. It consists of 26 identical receiving stations installed all over Belgium and one dedicated transmitter located in the south of Belgium. These receiving stations have been using analog commercial receivers, external sound cards as sampling device, and Spectrum Lab software to acquire the data. Since those receivers are not produced anymore and have suffered from failures due to aging at many different sites, the BRAMS team has decided to develop a new receiving station using a digital receiver, single-board computer, and in-house developed software. In this work, the new system will be presented and its performance will be compared to the performance of the analog system.

1 Introduction

The Belgian RAdio Meteor Stations (BRAMS) is a point-to-multipoint network with currently 26 radio receiving stations spread all over Belgium recording — under a fairly continuous regime — reflections from meteor trails of a signal generated by a dedicated transmitter located at Dourbes Geophysical Centre, which emits a pure sine wave at a frequency of 49.97 MHz with a constant power of 150 W (Lamy et al., 2011). The physical principle, known as radio forward scattering, states that the ionization trail produced by a meteoroid entering the Earth's atmosphere (meteor) can reflect a radio wave. Any receiver tuned to the transmitter's frequency, in principle, is capable of detecting that signal, also known as meteor echo. In forward scattering the transmitter and receiver are not located in the same place (McKinley, 1961).

Recently, many stations in the BRAMS network have experienced problems with their analog receiver. Until now, all failed units could be either repaired or replaced but this is not sustainable. A new type of receiver must now be chosen. A first candidate based on a software-defined radio (SDR) has been evaluated and its suitability will be presented here.

2 Current receiving stations

Most of the stations are basic receiving systems consisting of a single antenna (3-element Yagi), an analog receiver (ICOM IC-R75), an amplitude and frequency calibrator (developed at the Royal Belgian Institute of Space Aeronomy, BISA), a GPS clock, a sound card (a two-channel audio sampler) and a Windows-based PC running *Spectrum Lab*¹ software (Calders & Lamy,

2012). Figure 1 shows a diagram of the current BRAMS basic receiving station.

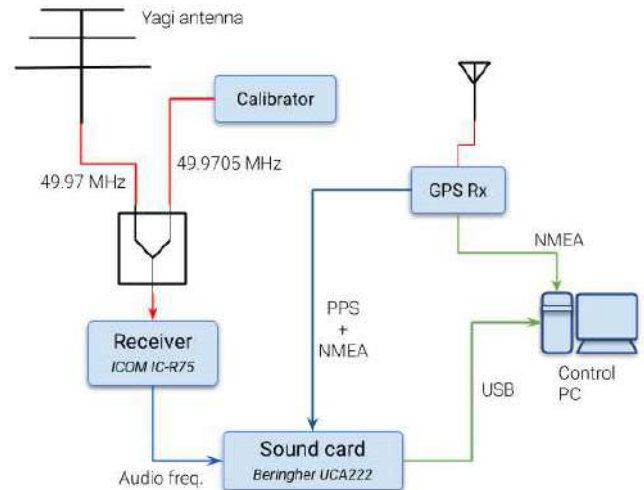


Figure 1 – Diagram of the components of the current BRAMS basic receiving station.

Most of the receivers have been operating continuously for several years. Many have already failed, some could be repaired because most of the failures have been of the same type (leading to a sharp drop in sensitivity), but new types of degradation have already been observed.

The IC-R75 is no longer produced, and alternative analog models are considerably more expensive. On the other hand, the market trend is that analog receivers are being replaced by software-defined radios (SDR).

In addition to those reliability and availability issues, there are also performance limitations with the current receivers:

¹<http://www.qsl.net/dl4yhf/spectral.html>.

- Limited dynamic range of 36 dB (see Table 1), which makes it impossible to observe weak and strong echoes simultaneously, and renders the system prone to desensitizing by strong interference.
- Sensitivity: noise temperature of about 1000 K
- Frequency instability, visible as a drift of the beacon in the data – the Local Oscillator (LO) is strongly dependent on temperature and cannot be locked to a reference.

A new type of receiver is needed in order to replace the IC-R75 and improve upon its performance, while keeping the cost low.

3 A new receiving station

After consideration of different alternatives, replacing the receiver and the data acquisition system using a low cost commercial SDR front-end and linux-based computer was the option finally selected.

Receiver

Several commercial SDRs were studied and tested. Finally, the SDRplay RSP2 proved to be the most suitable receiver to replace the IC-R75. The cost of this SDR, at the time of writing, lies around a few hundred euros, making it conveniently affordable. The unit has two $50\ \Omega$ SMA selectable inputs (plus an additional High-Z input). It delivers a 16-bit data stream from I and Q base-band signals through a USB port. Additionally, the RSP2 accepts an external frequency reference signal that can be used for LO stabilization.

The RSP2 performance has yet to be fully evaluated, but since the FUNcube Dongle Pro+ (FCDPP) – which was one of the SDR’s considered during the new receiver selection process – and the RSP2 have nearly the same analog front-end, it is reasonable to assume that they also share the same excellent performance that was measured on the FCDPP². Preliminary tests of the RSP2 at BISA have already shown very promising results.

Table 1 – Key performance features of IC-R75 and FCDPP receivers.

Parameter	Unit	IC-R75	FCDPP
Noise Temp.	K	≈ 1000	320
Dynamic Range	dB	36	61
P1dB ³	dBm	-102	-50
ENOB ⁴	–	6.0	14.3
Temp. Freq. Drift	Hz/ $^{\circ}$ C	10	0

²The FCDPP was eventually found unsuitable as it occasionally lost samples and had no input for an external frequency reference.

³The 1 dB compression point is the input power at which the actual gain deviates from the theoretical (linear) value by 1 dB.

⁴The effective number of bits is indicative of the dynamic range of the analog-to-digital conversion, taking the FFT processing gain into account.

Table 1 summarizes a comparison of key features of the original IC-R75 and the FCDPP receiver.

Control computer and software

A Raspberry Pi 3B+ (RPi) single-board computer was selected to control the RSP2, format and store the data. It has a *quad core ARM* processor running *Raspbian*, a free operating system based on Debian GNU/Linux optimized for the RPi hardware⁵.

In order to discipline the RPi clock, the Garmin GPS 18x LVS receiver currently installed on BRAMS basic receiving stations, is re-used. A dedicated electronic interface is employed to feed the NMEA frames and the 1-PPS signal to the RPi.

The data acquisition software has the following characteristics:

- Multi-threaded program written in C.
- Uses a proprietary application programming interface over USB.
- Decimates the data, resulting in a sampling rate of 6048 Sa/s. This is done to limit the total volume of data while remaining close to the 5512 Sa/s rate currently in use by the stations.
- Detects the upper side band (bandwidth: 2700 Hz).
- Saves the data in 300-second WAV files with time stamps (current BRAMS format).
- Network Time Protocol daemon (ntpd) configured to synchronise the system clock to the GPS signal.

Every 1008 samples a time stamp is created and stored with the data. Thus, in principle, the time of each sample is known.

Because of the non-synchronous nature of the operating system, the process that requests the time stamps will occasionally have to wait before being executed. This will result in scheduling jitter and offsets. This has indeed been observed in the raw data. Fortunately, the signal is sampled at a constant pace, *i.e.* without jitter, and the correct time can be retrieved by linear regression on sufficiently high number of time stamps (*e.g.* 300 seconds) in the post-processing stage.

The time-stamping method was tested using an RF continuous wave modulated by a one-pulse-per-second (PPS) signal from the GPS receiver during more than 15 hours (55913 pulses). After applying the time correction mentioned above, all the pulses occurred at the same decimal part of each second (Figure 2) and their envelopes overlaid neatly (Figure 3). The remaining time errors were then less than the sampling period (1/6048 s) or 166 μ s.

⁵<http://www.raspbian.org>

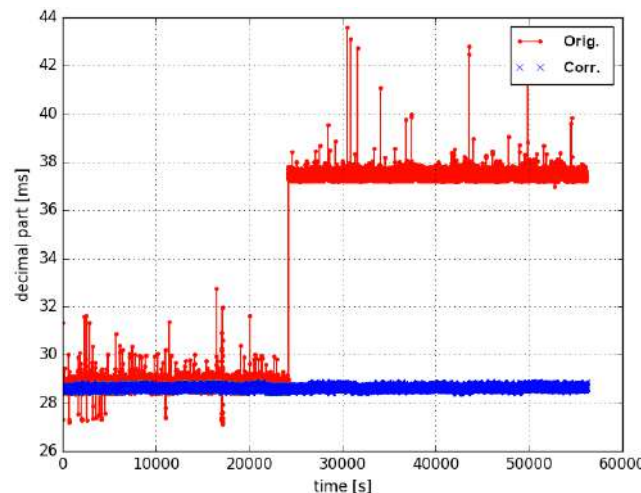


Figure 2 – Decimal part of the time stamp at trailing edge before and after correction.

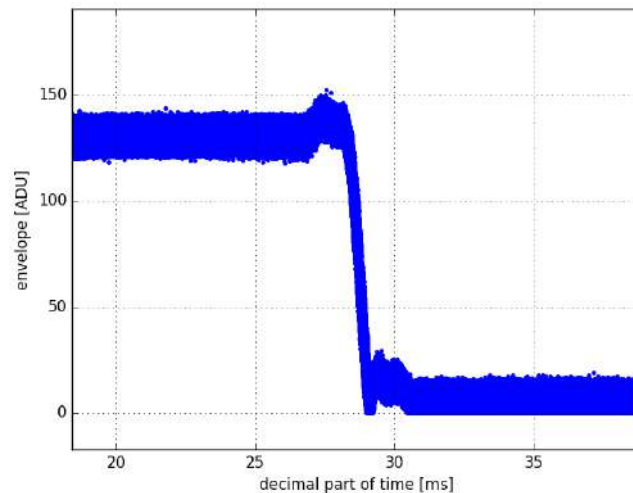


Figure 3 – 55913 overlaid trailing edges of 1-PPS after post-processing.

All stations that have internet access will be integrated in a *Hamashi VPN*⁶. They will be accessible remotely via ssh to allow remote upgrade and debugging.

Data transfer will be handled automatically via a http service.

4 First operational test

A simultaneous operational test on the original BRAMS station hardware and the proposed one (named v2.0 in this paper) was performed using the Uccle BRAMS station located in the premises of BISA facilities. An RF splitter was employed to input the incoming signals from the antenna+calibrator into each receiving system. Figure 4 shows a view of the cabinet with the setup of the test.

After weeks of registering observations, the resulting spectrograms allow to compare the performance of both systems working in parallel. Figure 5 shows the spectrograms of the same events recorded by each system. The

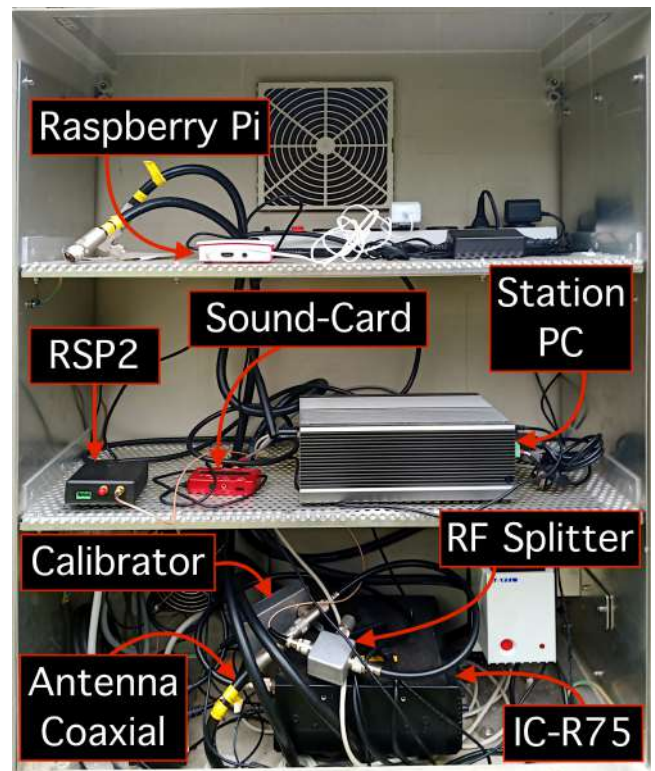


Figure 4 – View of the cabinet of the BRAMS station in Uccle during the tests.

similarity of the images demonstrates that the v2.0 station registers adequately the typical RF signals received by the BRAMS original receiving station, *i.e.* airplanes reflections, meteor echoes, and the fixed-frequency signal from the BRAMS beacon (Verbeeck, 2014). A lower noise floor is also easily noticeable in the v2.0, which shows less *snow-effect* on the background of the spectrogram.

5 Discussion

Our tests have proven the proposed replacement hardware for the BRAMS basic receiving stations to be an efficient and economically viable solution, more than suitable for the purpose of the project.

The better overall front-end performance and the adequate handling of data are promising indicators for a renewed basic BRAMS receiving station.

Some more testing is needed in order to fine-tune all aspects involved in the operation of the network. One extra physical feature which is being considered is to assemble all the replacement hardware in a single box, offering just the connectors to the different needed cables.

It is expected that the roll-out of the BRAMS receiving station v2.0 would start in 2020, and taking into account that the most time consuming part of the stations is already installed (antenna, GPS receiver, and its respective cabling), replacing the receiver and data acquisition system must be an easy operation which should not require too much effort nor time.

⁶<https://www.vpn.net>

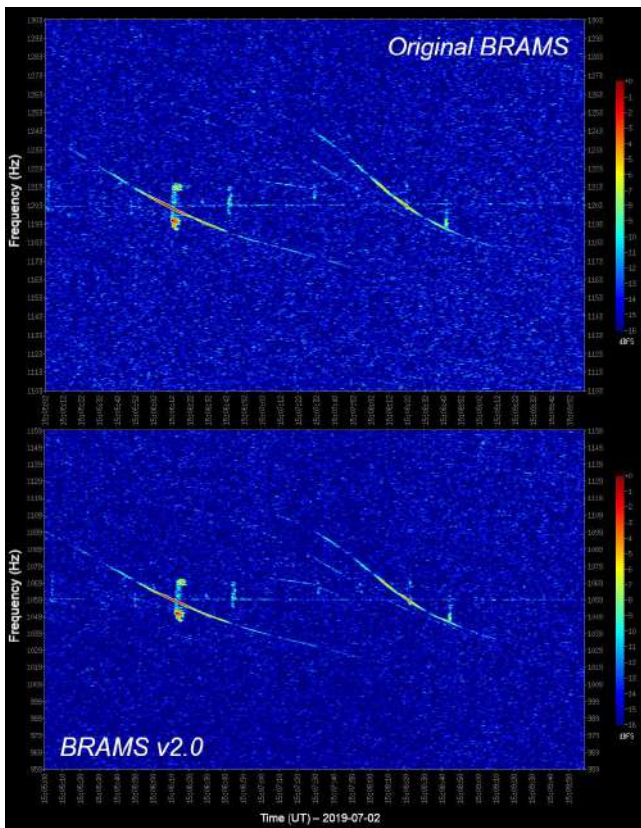


Figure 5 – Spectrograms from the same period of time obtained with the original BRAMS receiving configuration (top) and the proposed renewed one (below).

Acknowledgement

BRAMS is a project funded by the Solar-Terrestrial Centre of Excellence (STCE).

References

- Calders S. and Lamy H. (2012). “BRAMS: status of the network and preliminary results”. In Gyssens M. and Roggemans P., editors, *Proceedings of the International Meteor Conference*, Sibiu, 15–18 September 2011. IMO, pages 73–76.
- Lamy H., Ranvier S., de Keyser J., Calders S., Gamby E., and Verbeeck C. (2011). “BRAMS: the Belgian RAdio Meteor Stations”. In Cooke W. J., Moser D. E., Hardin B. F., and Janches D., editors, *Meteoroids: The Smallest Solar System Bodies*. pages 351–356.
- McKinley D. W. R. (1961). *Meteor science and engineering*. New York, McGraw-Hill.
- Verbeeck C. (2014). “An introduction to radio meteor astronomy”. In Gyssens M., Roggemans P., and Zoladek P., editors, *Proceedings of the International Meteor Conference*, Poznan, Poland, 22–25 August 2013. pages 57–69.

Mass determination of the iron meteoroids

David Čapek, Pavel Koten, Jiří Borovička, Vlastimil Vojáček, Pavel Spurný, and Rostislav Štork

Astronomical Institute of CAS, Ondřejov, Czech Republic

capek@asu.cas.cz

The initial mass of a meteoroid can be estimated from the video observations by two usual ways. If the meteor shows deceleration, the dynamical mass can be determined. The light curve together with knowledge of luminous coefficient allows determining the photometric mass. In case of small iron meteoroids there is one more way. The beginning height corresponds to reaching the melting temperature on the meteoroid's surface. These bodies are almost isothermal due to high heat conductivity of the iron and the beginning height simply depends on zenith angle of radiant, initial velocity, and initial mass. This method is however limited to smaller meteoroid sizes. We present the results from numerical modelling and simplified analytical theory.

1 Introduction

Borovička et al. (2005) described a population of meteors with only iron lines in their spectra. Most of these bodies have unusual light curves with rapid increase of brightness, low beginning heights, and low velocities. They have “asteroidal” orbits and they do not belong to any meteor stream. Campbell-Brown (2015) proved this population and found that they produce $\sim 3\%$ of meteors brighter than +3 mag and $\sim 6\%$ of fainter meteors (+6 mag to +3 mag maximum brightness range).

Čapek et al. (2019) considered that these meteors are produced by iron meteoroids, and fast removal of liquid iron as small droplets from the surface is a dominant ablation process. With these assumptions, they developed a model, which is able to explain most of the observed light curves of iron meteors.

2 Beginning height of iron meteors

The determination of the mass of iron meteoroids is a side product of the modelling the light curves and ablation of small iron meteoroids (Čapek et al., 2019). The basic principle of this method can be described on the following toy model.

The surface temperature of a meteoroid rises due to collisions with the atmospheric molecules. The ablation starts when it reaches the melting point of iron ($T_F = 1811$ K). The liquid iron is spraying off from the surface in small droplets, which quickly evaporate. The meteor becomes visible and corresponding altitude is the theoretical beginning height h_{beg} . (However, the actually observed beginning height depends on the observation instrument used.) If the meteoroid is sufficiently small and if it has sufficiently high thermal conductivity, then the whole volume of the meteoroid is almost isothermal. In this case, the energy E_h , which is necessary for the heating from the equilibrium temperature ($T_{eq} \approx 272$ K) to the melting temperature of iron is simply

$$E_h = mc(T_F - T_{eq}), \quad (1)$$

where c is the heat capacity and m is the meteoroid's mass. The energy received by the meteoroid due to

collisions with atmospheric molecules can be expressed as

$$E_{atm} = \frac{\Lambda}{2 \cos z} \int_{h=\infty}^{h_{beg}} \rho_{atm}(h) v^2 dh, \quad (2)$$

where Λ is the heat-transfer coefficient, S is meteoroid's cross section, and z is zenith distance of radiant. The atmospheric density ρ_{atm} exponentially decreases with altitude h . If we neglect radiative losses, then (1) and (2) lead to the following expression:

$$m = A \frac{v^6}{(\cos z)^3} \exp(-Bh_{beg}). \quad (3)$$

Therefore, the initial meteoroid mass depends on initial velocity, zenith angle of radiant and beginning height. (Constants A and B depend on shape and material properties of meteoroid, parameters describing the atmospheric density and heat-transfer coefficient.)

We developed more sophisticated model, which considers fast and random rotation of spherical iron meteoroid, free molecular flight regime, and the dependence of thermo-physical parameters on temperature. The model takes the radiative losses into account and the heat diffusion problem is solved numerically. The beginning of the ablation corresponds to reaching of the melting temperature on the surface of meteoroid. An example of the resulting dependence of initial mass on beginning height for zenith angle of 45° for four values of initial velocity can be seen in Figure 1. Here the solid curves correspond to numerical results. For lower mass, these curves can be approximated by exponential function according to (3):

$$\frac{m}{g} \cong 2 \times 10^{10} \left(\frac{v}{km/s} \right)^6 \frac{1}{(\cos z)^3} \exp \left(-0.534 \frac{h_{beg}}{km} \right) \quad (4)$$

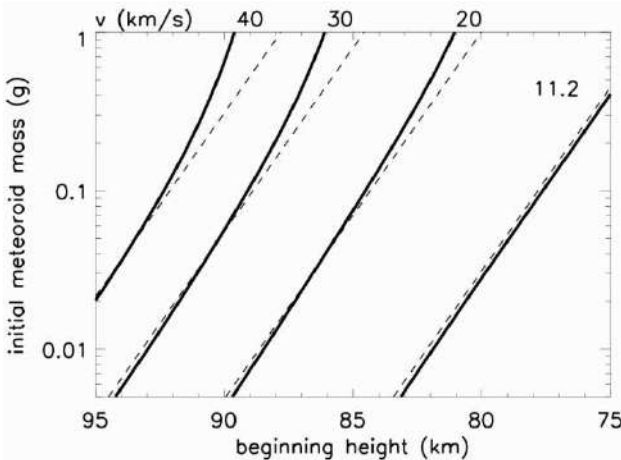


Figure 1 – Initial meteoroid mass as a function of beginning height for zenith angle of 45° and velocities 11.2, 20, 30, and 40 km/s. The solid curves correspond to numerical results and the dashed ones correspond to simplified analytical model.

3 Discussion

Equation (4) can be used for rough estimate of the initial mass of iron meteoroids. The masses of chondritic meteoroids cannot be determined this way due to their much lower thermal conductivity. Our results are reliable only for fainter iron meteors; beginning heights of larger bodies may be strongly affected by their shapes and spin states. Also the assumption of free molecular flow regime may not be fulfilled. Moreover, there is only weak dependence of beginning height on initial mass for larger bodies, which causes that small error in determination of beginning height leads to huge error in the estimated mass.

Acknowledgement

This work was supported by GACR grant 16-00761S.

References

- Borovička, J., Koten, P., Spurný, P., Boček, J., Štork, R. (2005). “A survey of meteor spectra and orbits: evidence for three populations of Na-free meteoroids”. *Icarus*, **174**, 15
- Campbell-Brown, M. (2015). “A population of small refractory meteoroids in asteroidal orbits”. *Planet. Space Sci.*, **118**, 8
- Čapek, D. Koten, P., Borovička, J., Vojáček, V., Spurný, P., Štork, R. (2019). “Small iron meteoroids. Observation and modelling of meteor light curves”. *Astronomy & Astrophysics*, **625**, A106

The study of meteoroid parameters with multi-techniques data

**Anna Kartashova¹, Yury Rybnov², Olga Popova², Dmitry Glazachev²,
Galina Bolgova¹, Vladimir Efremov²**

¹Institute of Astronomy of the Russian Academy of Sciences, Moscow, Russia

akartashova@inasan.ru

²Institute of Dynamics of Geospheres Russian Academy of Sciences, Moscow, Russia

Meteoroids are the source of information about the origins of our Solar System. They are among the most difficult objects to observe in the Solar system (we do not know in advance neither area on the celestial sphere, nor the time when the event occurs. Besides, a meteor flash in the atmosphere has duration few seconds or less.). The interaction of meteor particles with the atmosphere produces optical (actually meteors) and infrasound emissions. The meteor properties (mass, size, density etc.) are estimated based on the various observational data under different assumptions. The details of meteor-atmosphere interaction are poorly known, the parameters of meteor particles are determined with large uncertainty. Simultaneous registration of meteors by different techniques provides possibility to refine both the meteor parameters and models of particle interactions with the atmosphere. The goal of simultaneous observations is to decrease uncertainty in the meteoroid masses and study the formation and propagation of pressure pulses which are formed due to the interaction of meteoroids with the atmosphere.

The multi-technique (optical and acoustical) observations are carried out in the Institute of Astronomy RAS and Institute of Dynamics of Geospheres RAS from 2016 to the present time. The optical observations are carried out at three stations: Zvenigorod observatory of the Institute of Astronomy RAS (ZO INASAN), Geophysical observatory Mikhnevo of the Institute of Dynamics of Geospheres RAS (GPhO Mikhnevo) and the "Istra" station. Simultaneously with the optical observations the pressure variations are recorded at the ZO INASAN, GPhO Mikhnevo and IDG RAS in Moscow. The example of acoustic signals is shown in *Figure 1*.

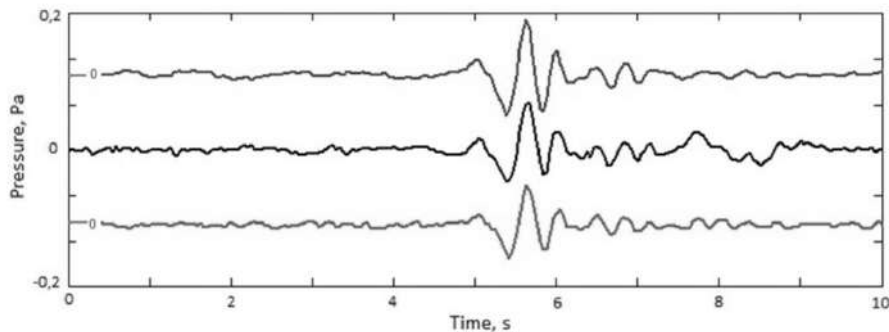


Figure 1. - Acoustic signal of the meteor 22.07.2017, 20:55:50. Signals recorded by 3 sensors are shown. Shown waveforms are filtered in the frequency range of 0.1-10 Hz.

As a result, few meteors were detected by both methods, and the meteoroid mass was estimated by various approaches. An example of the meteoroid mass estimates for two meteors are shown in the *Table 1*. The references given correspond to the papers from which appropriate assessment methodology were taken (Kartashova et al, 2017; Silber et al, 2014; Silber et al, 2015; Jacchia et al, 1967; Verniani, 1965; Jenniskens, 2006). The optical estimates are based on absolute magnitude, the acoustical estimates are based on signal frequency and amplitude. Two different models were applied to the meteors (Efremov et al, 2018).

Table 1. - The mass estimations by optic- acoustic method and the modelling data

№	ACOUSTIC		OPTIC			MODELLING	
	Mass range, g (Kartashova et al, 2017)	Mass, g (Silber et al, 2014; 2015)	Mass, g (Jacchia et al, 1967)	Mass, g (Verniani, 1965)	Mass, g (Jenniskens, 2006)	Mass, g Model 1 (Efremov et al, 2018)	Mass, g Model 2 (Efremov et al, 2018)
1	2.3-4.4	1	0.42	0.73	1.14	0.033	0.0218
2	1.1-3.3	2.7	0.40	0.68	1.06	0.15	0.0690

Comparison of meteoroid characteristics (*Table 1*) demonstrates a significant spread of values of masses (up to two orders of magnitude). The investigations will be continued and applied methods will be tested at increased number of meteors.

Acknowledgement

We thank Dr. A. Bagrov for his help with the observations. AK was partially supported by the Program LP RAS № 19-270.

References

- Efremov V.V., Popova O.P., Glazachev D.O. and Kartashova A.P. (2018). "Determination of the meteor particles properties from observational data". *Dynamic processes in geospheres*, **10**, 150-156.
- Jacchia L., Verniani F. and Briggs R. E. (1967). "An Analysis of the Atmospheric Trajectories of 413 Precisely Reduced Photographic Meteors". *Smithsonian Contributions to Astrophysics*, **10**, 1-139.
- Jenniskens P. (2006). "Meteor Showers and their Parent Comets". Cambridge, UK: Cambridge University Press, 804.
- Kartashova A., Rybnov Yu., Glazachev D., Popova O., Bolgova G. (2017). "The study of meteor events by multi-techniques observations", *Proceedings of IV All-Russian conference with international participation "Trigger effects in geosystems"*, 483-488.
- Silber E. A., Brown P. G. (2014). "Optical Observations of Meteors Generating Infrasound – I: Acoustic Signal Identification and Phenomenology". *JASTP*, V. 119, pages 116-128.
- Silber E., Brown P., Krzeminski Z. (2015). "Optical observations of meteors generating infrasound – II Weak Shock Theory and Validation". *JGR*, V. 120, Issue 3, pages 413-428.
- Verniani F. (1965). "On the Luminous Efficiency of Meteors". *Smithsonian Contributions to Astrophysics*, **8**, 141.

Simulation of meteors by TC-LIBS: Advantages, limits and challenges

Martin Ferus,¹ Anna Křivková,^{1,2} Lukáš Petera,^{1,3} Vojtěch Laitl,¹ Libor Lenža,^{1,4} Jakub Koukal,⁴ Antonín Knížek,^{1,3} Jiří Srba,⁴ Nikola Schmidt,^{5,6} Petr Boháček,⁵ Svatopluk Civiš,¹ Miroslav Krůš,⁷ Jan Kubát,⁸ Lucie Paloušová,⁸ Elias Chatzitheodoridis,⁹ and Petr Kubelík¹

¹ J. Heyrovský Institute of Physical Chemistry, Czech Academy of Sciences, Dolejškova 3, CZ 18223, Prague 8, Czech Republic.

martin.ferus@jh-inst.cas.cz

² Faculty of Nuclear Sciences and Physical Engineering, Czech Technical University in Prague, Břehová 78/7, 115 19 Prague 1, Czech Republic.

³ Charles University in Prague, Faculty of Science, Department of Physical and Macromolecular Chemistry, Albertov 2030, CZ12840, Prague 2, Czech Republic.

⁴ Valašské Meziříčí Observatory, Vsetínská 78, CZ75701 Valašské Meziříčí, Czech Republic.

⁵ Charles University in Prague, Institute of political studies, Faculty of Social Sciences, U Kříže 8, 158 00, Praha 5, Czech Republic.

⁶ Institute of international relations Prague, Nerudova 3, 118 50 Praha 1, Czech Republic.

⁷ Institute of Plasma Physics, Czech Academy of Sciences, Za Slovankou 1782/3, 182 00 Prague 8, Czech Republic.

⁸ Crytur spol. s r.o., Na Lukách 2283, 511 01 Turnov, Czech Republic.

⁹ National Technical University of Athens, School of Mining and Metallurgical Engineering, 9 Heroon Polytechneiou str.; GR-15780 Zografou, Athens, Greece.

Important features in meteor spectra are usually interpreted by synthetic convolution of lines extracted from databases. However, we developed an entirely new approach in this field. Instead of the aforementioned one, experimental techniques based on ablation of real meteorite samples using a wide range of laser sources are exploited within our method. We performed several experiments in order to provide spectra of several molecular, radical and ion or molecular ion species that are likely to appear in meteor or cometary impact plasma. The spectra are recorded by a high-resolution laboratory Echelle spectrograph and, simultaneously, by a high-resolution Meteor Spectral Camera for real meteor observation. In this manner, we show that instead of theoretical spectra simulation, laboratory experiments can be used at least for the qualitative evaluation of the observational data and for the assignment of important spectral features in meteor emission spectra. We also investigate ablation spots for the future estimation of parameters of a high-power laser, which is used for remote LIBS applied in astronautics.

1 Introduction

The most remarkable advantage of comparative measurements using laser-induced breakdown spectroscopy (hereinafter just LIBS) lies in the applicability of this method to the real-time *in-situ* analysis of any sample of real meteorites without any preceding treatment, preparation, or isolation. Laser ablation plasma is generated in the laboratory under strictly defined conditions and the chemical elements are evaporated together with the whole matrix, mimicking the meteoroid or asteroid descent (Ferus et al., 2018a, 2019). These attributes put LIBS in line for a wide range of laboratory studies revealing physical and chemical effects during the atmospheric entry of an extra-terrestrial body, as well as its impact on a planetary surface (Ferus et al., 2015b).

More than 15 years ago, our laboratory enrolled in research that was mainly focused on the investigation of chemical consequences of early planetary bombardment during the post-accretion period after the dissolution of a

protoplanetary disc. During the formation of the Sun, a disc of material, which consisted mainly of gas and small dust particles, orbited the new-born star. Over a few tens of millions of years, particles from the disc collapsed and formed what today are the planets and asteroids of our Solar system. This process eventually led to frequent and massive impacts on the proto-Earth (Canup and Asphaug, 2001). The impact frequency slowly decreased over time, only to rise again during the Late Heavy Bombardment (LHB) about 4-3.85 Gyr ago (Koeberl, 2006). The LHB phenomenon has been explained by gravitational resonance interactions of Jupiter with Neptune and other gas giants (Tsiganis et al., 2005; Nesvorný and Morbidelli, 2012). This transient instability of the resonance ratios led to a change in Jupiter's orbit as well as the ejection of asteroids and comets from their previously stable orbits. The would-be observed effect on Earth was a 10-fold increase in the frequency of extraterrestrial body impacts relative to the frequency immediately before LHB (Morbidelli et al., 2012; Geiss and Rossi, 2013). This in effect meant 10^9 tons of

impacting material per year (Koeberl, 2006). Typical impact velocities are estimated to have increased from 9 km s⁻¹ to 21 km s⁻¹. Moreover, the gravitational cross-sections ratio of the Moon and the Earth is approximately 1:17, which means 17 impact basins should have been formed on the Earth per one lunar basin (Bottke et al., 2012). These lunar craters are still visible nowadays and their age and origin have been successfully ascribed to the LHB.

The impact frequency decreased again after the LHB period until 3.8 Gyr ago and since then it has not much fluctuated. Our investigations show that extra-terrestrial body impacts were a major source for mineral formation, of volatiles (i.e., water), and of energy for chemical transformations. This raises a question of the influence on the early Earth's environment, more specifically the decomposition or synthesis of prebiotically relevant compounds and early chemical evolution of our planet. To model such conditions as precisely as possible, the best currently available approach is to simulate the impact plasma, for a high-power laser source is especially suitable.

During the last two decades, our team demonstrated several experiments mostly focused on the chemical consequences of hypervelocity impacts on an atmosphere or their interaction with solid or liquid surfaces (Babankova et al., 2006). Most studies have so far been focused on the impact-induced synthesis of biomolecules (Šponer et al., 2016) such as canonical nucleobases (Ferus et al., 2012, 2014, 2015a, b, 2017c), sugars (Civiš et al., 2016b) and amino acids (Civiš et al., 2004) and on the transformations of atmospheric molecules on early terrestrial planets (Civiš et al., 2008), mainly on either formation or decay of prebiotic substances such as formamide (Ferus et al., 2011), isocyanic acid, (Ferus et al., 2018c), hydrogen cyanide (Ferus et al., 2017b), acetylene (Civiš et al., 2016a), methane, (Civiš et al., 2017) or carbon monoxide (Civiš et al., 2008; Ferus et al., 2009).

Apart from the chemical consequences of the impacts, another important topic is the investigation of physics and the spectroscopic parameters of atmospheric entry and impact (Madiedo et al., 2013), (Jenniskens, 2007). Indeed, the chemical composition of distant objects and events in the universe can only be determined using spectroscopic techniques. To understand the observed spectra, laboratory experiments must be performed to provide some comparable spectral features of individual systems under controlled physical conditions, chemical conditions and concentrations of individual atomic or molecular species, temperature, pressure, and electron density (Ferus et al., 2017a, 2018a, 2019).

In scope of such research, the understanding of the meteor spectra is crucial. Meteoroid source bodies, asteroids, are generally remnants from the materials that first formed the planetesimals and planets. Meteorites, on the contrary, are pieces of asteroids on Earth that allow us to measure many of the properties of their parent bodies

in detail. However, a fundamental problem exists in linking specific meteorites to their parent bodies (primary matter, asteroids, and comet nuclei). Moreover, most bodies are evaporated and disintegrated completely during their descent and their emission spectra measured using spectrographs are therefore the only record of their chemical composition. Only in the specific cases that the object is found as a meteorite and its spectrum has been recorded a detail spectroscopic study can lead to the full understanding of the meteor spectra, the composition of the parent body, its origin, its chemistry *etc.* The in-depth description and understanding of their behaviour in the atmosphere is therefore a challenging scientific problem whose studying is definitely rewarding. When a body enters the Earth's atmosphere, it is immediately surrounded by a meteor plasma and interacts with the highest layers of the Earth's atmosphere at very high speeds (up to tens of kilometres per second). Descent of a meteoroid through the atmosphere leads to rapid heating, surface ablation and parent body disintegration. The initial height of a meteoroid ablation (early stage of the light – visible – part of atmospheric trajectory) depends on the geocentric entry speed and the initial mass. For known major meteor showers with retrograde orbit (*e. g.* Leonids, Perseids, Orionids), and sporadic meteors with high geocentric velocity, the initial height of ordinary meteors varies between 120 km and 100 km. On the contrary, for meteor showers and sporadic meteors with low geocentric velocities (*e. g.* Phoenicids, Arietids, Drakonids), the initial height is lower and ranges between 90 and 80 km. In the case of showers with high geocentric speeds, *e. g.* Leonids or Orionids, some meteors occur at a very high initial height, which in rare cases can reach up to 150 km. The lowest point of meteoroid visible atmospheric trajectory (end of ablation process) depends, alongside with geocentric speed and initial mass, also on the zenithal angle of entry into the atmosphere. Meteors with low geocentric velocity and the mass in order of kg may have the visible path ending height between 30–50 km above the Earth's surface.

Meteoroids called Earth-grazers have a special trajectory. They enter the Earth's atmosphere at a very small angle and, in case of a suitable combination of low geocentric speed and initial mass in order of kilograms, the body fails to fully vaporize and continues along new heliocentric orbit with significantly different elements.

In previous studies where the LIBS method was used (Ferus et al., 2018a, 2019), we demonstrated that the emission intensity of a particular spectral line of a studied analyte depends not only on the physical parameters of the line and the quantity of the emitting element but also on the matrix where the analyte is embedded. This matrix dependency leads to the necessity of calibration curves or matrix-matched standards, which in some practical situations, including samples of meteorites, are simply unavailable. Ciucci et al., however, proposed a novel Calibration-Free Laser Induced Breakdown Spectroscopy (CF-LIBS) procedure to overcome the mentioned matrix effect (Ciucci et al., 1999). The CF-LIBS method is based

on a direct analysis of emission lines of an analyte together with the matrix, instead of looking at the matrix as an independent problem. Using this method, we analysed a wide range of chondrite meteorites and developed all the subsequent steps of data processing. Their results indicated that the calibration-free method was suitable for meteor analysis and we therefore subsequently exploited those procedures for the interpretation of two bright bolides - Perseid and Leonid - meteor spectra (Ferus et al., 2018a, 2019). Moreover, as mentioned above, we used the reference experimental spectra of meteorite ablation, laser induced breakdown (LIDB) in the air and glow discharge in the air for the data comparison.

In our previous studies (Ferus et al., 2018a, 2019), we demonstrated the calibration free analysis of a meteor spectrum and we created a catalogue of main meteor spectral features based on ablation experiments using terawatt-class laser (TC-LIBS). Regarding the works of other authors focused on laser-based laboratory studies related to astrophysics and astrochemistry, we should note publications by Hawkes (Hawkes et al., 2008) proposing that laboratory based laser ablation techniques can be used not only to study the size of the meteor luminous region, but also to predict spectral features, estimate the luminous efficiency factor, and assess the role of chemically differentiated thermal ablation of meteoroids. Furthermore, Milley (Milley et al., 2007), simulated meteor luminosity through laser ablation of meteorites and in 2017, Ebert (Ebert et al., 2017) simulated the virtually instantaneous melting of target rocks during meteorite impacts. Alongside with these studies, the simulated space weathering together with the deflection of asteroids by lasers remains the most studied research topic connected with application of lasers in this field. Deflection of asteroids and comets by lasers was proposed by Park and Mazanek (2003), and recently, Aristova et al. (2018) studied impact physics of nuclear explosion on hazardous asteroids. Moroz et al. (1996) simulated the optical effects of impact melting and repeated crystallization on asteroidal surfaces using laser ablation and Kurahashi et al. (2002) conducted laser ablation laboratory simulation of space weathering focused on the source of difference between reflectance spectra of ordinary chondrites and their parent bodies: S-type asteroids. Loeffler et al. (2008) studied the effect of redeposition of impact-ejecta on mineral surfaces using laser ablation.

2 Experimental Part

Complex spectra within the entire UV/VIS-range have been recorded by the High-Resolution Echelle Spectra Analyzer ESA 4000 (LLA Instruments GmbH, Germany). The optical analyser unit enables spatial and temporal resolved image of lowest spectral intensities. The resolution is a few pm in the range 200–780 nm with resolution of 0.005 nm (200 nm) to 0.019 nm (780 nm). Simultaneously, the spectra have been recorded for direct calibration by a common astronomical spectroscopic

camera, directly employed in observation of real meteors for comparative measurements. We have used the high-resolution PointGrey Grasshopper3 GS3-U3-32S4M-C camera with high quantum efficiency (QE= 76%, 525 nm), dynamical range (71.34 dB) utilising the CMOS Sony Pregius chip with resolution of 2048×1536 px, and a grating of 1000 lines/mm that allows a resolution of 0.48 nm/px. The spectral intensity recorded by the instrument is calibrated using the following approaches that are usually applied by our team: calibration to standard sources (deuterium lamp, tungsten source) and calibration using the standard spectra of Venus. Wavelength calibration is achieved using high resolution data and standard wavelengths from calibration sources (deuterium lamp). For spectroscopic studies of meteors, we also use an older system based on spectrographic cameras equipped with QHY5LII-M hardware, with a 1280×960 px CMOS chip and an Tamron objective (f/1.00; F/3–8 mm) using a 1000 lines/mm grating, which allows a resolution of up to 0.97 nm/px. In our measurements, for every sample of meteorite, the Echelle spectrograph was set to trigger 1 μ s after the laser pulse with the gate open for 2 μ s for a total accumulation of 1 signal after 1 large laser shot. The PALS laser has a repetition rate of 30 minutes, necessary time to cool down the system. An additional low-resolution observational spectrograph opened its gate for 1 s, after being triggered by the laser system.

The plasma shock wave induced by the impact of a meteoroid was simulated using the high-power laser PALS (Prague Asterix Laser System). The laser beam was focused on the sample—which has been placed in the interaction chamber—by a plano-convex lens with a diameter of 20 cm and a focal length of 50 cm. The ablation of the meteorite's surface has been done with a single laser pulse with energy of 600 J (time interval about 400 ps, wavelength of 1.315 μ m). All manifestations connected with creation of high-energy plasma fireball take place: temperature rising to several thousand of K, shock expansions of plasma ejected from the surface, and emission of secondary hard radiation (UV–VUV, XUV, X-Ray). All the experiments have been performed under a pressure of 2 mbar, corresponding to altitudes typical for the beginning of the meteoroid body ablation in the atmosphere (i.e., above 110 km).

The meteoroid plasma was also simulated in our laboratory via the laser ablation of meteorite samples using a Lambda Physik (ArF) excimer laser. The laser emits ~10-ns pulses with a wavelength of 193 nm and an energy of 200 mJ. The laser beam has been focused using a calcium fluoride lens (focal length of 50 mm) onto a solid target (sample of meteorite) attached to an XYZ rotation stage. In a similar manner, the irradiation has been also performed using a Nd:YAG laser (6 ns, 1064 nm, 450 mJ) and a femtosecond Ti:SAF laser (50 fs, 810 nm, 1 mJ). The rotation system with the holder of the particular meteorite sample was placed in a vacuum interaction chamber, equipped with a collimator that was

connected similarly to the arrangement of the terawatt PALS laser, in a setup with the high-resolution Echelle Spectrograph (ESA 4000, LLA Instruments GmbH, Germany). The low-resolution spectrum was simultaneously measured using an astronomical spectrograph.

To visualise the ablation spots on the samples we used the electron microscope located at the School of Mining and Metallurgical Engineering of the National Technical University of Athens, Greece. This is a JEOL 6380LV electron microscope equipped with an EDS chemical analysis system from Oxford Instruments. The backscattered topography-composition imaging mode was used to reveal both chemical and topographical information. All analyses have been performed in a vacuum of about 30 Pa (Low-Vacuum mode) to preclude from surface charging and to avoid chemical modifications of the surface by coating with conducting metals usually employed in electron microscopy to avoid charge accumulation on the surface of the samples.

3 Results and Discussion

In order to validate this approach, there are several points to be considered. Firstly, a significant parameter for studying the plasma during atmospheric entry is its temperature. The meteor plasma temperature is more or less a rigid parameter and reaches approximately the 5000 K. The temperature exhibits only a slight dependence on the impact velocity or mass of the infalling object. The temperature range is usually 4000 – 5800 K. The laser impact plasma, on the other hand, has a different time-evolution than the infalling object plasma. Directly after the sub-nanosecond pulse of the laser, its energy is transformed into simulated atmospheric entry or impact plasma. A tiny spot at the impact site with large energy density produces extremely charged ions and temperatures of about 7 eV, *i. e.* up to 100 000 K. This ‘ignition stage’ is however very limited in time scale and we therefore do not expect any chemically-relevant behaviour. Also, this stage of the plasma development is not spectroscopically observable due to continuum emission from the system. Two microseconds after the laser pulse, characteristic emission of atomic lines with temperature estimated in previous works of Babanková to be about 4500 K arises in the case of gas phase experiments. According to our chemical models, this is related to ignition of radical reactions and decomposition of the present chemical compounds. (Civiš et al., 2016a).

Under the collision conditions, the excited states usually decay faster than may be predicted by the transition dipole moments. Conversely, in collisional excitations and during the related energy transfer, several short living atomic states can exhibit longer emission. During the afterglow, it is assumed that the Boltzmann distribution among excited states is maintained. Finally, according to chemical models, some background chemical and physical processes may also occur among reactive species on milliseconds timescales. Apart from the ignition state the laser impact plasma therefore is a valid model of the

impact plasma of an extra-terrestrial body in the sense of temperature. Other parameters, such as the species number density (concentration), are indeed easily adjustable during the experimental procedure.

Surprisingly, a different behaviour is exhibited by plasma formed after ablation of solid targets. Our measurements reveal that laser-induced breakdown of meteorite surfaces exhibit temperatures about 10 000 K for TC-LISB but only about 6000 K for excimer lasers. This is closely related to the behaviour of frontal shockwave created in front of descending meteoroid body. Based on our measurements, typical values of electron densities estimated for laser induced plasma on meteorite surfaces are in order of 10^{16} cm^{-3} decreasing during microseconds after the laser initiation. Real meteor trails are estimated to exhibit electron densities ranging from 10^{12} to 10^{14} cm^{-3} (Ferus et al., 2018b) and references therein), however, in the frontal shock wave exhibiting very high temperatures, the situation can be different.

In our recent paper (Ferus et al., 2019), we have highlighted a major advantage of laser experiments under laboratory-controlled conditions for the production of precise tables of main spectral features observed in meteor spectra. Meteor plasma is formed after an evaporation of a very complex matrix – rocks and minerals embedded in the meteoroid or asteroid body. Only precise experiments can indeed show the major coincidences of spectral lines, positions of spectral features formed as result of particular lines and the convolution the observed spectrum. The peak maximum of an individual spectral feature can be different for a particular composition of the matrix and also for different temperatures. Hence, the common procedure of spectral lines (or rather spectral features) assignment in meteor spectra and the calibration of meteor camera cannot be precise if only theoretical tables are taken into account. Instead, we strongly propose that the spectral lines be assigned using the data provided in our recent study for ablation experiments of real meteorite samples.

Example meteor spectra compared with experimental TC-LIBS and standard laboratory LIBS spectrum recorded for a chondrite sample are depicted in Figure 1 (next page). Panel A shows the spectra of two examples of Leonid meteor shower (2016), famous very bright bolide Ždár (December 16, 2014), and simulated ablation spectra together with real ablation spectra of a chondrite specimen provided by Excimer laser and also spectra of gas-phase LIDB of several gaseous mixtures (methane, hydrogen, nitrogen) recorded at terawatt laser PALS. Panel B shows the spectrum of TC-LIBS recorded at PALS infrastructure. The red envelope represents the low-resolution spectrum that has been recorded simultaneously by the astronomical spectrograph, while the black lines indicate a spectrum recorded by high-resolution Echelle instrument.

We expect that precise measurement under laboratory conditions can also provide important parameters for the design of future space missions intended to direct

investigation of elemental compositions of bodies in the asteroid belt using remote high-resolution spectroscopy of laser-induced ablation plasma over their surfaces. State-of-the-art laboratory laser sources are able to ablate $\sim \text{mm}^2$ size spots while the plasma emission is measured very close to the target (*e. g.* Nd:YAG or Excimer providing energy in order of 10^{-2} J in sub-nanosecond ranges).

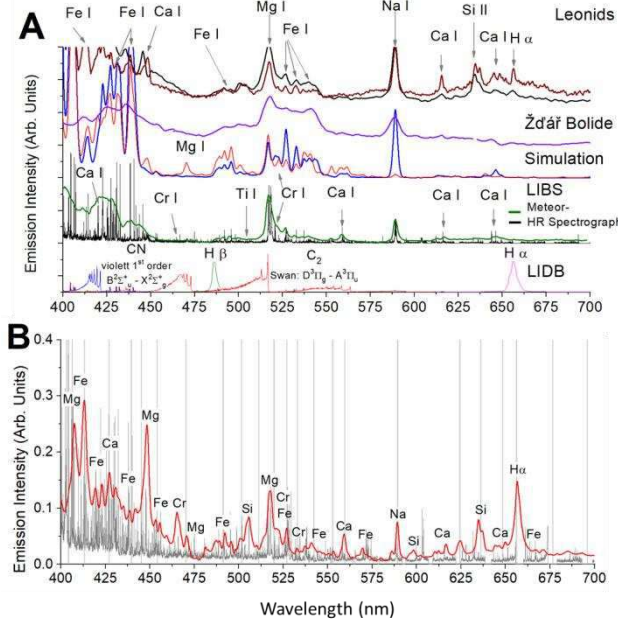


Figure 1 – A comparison of several meteor spectra, simulated and experimental LIBS (Panel A) with TC-LIBS spectrum recorded by high resolution Echelle spectrograph and meteor camera (Panel B). The specific line list for spectral features recorded using high power laser is supplied in Ferus et al. (2019).

TC-LIBS performed for instance by high-power facility PALS is yet able to evaporate about 1 cm^2 (energy of 600 J). Our survey of craters performed by Optical Microscopy and Scanning Electron Microscopy (SEM) shows that high-power lasers typically create an ablation spot of $10^2 \mu\text{m}$ in depth and about 1 cm (power of 600 J) in diameter in one laser shot, while Nd:YAG laboratory laser source of 600 mJ energy creates a spot with $10^1 \mu\text{m}$ in depth and diameter of 1 mm. Only a series of several hundreds of pulses can therefore create an ablated area comparable in depths and diameter with a single shot of large terawatt laser. The corresponding example is provided in Figure 2. Panel A shows the ablation spot of PALS laser examined with electron microscopy, panel B shows a detail of this area. Panel C shows an example of microscopic mapping of a crater created by about 1000 pulses of Nd:YAG laser on rotating sample of a chondritic meteorite.

The concluding comparison of laser ablation experiments with meteor plasma is provided in Table 1. First of all, it should be noted that ablation experiments represent the only state-of-the-art method for the simulation of meteor plasma. Other methods (flames, electric discharges or induced plasma sources etc.) require dissolution or further reprocessing of the material. Hypervelocity guns may serve as a remarkably good model for target

experiments but the projectile must usually be manufactured of copper or steel. Original sample of a meteorite cannot be directly fired by the gun.

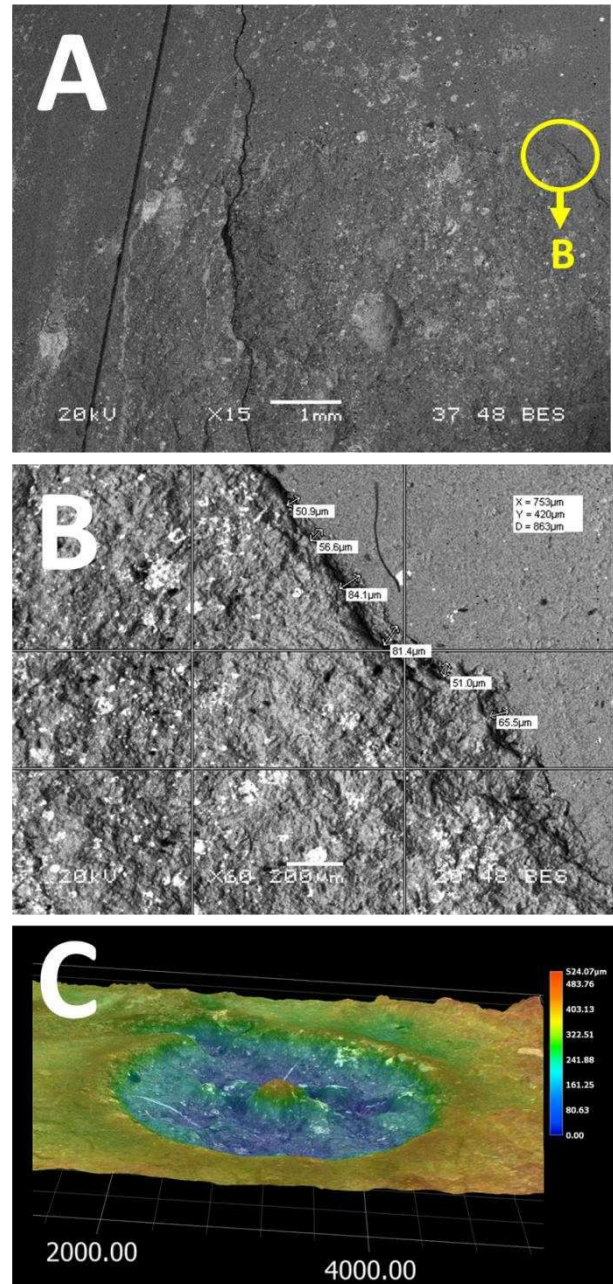


Figure 2 – An example of laser ablation spot survey performed by electron microscope for an ablation spot after a single pulse of terawatt laser facility PALS (panel A and detailed in panel B). Relief measurement of ablation spot after about 1000 pulses of standard Nd:YAG laser (Panel C).

Table 1 – Parameters of ablation plasma induced by several laser sources: ArF excimer laser, Nd:YAG laser, Ti:SAF laser and terawatt laser PALS. T is temperature expressed in K, n_e is electron density expressed in number of electrons per cm^3 .

	ArF Excimer	Nd:YAG	Ti:SAF	PALS
T [K]	6 965	8 169	8 343	10 274
$n_e [\text{cm}^{-3}]$	3.97×10^{16}	5.83×10^{16}	6.27×10^{16}	5.34×10^{16}

This means that the target as well as plasma formed after interaction is inevitably contaminated by the projectile material. Moreover, the typical speed of the projectile

reaches 10 km s^{-1} , which is actually the lowest possible velocity of a meteoroid. Furthermore, any observable plasma is created only after the collision with the target and such kind of experiments therefore cannot simulate the airglow around the meteoroid body. In comparison, laser ablation technique performed particularly by the terawatt-class laser (TC-LIBS) provides large volume of plasma (around 1 l) and evaporates significantly large surface of a meteorite specimen (about 1 cm^2). Although the physical initiation differs from meteoroid ablation, this technique has ambitions to provide real simulation of meteor chemistry and physics. However, it is necessary for the further research to test different laser energies, time scales after laser initiation, laser pulse lengths, buffer air speed and pressure etc. in order to approach all the parameters of extraterrestrial body atmospheric entry and the impact conditions.

4 Conclusion

Our explorations of advantages and limits of high-power laser application for laboratory simulation of chemical and physical consequences of an extraterrestrial body atmospheric entry as well as the extrapolation of technical parameters of high-power laser systems for space applications show that, first of all, all the spectral features can be studied on laboratory level for any complex matrix and laser sources can be used for LIBS in astronautics. Additionally, the physical parameters of high-power laser sources for deflection or destruction of potentially hazardous objects or for remote LIBS exploration of elemental composition of bodies in the asteroid belt can be defined based on laboratory experiments. The main advantage of high-power laser application in laboratory astrochemistry and astrophysics is that they represent clear sources of energy directly delivered to vacuum sealed vessels or interaction chambers for chemical and physical experiments. The system is not contaminated by any other material and all the phases (buffer gas atmosphere, solid or liquid interaction target) represent neat materials with well-defined chemical composition. In such a set-up, we can study all the manifestations of high-power plasma in a well-controlled system without the influence of material introduced from the outside (projectile, electrodes etc). Moreover, especially harsh conditions (temperatures over 4000 K or manifestation of a shock wave) cannot be simulated by other techniques whilst using our experimental set-up, the starting conditions such as pressure, temperature and chemical composition can easily be tuned and kept. Even though all the parameters cannot be simulated even with high-power lasers, this technique still represents better starting system for peak parameters extrapolation that engagement of small-scale laboratory systems such as small lasers. Serious disadvantage of this kind of experiments, however, lies in the different kind of high energy plasma initiation (e. g. real high-speed atmospheric entry and ablation of the solid material by collisions with gas phase air molecules compared to the simulation by melting the solid target surface by laser light and its subsequent evaporation to

the gas phase). High-power laser facility PALS also provides only very small number of pulses per day (1 every 30 minutes), which seriously limits the range of experimental conditions whose influence can be explored.

Acknowledgement

The research is supported by the Czech Science Foundation within the project reg. no. 18-27653S, ERDF/ESF "Centre of Advanced Applied Sciences" (No. CZ.02.1.01/0.0/0.0/16_019/0000778) and grant TL01000181 of the Technological Agency of the Czech Republic. We greatly acknowledge assistance of Keyence company and a great help of Mr. Martin Rybín from Crytur spol. s r. o. (Na Lukách 2283, 51101 Turnov, Czech Republic) for the measurement of a crater relief.

References

- Aristova EY, Aushev AA, Baranov VK, et al (2018) Laser Simulations of the Destructive Impact of Nuclear Explosions on Hazardous Asteroids. *J Exp Theor Phys* 126:132–145. doi: 10.1134/S1063776118010132
- Babanková D, Civiš S, Juha L (2006) Chemical consequences of laser-induced breakdown in molecular gases. *Prog Quantum Electron* 30:75–88. doi: 10.1016/j.pquantelec.2006.09.001
- Bottke WF, Vokrouhlický D, Minton D, et al (2012) An Archaean heavy bombardment from a destabilized extension of the asteroid belt. *Nature* 485:78–81. doi: 10.1038/nature10967
- Canup RM, Asphaug E (2001) Origin of the Moon in a giant impact near the end of the Earth's formation. *Nature* 412:708–712. doi: 10.1038/35089010
- Ciucci A, Corsi M, Palleschi V, et al (1999) New Procedure for Quantitative Elemental Analysis by Laser-Induced Plasma Spectroscopy. *Appl Spectrosc* 53:960–964. doi: 10.1366/0003702991947612
- Civiš M, Ferus M, Knížek A, et al (2016a) Spectroscopic investigations of high-density-energy plasma transformations in a simulated early reducing atmosphere containing methane, nitrogen and water. *Phys Chem Chem Phys* 18:27317–27325
- Civiš S, Babankova D, Cihelkat J, et al (2008) Spectroscopic investigations of high-power laser-induced dielectric breakdown in gas mixtures containing carbon monoxide. *J Phys Chem A* 112:7162–7169. doi: 10.1021/jp712011t
- Civiš S, Juha L, Babankova D, et al (2004) Amino acid formation induced by high-power laser in CO₂/CO-N-2-H₂O gas mixtures. *Chem Phys Lett* 386:169–173. doi: 10.1016/j.cplett.2004.01.034
- Civiš S, Knížek A, Ivanek O, et al (2017) The origin of methane and biomolecules from a CO₂ cycle on terrestrial planets. *Nat Astron* 1:721–726

- Civiš S, Szabla R, Szyja B, et al (2016b) TiO₂-catalyzed synthesis of sugars from formaldehyde in extraterrestrial impacts on the early Earth. *Sci Rep* DOI: 10.1038/srep21280. doi: <https://doi.org/10.1111/maps.12809>
- Ebert M, Hecht L, Hamann C, Luther R (2007) Laser-induced melting experiments Simulation of short-term high-temperature impact processes. *Meteorit. Planet. Sci.* 52, 1475–1494. doi: <https://doi.org/10.1111/j.1365-272X.2007.01742.x>
- Ferus M, Civiš S, Mládek A, et al (2012) On the Road from Formamide Ices to Nucleobases: IR-Spectroscopic Observation of a Direct Reaction between Cyano Radicals and Formamide in a High-Energy Impact Event. *J Am Chem Soc* 134:20788–20796. doi: 10.1021/ja310421z
- Ferus M, Knížek A, Civiš S (2015a) Meteorite-catalyzed synthesis of nucleosides and other prebiotic compounds. *Proc Natl Acad Sci U S A* 112:.. doi: 10.1073/pnas.1507471112
- Ferus M, Koukal J, Lenža L, et al (2017a) Recording and Evaluation of High Resolution Optical Meteor Spectra and Comparative Laboratory Measurements Using Laser Ablation of Solid Meteorite Specimens. In: 2017 19th International conference on transparent optical networks (ICTON). IEEE, 345 E 47th St., New York, NY 10017 USA
- Ferus M, Koukal J, Lenža L, et al (2018a) Calibration-free quantitative elemental analysis of meteor plasma using reference laser-induced breakdown spectroscopy of meteorite samples. *Astron Astrophys* 610:A73. doi: 10.1051/0004-6361/201629950
- Ferus M, Koukal J, Lenža L, et al (2018b) Calibration-free quantitative elemental analysis of meteor plasma using reference laser-induced breakdown spectroscopy of meteorite samples. *Astron Astrophys* 610:A73. doi: 10.1051/0004-6361/201629950
- Ferus M, Kubelík P, Civiš S (2011) Laser Spark Formamide Decomposition Studied by FT-IR Spectroscopy. *J Phys Chem A* 115:12132–12141. doi: 10.1021/jp205413d
- Ferus M, Kubelík P, Knížek A, et al (2017b) High Energy Radical Chemistry Formation of HCN-rich Atmospheres on early Earth. *Sci Rep* 7:Article number: 6275. doi: 10.1038/s41598-017-06489-1
- Ferus M, Kubelík P, Petera L, et al (2019) Main spectral features of meteors studied using a terawatt-class high-power laser. *Astron Astrophys* 630:A127. doi: 10.1051/0004-6361/201935816
- Ferus M, Laitl V, Knížek A, et al (2018c) HNCO-based synthesis of formamide in planetary atmospheres. *Astron Astrophys* 616:A150. doi: 10.1051/0004-6361/201833003
- Ferus M, Matulková I, Juha L, Civiš S (2009) Investigation of laser-plasma chemistry in CO-N₂-H₂O mixtures using O-18 labeled water. *Chem Phys Lett* 472:14–18. doi: 10.1016/j.cplett.2009.02.056
- Ferus M, Michalčíková R, Shestivská V, et al (2014) High-Energy Chemistry of Formamide: A Simpler Way for Nucleobase Formation. *J Phys Chem* 118:719–736
- Ferus M, Nesvorný D, Šponer JJE, et al (2015b) High-energy chemistry of formamide: A unified mechanism of nucleobase formation. *Proc Natl Acad Sci* 112:657–662. doi: 10.1073/pnas.1412072111
- Ferus M, Pietrucci F, Saitta AM, et al (2017c) Formation of nucleobases in a Miller–Urey reducing atmosphere. *Proc Natl Acad Sci* www.pnas.org/cgi/doi/10.1073/pnas.1700010114
- Geiss J, Rossi AP (2013) On the chronology of lunar origin and evolution Implications for Earth, Mars and the Solar System as a whole. *Astron Astrophys Rev* 21:.. doi: 10.1007/s00159-013-0068-1
- Hawkes RL, Milley EP, Ehrman JM et al. (2008) What can we learn about atmospheric meteor ablation and light production from laser ablation? *Earth Moon Planets* 102, 331–336 doi: <https://doi.org/10.1007/s11038-007-9186-y>
- Jenniskens P (2007) Quantitative meteor spectroscopy: Elemental abundances. *Adv Sp Res* 39:491–512. doi: 10.1016/j.asr.2007.03.040
- Koeberl C (2006) Impact processes on the early Earth. *Elements* 2:211–216. doi: 10.2113/gselements.2.4.211
- Kurahashi E, Yamanaka C, Nakamura K, Sasaki S (2002) Laboratory simulation of space weathering: ESR measurements of nanophase metallic iron in laser-irradiated materials. *EARTH PLANETS Sp* 54:E5–E7. doi: 10.1186/BF03352448
- Loeffler MJ, Baragiola RA, Murayama M (2008) Laboratory simulations of redeposition of impact ejecta on mineral surfaces. *Icarus* 196:285–292. doi: 10.1016/j.icarus.2008.02.021
- Madiedo JM, Trigo-Rodriguez JM, Konovalova N, et al (2013) The 2011 October Draconids outburst - II. Meteoroid chemical abundances from fireball spectroscopy. *Mon Not R Astron Soc* 433:571–580. doi: 10.1093/mnras/stt748
- Milley EP, Hawkes RL, Ehrman, JM (2007) Meteor luminosity simulation through laser ablation of meteorites. *Mon. Not. R. Astron. Soc.* 382, L67–L71, doi: <https://doi.org/10.1111/j.1745-3933.2007.00390.x>
- Morbidelli A, Marchi S, Bottke WF, Kring DA (2012) A sawtooth-like timeline for the first billion years of lunar bombardment. *EARTH Planet Sci Lett* 355:144–151. doi: 10.1016/j.epsl.2012.07.037

Moroz L V, Fisenko A V, Semjonova LF, et al (1996) Optical effects of regolith processes on S-asteroids as simulated by laser shots on ordinary chondrite and other mafic materials. *Icarus* 122:366–382. doi: 10.1006/icar.1996.0130

Nesvorný D, Morbidelli A (2012) Statistical Study of the Early Solar System's Instability with Four, Five, and Six Giant Planets. *Astron J* 144:20–68. doi: 10.1088/0004-6256/144/4/117

Park SY, Mazanek DD (2003) Mission functionality for deflecting earth-crossing asteroids/comets. *J Guid Control Dyn* 26:734–742. doi: 10.2514/2.5128

Šponer JE, Szabla R, Góra RW, et al (2016) Prebiotic synthesis of nucleic acids and their building blocks at the atomic level - merging models and mechanisms from advanced computations and experiments. *Phys Chem Chem Phys* 18:20047—20066. doi: 10.1039/c6cp00670a

Tsiganis K, Gomes R, Morbidelli A, Levison HF (2005) Origin of the orbital architecture of the giant planets of the Solar System. *Nature* 435:459–461. doi: 10.1038/nature03539

A spectral mystery

Bill Ward

International Meteor Organisation, Glasgow, Scotland, UK.

Bill_meteor@yahoo.com

This paper investigates the claim that a spectrum obtained by E. Majden, Vancouver, Canada, 1997, was unmeasurable. A solution to this problem is suggested.

1 Introduction

In February 2019 the author was contacted by Ed Majden with a request for assistance. Mr Majden is a long time and experienced meteor observer and meteor spectroscopist based in Vancouver, Canada. On June 9, 1997, Mr Majden was investigating the use of plastic film gratings for meteor spectroscopy. On the evening in question he recorded a bright meteor with his medium format camera system. This had 750 lines/mm grating mounted in front of a 75mm lens set to f4. The film used was Kodak Tri-X. Mr Majden comments that it appeared to be around mag -4 (Majden, 1998).

On processing the film an excellent spectrum had been captured.

Also on the film was a spectrum of the star Vega. Mr Majden sent the image to what he referred to in private communications as several experts. However, the image was returned with the comment that due to differences in the dispersion between Vega and the assumed lines in the spectrum, the spectrum, as such, was unmeasurable!

2 Unmeasureable ...?

After further email correspondence on the issue and several failed attempts working with a very low resolution image originally sent, the author enquired as to whether the original negative was still available. Fortunately it was (Figure 1). The image was scanned with an Epson photo perfection 1035 at 600 dpi and 16 bit depth. Due to the brightness of the meteor many of the lines were saturated (Figure 2).

The image contained an excellent wide field spectrum of Vega which could be used as a calibration. The processing was done using the Visual Spec software. Using the hydrogen Blamer lines on the image yielded a dispersion of approximately 1.8 nm/pix. It should be noted that the pixel figure is from the “pixels” produced by the scanning.

Turning attention to the spectrum. By visual inspection several prominent line groupings could be easily identified. By taking spectrum sections through the trail lines could be fitted and it was straightforward to then identify the individual prominent lines. However this resulted in a dispersion of approximately 0.8 nm/pix. This was a surprise as all things being equal the dispersion should have been the same!

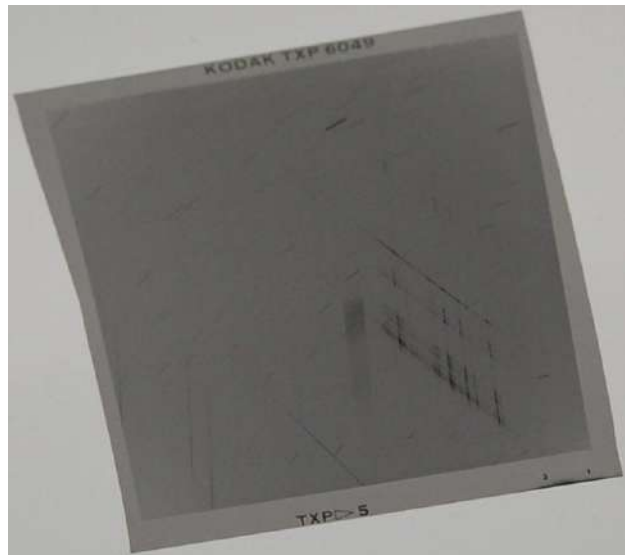


Figure 1 – Original negative of the spectrum



Figure 2 – Meteor spectrum and spectrum of Vega

3 A Puzzle

Physical optics dictates the function of light passing through a grating and it is well established physics. What could be the problem? The first course of action was to re-measure everything from scratch! This resulted in exactly the same result. Using the H Balmer lines gave the graph in Figure 3 and the assumption of particular meteor lines gave the spectrum in Figure 4.



Figure 3 – Assumed hydrogen spectrum

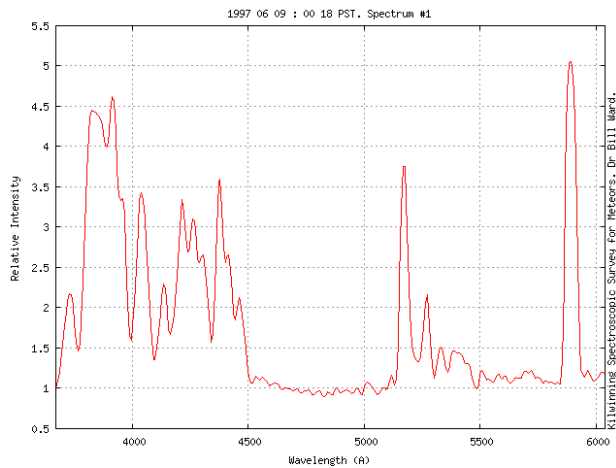


Figure 4 – Assumed meteor spectrum

Both of these results, on their own, would seem entirely reasonable. Knowing the configuration of the optics and the resulting disparity in dispersions clearly indicated there was an error somewhere!

Attempts were made to fit lines in the meteor spectrum using the dispersion of the hydrogen line spectrum as there should be no ambiguity of the lines in this spectrum. This resulted in meteor spectra that made no sense whatsoever. Even if it was accepted that the spectrum was itself very unusual, the various patterns of lines, in particular well known Fe lines, did not give any meaningful results compared to other existing spectra (Ward, 2016).

4 Detector Sensitivity

It was at this point that a moment of inspiration occurred!

When reviewing spectra taken with the authors own video cameras it was noticed that some spectra had no or very faint blue lines. This is due to the optoelectronic characteristics of silicon as a photo sensor. Silicon is much more sensitive to red and near IR photons than blue. However, although the quantum efficiency is low, film emulsion is the reverse. That is, it is relatively more sensitive to blue than red.

Considering the hydrogen spectrum, if the lines as originally assumed were not in fact correct, could this resolve the problem? If the film is not actually recording red perhaps the furthest “red” line on the Vega spectrum is not H alpha, but rather H beta. Re-assigning and re-measuring the hydrogen lines gave spectrum in Figure 5. Using this calibration the dispersion becomes approximately 0.8 nm/pix!



Figure 5 – Corrected hydrogen spectrum

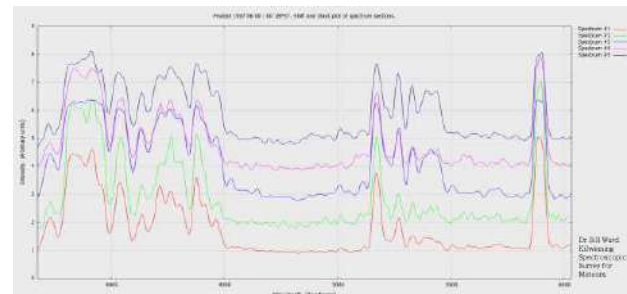


Figure 6 – Section through bright flares in meteor spectrum

5 Conclusion

Now that the two dispersions have been shown to be the same in reality, it can be concluded that it may have been a misidentification of the hydrogen lines that lead to the determination that the spectrum was unmeasurable! What is surprising is that the “experts” gave up so easily!

Figure 6 shows a plot of several sections through the trail of the meteor.

References

- Majden E (1998) “Meteor spectroscopy with inexpensive holographic gratings.” Journal of the Royal Astronomical Society of Canada. 92: 91-92. April 1998
- Ward B (2016) “Meteor Spectra”. The Astronomer, 52, 623, 294, 2016

MeteorFlux Reloaded

Sirko Molau¹

¹Arbeitskreis Meteore e.V, Germany

sirko@molau.de

In 2011, Geert Barentsen introduced MeteorFlux – a Web application to generate flux density graphs from video data of the IMO Video Meteor Network. It has been extensively used for almost every meteor shower analysis of IMO network data ever since. The tool received some improvements in 2013 and had been migrated to a new hardware platform in 2018, but despite a large number of long-term feature requests it was never really extended. Earlier this year, the tool finally received some functional upgrades, which will be discussed in this paper.

1 Introduction

MeteorFlux is a Web application that was developed in 2011 by Geert Barentsen. It aims at visualizing flux data collected by the IMO network. MeteorFlux has been the basis for numerous meteor shower analyses since then. A real-time flux viewer was implemented as proof-of-concept for the 2011 Draconids outburst¹. Further enhancements were implemented for the 2013 Meteoroids conference.

Thereafter, the programmer did not have the time to work further on MeteorFlux. Some functions were prepared in the user interface but never completed, and also many new ideas and feature requests remained unimplemented for years. In 2017 the situation deteriorated, because even the ingest of new data became impossible.

At the 2017 IMC, a team of high school students from Petnica science center indicated interest to step in and take over responsibility for MeteorFlux. Unfortunately, their enthusiasm vanished soon. A few months later, only Vladimir Nikolić was left to help. He deployed the software on a new AWS cloud server owned by the author, and MeteorFlux was relaunched under a new URL².

This initiative preserved the previous state and MeteorFlux could be further used to generate flux graphs from IMO network data, but new features were still missing.

2 Problem

As programmer of MetRec, the author is knowledgeable about the C programming language under the DOS and Windows PC operating system (Figure 1). MeteorFlux, however, has a completely different technology stack (Figure 2).

- runs on Ubuntu Linux,
- is deployed on a virtual server in the cloud (more specifically, an AWS EC2 instance),
- is using a Web-Application server based on uWSGI and NGINX,

- uses the Bootstrap framework and Javascript code for client-side functions,
- is using server-side functions written in Python, and
- a local PostgreSQL database with stored procedures.

Prior to this project, I had little to no experience with that technology stack at all.



Figure 1 – MetRec technology stack.



Figure 2 – MeteorFlux technology stack.

¹ <http://www.imonet.org/draconids>

² <https://meteorflux.org>

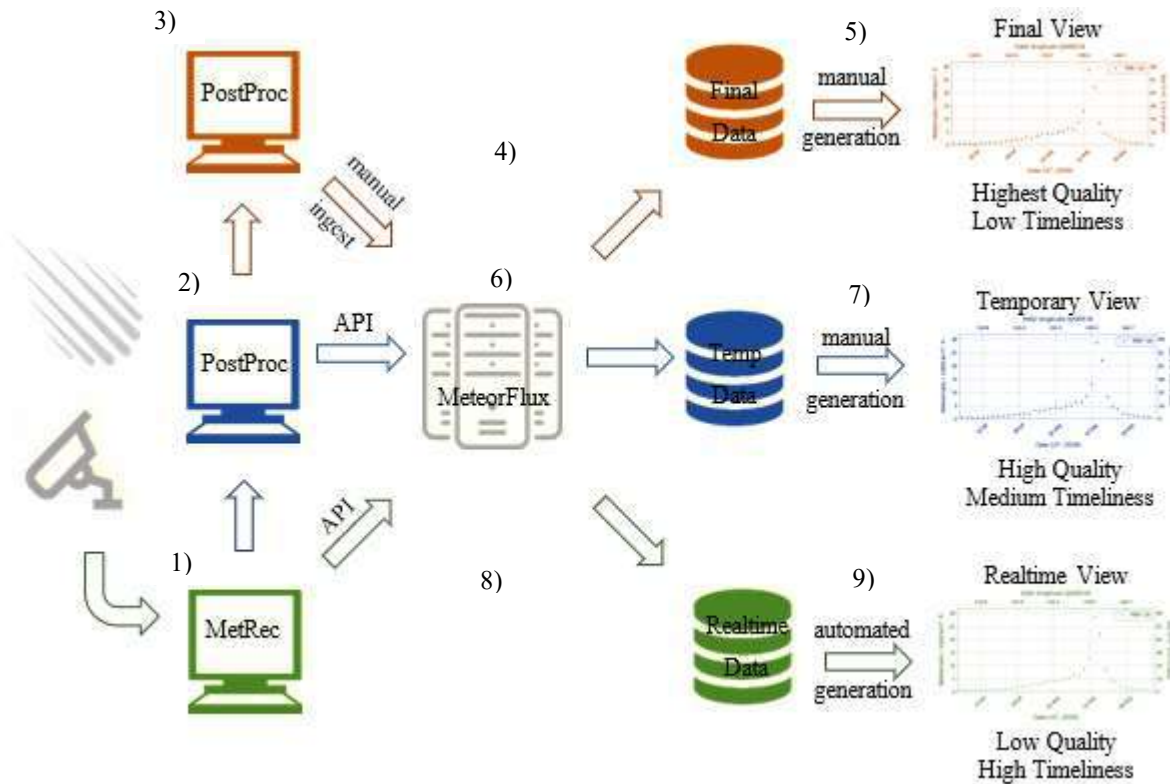


Figure 3 – Vision of different data flows in MeteorFlux.

3 Solution

Once MeteorFlux was running on a virtual server of my own, I had full access to the system and could analyze it more thoroughly. Among others, MeteorFlux contained a function to filter observations for a minimum radiant altitude. When I had the requirement for a maximum radiant altitude filter in May 2019, I tried to implement that function by copy & paste some lines of the existing source code. I succeeded within only two days.

This gave me sufficient self-confidence to follow the approach, and step by step I tackled and solved more complex tasks. With every new feature, I gained more insight into the code. In the end I was able to add a completely new interface to MeteorFlux.

As of today, I would not be able to reprogram MeteorFlux from scratch, but I understand the structure of MeteorFlux and gained basic insight into the whole technology stack.

4 Vision

So far, MeteorFlux supported just one data flow (Figure 3):

- 1) the video stream of the camera is digitized and automatically analyzed by MetRec
- 2) the observation is post-processed by the observer (e.g. false detections are removed)
- 3) the observation is checked for a second time with PostProc by an IMO network admin
- 4) the flux data are uploaded to the MeteorFlux server and manually ingested into the final database

- 5) the Web user interface allows to manually create flux density plots with various settings

With the four-eyes principle at post-processing, highest data quality is assured, but due to the long processing pipeline, the available data has only low timeliness.

In the vision of an alternative data flow, the observer would be able to upload the data automatically after post-processing to MeteorFlux (Figure 3, 6). They would be stored in a temporary database, and the same Web user interface could be used for generating flux density plots of still high quality and with improved timeliness (Figure 3, 7).

Finally, the real-time flux viewer that was piloted in 2011, should be properly implemented. In this new data flow, MetRec would efficiently upload observational data every minute during the observation to MeteorFlux (Figure 3, 8), where they would be stored in a real-time database. At the server-side, standard flux density plots with fixed parameters could be generated automatically for all active meteor showers (Figure 3, 9). They would have low quality because of false detection, but the best possible timeliness.

5 Implementation

Final View

MeteorFlux functions that have been missing since 2013 were implemented by the author in summer 2019, together with all other features that had been requested for years:

- the begin and end date for data selection can be entered alternatively as date or as solar longitude,
- two data sets can be plotted in one graph (same or different shower),
- various parameters (shower, year, binning parameter, camera set, population index, ...) can be adjusted for the second data set,

- the second data set can be scaled and offset,
- analog sliders for binning parameters, which prevented reproducible results so far, are replaced by discrete input fields,
- data can be filtered by camera, observer, and country,
- data can be filtered by a radiant altitude interval and by minimum stellar limiting magnitude,
- the plot can be switched between flux density and particle density e.g. for better comparison with visual data analyses of IMO,
- download functions for PNG, PDF and CSV files are offered,
- additional tables provide statistics on contributing cameras and observers,
- traffic is encrypted by switching from HTTP to HTTPS,
- session data from VMO files are ingested into the database (for future use).

These new functions make the Web user interface much more powerful and user-friendly than before.

Temporary View

For the second data flow, a new API was implemented. The PostProc software can upload flux data after post-processing as ZIP file via a HTTP POST request to the MeteorFlux server. Temporary data are manually deleted from the database as soon as the corresponding final data set is ingested via the original data flow.

With a check-box in the browser the user can switch between the final and temporary database. All options to control data selection and plotting are identical.

Real-time View

The implementation of the real-time data flow was more challenging. Another API was implemented, where MetRec is uploading short JSON messages with observational data to the MeteorFlux server every minute. Data are stored in a separate real-time database with its own scheme, and automatically deleted after seven days.

Every five minutes, a cron job at the MeteorFlux server creates flux density graphs with fixed parameters for every active shower. For generating the plots, the same internal API is used as for the Web user interface.

Real-time flux density graphs and additional camera / observer statistics can be accessed via an own URL³ (Figure 4). In addition, all relevant data are provided in a JSON structure⁴, so that the real-time flux density graphs can be integrated into other web pages easily. It has in fact been integrated into the IMO homepage since the 2019 IMC.

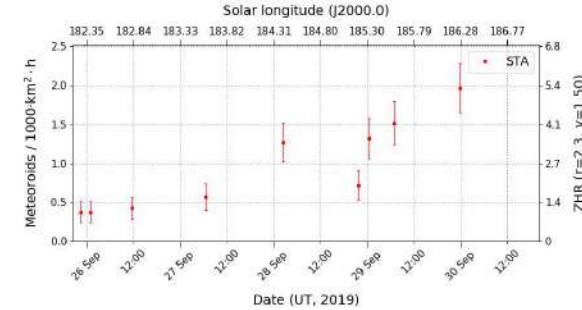
As add-on, a Google Maps API was integrated to depict the locations of the currently active cameras (Figure 5).

MeteorFlux 2.1 Realtime Viewer

Below you find the real-time flux profiles for currently active meteor showers. Note that these data are unchecked and error-prone. Use the [main page](#) for quality-checked data.

Last update: 2019/09/30 20:20:01 UT

[DAU](#) [DSX](#) [STA](#) [NTA](#) [SPO](#) [Cameras](#)



Flux data table:

Time [UT]	Solarlon [°]	Teff [h]	ECA [$10^3 \text{ km}^2 \text{ h}^{-1}$]	# Met	Flux [$10^3 \text{ km}^{-2} \text{ h}^{-1}$]	Particle [10^7 km^{-3}]	ZHR
2019-09-25 22:00	102.290	24.5	20.1	7	0.4 ± 0.1	3.6 ± 1.4	1.0
2019-09-26 01:01	102.294	18.5	20.0	7	0.4 ± 0.1	3.9 ± 1.4	1.0

Figure 4 – MeteorFlux real-time viewer.

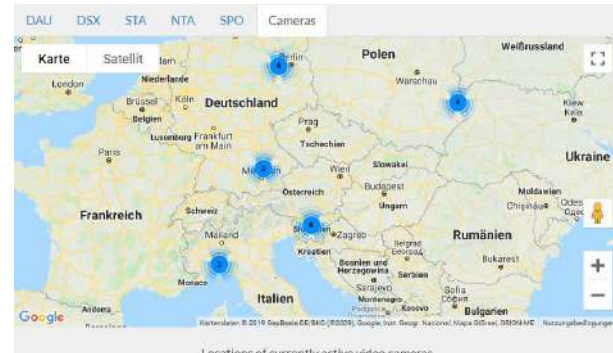


Figure 5 – Google Maps integration in the real-time viewer.

6 Results and Outlook

At the time of the 2019 IMC, MeteorFlux is not only back to life, but it has been extended by numerous long-awaited features. With these, observers have better transparency on their contribution to the analyses, and new data flows provide more flexibility and a much better timeliness.

Naturally, a number of new ideas were born during the implementation, which can now be tackled piece by piece. Some examples:

- implementation of outlier rejection filters for better real-time flux density graphs,
- proper population index and zenith exponent correction,
- automated calculation of population index graphs from data,
- implementation of camera-specific perception coefficients.

The past few months provided me with a hands-on training for a completely new technology stack. The implementation of new MeteorFlux features was particularly rewarding, because contrary to MetRec new functions become immediately available and usable.

³ <https://meteorflux.org/rt>

⁴ <https://meteorflux.org/rt/shower.json>

Double and triple meteor detections

Ilias Fernini^{1,2}, Mohammed Talafha¹, Aisha Al-Owais¹, Yousef Eisa Yousef Doostkam¹, Maryam Sharif¹, Masa Al-Naser¹, Shahab Zarafshan¹, Hamid Al-Naimiy^{1,2}, Ahmad Hassan Harriri¹, Issam Abu-Jami¹, Salma Subhi, Yahya Al-Nahdi¹, Ridwan Fernini¹, Anas Omar Adwan¹

¹ Sharjah Academy for Astronomy, Space Sciences and Technology, University of Sharjah, Sharjah, United Arab Emirates

Ifernini@sharjah.ac.ae, mtalafha@sharjah.ac.ae, aalowais@sharjah.ac.ae,
aadwan@scass.ae, ssubhi@sharjah.ac.ae, Rfernini@sharjah.ac.ae

² University of Sharjah

U15106538@sharjah.ac.ae, U00042517@sharjah.ac.ae, u15104934@sharjah.ac.ae,
alnaimiy@sharjah.ac.ae, U14112271@sharjah.ac.ae, u15105490@sharjah.ac.ae,
ijami@sharjah.ac.ae, u14210365@sharjah.ac.ae

A prominent meteor monitoring network known as the UAEMMN was developed in the United Arab Emirates in September 2018. The network consists of three towers located in different parts of the country, each equipped with 17 cameras of different lenses. The total number of meteors observed as of June 2019 is 9,992 with 956 being double detections and 86 triple detections. Furthermore, we are developing a smart UAV to detect meteorites at the possible meteorite landing sites.

1 Introduction

The sky is embellished with countless beautiful stars and often accessorized with numerous mesmerizing fireballs. In the Gulf region, specifically in the United Arab Emirates (UAE), a prominent meteor monitoring network has been developed and operated by the Sharjah Academy for Astronomy, Space Sciences, and Technology under the sponsorship of the UAE Space Agency (UAESA). In September 2018, the first tower was installed in Sharjah (25.285922 N, 55.463625 E) at the academy. In October 2019, the third tower – in terms of location order – was installed in the southern side of the country in Liwa (23.104722 N, 53.754828 E). The second and last tower joined the network in January 2019 and was installed in Al-Yahar (24.235611 N, 55.539645 E). This tower has been placed between the first and third to fill any uncovered region and increase the number of double and triple detections to create orbits and facilitate the task of locating possible meteorites. The network is quite similar to the other networks like the European Fireball Network in Germany (Flohrer et al., 2012), the CAMS Network in the US (Jenniskens et al., 2011), the one in the Armagh Observatory (Atreya and Christou, 2006), and several others. However, what distinguishes this network is the camera orientation per tower where we have organized a different arrangement for the cameras when compared to other stations.

2 System set-up

The full network is shown in Figure 1, along with the STK simulation coverage where the green color represents the 8 mm cameras, the red 6 mm cameras, and the yellow 2 mm cameras. Each tower has 16 cameras arranged in a ring-like structure, centered with a wide-angle camera to cover any missing area of the sky left out by the complementing cameras.

Each tower is made up of three levels as denoted in green in Figure 2. The first level is the computer room where camera wires are attached to the CPU. The second level is a storage area and air conditioning compressor, finally, the third level is where the cameras are placed around the circular edge of the tower. All of the wires extend from the top to the ground level.

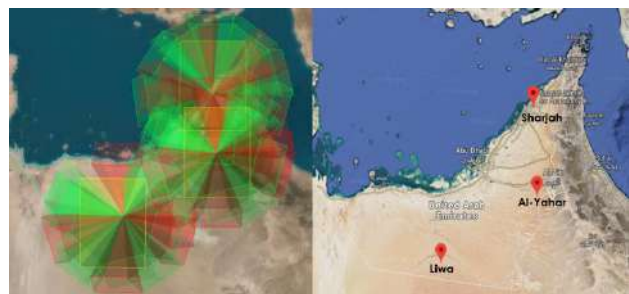


Figure 1 – The UAEMMN towers locations and STK simulation.



Figure 2– The UAEMMN towers (Sharjah, Al-Yahar, and Liwa).

3 Observations

The meteors detected and observed by the system often range from faint meteors to bright fireballs, and with the help of the UFO Analyzer¹ software, the magnitude of each meteor is measured alongside its other characters like the duration, its angular velocity, etc. Very bright meteors were observed when the very first tower was installed, with fireballs reaching up to -8 apparent magnitude. With the addition of two more towers located in the desert away from any city lights, at least one bright fireball was observed every month. As for meteors, they appear dazzling in the UAE sky almost every night, ranging from meteors with an apparent magnitude of 4 until the threshold of a fireball. It is worth mentioning that bright meteors are better detected in Liwa (the farthest from the city), followed by Al-Yahar, and finally the Sharjah tower. An example of a fireball captured by the third tower is shown in Figure 3.



Figure 3 – A bright fireball observed on April 30, 2019, from the third tower.

Overall, from September 2018 up to June 2019 we have observed around 9,992 meteors of which 956 were double detections and 86 triple detections. Figure 4 shows the number of detections per month. The highest number of meteors detected took place in Liwa (third station) in

December 2018, the month of the annual Geminids meteor shower.

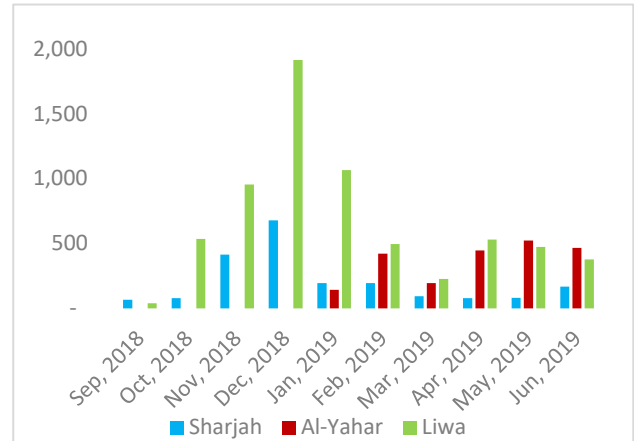


Figure 4 – Observed meteors from September 2018 to June 2019.

4 Double detections

The double and triple detections are calculated by a Python program, where folders of the three towers are read, then files with matching timings within a threshold of 3 seconds are considered double detection candidates.

In addition to timing, the distance between the towers also plays a vital role. The distance between the first and second tower is 116 km while the second and third towers are 221 km apart; however, the distance between the first and third is 300 km. Although the distance between the first and second tower is the shortest, the double detections are not higher since the first tower is located in a region of relatively high light pollution. Nevertheless, double detections appear mostly between the second and third towers due to them being in a desert location. After analyzing meteor videos by UFO Analyzer, the output “CSV” folder is fed into the UFO Orbit software to determine the radiant points of the double detected meteors, and the trail map which illustrates the paired path of the double detected meteors. Furthermore, the ground map shows where the meteor has been observed (Figure 5). The yellow line represents the distance (in kilometers) of the observed location, which varies from 9.6 km to 128 km, while the green color represents the path of the meteor.

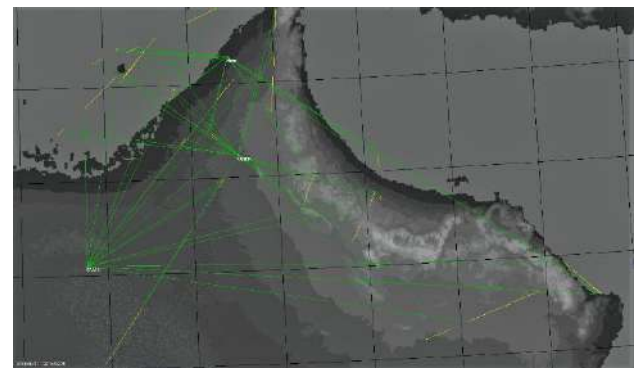


Figure 5 - June's 2019 double and triple detections

¹ http://sonotaco.com/soft/e_index.html

5 Triple detections

Although triple detections are expected to be relatively high since there are three available towers, such detections have been rare. This may be because of the locations of the towers since the three towers can only see the same meteor in the north-west of the country.

Moreover, because the first tower is within city limits, it seldom observes the meteors observed by both the second and third tower. Table 1 lists the number of meteors detected during June 2019, where we observed a total of 1,010 meteors. To get a total number without duplications, we subtracted the double detections from the total detections, and added the triple detections; hence leading to an exact total of 803 observed meteors. The second tower (Al-Yahar) with the third one (Liwa), scored a higher number of double detected meteors.

Table 1 - June's 2019 detections (single, double, and triple).

Towers	Detection Number
Sharjah	166
Al-Yahar	377
Liwa	467
Sharjah & Liwa	34
Sharjah & Al-Yahar	96
Liwa & Al-Yahar	107
Triple Detections	30
Double Detections	237
Exact Double Detections	207
Total	1,010
Exact total	803

6 Conclusion

Detecting meteors in the UAE sky has now become feasible with the UAEMMN. In addition, the UFO software has made meteorite searches much more efficient and easier. Currently, we are planning to add at least two more towers to cover the gaps in the western-northern part of the country. Also, we have created a platform where individuals in the region can enter the details of a meteor observed by them. By allowing the public to interact with us, our network detection rate would increase, and the sense of awareness regarding space debris will increase. Additionally, after determining the observed location, a triangulation calculation would be carried out to approximate the possible fall area, then a UAV trained on recognizing meteorite images using machine learning would be sent to scan the area.

Acknowledgment

We would like to express our gratitude to the UAE Space Agency as they have supported this project by a grant (J06-2016-001). We would like to thank the UAE National Center for Meteorology and Seismology (NCMS) for letting us the use of their weather station locations to implement the second and third towers.

References

- Atreya, P. & Christou A. (2006). "The Armagh Observatory meteor camera system." In Bettonvil F. and Kac J., editors, *Proceedings of the International Meteor Conference*, Roden, The Netherlands, 14-17 September 2006. IMO, pages 141-145.
- Flohrer, J., Oberst, J., Heinlein, D., & Grau, T. (2012). "The European Fireball Network 2011 – Status of Cameras and Observation Results in Germany". European Planetary Science Congress, Madrid, Spain 23-28 September 2012.
- Jenniskens, P., Gural, P., Dynneson, L., Grigsby, B., Newman, K., Borden, M., Koop, M. & Holman, D. (2011). "CAMS: Cameras for Allsky Meteor Surveillance to establish minor meteor showers." *Icarus*, 216(1), pages 40-61.

Minor meteor shower anomalies 2018: predictions and observations

Jürgen Rendtel¹

¹ Leibniz-Institut für Astrophysik, An der Sternwarte 16, 14480 Potsdam
and International Meteor Organization, Eschenweg 16, 14476 Potsdam, Germany
jrendtel@web.de

Predictions of possible meteor shower activity based on meteoroid stream modelling is regularly provided with the Meteor Shower Calendar. We use different data sets to verify predictions. The selected events of 2018 include the η -Aquariids (activity enhancement related to ancient Maya recordings), the September ε -Perseids (slight rate enhancement from model assumptions) and the December φ -Cassiopeids (assumed to be related to the past Andromedids). These three events did not yield conclusive activity in the available data, while the Draconids yielded higher rates than predicted. The main conclusion is to alert many observers to improve the data sample particularly for weak shower activity.

1 Introduction

The IMO Meteor Shower Calendar, published annually since 1989, includes predictions of meteor shower activity based on model calculations issued by various researchers and provided usually as personal communication during the calendar preparation phase in the middle of the preceding year. There at least two intentions to publish these predictions, even if they concern only vague chances of minor events:

1. We want to monitor the meteor activity by different techniques, including visual data. Visual observers, however, concentrate their efforts to major showers and an additional alert is helpful.
2. Providing observational data of modelled events may be used for verification of the model parameters. This holds for both “positive” and “negative” results.

In the 2018 Calendar (Rendtel, 2017), apart from the annual shower returns, we listed the events given in Table 1. The authors listed in the “source” column provided me with their modelling results in the preparation phase of the Shower Calendar (which is May of the preceding year).

The optical data comprise the ZHR obtained from the IMO’s Visual Meteor DataBase and the meteoroid flux density (hereafter shortened as flux) from the IMO Video Meteor Network and the new launched fluxviewer. Further, we use the “radio ZHR” as derived from Hirofumi Sugimoto from radio forward scatter data (see description given in Rendtel, Ogawa and Sugimoto, 2016). Unfortunately, we cannot analyse several of the events due to lack of data. This may concern real gaps in the data recordings or the shower activity has not been derived from the data. Here we describe results concerning the events with some data within or very close to the interesting intervals.

2 Eta Aquariid “Maya-peak”

This possible activity predicted by Kinsman and Asher (2017a) is fascinating as it combines historical notes and their interpretation with modern methods of meteoroid orbit evolution (Kinsman and Asher, 2017). The expected timings for the encounter of the 164BC-trail in 2018 were given as

- May 3, 19^h11^mUT ($\lambda_{\odot} = 43^{\circ}042$)
- May 5, 05^h49^mUT ($\lambda_{\odot} = 44^{\circ}441$)
- May 5, 07^h34^mUT ($\lambda_{\odot} = 44^{\circ}511$)

Unfortunately, the observing circumstances are generally difficult and substantial data can only be obtained from locations south of about 40° N. The shower is well visible from the southern hemisphere, but the number of observers is small. In 2018, the waning gibbous Moon added a problem (last quarter on May 8) as it illuminated the essential morning hours. Hence we have no continuous coverage of the interesting period with visual observations (no overlap of the observing periods). However, we can combine data of visual observations with video flux density (later shortened as flux) data of the IMO Video Meteor Network, using the new fluxviewer (Molau, 2020). Further, the radio ZHR derived forward scatter data are available.

Both optical data sets (Figure 1) cover only a portion of the suspected interval with large gaps. The first of the listed positions ($\lambda_{\odot}=43^{\circ}042$) is not covered at all and the last available data point at $\lambda_{\odot} = 44^{\circ}43$ excludes the last position which was mentioned as most promising by Kinsman and Asher (2017a). There is no rate or flux increase in the covered periods. However, we find that right at the end of both the visual ZHR and the video flux show a decrease which at least confirms that the two independent data sets reveal identical information. The general level of the ZHR and flux, respectively, are at the annual average level or slightly below the level found in the recent returns. The radio forward scatter data are continuous and the derived ZHR shows a maximum at $\lambda_{\odot} = 43^{\circ}05$ which might

Table 1 – Possible rate anomalies as compiled in the 2018 Meteor Shower Calendar.

Date and time (UT)	Description and source	Data available in 2018 and results
May 03, 1911	η -Aquariids (031 ETA), possible activity derived from Maya	Section 2
May 05, 05–08	recordings (Kinsman & Asher)	
Sep 09, 1912	September ε -Perseids (208 SPE), weak activity (Sato)	Section 3
Sep 20, 1324	Possible meteors of 2009 SG ₁₈ from radiant in Cepheus (Vauvaillon)	No data reported
Oct 06, 0216	October Camelopardalids (281 OCT) (Lyytinen)	Details see Rendtel (2018)
Oct 08, 2333	Draconids (009 DRA), ZHR 10–15 (Vauvaillon, Maslov)	Section 6
Oct 09, 0014	Draconids, ZHR 20–50 (Sato)	
Nov 22, 0050	α -Monocerotids (246 AMO), possible minor activity (Sato)	Section 4
Dec 01–07	December φ -Cassiopeids (446 DPC) – meteoroids which appeared as Andromedids of 3D/Biela, weak activity in early December (Wiegert et al., 2013)	Section 5
Dec 22, 19–20	Ursids (015 URS), possible filament (Jenniskens 2006)	No reports close to filament position

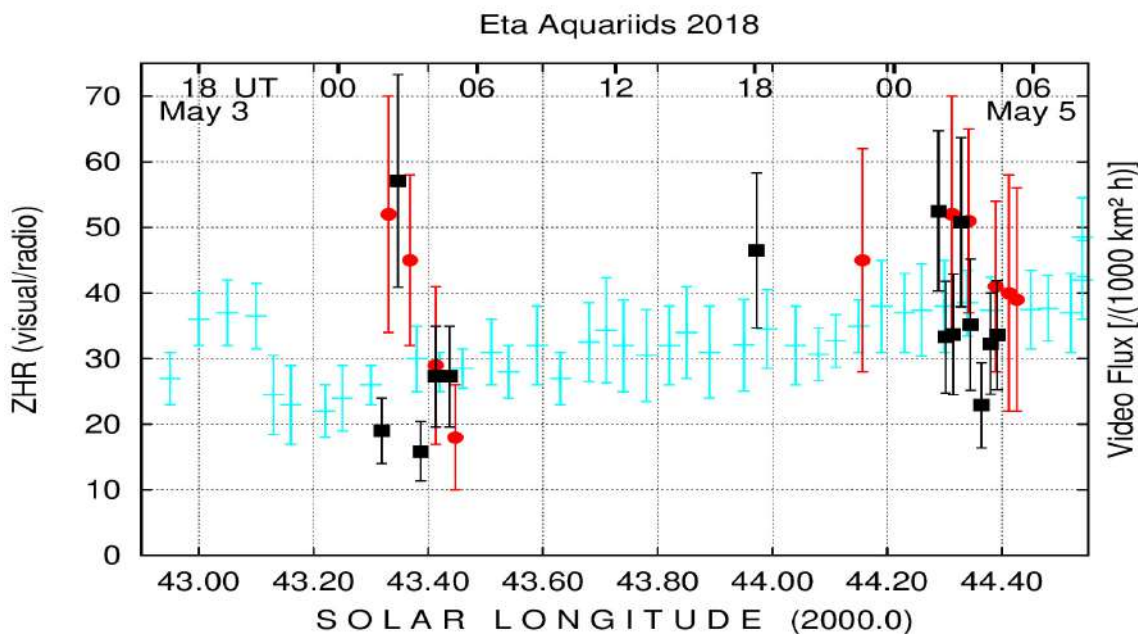


Figure 1 – Visual ZHR (dots), video flux density (squares) and radio ZHR (crosses) of the η -Aquariids in the interval of the possible encounter of the 164BC trail dust. $\lambda_{\odot} = 43^{\circ}00$ corresponds to 2018 May 3, 18^h00^m; 44^h40^mUT, respectively.

be associated with the May 3 timing. Interestingly, the first visual ZHR data between 43°33 and 43°45 may indicate a descent from higher values. The video flux data, with one high value at 43°35, do not support a systematic structure here. An identification of just one enhanced flux value does not seem appropriate given the limited sample, even if it coincides with the highest visual ZHR. On May 5, the radio ZHR has no obvious feature in the studied interval, but an increase 4–6 hours later at $\lambda_{\odot} = 47.7^{\circ} \pm 0.2^{\circ}$ which is close to the annual, broader ETA-maximum.

The available data contain no structure which may be reliably associated with the position derived from the inscriptions of the Maya period and the subsequent integration of the orbit evolution.

3 Minor September ε -Perseid activity?

The conditions for this far northern radiant are usually favourable for the potential observing latitudes as the duration of the night is long enough to establish overlapping observing periods. However, it seems that minor events do not create the same attention as possible peculiarities predicted for major showers or intense outbursts. Mikiya Sato (personal communication) made a prediction based on some assumptions:

- (1) the activity in recent years was caused by a long periodic cometary object,
- (2) the events observed in 2008 and 2013 are related to one dust trails, and
- (3) the 2013 encounter was closest to the potential parent (for timing).

This would hint at a minor activity enhancement on 2018 September 9, 19^h12^mUT ($\lambda_{\odot} = 166.801^{\circ}$).

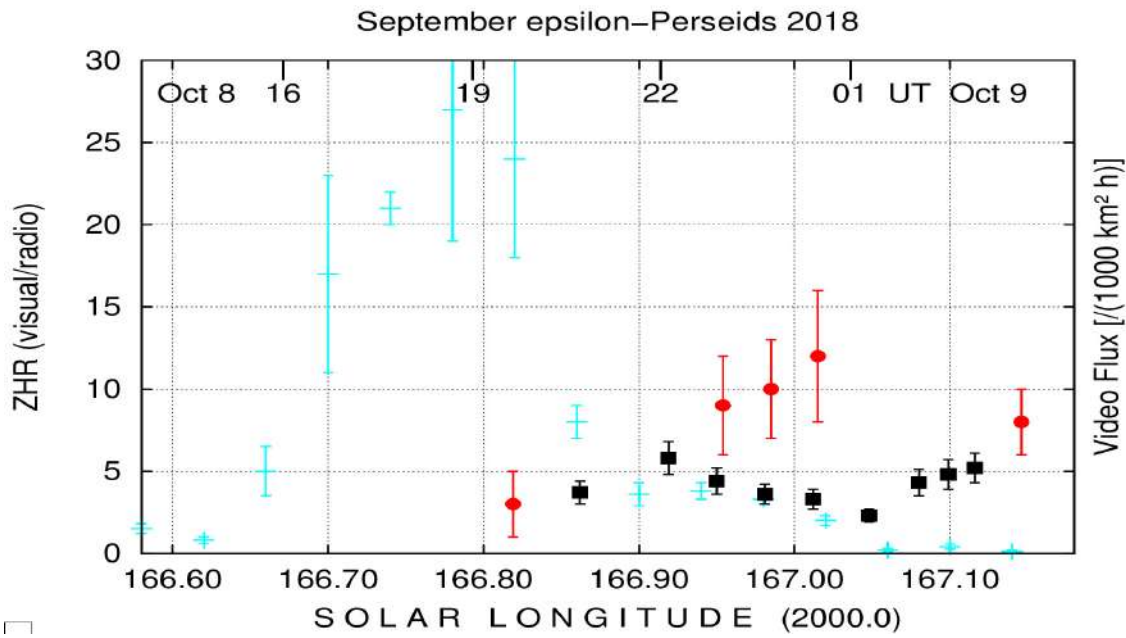


Figure 2 – Visual ZHR (dots), video flux density (squares) and radio ZHR (crosses) of the September ε -Perseids in 2018 close to the period of possible activity on September 9 between 16^h and 19^h UT (corresponding to $\lambda_{\odot} = 166^{\circ}7$ to $166^{\circ}8$.

Again, we use visual, video and radio data (Figure 2). Despite the possibly good astronomical conditions, the 2018 visual data set comprises only 45 shower meteors close to the period of interest, collected by 11 observers. Our first visual data point is already later than the predicted position; observers placed east of Europe did not submit reports. Unfortunately, the video data also do not provide a complete flux density profile. The only continuous data set is the radio ZHR. However, the level seems to be overestimated. This was already found in a previous analysis of minor shower data (Rendtel, Ogawa and Sugimoto, 2017). In that paper, a calibration with a factor of 0.25 was found to be appropriate. This would then yield a peak radio ZHR of about 7 instead of 27 in 2018.

The three data sets provide us with no consistent information. The continuous profile of the radio ZHR shows a clear and single maximum at $166^{\circ}78$. This is very close to the predicted position. However, the annual maximum also occurs at $166^{\circ}7$ and thus the slightly skew profile does not include a clue to an additional activity shortly after this. The two optical data sets seem to be rather contradictory. While the video flux profile has a dip at $167^{\circ}05$ and no obvious enhancement before that, the visual ZHR reaches a maximum virtually at the same position ($166^{\circ}02$). Hence it seems likely that we see mainly statistical fluctuations, particularly given the small samples of the visual observations. At least, there was nothing comparable to any of the previous returns. According to Lyytinen, the next impressive SPE return is not due before 2040.

4 α -Monocerotids

Obviously, due to bad observing conditions and moonlight interference, the period of possible minor activity

of the α -Monocerotids on 2018 November 22 which may have indicated further rate increases in 2019 and other years is not covered by visual and radio forward scatter data (referring to the activity analysis shown on Sugimoto's web page <http://www5f.biglobe.ne.jp/~hro/Flash-e/index.html>) in 2018. For this shower we find only one value from the video flux density showing an enhancement which is centered at $\lambda_{\odot} = 239^{\circ}73$ (2018 November 22, 08^h38^mUT). This differs a lot from Sato's prediction and as we have no "real profile" but only one flux value which is apparently higher than the annual average suggests. But from this we cannot derive an enhancement at a certain position. As a result, we cannot give any conclusive answer to the question whether the shower had any density fluctuation at the predicted position.

5 December φ -Cassiopeids

This case is another very interesting combination for different reasons. The shower is considered as successor of the famous Andromedids caused by the (currently inactive) comet 3D/Biela as pointed out by Wiegert et al. (2013). Due to the orbital evolution of the meteoroids, the radiant should now be located at another position, in Cassiopeia at $\alpha = 24^{\circ}$, $\delta = 50^{\circ}$. Thus observations would confirm both the radiant position and possible activity. Weak activity was recorded by the Canadian CMOR radar on 2011 December 5 at $\lambda_{\odot} = 252^{\circ}8$. The meteoroids were predominantly small and the rate corresponded to a ZHR of 50 (Wiegert et al., 2011). The DPCs showed up again in 2013 (peak at $\lambda_{\odot} = 255^{\circ}$) with an activity of about what it was in 2011 (Peter Brown, personal communication, 13 September 2019). In 2018, the CMOR data showed no detectable rates.

Contrary to the two events described above, there was

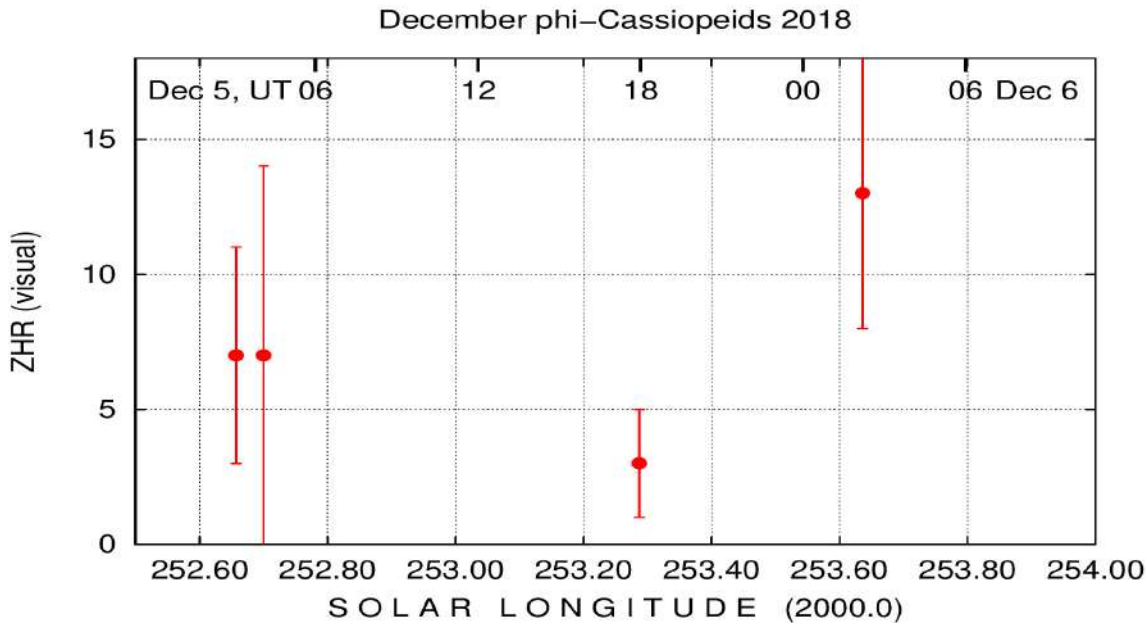


Figure 3 – Visual ZHR of the December φ -Cassiopeids in 2018 on December 5–6, close to the center of the period of possible activity around $\lambda_{\odot} = 254^{\circ}$.

no specific time for detectable activity given and observers were more or less asked to cover several nights “in early December”, centered at $\lambda_{\odot} = 254^{\circ}$, which is approximately 2018 December 6, 10^hUT. As already pointed out in the previous section, it is difficult to activate observers in such periods for several nights, which for many locations bring poor or at least uncomfortable observing conditions. So the check of the available data shown in Figure 3 yields no clear indication of meteors which can be associated to the DPC.

There were only six visual observers active in the first week of December. A total of 15 potential DPC meteors does not provide conclusive information. As a result we may calculate four intervals which contain 12 of these shower meteors. The last data point on December 5/6 yields the highest ZHR. However, it needs to be noted that this is comprised of data from two observers, both under regular conditions – one reported 6 DPC candidates, the other zero.

The video analysis of this month has not yet performed at this moment. Since the shower is not included in the database for the routine analysis, the fluxviewer (then using the temporary data) does not help because potential DPC meteors are not labelled as such.

We face a similar situation with the radio data. In a personal communication, Hirofumi Sugimoto said that he has no data available for this possible shower in 2018.

So the conclusion is, again, that the available data do not give a clue to the shower activity in 2018. Peter Brown summarized, that the DPC is an odd shower of occasional high activity, certainly worth monitoring. Wiegert et al.’s modelling suggests there could be enhanced activity again similar to 2008 or 2011. The next good chance to observe this shower will occur in 2023 (radiant at $\alpha = 29^{\circ}$, $\delta = +47^{\circ}$, peak position at

$\lambda_{\odot} = 250^{\circ}$ (Wiegert et al., 2013)).

6 Draconids

The return of the 2018 Draconids deserves a detailed analysis. Here we add just a brief description as an example of a confirmed activity and a case which showed a much higher activity than predicted. Observers should have this possibility in mind when thinking about an observing session with unknown chances.

For this shower we had three predictions given in the IMO Meteor Shower Calendar for 2018 (Rendtel, 2017) which are summarised as follows:

Sato:	Dust trail of 1953, disturbed, ZHR 20–50, October 9, 00 ^h 14 ^m UT
Maslov:	Several dust trails of low density, “best” the 1953 trail, ZHR \approx 15, October 8, 23 ^h 34 ^m UT
Vaubaillon:	Draconid evolution calculated from recent parent comet ephemeris, ZHR \approx 15, October 8, 23 ^h 31 ^m UT

In reality, observers were rewarded with an unusually high activity lasting for more than four hours: the ZHR reached 150 (Figure 4), exceeding the expectations a lot. Visual and video data confirm structures within the stream which are found in both data sets. The ZHR reached a first peak close to 23^hUT, followed by some variations seen in both the visual and video data. A late peak occurred shortly after 01^hUT, and the activity subsequently decreased towards the (European) morning hours. Seen the large variation of the radiant elevation during the observing period (from about 60° in the evening to about 20° in the morning, depending on the latitude), and the good coincidence of both

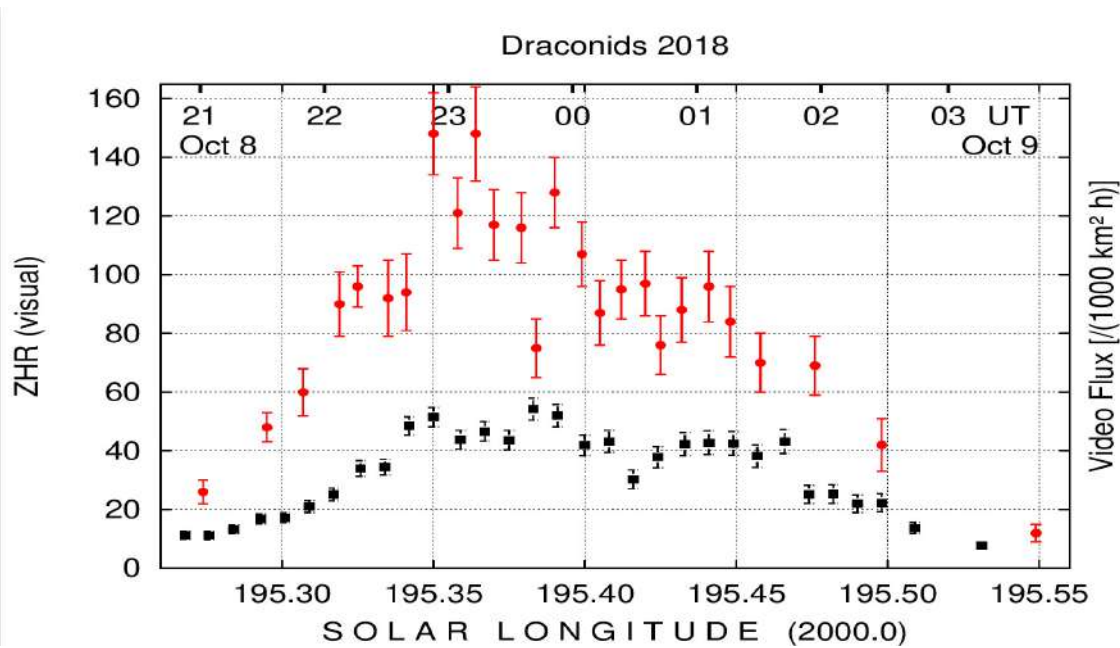


Figure 4 – Visual ZHR (dots) and video meteor flux density (squares) of the Draconid outburst on 2018 on October 8–9 using $r = 2.30$ for the entire profile. For both graphs we required at least 50 Draconid meteors per bin.

graphs, we may conclude that the visual observers were careful enough with the shower association. Details of these data sets are subject of a separate paper on the Draconids.

The derived radio ZHR at Sugimoto's web page reaches a peak value of about 140 which is in good agreement with the optical data. This indicates that the calibration of the radio ZHR may be more complex than just applying a constant factor. Since we will make use of the continuous radio recordings to find short outbursts or unusual activity this aspect needs further elaboration.

7 Conclusions

Three events analysed in this paper, did not show significant rates close to the predicted times. In the case of the ETA, the temporal coverage was not sufficient. The SPE rate and flux data do not yield a consistent image and the promising time according to the modelling was not covered by optical observations. Finally, the DPC activity basically remained below the detection limit mainly due to very limited temporal coverage.

Many observations, like the video and radio forward scatter systems, run (more or less) continuously. Nevertheless, in some cases the information about the event to look for needs to be implemented beforehand. Otherwise, it requires extra work to re-analyse the recordings.

The radio forward scatter analysis seems to be limited to either significant activity increases or to events which happen in periods with no other (dominant) activity as it depends on reference periods before (or after) the period under study. This probably affected the DCP period, because of numerous sources being active in early December.

Regarding the visual observers, there is a bias towards the major showers in all years. It seems difficult to alert enough observers to record visual data in one or two nights during a period known as usually poor in terms of meteor rates. Experience has shown that alerts may work in regional or national groups if the lunar conditions are favourable and the weather is expected to be good. Examples are the October Camelopardalids in 2018 (Rendtel and Molau, 2018) and the Draconids in 2018 (Rendtel, 2018) when we were able to alert German observers in time by personal mails. So we recommend that e.g. local groups inform their members shortly before predicted events are due and encourage to collect data. All such data is welcome, and bear in mind that the result may also be a “zero”.

Acknowledgements

Thanks to all observers who tried to collect data in and around the intervals which were supposed to show unusual activity.

Once we noted incoming data concerning the DPC, Vincent Perlerin immediately included the shower into the active meteor shower list of the input form which allowed us to collect the respective data.

Thanks to Sirko Molau for making video data available through the new fluxviewer webpage.

References

- Kinsman J.H., Asher D.J. (2017a). “Evidence of Eta Aquariid outbursts recorded in the classic Maya hieroglyphic script using orbital integrations”. *Planetary and Space Science*, **144**, 112–125.

- Rendtel J. (2017). “2018 meteor shower calendar”.
IMO_INFO (2-17).
- Rendtel J. (2018). “Oktober 2018: Draconiden-Outburst,
Camelopardaliden-Aktivität und normale Orioniden”.
Meteoros, **21**, 246–249.
- Rendtel J., Molau S. (2018). “October Camelopardalid
outburst 2018 October 6”. *WGN, Journal of the
IMO*, **46**, 173–175.
- Rendtel J., Ogawa H., Sugimoto H. (2016). “Quadrantids
2016: observations of a short pre-maximum
peak.” *WGN, Journal of the IMO*, **44**, 101–107.
- Wiegert P.A., Brown P.G., Weryk R.J., Wong D.K.
(2013). “The return of the Andromedids meteor
shower”. *Astronomical Journal*, **145**, article id. 70,
11 pp. DOI: 10.1088/0004-6256/145/3/70
- “Visual Meteor Data Base”, IMO webpage, http://www.imo.net/members/imo_vmdb/download

School of Meteor Astronomy at Petnica Science Center

Dušan Pavlović¹, Vladimir Lukić¹

¹ Petnica Science Center, Valjevo 14104, Serbia
dusan.pavlovicc@gmail.com

From 2009, Petnica Science Center and Petnica Meteor Group organized a specific program for high school students every year, to teach them basics of meteor astronomy. The program is designed for students to learn about the basic problems of meteor science, basic observational techniques and the broader context of meteor science (from planetary sciences perspective to meteoritics). Along with the lectures and demonstrations, the school is equally focused on the projects on which students are working during the school (and after it), from which some expanded even to the level of IMC contributions in the past years. The main idea is to educate youngsters about the meteor science and give them a framework to recognize and interpret the problems which meteor science had in the past, and the modern problems which are accessible to them, and to develop the reasoning needed to solve them. Also, the School of Meteor Astronomy is the introductory program for most of the Petnica Meteor Group visual observers. We will present the basic structure, ideas and methods of our educational system in the hope that this can become a model or an inspiration for other meteor groups and institutions, because we had a strong opinion that education of this kind is necessary for the amateur meteor community to develop.

Meteor pairs among Geminids

Pavel Koten¹, David Čapek¹, Pavel Spurný¹, Rostislav Štork¹, Vlastimil Vojáček¹, and Jan Bednář²

¹ Astronomical Institute of CAS, Ondřejov, Czech Republic

koten@asu.cas.cz

² Faculty of Electrical Engineering, Czech Technical University, Prague, Czech Republic

Inspection of the archived video data revealed several of Geminid meteors which appear in pairs. Higher than statistically expected number of random pairs was found during the night of December 13-14, 2006. Moreover, one triplet of Geminid meteors was recorded, too. Both time and spatial separations of the meteoroid particles suggest that the most probable place where the separation could occur is up to 4 million kilometres from the Earth up to one day before the encounter with our planet.

1 Introduction

The existence of the pairs and larger groups of the meteors was already investigated in several papers. Although there were several positive detections of such clusters – e.g. Hapgood and Rothwell (1981), Piers and Hawkes (1993), Kinoshita et al. (1999), Watanabe et al. (2002), Watanabe et al. (2003), Koten et al. (2017) etc. – the general prospect is rather negative. Porubčan et al. (2002) statistically analysed radar data on several meteor showers and found that among young streams the grouping is possible, but among older stream they did not find any evidence for such behaviour. Also, Gural and Jenniskens (2000) did not see clustering among 1999 Leonids but rather a uniformly random temporal distribution of the particles.

When digitalizing older videotapes of our video observation archive we recognized a relatively higher number of meteors which appear in pairs. It was the case of the 2006 Geminid observation campaign, therefore we decided to investigate the possibility that the pairs can be present within this relatively old meteor shower.

2 Observations, data processing

The analogue observations were carried out by the S-VHS cameras connected with Mullard XX1332 image intensifiers and 50 mm lenses since 2005. The cameras were usually deployed at the Ondřejov and Kunžak stations. Distance between them is 92.5 km, the azimuth of the southern station is 340° (e.g. Koten et al., 2004).

The digitalized records were measured by MAIAMetPho software (Koten et al., 2016). The atmospheric trajectories and heliocentric orbits were calculated using standard procedures (Borovička, 1990). Some meteors were observed only from one station. In such cases, it was supposed that they belong to Geminid meteor shower and their atmospheric trajectories were calculated using the shower initial velocity. If the prolonged line of the meteor flight deviated less than 5 degrees from the Geminid radiant they were marked as the shower members.

Up to now 3.5 hours of the observations carried out on the night December 13 to 14, 2006 were analysed. 350 single and double station meteors were recorded during this period. About 230 Geminids were among them. When two consecutive meteors appeared within less than 2 seconds they were selected as possible candidates for the meteor pair. Having this condition 9 pairs were found. One of them was actually a triplet of meteors.

3 Statistics of random appearance

When searching for the meteor pairs and clusters the Poisson distribution can be taken into account (Sampson, 2007). The expected number of random appearances N is given by the equation:

$$N = n \frac{\mu^x}{x!} e^{-\mu},$$

where n is the number of intervals, μ is the number of meteors per interval and x is the number of meteors within the cluster. If the interval is 2 seconds, the number of intervals per hour is 1800. Taken into account ZHR for Geminids to be about 100 then $\mu = 0.056$. If we look for a pair, $x = 2$. The probabilities of random appearance for several parameters are summarized in Table 1.

Table 1 – Statistical number of random pairs in one hour of observations.

Δt	n	μ	x	N
2 s	1800	0.056	2	2.7
1 s	3600	0.028	2	1.4
1 s	3600	0.028	3	0.013

As the majority of selected cases occurred within 1 second ($\Delta t = 1$ s), we can expect 5 – 6 random pairs of Geminid meteors within the observational period of 3.5 hours. Note that an actual number of random appearance is probably even lower since visual ZHR was taken into

account. The hourly rates for narrow field-of-view camera ($\Theta = 44^\circ$) usually does not reach visual values.

Therefore at least some of 9 pairs observed per 3.5 hours are from the statistical point of view non-random cases. When three meteors within 1 second are recorded, we can expect only 0.05 of random cases within this observation interval.

4 Geminid pairs

With known atmospheric trajectories of all potential candidates, their spatial distances were calculated. If the meteors appeared at the same time, the positions for the same frame were taken into account. If not, the average movement per one frame was calculated for the second meteor and then its hypothetical position for the initial frame of the first one was deduced. Having this location, the spatial distance of both meteors was calculated.

Table 2 – Summary of the results for recorded pairs. The error of ΔD determination is up to 1 km.

Meteors	Δt [s]	ΔD [km]
0C613xxx		
040, 041	0.40	28.6
069, 070	0.16	22.6
090, 091	0.36	21.5
130, 131	0.88	43.1
153, 154	1.30	70.4
196, 197	0.14	72.8
255, 256	1.08	101
308A, 308B	0.76	36.4

Let's look at the meteors 06C13069 and 0C613070 recorded at 23:03:04 UT as an example. The second one started only 4 frames later than the first one, i.e. $\Delta t = 0.16$ s. As Figure 1 shows, both meteors occurred at a similar range of heights. The photometric masses of both meteors were $2.1 \cdot 10^{-3}$ g and $5.5 \cdot 10^{-4}$ g. Spatial distance ΔD between them was 22.6 km. 3D view of their atmospheric trajectories is shown in Figure 2. When projected on the ground both meteors occurred in a small area of 23.25×17.7 km, which means about 295 km^2 .

Other candidate meteors were processed in the same way. The results are summarized in Table 2. The spatial distances are between 20 and 100 km. Majority of the pairs occurred within 1 second with only two exceptions when the time separation was a bit above 1 second.

Moreover also a triplet of Geminid meteors was detected at 0:30:22 UT. The composite image of all three meteors is shown in Figure 3. The meteor 260A was followed by 0.6 s by 260B. The smallest distance between them was 41.6 km. The 261 was observed 0.3 s later separated from 260A by 82 km. The spatial distance between 260B and 261 was 92 km. When projected on the ground all three

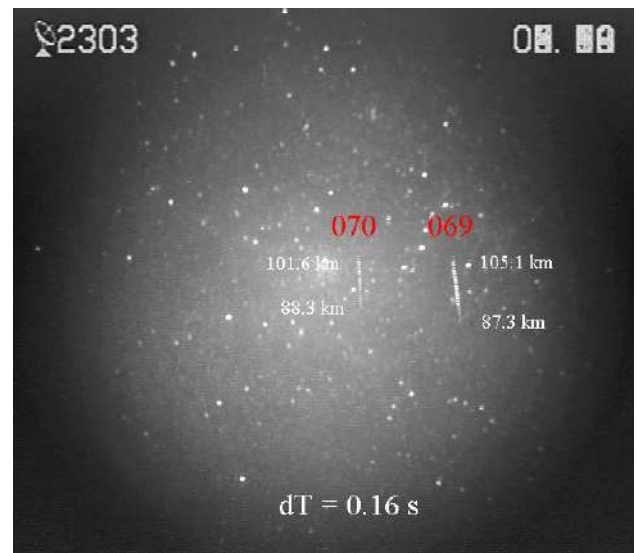


Figure 1 – The composite image of two Geminid meteors 06C13069 and 06C13070 which appeared within 0.16 s.

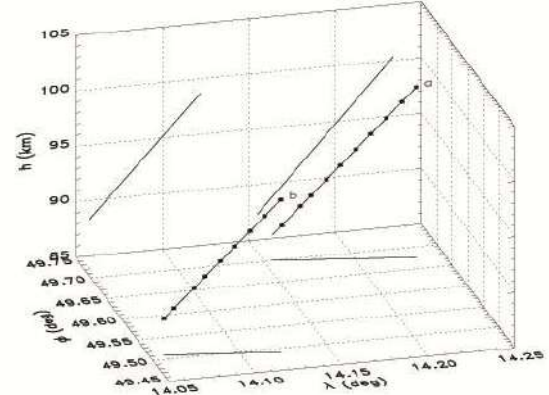


Figure 2 – The 3D map of the atmospheric trajectories of the meteors 06C13069 and 06C13070. X-axis represents the geographic longitude, y-axis the geographic latitude and z-axis the height.

meteors cover the area smaller than 4000 km^2 as shown on Figure 4.

Altogether we have 8 pairs and 1 triplet – this can be supposed as 3 other pairs. Sure that it is still small number statistics, but it is higher than the expected number of random appearance. When plotting ΔD vs. Δt we can see that distance increases with increasing time separation. The plot is shown in Figure 5. The question arises – does this plot suggest that the separation of the meteoroids occurred relatively shortly before the observation?

5 Origin of pairs

Assuming that the pairs are real cases we can discuss their possible origin. With masses of order 10^{-2} to 10^{-4} g and distances up to 100 km we can suppose three possible scenarios:

- a) direct release from the parent body,
- b) separation within the atmosphere,
- c) separation in the vicinity of the Earth.

Direct release from the parent body

The parent body of the Geminid meteor shower is asteroid 3200 Phaeton. At this moment we do not discuss how and when the release of the particles from the asteroid body occurred. The ejection velocities for the particles from the surface of Phaeton vary according to different models between 0.5 and 0.9 km.s^{-1} (Ryabova, 2013).

100 km distance is reached within about 3 minutes if the particles are released perpendicularly at a velocity of 0.5 km.s^{-1} . If the angle between velocity vectors of the particles is only 5° , it takes about 40 minutes to reach 100 km distance. Therefore even if the particles were released at a very similar velocity they can reach a distance of 100 km in a very short time in comparison with the time of orbital evolution. Moreover, the orbital evolution is different for the particles of different masses. From this point of view a direct release of the pair from the surface of the parent body is an unrealistic scenario.

Separation within the atmosphere

The geocentric velocity of the Geminid meteor shower is about 34 km.s^{-1} . Duration of such faint meteor as we observe is usually shorter than 1 second. To reach gaps between 20 and 100 km within such a short time interval requires the separation velocities of 10 to 100 km.s^{-1} . Such high velocities are impossible. Moreover, the trails of the meteors in the pairs are parallel when observed, which also suggests that the separation cannot happen very shortly before the observation.

Thus we can exclude this scenario, too.

Separation in the vicinity of the Earth

Let's assume the separation velocity of the particles to be about 1 m.s^{-1} . That such assumption is realistic, is shown for example in the paper of Hapgood and Rothwell (1981), which supposed velocities between 0.6 and 6.6 m.s^{-1} .

The distance between 20 and 100 km can be reached within 5.6 and 27.8 hours at this velocity. If the entry velocity of the Geminid meteor is about 39 km.s^{-1} the separation can occur 0.79 to 3.9 million kilometres from Earth.

6 Summary

This paper reports the very first results of the project dedicated to meteor pairs and clusters study. The number of included cases is still small. More potential candidates will be studied in the coming months.

Higher number of pairs than expected from random distribution was found for the video observation of the 2006 Geminid meteor shower. The detailed analysis of their atmospheric trajectories shows that distances between meteoroid pairs were up to 100 km. Moreover, one triplet of meteors was detected, too.

If the pairs are real than the separation of the meteoroids occurred most probably shortly before they reach Earth – up to one day at the distances up to 4 million kilometres.

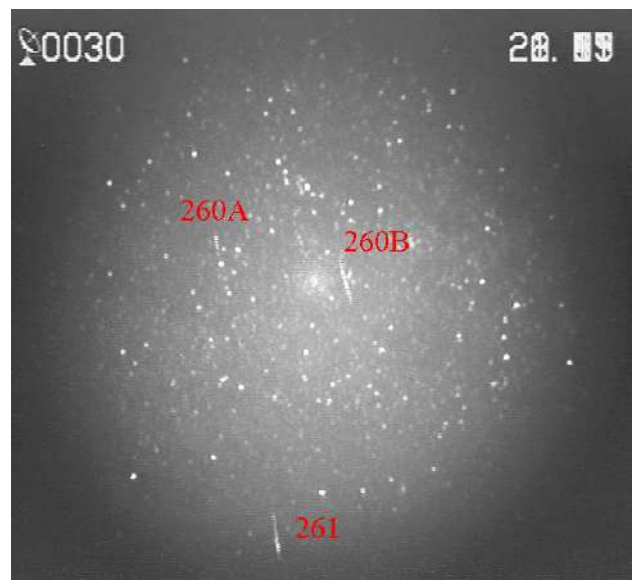


Figure 3 – The composite image of the Geminid triplet 06C13260A, 260B and 261.

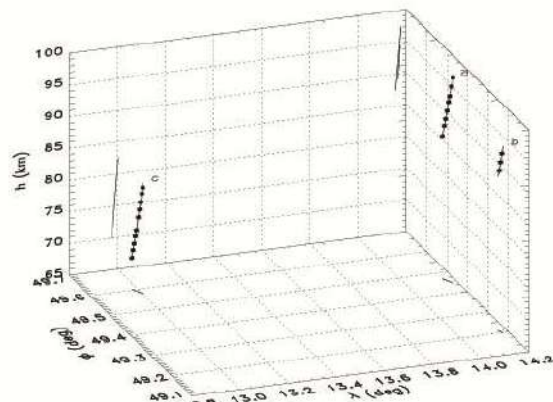


Figure 4 – The 3D plot of the Geminid triplet 06C13260A, 260B and 261 in the atmosphere.

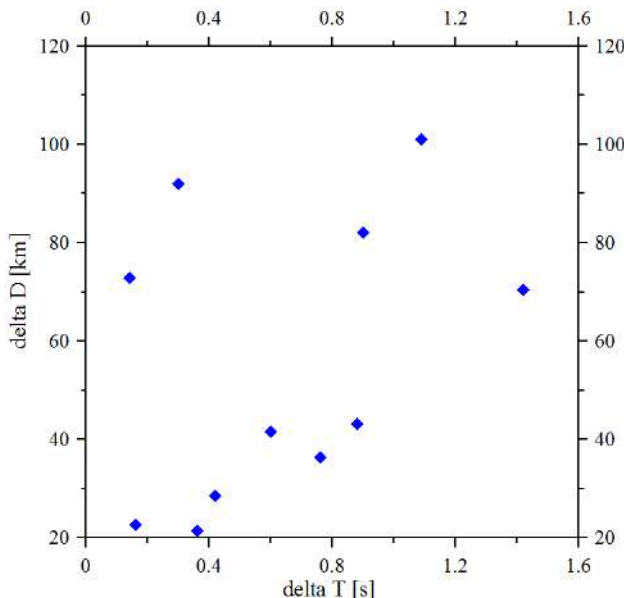


Figure 5 – Plot of the distance as a function of time delay for all Geminid pairs. Triplet is separated into 3 pairs for this plot.

Acknowledgement

This work was supported by grants number 17-05840S and 20-10907S from the Grant Agency of the Czech Republic and the Institutional Project RVO:67985815.

References

- Borovička J. (1990). "The comparison of two methods of determining meteor trajectories from photographs". *Bulletin of the Astronomical Institutes of Czechoslovakia*, **41**, 391-396.
- Gural P. S. and Jenniskens P. (2000). "Leonid Storm Flux Analysis from One Leonid Mac Video AL50R". (2000). *Earth, Moon and Planets*, **82**, 221-247.
- Hapgood M. A. and Rothwell P. (1981). "Fragmentation of a meteor in near-earth space". *Nature*, **290**, 384-386.
- Kinoshita M., Maruyama T., Sagayama T. (1999). "Preliminary activity of Leonid meteor storm observed with a video camera in 1997". *Geophysical Research Letters*, **26**, 41-44.
- Koten P., Borovička J., Spurný P., Betlem H., Evans S. (2004). "Atmospheric trajectories and light curves of shower meteors". *Astronomy & Astrophysics*, **428**, 683-690.
- Koten P., Štork R., Páta P., Fliegel K., Vítek S., (2016). "Simultaneous analogue and digital observations and comparison of results". In Roggemans A. and Roggemans P., editors, *Proceedings of the International Meteor Conference*, Egmond, The Netherlands, 2-5 June 2016. IMO, pages 133–136.
- Koten P., Čapek D., Spurný P., Vaubaillon J., Popek M., Shrbený L. (2017). "September epsilon Perseid cluster as a result of orbital fragmentation". *Astronomy & Astrophysics*, **600**, A74.
- Piers P. A. and Hawkes R. L. (1993). "An unusual meteor cluster observed by image-intensified video". *WGN, Journal of the IMO*, **21**, 168-174.
- Porubčan V., Tóth, J., Yano H. (2002). "On fragmentation of meteoroids in interplanetary space". *Contributions of the Astronomical Observatory Skalnaté Pleso*, **32**, 132-144.
- Ryabova G. O. (2013). "Modeling of meteoroid streams: The velocity of ejection of meteoroids from comets (a review)". *Solar System Research*, **47**, 219-238.
- Sampson R. D. (2007). "Modelling Meteor Clusters". *Journal of the Royal Astronomical Society of Canada*, **101**, 57-58.
- Watanabe J.-I., Sekiguchi T., Shikura M., Naito S., Abe S. (2002). "Wide-Field TV Observation of the Leonid Meteor Storm in 2001: Main Peak over Japan". *Publications of the Astronomical Society of Japan*, **54**, L23-L26.
- Watanabe J.-I., Tabé I., Hasegawa H., Hashimoto T., Fuse T., Yoshikawa M., Abe S., Suzuki B. (2003). "Meteoroid Clusters in Leonids: Evidence of Fragmentation in Space". *Publications of the Astronomical Society of Japan*, **55**, L23-L26.

Analysis of a boulder in the surroundings of 67P

J. Marin-Yaseli de la Parra¹, M. Kueppers¹ and the OSIRIS team²

¹ ESA European Space Astronomy Centre (ESAC), Camino bajo del Castillo s/n, Urb. Villafranca del Castillo, P.O. Box 78, 28691 Villanueva de la Cañada, Madrid, Spain

² Max-Planck-Institute for Solar System Research, Göttingen, Germany

jmarin@sciops.esa.int

Comet 67P/C-G is a dusty object. As it neared its closest approach to the Sun in late July and August 2015, instruments on Rosetta recorded a huge amount of dust enshrouding the comet including larger boulders.

1 Introduction

The dust is connected to the comet's proximity to the Sun; its heat causes the comet's nucleus to release gases into space, lifting the dust along. Spectacular jets were also observed, blasting more dust away from the comet. This disturbed, ejected material forms the coma, the gaseous envelope encasing the comet's nucleus, and can create a beautiful and distinctive tail. A single image from Rosetta's OSIRIS instrument can contain hundreds of dust particles and grains surrounding the 4 km-wide comet nucleus. Sometimes, even larger chunks of material left the surface of 67P/C-G – as shown here. The sizeable chunk in this view (Figure 1) was spotted a few months ago by astrophotographer Jacint Roger from Spain, who mined the Rosetta archive, processed some of the data, and posted the finished images on Twitter as an animated GIF. He spotted the orbiting object in a sequence of images taken by Rosetta's OSIRIS narrow-angle camera on 21 October 2015. At that time, the spacecraft was over 400 km away from 67P/C-G's centre.

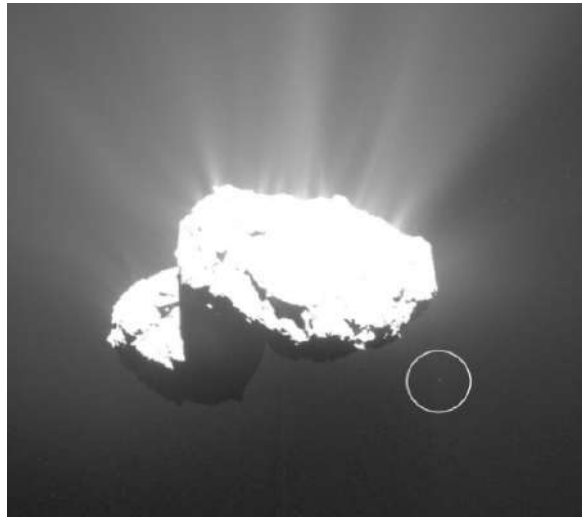


Figure 1 – The boulder image was recently published in ESA webpage. Credits by: ESA Rosetta MPS OSIRIS UPD LAM IAA SSO INTA UPM DASP IDA J. Roger (CC BY-SA 4.0).

During the perihelion phase of the orbit of Churyumov-Gerasimenko, a huge number of dust particles were discovered with the WAC and NAC cameras of the OSIRIS instrument. One single frame may contain hundreds

of particles from millimeter to decimeter sizes in the nearby coma of the comet. Dust jets increase the halo of dust around the comet. That helps for calculating the average mass loss rate per period.

Calculations are not so simple since two situations may occur. The diurnal thermal cycle plus the irregularities in the shape of the comet produce a flow of particles from the southern hemisphere to the northern and most particles are redeposited. However some areas, like the Hapi region, are eroded by around 1.0 ± 0.5 m per orbit. Some other areas are growing with deposits of dust creating moving shifting dunes. Some other particles are able to escape from the coma on open trajectories. An example of an escaped particle is shown in Figure 2. It was ejected in the morning of 2015 October 21. The image shows an open trajectory with a period of time of 1 hour.

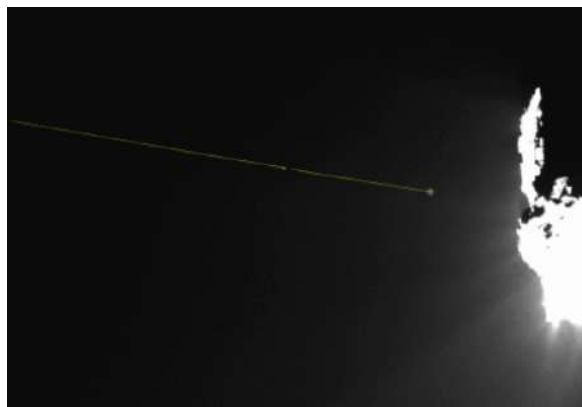


Figure 2 – An example of an ejecting boulder escaping from the gravity of the comet.

2 Methodology

It has been considered that the particle moved in the same plane perpendicular to the boresight of the camera. This is not correct. But the brightness of the pixels that conformed the boulder and the evolution of the trajectory indicates the angle between the boresight and the real plane of the orbit is not very big for a first approximation. A first determination of the size of the particle yielded a diameter between 3.5 and 4 metres. It can be observed that the particle distance from the centre of the comet increases with time.

After the first set of data made with 123 frames the boulder entered into the brightest area of the coma and the error value of the measures increases. Figure 3 shows the evolution of the boulder trajectory inside the coma. It is very interesting that theoretically the same boulder may have crossed the coma again since I identified another boulder of the same size on a very similar trajectory. Figure 4 shows the previous orbit and the identification of the second orbit.

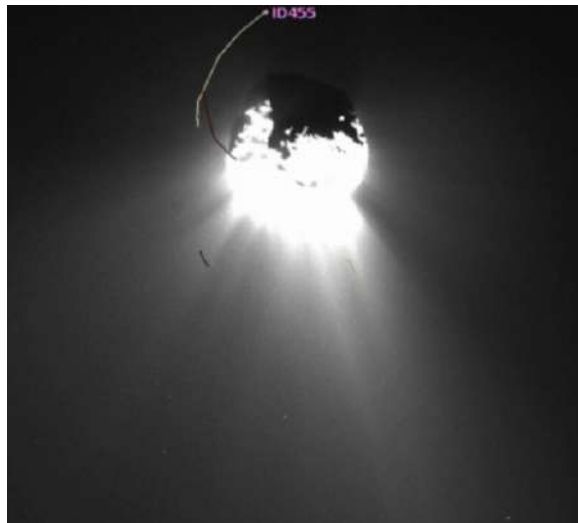


Figure 3 – The boulder trajectory determined with Image J using a tracking algorithm.

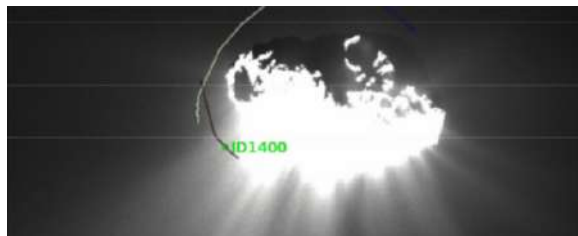


Figure 4 – After crossing the coma, a black trajectory can be observed visually overlapping the previous set of data.

If they are the same particle, the period of such orbit would last almost 2 days (compared to the 12 hours rotation of the comet) and a rough estimation of its relative velocity from the center of the comet would be around 0.5 km/h. According to Bertini et al. (2015), so far there are no clues which indicate that a satellite could describe stable trajectories along long periods of time since its survival would have been jeopardized by many adverse events. However this studies were based of outburst that were not strong enough to eject large objects. During the set of data described in this document, there are evidences of large boulders being ejected (see above). However a further study with predicted trajectories simulations could clarify if this boulder might be a stable “Churymoon” though the detailed observation of posterior images. So far it clearly present evidences of describing a closed trajectory around 67P. The radius of the orbit varies from 2.4 to 3.9 km and the Churymoon would have a diameter of less than 4 metres. It is very likely that the perturbations from the gas coma outflow models though the dust motion (Marschall et al., 2016; Keller et al., 2015; Thomas et

al., 2015) would limit this satellite lifetime to a small number of orbits around 67P.

After crossing the coma, a black trajectory can be observed visually overlapping the previous set of data. The analysis performed was developed using Trackmate platform for single-particle tracking (Tinevez et al., 2016).

Acknowledgements

OSIRIS was built by a consortium of the Max-Planck-Institut für Sonnensystemforschung, Göttingen, Germany, CISAS University of Padova, Italy, the Laboratoire d’Astrophysique de Marseille, France, the Instituto de Astrofísica de Andalucía, CSIC, Granada, Spain, the Research and Scientific Support Department of the European Space Agency, Noordwijk, The Netherlands, the Instituto Nacional de Técnica Aeroespacial, Madrid, Spain, the Universidad Politécnica de Madrid, Spain, the Department of Physics and Astronomy of Uppsala University, Sweden, and the Institut für Datentechnik und Kommunikationsnetze der Technischen Universität Braunschweig, Germany. The support of the national funding agencies of Germany (DLR), France (CNES), Italy (ASI), Spain (MEC), Sweden (SNSB), and the ESA Technical Directorate is gratefully acknowledged.

References

- Bertini I., et al. (2015). “Search for satellites near comet 67P/Churyumov-Gerasimenko using Rosetta/OSIRIS images.” *Astronomy & Astrophysics*, **583**, id.A19, 8 pp.
- Keller H.U., et al. (2015). “The changing rotation period of comet 67P/Churyumov-Gerasimenko controlled by its activity.” *Astronomy & Astrophysics*, **579**, id.L5, 4 pp.
- Marschall R., et al. (2016). “Modelling observations of the inner gas and dust coma of comet 67P/Churyumov-Gerasimenko using ROSINA/COPS and OSIRIS data: first results.” *Astronomy & Astrophysics*, **589**, id.A90, 17 pp.
- Thomas N., et al. (2015). “Redistribution of particles across the nucleus of comet 67P/Churyumov-Gerasimenko.” *Astronomy & Astrophysics*, **583**, id.A17, 18 pp.
- Tinevez J.-Y. et al. (2016). “Trackmate: 2.7.4-Snapshot Release (Includes Findmaxima Detector)” Zenodo, February 12 2016, DOI: 10.5281/zenodo.45973

Parent bodies of some minor showers

Luboš Neslušan¹ and Mária Hajduková²

¹ Astronomical Institute, Slovak Academy of Sciences, 059 60, Tatranská Lomnica, Slovakia
ne@ta3.sk

² Astronomical Institute, Slovak Academy of Sciences, Dúbravská cesta 9, 845 04 Bratislava,
Slovakia
astromia@savba.sk

This is a summary of selected studies in which we mapped whole meteor shower complexes of chosen parent bodies. The results are based on the same modelling procedure of meteoroid streams, which may provide new parent bodies, predict new meteor showers, find new relationships between a parent body and a shower, and confirm or exclude previously suggested relationships. Here we present the modelled meteoroid streams of four comets C/1964 N1, C/1975 T2, C/1979 Y1 and C/1963 A1, each causing at least one meteor shower in the Earth's atmosphere.

1 Summary

Studying the dynamical evolution of a meteoroid stream for a suitably long period can reveal alterations of the initial orbital corridor in which the orbit of the parent body is commonly situated. Alternative corridors of orbits are formed as a result of the influence of the gravitational perturbations of big planets and non-gravitational forces. If more than a single corridor of a given stream passes through the Earth's orbit, we observe several meteor showers associated with the same parent body.

For the stream modelling we used the procedure developed by Neslušan (1999), modified in Tomko & Neslušan (2012), and recently described in detail in Tomko & Neslušan (2019). For several perihelion passages of the parent comets we simulated associated streams using various strengths of the Poynting-Robertson effect, as described in Klačka (2014). We analyzed those parts of the streams which approached the Earth's orbit. The theoretical showers were compared with real meteor showers, which were selected from several meteor databases using the "break-point" method suggested by Neslušan et al. (2013). We used the photographic catalogues of the IAU MDC (Neslušan et al., 2014), video data from the IAU MDC CAMS database (Jenniskens et al., 2011, 2016), the SonotaCo catalogue (SonotaCo, 2009, 2016), the EDMOND database (Kornoš et al., 2014) and a collection of older radar data (Lindblad, 2003).

We also identified predicted showers with showers from the IAU MDC list (Jopek & Kaňuchová, 2014). A predicted shower which was not identified with any of the showers from the list, but for which we found a real counterpart, was suggested as a new meteor shower. We obtained the following results:

Our model of the C/1964 N1 (Ikeya) stream implies the existence of four distinct filaments that approach Earth's orbit (Neslušan & Hajduková, 2018a,b). They correspond to the showers July ξ -Arietids, #533, ϵ -Geminids, #023, and to ξ -Geminids, #178, although this relationship is rather uncertain. A real counterpart of the fourth filament was not found in the databases.

The meteoroid stream of the C/1975 T2 (Suzuki-Saigusa-Mori) does not split; theoretical particles which cross the Earth's orbit create a single meteor shower, which we identified with λ -Ursae Majorids, #524 from the IAU MDC list of showers. We can conclude that the comet is a parent body of this shower and, at the same time, we can exclude the comet's association with other showers (Hajduková & Neslušan, 2019).

The stream of comet C/1979 Y1 (Bradfield) divides into two parts which cross the Earth's orbit causing two regular showers (Hajduková & Neslušan, 2017). Due to a stronger P-R drag, the stream also crosses the Earth's orbit in other sections, creating transitory showers which are expected to survive for a limited period and to consist of particles of sizes in a narrow interval. The identification showed that one of the regular filaments represent the established shower July Pegasids, #175. The second regular theoretical shower was found among real meteors but not identified with any showers from the IAU MDC list. Thus, we suggest it is a new shower and name it α -Microscopiids. We also identified one of the transitory filaments to γ -Bootids, #104; however, it is a shower represented only by 2 meteors in the list at the moment.

Comet C/1963 A1 (Ikeya) is, according to our simulations, the parent body of five meteor showers (Neslušan & Hajduková, 2019). Three of the predicted showers were identified with π -Hydrids, #101, δ -Corvids, #729 and, less certainly, with November α -Sextantids, #483. The fourth prediction is a new meteor shower, which we named ϑ -Leonids. The last shower was predicted to have few members, and hence no real counterpart was found in the databases.

The mean geophysical parameters of the real meteor showers are summarized in Table 1., and their mean orbital elements in Table 2. The real showers were separated according to our predictions from three video databases, CAMS (Jenniskens et al., 2016), SonotaCo (SonotaCo, 2009) and EDMOND (Kornoš et al., 2014).

Table 1 – Mean geophysical parameters of the real meteor showers related to the streams of four chosen comets. Symbols used: Cat.No. - working numbers used in original papers (listed under references) which correspond to a specific modifications of the particular shower separated from various databases (C - CAMS, S - SonotaCo, E - EDMOND) using different threshold values of the Southworth-Hawkins D-discriminant, D_{lim} ; $\langle\lambda_{\odot}\rangle$ - mean solar longitude, $\langle\alpha\rangle$ and $\langle\delta\rangle$ - mean equatorial coordinates of geocentric radiant, $\langle V_g \rangle$ and $\langle V_h \rangle$ - mean geocentric and heliocentric velocities, N - number of meteors in given modification.

Cat. No.	D_{lim} [1]	$\langle\lambda_{\odot}\rangle$ [deg]	$\langle\alpha\rangle$ [deg]	$\langle\delta\rangle$ [deg]	$\langle V_g \rangle$ [km s $^{-1}$]	$\langle V_h \rangle$ [km s $^{-1}$]	N [1]	parent body
July ξ-Arietids #533 (Neslušan & Hajduková, 2018a,b)								
25C	0.10	113.2 ± 7.4	36.2 ± 5.5	8.9 ± 2.1	68.8 ± 0.5	41.1 ± 0.5	18	C/1964 N1
3S	0.08	101.3 ± 34.9	35.3 ± 3.2	8.9 ± 1.2	69.4 ± 0.4	41.7 ± 0.3	20	
ϵ-Geminids #23 (Neslušan & Hajduková, 2018a,b)								
14C	0.10	195.2 ± 7.8	96.0 ± 6.9	27.3 ± 1.0	70.4 ± 0.2	41.7 ± 0.2	9	C/1964 N1
20S	0.09	153.8 ± 81.3	92.2 ± 5.7	27.2 ± 0.9	70.5 ± 0.6	41.7 ± 0.5	10	
λ-Ursae Majorids #524 (Hajduková & Neslušan, 2019)								
C-1	0.13	214.6 ± 2.4	156.1 ± 3.2	48.0 ± 1.9	61.6 ± 1.2	41.8 ± 0.6	9	C/1975 T2
S-1	0.08	214.4 ± 1.1	157.5 ± 1.7	49.7 ± 1.1	60.8 ± 0.7	42.0 ± 0.4	21	
E-1	0.10	214.6 ± 1.3	157.7 ± 1.5	49.4 ± 0.8	60.8 ± 0.8	41.9 ± 0.4	19	
July Pegasids #175 (Hajduková & Neslušan, 2017)								
C	0.17	110.8 ± 5.5	350.0 ± 4.6	11.7 ± 1.6	64.1 ± 1.1	41.0 ± 1.0	81	C/1979 Y1
New meteor shower α-Microskopiids (Hajduková & Neslušan, 2017)								
C	0.19	294.8 ± 7.4	227.8 ± 6.8	-30.2 ± 2.8	64.8 ± 1.7	42.0 ± 1.5	10	C/1979 Y1
S	0.15	291.9 ± 7.5	224.4 ± 6.3	-30.8 ± 2.3	64.3 ± 1.3	41.8 ± 0.8	5	
New meteor shower ϑ-Leonids (Neslušan & Hajduková, 2019)								
S	$0.086 - 0.137$	235.3 ± 9.0	161.4 ± 7.0	13.0 ± 3.3	70.2 ± 0.7	41.4 ± 0.5	17	C/1963 A1
November α-Sextantids, #483 (Neslušan & Hajduková, 2019)								
C	$0.115 - 0.166$	222.9 ± 18.3	142.4 ± 13.4	1.4 ± 4.7	70.4 ± 1.1	42.6 ± 0.7	24	C/1963 A1
S	$0.085 - 0.145$	221.9 ± 5.9	140.6 ± 4.2	4.0 ± 2.0	69.9 ± 0.8	41.5 ± 0.7	17	
E	$0.185 - 0.227$	215.3 ± 10.0	136.8 ± 7.4	1.2 ± 3.2	68.4 ± 1.5	41.5 ± 0.6	31	
π-Hydrids, #101 (Neslušan & Hajduková, 2019)								
S	$0.036 - 0.078$	314.2 ± 5.2	207.2 ± 4.1	-20.0 ± 1.7	70.6 ± 0.6	42.0 ± 0.5	28	C/1963 A1
E	$0.115 - 0.138$	315.6 ± 8.1	209.5 ± 6.2	-20.3 ± 2.6	69.5 ± 0.8	40.7 ± 0.6	16	
δ-Corvids, #729 (Neslušan & Hajduková, 2019)								
S	$0.040 - 0.094$	287.8 ± 6.1	189.0 ± 4.3	-14.8 ± 1.7	71.5 ± 0.4	42.1 ± 0.3	15	C/1963 A1

Table 2 – Mean orbital elements of the real meteor showers related to the streams of four chosen comets. Symbols used: Cat.No. - working numbers used in original papers (listed under references) which correspond to a specific modifications of the particular shower separated from various databases (C - CAMS, S - SonotaCo, E - EDMOND) using different threshold values of the Southworth-Hawkins D-discriminant, D_{lim} ; $\langle q \rangle$ - mean perihelion distance; $\langle a \rangle$ - mean semi-major axis; $\langle e \rangle$ - mean eccentricity; $\langle \omega \rangle$ - mean argument of perihelion; $\langle \Omega \rangle$ - mean longitude of ascending node; and $\langle i \rangle$ - mean inclination to the ecliptic.

Cat. No.	$\langle q \rangle$ [au]	$\langle a \rangle$ [au]	$\langle e \rangle$ [1]	$\langle \omega \rangle$ [deg]	$\langle \Omega \rangle$ [deg]	$\langle i \rangle$ [deg]	parent body
July ξ-Arietids #533 (Neslušan & Hajduková, 2018a,b)							
25C	0.854± 0.036	75.8± 231.1	0.944± 0.040	312.5± 5.7	293.2± 7.4	170.7± 1.4	C/1964 N1
3S	0.857± 0.027	20.6± 35.6	0.992± 0.028	313.4± 4.3	292.2± 4.4	171.1± 1.5	
ϵ-Geminids #23 (Neslušan & Hajduková, 2018a,b)							
14C	0.905± 0.032	28.6± 16.8	0.960± 0.018	215.7± 6.0	195.2± 7.8	172.6± 1.8	C/1964 N1
20S	0.907± 0.030	5.9± 14.9	0.967± 0.040	215.6± 6.1	191.8± 6.5	173.2± 1.6	
λ-Ursae Majorids #524 (Hajduková & Neslušan, 2019)							
C-1	0.917±0.007	245.9±428.4	0.958±0.049	147.5±1.6	214.6±2.4	118.3±3.9	C/1975 T2
S-1	0.920±0.007	29.2± 35.4	0.976±0.035	148.3±1.7	214.4±1.1	115.2±1.9	
E-1	0.918±0.009	19.1± 27.6	0.966±0.036	147.7±2.2	214.6±1.3	115.3±1.8	
July Pegasids #175 (Hajduková & Neslušan, 2017)							
C	0.582±0.042	259± 427	0.961±0.054	262.8±5.4	110.8±5.5	148.7±1.8	C/1979 Y1
New meteor shower α-Microskopiids (Hajduková & Neslušan, 2017)							
C	0.457±0.063	308± 477	0.982±0.063	265.1±8.4	114.8±7.4	151.9±3.9	C/1979 Y1
S	0.456±0.051	35± 37	0.971±0.031	264.8±6.4	111.9±7.5	148.5±3.6	
New meteor shower ϑ-Leonids (Neslušan & Hajduková, 2019)							
S	0.854± 0.037	19.8± 21.9	0.925± 0.039	136.1± 6.9	235.3± 9.0	171.2± 2.2	C/1963 A1
November α-Sextantids, #483 (Neslušan & Hajduková, 2019)							
C	0.889± 0.063	599.± 484.	1.024± 0.060	324.7± 12.9	42.9± 18.3	158.0± 5.5	C/1963 A1
S	0.913± 0.029	16.4± 22.6	0.928± 0.056	327.0± 6.2	41.9± 5.9	160.8± 2.6	
E	0.855± 0.049	16.7± 20.0	0.936± 0.051	316.3± 9.5	35.3± 10.0	153.3± 7.4	
π-Hydrids, #101 (Neslušan & Hajduková, 2019)							
S	0.871± 0.030	26.1± 31.6	0.963± 0.037	40.0± 5.9	134.2± 5.2	165.1± 2.1	C/1963 A1
E	0.873± 0.039	8.0± 6.0	0.864± 0.049	40.5± 8.2	135.6± 8.1	165.8± 3.8	
δ-Corvids, #729 (Neslušan & Hajduková, 2019)							
S	0.969± 0.012	37.0± 36.0	0.970± 0.029	12.6± 6.5	107.8± 6.1	162.7± 2.0	C/1963 A1

Acknowledgements

The work was supported by the Slovak Scientific Grant Agency, grant No. VEGA 2/0037/18, and by the Slovak Research and Development Agency, contract No. APVV-16-0148.

References

- Hajduková M. and Neslušan L. (2017). “Regular and transitory showers of comet C/1979 Y1 (Bradfield)”. *A&A*, **605**, A36.
- Hajduková M. and Neslušan L. (2019). “Modeling of the meteoroid stream of comet C/1975 T2 and λ -Ursae Majorids”. *A&A*, **627**, A73.
- Jenniskens P., Gural P. S., Dynneson L., Grigsby B. J., Newman K. E., Borden M., Koop M., and Holman D. (2011). “CAMS: Cameras for Allsky Meteor Surveillance to establish minor meteor showers”. *Icarus*, **216**, 40–61.
- Jenniskens P., Nénon Q., Albers J., Gural P. S., Haberman B., Holman D., Morales R., Grigsby B. J., Samuels D., and Johannink C. (2016). “The established meteor showers as observed by CAMS”. *Icarus*, **266**, 331–354.
- Jopek T. J. and Kaňuchová Z. (2014). “Current status of the IAU MDC Meteor Showers Database”. *Meteoroids 2013*, pages 353–364.
- Klačka J. (2014). “Solar wind dominance over the Poynting-Robertson effect in secular orbital evolution of dust particles”. *MNRAS*, **443**, 213–229.
- Kornoš L., Koukal J., Piffi R., and Tóth J. (2014). “ED-MOND Meteor Database”. In Gyssens M., Roggeman P., and Zoladek P., editors, *Proceedings of the International Meteor Conference, Poznan, Poland, 22-25 August 2013*. pages 23–25.
- Lindblad B. A. (2003). “IAU Meteor Database of radar orbits version 2003”. *private communication*.
- Neslušan L. (1999). “Comets 14P/Wolf and D/1892 T1 as parent bodies of a common, alpha -Capricornids related, meteor stream”. *A&A*, **351**, 752–758.
- Neslušan L., Porubčan V., and Svoreň J. (2014). “IAU MDC Photographic Meteor Orbits Database: Version 2013”. *Earth Moon and Planets*, **111**, 105–114.
- Neslušan L., Svoreň J., and Porubčan V. (2013). “The Method of Selection of Major-Shower Meteors Revisited”. *Earth Moon and Planets*, **110**, 41–66.
- Neslušan L. and Hajduková, M. J. (2018a). “Meteoroid stream and meteor showers of comet C/1964 N1. Part II”. *Contributions of the Astronomical Observatory Skalnaté Pleso*, **48:4**, 554–583.
- Neslušan L. and Hajduková M. (2018b). “Meteor showers of comet C/1964 N1 (Ikeya)”. *A&A*, **616**, A162.
- Neslušan L. and Hajduková M. (2019). “Long-period comet C/1963 A1 (Ikeya), the probable parent body of π -Hydrids, delta-Corvids, November α -Sextantids, and θ -Leonids”. *A&A*, **accepted**.
- SonotaCo (2009). “A meteor shower catalog based on video observations in 2007-2008”. *WGN, Journal of the International Meteor Organization*, **37**, 55–62.
- SonotaCo (2016). “Observation error propagation on video meteor orbit determination”. *WGN, Journal of the International Meteor Organization*, **44**, 42–45.
- Tomko D. and Neslušan L. (2012). “Search for New Parent Bodies of Meteoroid Streams Among Comets. I. Showers of Comets 126P/1996 P1 and 161P/2004 V2 with Radiants on Southern Sky”. *Earth Moon and Planets*, **108**, 123–138.
- Tomko D. and Neslušan L. (2019). “Meteoroid-stream complex originating from comet 2P/Encke”. *A&A*, **623**, A13.

Where are the missing fireballs?

Keresztfuri A.¹, Steinmann V.^{1,2}

¹ Research Centre for Astronomy and Earth Sciences, Konkoly Thege Miklos Astronomical Institute, MTA Centre for Excellence
keresztfuri.akos@csfk.mta.hu

² Eotvos Lorand University of Sciences, Department of Physical Geography
steinmann.vilmos@csfk.mta.hu

The areal density of small and young craters was analyzed on the Moon and compared to atmospheric blast observations in the Earth. Focusing on the events produced by 0.15–0.32 m diameter exploded meteoroids, these would have produced 3.0–6.5 m sized craters on the Moon at the target area. Surveying the areal density of this size category craters gave 81 or 140 Ma accumulation period for them, according to different approaches. Comparing this to the number of observed atmospheric bolides, the expected number of impact craters would only be 0.03–0.06% of the observed number, suggesting that many fireballs burn up without notice in the Earth atmosphere.

1 Introduction

Crater formation on the Earth and the Moon is caused by the same bombardment rate, but the Earth atmosphere filters out the smaller object (below few dozen meter diameter). As a results, monitoring the Lunar surface for fresh impact events and recent cratering rate, the total possible number of the fireballs burned up in the Earth atmosphere could be estimated.

Several projects exist presently that are monitoring the Earth atmosphere (Koschny et al. 2019), thus it is worth to compare the atmospheric observation of impact rate and the Lunar crater observations based estimations.

2 Background of cratering rate

It is relatively poorly known what is the flux of impacting bodies in the intermediate size range (0.2–20 m, Drolshagen et al. 2019), produce the most often observed category of fireballs. Because of the large number of near-Earth asteroids orbit the Sun (Brown et al., 2002, Bottke et al., 2002, Losiak et al. 2016) they occasionally hit the Earth (Hargitai, 2009) or explode in the atmosphere (Bland and Artemieva, 2003). The filtering of atmosphere and the active surface erosion make it difficult to extrapolate the current impact rate using only the Earth surface. But the Moon is ideal for such analysis.

Global coverage of high resolution data from Lunar Reconnaissance Orbiter (LRO) mission (Jolliff et al., 2011; Losiak et al., 2009; Scholten et al., 2012; Waters et al., 2010) is available already. Recent attempts are being made to analyse statistically craters below 100 m diameter (Banks et al., 2012; Braden et al., 2014; Watters et al., 2012). The behavior of small impact craters is poorly known and recent degradation might happen (Mahanti et al., 2016), influencing the estimated age values. Very recent lunar craters, which formed between the acquisition of two images of the same area, could be also identified (Daubar et al., 2011; McBeath 2010, Oberst et al., 2012, Rainer and Danielle 2008, Zimnkoval

2017), while impact flashes were also observed from the Earth by (Madeido et al., 2014; Robinson et al., 2015; Speyerer et al., 2016).

3 Methods

During the estimation of fireball rate, images of Lunar craters and related age estimation, fireball rate monitoring from the Earth surface, and satellite based fireball occurrence data were analyzed and evaluated together. For the crater analysis on the Moon high resolution LROC images were used, the analysis was done with CraterTool (Kneissl et al., 2011) and CraterStat (Michael et al., 2010) software using the chronology system from Neukum (2001) for a separated size group (see the reasons later) and for all craters in the given area.

Those surface structures were considered as craters, if they had a more solar illuminated (brighter) part and opposite to this a less illuminated (darker) area, and together they formed a roughly circular shaped structure. Only the areas, which were smooth, not tilted, and provided a flat homogeneous surface for firm crater identification, were considered.

Age of a terrain is usually estimated using all craters in the area, but could also be determined for different crater size domains separately, as differently sized craters represent the rough age of different depth of the regolith layer. Different sized craters also have different lifetime on the lunar surface, where the smaller ones eroded faster – smaller impacts are more frequent and influence a shallower layer of the regolith than the rare larger impact events. In this work both approaches (selected crater group and all craters) were used. The results of age estimation are presented on diagrams with indicating crater size domains on the horizontal and spatial density of the craters in the vertical axis. The data points in such diagrams are arranged along tilted lines (called isochrones), usually in the smaller crater size domain (as larger craters positioned rightward rarely occur at a given surveyed area). Approaching the limit of spatial

resolution of the images (going leftward on the diagrams, the firm identification is getting more difficult, thus craters smaller than about 2 m were not counted, and here the distribution curve bents down).

Considering Earth surface based observations, the following datasets could be analyzed. They provide useful constrains (Ames et al. 2007), however they do not provide a global coverage of events nor in spatial neither in temporal terms. Useful statistics are available from camera systems being maintained in Canada (Brown et al. 2010, Weryk et al. 2008), Czech Republic (Spurny et al. 2007), Spain (Trigo-Rodríguez et al. 2004), a continent wide European Fireball Network (Oberst et al. 1998), Australia (Bland et al. 2003, Howie et al. 2017), and the US (Cooke and Moser 2012). The fireball events reported by the American Meteor Society in 2018 was 4301 (AMS), however most of these events are much smaller in energy than the typical ones used in this work.

Although several fireball observation projects are running currently, none one them provides global coverage and none is searching for daytime events regularly and successfully. Thus space based Earth atmosphere monitoring data were also applied in this work. The Center for Near Earth Object Studies (NASA CNEOS, Chodas 2018, Zhao 2010) maintains a global and homogeneous database for bright fireball and bolide events, using U.S. Government sensors recordings onboard geosynchronous elliptical orbit satellites. The system recorded fireball events between 14 May 1988 and 12 March 2018. Beside the date and location, the brightness is also recorded and provides data to calculate released kinetic energy.

The connection between lunar crater size and Earth atmospheric explosions establishes the kinetic energy (KE in Joule, and in KT in TNT kilotonnes). For simple craters using average impact speeds at the Earth solar distance, the radius of the impactor body is roughly equal of the 1/10 radius of the produced craters (for example a 10 meters diameter (5 m radius) craters have a diameter of 1 m (0.5 m radius) (Walsh et al. 2003).

4 Results

Based on the authors' earlier survey (Keresztsuri A., Steinmann V. 2017) of 0.1-0.2 km² areas, altogether 1.55 km² were surveyed and 2784 craters were identified of sizes between 2 and 102 m diameter (most of them below 20 m diameter), the spatial density ranging between 388-542 crater/km². The calculated ages show the accumulation periods of all craters at a given area, which ranged between 30 and 170 million years (Ma). The range is moderately large as the cratering process is a stochastic one and random fluctuation influences it.

For visualization Figure 1 shows an example area on the Moon, while in Figure 2 an example crater size frequency distribution (SFD) curve, presenting a "conservative"

approach to the surface age, used below as a reference. The target area was an average, non-sloping mare terrain in M117582609LC image, counting craters in a 0.24 km² terrain, near to the Lalande crater (S 4°24' W 8°35', Figure 1).

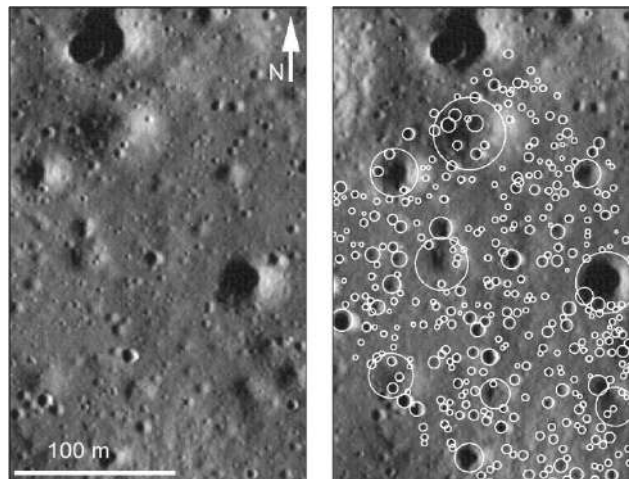


Figure 1. Example of LROC mage of the Lunar surface (left), and with the counted craters' silhouettes (right).

Two cases were considered for age estimation: only one Lunar crater size (and corresponding atmospheric blast class), and all crater size classes (and all corresponding atmospheric blast classes). The most populated class (3-6.4 m sized craters and 9.99E+09-9.98E+10 J explosions) gave an age estimate of 82 Ma (these craters accumulated during this period). The second case using all observed craters gave 140 Ma (that corresponds to all observed explosions in the whole range). The number of fireball events was translated to spatial density from global occurrence on the Earth to local occurrence on a given sized Lunar surface, and the extrapolation also covered the number of expected events from 29.83 years to the above listed two age values.

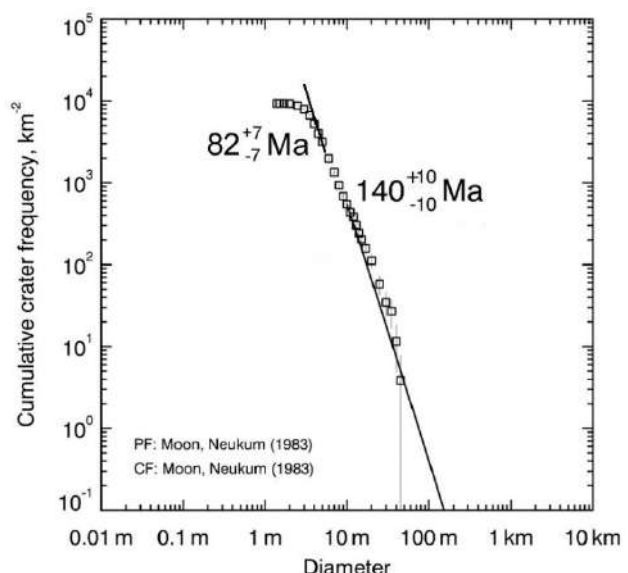


Figure 2. Example of the crater age estimation for the most common crater diameter range (top) between 2.98-6.42 m (giving an age of 80 Ma); and for all craters

(bottom) also with fitted age for a larger range (all observed craters, giving an age of 140 Ma).

Having a rough estimation on the impact rate from the Moon, the data could be linked to the fireball observations from the Earth if one calculates the released energies. The impact of a given size and speed body produces a given diameter crater – while the energy from an airblast in the Earth atmosphere could also be estimated using the maximal brightness of the given fireball or bolide explosion.

Using this approach, it can be estimated how many craters of this bombardment rate would have been produced on the Moon surface using two age values only from the most populated diameter category (2.98–6.42) linked to 82 Ma, and the age using all sized lunar craters (corresponding to a wider explosion category), was found to be 140 Ma.

Fireball and bolide observations

The most homogeneous observational data are available in the CNEOS database, recording 729 events between 14 May 1988 and 12 March 2018, 452 of which were in the 10^9 - 10^{10} KE range during almost 30 years. Among the observed ones the smallest fireball cause about 3 m crater with energy of $2E+10$ KE. The areal density of the atmospheric blasts was extrapolated to the whole area of Earth. The corresponding crater diameter range (second column in Table 1) shows the crater size that the given category of atmospheric blast would have produced if it had happened on the Lunar surface. The values range from 2.42 crater/km² to 0.11 crater/km² for the corresponding duration at differently sized craters (82 Ma and 140 Ma respectively).

Although several projects record bright fireball events in the Earth atmosphere, the burn up occurrence of dm-m sized impactor in the Earth atmosphere is poorly known. The main data source for this “fireball rate” was the CNEOS database (see the Method section). These numbers were compared to the observed areal density of lunar craters at the same size ranges in the Discussion section, to evaluate what fraction of the atmospheric blasts has been observed.

5 Discussion

According to the listed results and comparing the observed Lunar crater’s areal density with the

atmospheric blast observations on Earth, the occurrence of fireballs was extrapolated to the Moon (as they would produce craters there) and compared to the observed surface crater density, that formed during the corresponding duration.

Table 2. Comparison of the measured lunar craters’ areal density and the observed terrestrial fireballs’ occurrence with their corresponding areal density of craters they would produce during 82 Ma on the lunar surface.

Crater diameter (m)	Age of Lunar craters (Ma)	Areal density of Lunar craters (km ⁻²)	Areal density of atmospheric blasts (km ⁻²)
0 - 2.98	46	6.82×10^7	-
2.98 – 6.42	82	3.2×10^6	2.42
6.42 – 13.8	143	7.46×10^7	2.25
13.8 – 29.53	236	1.13×10^7	0.53
29.53 – 48.99	343	1.76×10^8	0.11

The crater size category <2.98 m corresponds to most atmospheric blasts. Starting from the observed 1635 lunar craters in the 2.98–6.42 m class, 6540 of them formed during 82 Ma at 1 km², and during this period 3.3×10^{12} such scale blast events should occur around the whole globe of the Earth, which means 4.02×10^4 (4020) annually. Including larger lunar craters with the 140 Ma accumulation duration, 2431 craters were produced and 4615 bolide events/year are expected. Extrapolating from these two numbers (corresponding to the 82 and 140 Ma accumulation periods) and the 29.83 years duration of the CNEOS survey, about 120,000 and 206,000 events should have been observed instead of the recorded 428 during these three decades. The difference is about a thousand times – although it is difficult to estimate exactly (as stochastic fluctuation might also influence the Lunar crater population), but the difference between the expected and observed atmospheric blasts on the Earth is definitely large, 0.03% and 0.06% respectively for the two different estimated ages.

fireball observations				lunar crater observations		
Kinetic Energy (J)	Corresponding crater diameter range (m)	Number of bolides by NASA	Hypothetical number of bolides (during lunar age)	Corresponding age of the lunar surface (Ma)	Lunar crater number	Areal density (crater/km ²)
9.99×10^9 - 9.98×10^{10}	2.98–6.42	452	1.24×10^9	82	1635	6540
9.98×10^{10} - 9.92×10^{11}	6.42–13.8	241	1.15×10^9	143	381	1524
9.92×10^{11} - 9.71×10^{12}	13.8–29.53	35	2.75×10^8	236	58	232
9.71×10^{11} - 4.43×10^{13}	29.53–48.99	5	5.72×10^7	343	9	36
$4.43 \times 10^{13} <$	48.99 <	1	-	-	-	-

Table 1. The number and the areal density of the terrestrial atmospheric blasts (left columns). The fourth column shows how many terrestrial fireballs would be observed on the Earth during the corresponding age of the analysed crater size class on the Lunar surface (in Ma). The diameter intervals were selected according to the exponent of the blast energy, thus the class boundaries are specific. The age of the analysed lunar area is the same in all categories.

Working in the reverse order, estimating the areal density of Lunar craters from the observed atmospheric blasts on the Earth is also possible. The events of $10^9\text{--}10^{10}$ KE would have produced 2.98–6.42 m sized craters on the Moon. Calculating with the 82 Ma only, 0.58 craters would have been formed at a 0.25 km^2 area (0.03% of the observed craters). Considering the 140 Ma age data, the observed fireballs rate that would have been produced is 1.61 craters at a 0.25 km^2 , (0.06% of the observed number).

Considering that the observed fireball rate in roughly 30 years, extrapolating it to the 82 or 140 Ma durations, there are large differences between the Lunar observation and Earth atmospheric blasts numbers. There are many fewer craters expected to form based on atmospheric blast observations than were found on the Moon. The difference decreases toward the larger object and crater size, but it still exists.

Evaluating the reasons for the difference, the following possibilities are relevant: The CNEOS database does not contain all of the events, which is definitely true. There could be some errors in the age estimation of lunar craters size frequency distribution based surface age estimation, specifically related to relatively recent ages and small craters. Here the equilibrium conditions (Povilaitis et al. 2018, Xiao and Werner 2015) possibly increase the error level especially for the small craters, below 10 m diameter (Keresztsuri and Steinmann 2018), but unfortunately this error is poorly known. However the results indicate that there is a large field of possibility for the emergence of currently unobserved fireballs. This might be because of daytime periods, cloudy sky, locations above the ocean and desert areas.

Good possibilities exists for projects that aim the above mentioned uncovered domain. These include the NEMO citizen science project (Drolshagen et al. 2019), which capture fireballs. Although the recording of daylight fireball events is difficult (Egal et al. 2016), there are successful examples (Docobo et al., 2017, Roggemans 2019) and improvement is expected in this domain (Blanch et al. 2017, Colas et al. 2014, Koschny et al. 2008). Using cheap digital cameras and automatized image analysis by machine learning algorithms, and exploitation of different databases (Rudawska et al. 2015), even daylight or twilight fireball detection (Roggemans 2019, Przemyslaw 2019) might became possible in the near future.

6 Conclusion

Using Lunar surface images and the small crater occurrence there and comparing the areal density to the occurrence of atmospheric explosions by fireballs on the Earth, the rough scale of optically unobserved fireball events could be estimated. Analyzing the NASA published CNEOS database, the most frequent bolides are caused by 0.15–0.32 m meteoroids, and would produce 3–6.5 m sized craters on the Moon. Starting from the currently accepted crater production and retention rates, the analyzed lunar surface area is 81 Ma old (calculating only with the small craters) or 140 Ma old (calculating with all craters).

Comparing the observed atmospheric bolide rate with the Lunar cratering rate, the expected number of impact craters would have been only 0.03–0.06% of the observed one. The difference is probably related to observational selection effect, caused by the lack of recording in daytime, above the oceans and non-inhabited land areas as well as bad weather periods. The argumentation suggests many impact events could happen undetected, thus improvement of detecting methods and development of new ones are necessary.

Acknowledgement

This project has been supported by Excellence of Strategic R&D centres (GINOP-2.3.2-15-2016-00003) of NKFIH, funded by EU R&D project. The support from the EUHUNKPT 2019 and the NEOMETLAB projects are also acknowledged.

References

- Ames A.P., Huyck J. L., Butler C. E., Johnson B. C., Pickering E., Nemiroff R. J. (2007). Determination of the 2006 Sporadic Fireball Rate from Continuous CCD Fisheye Monitoring. *Bulletin of the American Astronomical Society* 39, p.829.
- Beech M. (2008). Meteors over the Moon. *WGN* 36, 33–36
- Banks M.E., Watters T.R., Robinson M.S., Tornabene L.L., Tran T., Ojha L., Williams N.R., (2012). Morphometric analysis of small-scale lobate scarps on the Moon using data from the Lunar Reconnaissance Orbiter, *Journal of Geophysical Research: Planets* 117, E00H11.
- Blanch E., Trigo-Rodríguez J.M., Madiedo J.M., Lyytinen E., Moreno-Ibáñez M., Gritsevich M., Altadill D. (2017) Detection of Nocturnal and Daylight Bolides from Ebre Observatory in the Framework of the SPMN Fireball Network. *Assessment and Mitigation of Asteroid Impact Hazards, Astrophysics and Space Science Proceedings* 46, p. 185.

- Bland P.A., Artemieva N.A. (2003). Efficient disruption of small asteroids by Earth's atmosphere. *Nature* 424, 288-291.
- Bottke W.F., Morbidelli A., Jedicke R., Petit J.-M., Levison H.F., Michel P., Metcalfe T.S. (2002). Debiased Orbital and Absolute Magnitude Distribution of the Near-Earth Objects. *Icarus* 156, 399-433.
- Braden S.E., Stopar J.D., Robinson M.S., Lawrence S.J., van der Bogert C.H., Hiesinger H., (2014). Evidence for basaltic volcanism on the Moon within the past 100 million years. *Nature Geosci.* 7, 787-791.
- Brown P., Spalding R. E., ReVelle D. O., Tagliaferri E., Worden S.P. (2002). The flux of small near-Earth objects colliding with the Earth. *Nature* 420, 294-296.
- Brown P., Weryk R.J., Kohut S., Edwards W.N., Krzeminski Z. (2010). Development of an All-Sky Video Meteor Network in Southern Ontario, Canada The ASGARD System. *WGN* 38, 25-30.
- Chodas, P. 2018. Twenty Years of Tracking Near-Earth Objects: The Role of JPL's Center for NEO Studies (CNEOS). American Astronomical Society, DPS meeting #50, id.111.03.
- Colas F., Zanda B., Bouley S., Vernazza P., Gatacccea J., Vaubaillon J., Marmot C., Kwon M., Audureau Y., Rotaru M. (2014). FRIPON, a French fireball network for the recovery of both fresh and rare meteorite types. *Asteroids, Comets, Meteors* 2014. Proceedings, ed. by Muinonen et al.
- Cooke W.J., Moser D.E. (2012). The status of the NASA All Sky Fireball Network. *Proceedings of the International Meteor Conference*, Sibiu, Romania, Eds.: Gyssens, M.; and Roggemans, P. International Meteor Organization, ISBN 2978-2-87355-023-3, pp. 9-12.
- Daubar I.J., McEwen A.S., Byrne S., Dundas C.M., Keska A.L., Amaya G.L., Kennedy M., Robinson M.S. (2011). New craters on Mars and the Moon. *42nd Lunar Planet. Sci. Conf.* abstract 2232.
- Drolshagen E., Koschny D., Mialle P., Pilger C., Vaubaillon V., Drolshagen G., Poppe B. (2019). Combination of infrasound signals and complementary data for the analysis of bright fireballs. *Planetary and Space Science*, in Press.
- Docobo J.A., Campo P.P., Trigo-Rodríguez J.M., Madiedo J.M. (2017). A Very Bright Daylight Bolide Witnessed on May 17, 2016 Over Galicia, Spain. *48th Lunar and Planetary Science Conference*, abstract 1883.
- Egal A., Kwon M.K, Colas F., Vaubaillon J., Marmo C. (2016). The challenge of meteor daylight observations. *Proceeding of the International Meteor Conference*, Egmond, 73.75.
- Hargitai, H. 2009. Water Ejecta of Marine Impacts and Ice Meteorites. *40th Lunar and Planet. Sci. Conf.*, abstract 2439
- Howie R.M., Paxman J., Bland P.A., Towner M.C., Cupak M., Sansom E.K., Devillepoix H.A.R. (2017). How to build a continental scale fireball camera network. *Experimental Astronomy* 43, 237-266.
- Jolliff B.L., Wiseman S.A., Lawrence S.J., Tran Thanh N., Robinson M.S., Sato H., Hawke B.R., Scholten F., Oberst J., Hiesinger H., van der Bogert C.H., Greenhagen B.T., Glotch T.D., Paige DA., (2011). Non-mare silicic volcanism on the lunar farside at Compton-Belkovich. *Nature Geosci.* 4, 566-571.
- Keresztsuri A., Steinmann V. (2017). Characteristic of small young lunar impact craters focusing on current production and degradation of the Moon. *Planetary and Space Science* 148; 21-27.
- Keresztsuri A., Steinmann V. (2018). Terra-mare comparison of small young craters on the Moon: size distribution, depth and secondary sources. *Icarus* 322, 54-68.
- Kneissl T., van Gasselt S., Neukum G. (2011). Map-projection-independent crater size-frequency determination in GIS environments — New software tool for ArcGIS; *Planetary and Space Science* 59, 1243-1254.
- Koschny D., McAuliffe J., Barentsen G. (2008). The IMO Virtual Meteor Observatory (VMO): Architectural Design. *Earth, Moon, and Planets* 102, 247-252.
- Koschny D., Soja R., Engrand C., Flynn G.J., Lasue J., Levasseur-Regourd A.-C., Malaspina D., Nakamura T., Poppe A.R.; Sterken V.J.; Trigo-Rodríguez J.M. (2019). Interplanetary Dust, Meteoroids, Meteors and Meteorites. *Space Science Reviews* 215(4), id. 34, 62.
- Losiak A., Wilhelms D. E., Byrne C. J., Thaisen K. G., Weider S. Z., Kohout T., O'Sullivan K., Kring D.A. (2009). A New Lunar Impact Crater Database. *40th Lunar and Planet. Sci. Conf.*, abstract 1532.
- Losiak A., Wild E.M., Geppert W.D., Huber M.S., Jõeleht A., Kriiska A., Kulkov A., Paavel K., Pirkovic I., Plado J., Steier P., Välijä R., Wilk J., Wisnioski T., Zanetti M. (2016). Dating a small impact crater: An age of Kaali crater (Estonia) based on charcoal emplaced within proximal ejecta. *Meteoritics & Planetary Science* 51, 681-695.
- Mahanti P., Robinson M.S., Thompson T.J., Henriksen M.R. (2016). Small lunar craters at the Apollo 16 and 17 landing sites - morphology and degradation. *Icarus* 299, 475-501.

- Madiedo J.M., Ortiz J.L., Morales N., Cabrera-Cano J. (2014). A large lunar impact blast on 2013 September 11. *Mon. Not. R. Astron. Soc.* 439, 2364–2369.
- McBeath A. (2010). SPA Meteor Section Results: 2006. *WGN* 38, 184–192.
- Michael G.G., Neukum G. (2010). Planetary surface dating from crater size-frequency distribution measurements: Partial resurfacing events and statistical age uncertainty; *Earth and Planetary Science Letters* 294, 223–229.
- Neukum G., Ivanov B.A., Hartmann W.K. (2001). Cratering records in the inner Solar System in relation to the lunar reference system. *Space Sci. Rev.* 96, 55–86.
- Oberst J., Christou A., Suggs R., Moser D., Daubar I.J., McEwen A.S., Burchell M., Kawamura T., Hiesinger H., Wünnemann K., Wagner R., Robinson M.S. (2012). The present-day flux of large meteoroids on the lunar surface- A synthesis of models and observational techniques. *Planetary and Space Science* 74, 179–193.
- Oberst J., Molau S., Heinlein D., Gritzner C., Schindler M., Spurný P., Ceplecha Z., Rendtel J., Betlem H. (1998). The "European Fireball Network": Current status and future prospects. *Meteoritics & Planetary Science* 33, 49–56.
- Povilaitis R.Z., Robinson M.S., van der Bogert C.H., Hiesinger H., Meyer H.M., Ostrach L.R. (2018). Crater density differences: Exploring regional resurfacing, secondary crater populations, and crater saturation equilibrium on the moon. *Planetary and Space Science* 162, 41–51.
- Przemyslaw Z. (2019). Beta Taurids video campaign. International Meteor Conference, Ballmannsruh, Germany. p. 16.
- Rainer A., Danielle M. (2008). Meteoroid Environment Workshop and Call for Lunar Impact Observations. *WGN* 36, 83–86.
- Robinson, M.S., Boyd, A.K., Denevi, B.W., Lawrence, S.J., McEwen, A.S., Moser, D.E., Povilaitis, R.Z., Stelling, R.W., Suggs, R.M., Thompson, S.D., Wagner R.V., 2015. New crater on the Moon and a swarm of secondaries. *Icarus* 252, 229–235.
- Roggemans P. (2019). Bright daylight fireball April 6, 2019 above Krasnoyarsk, Russia. *eMeteorNews* 4(3), ISSN 2570-4745, p. 197.
- Rudawska R., Matlovič P., Tóth J., Kornoš L. (2015). Independent identification of meteor showers in EDMOND database. *Planetary and Space Science* 118, 38–47.
- Scholten F., Oberst J., Matz K.-D., Roatsch T., Wählisch M., Speyerer E.J., Robinson M.S., (2012). GLD100: The near-global lunar 100 m raster DTM from LROC WAC stereo image data. *Journal of Geophysical Research: Planets* 117, CiteID E00H17.
- Speyerer E.J., Povilaitis R.Z., Robinson M.S., Thomas P.C., Wagner R.V. (2016). Quantifying crater production and regolith overturn on the Moon with temporal imaging. *Nature* 538, 215–218.
- Spurný P., Borovička J., Shrbený L. (2007). Automation of the Czech part of the European fireball network: equipment, methods and first results. *Near Earth Objects, our Celestial Neighbors: Opportunity and Risk, Proceedings if IAU Symposium 236*. Ed: Valsecchi G.B., Vokrouhlický D., Milani A.. Cambridge: Cambridge University Press, 121–130.
- Trigo-Rodríguez J.M., Castro-Tirado A.J., Llorca J., Fabregat J., Martínez V.J., Reglero V., Jelínek M., Kubánek P., Mateo T., de Ugarte Postigo A. (2004). The Development of the Spanish Fireball Network Using a New All-Sky CCD System. *Earth, Moon, and Planets* 95, 553–567.
- Walsh A.M., Holloway K.E., Habdas P., de Bruyn J.R. (2003). Morphology and Scaling of Impact Craters in Granular Media. *Physical Review Letters* 91(10), id. 104301.
- Watters T.R., Robinson M.S., Banks M.E., Tran T., Denevi B.W. (2012). Recent extensional tectonics on the Moon revealed by the Lunar Reconnaissance Orbiter Camera. *Nature Geosci* 5, 181–185.
- Watters T.R., Robinson M.S., Beyer R.A., Banks M.E., Bell J.F., Pritchard M.E., Hiesinger H., van der Bogert C.H., Thomas P.C., Turtle E.P., Williams N.R. (2010). Evidence of Recent Thrust Faulting on the Moon Revealed by the Lunar Reconnaissance Orbiter Camera. *Science* 329, 936–940.
- Weryk R.J., Brown P.G., Domokos A., Edwards W.N., Krzeminski Z., Nudds S.H., Welch D.L. (2008). The Southern Ontario All-sky Meteor Camera Network. *Earth, Moon, and Planets* 102, 241–246.
- Xiao Z., Werner S.C. (2015). Size-frequency distribution of crater populations in equilibrium on the Moon. *Journal of Geophysical Research: Planets* 120, 2277–2292.
- Zimníková P. (2017). Lunar impact flashes. *WGN* 45, 111–114.
- Zhao H.B. (2010). Survey and Risk Assessment of Near Earth Asteroids. *Acta Astronomica Sinica* 51, 324–325.

Impact fluxes on the Columbus module of the ISS: survey and predictions

Gerhard Drolshagen¹, Maximilian Klaß¹, Robin Putzar⁴, Detlef Koschny^{2,3} and Björn Poppe¹

¹CvO Universität Oldenburg, Germany

gerhard.drolshagen@uol.de

maximilian.klass@uol.de

bjoern.poppe@uol.de

²ESA/ESTEC, 2201 AZ Noordwijk ZH, The Netherlands

detlef.koschny@esa.int

³Chair of Astronautics, TU Munich, Germany

⁴Fraunhofer Institute for High-Speed Dynamics, Ernst-Mach-Institut, Freiburg, Germany

Robin.Putzar@emi.fraunhofer.de

Launched in 2008, the Columbus module of the International Space Station (ISS) has by now been exposed for more than 10 years to fluxes from micrometeoroids and space debris particles. Numerous impact craters are present on its outer surfaces. A group of researchers from various German entities has initiated an impact survey of outer surfaces of the Columbus module. Such a survey was supported by ESA and NASA and finally carried out in September 2018 using a video camera on the Canadian robot arm. Impact features bigger than a few hundred microns are visible. With its large size of several tens of square meters and its long exposure duration, the surfaces of the ISS modules provide a unique opportunity to record fluxes or particles in space before they enter the atmosphere. A systematic analysis of the impact craters is ongoing. This is done in several steps: Combining the different video sequences, identifying impact craters, measuring them and converting measured crater sizes to particle diameters. The results will be compared to existing meteoroid and space debris flux models and, if required, will lead to improved flux and population models. In this paper, the details of the impact survey are discussed, and impact flux predictions are presented.

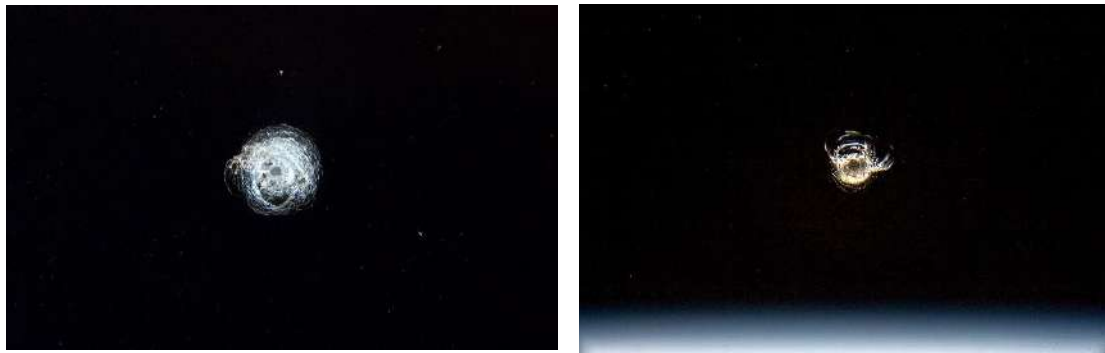


Figure 1: Impact craters on Soyuz spacecraft window, crater size: 3-4 mm. Image credit: Alexander Gerst, ESA

1 Introduction

Meteoroid and space debris flux models are very important for spaceflight. Accurate flux models are essential to precisely calculate the risk of impacts on a given spacecraft and to assess the threat such impacts pose to crew and equipment. Naturally, these flux models require frequent validations and/or updates in order to maintain their accuracy. Each new piece of hardware in Earth's orbit is a potential source for new debris particles. Conclusively, one should compare theoretical flux-predictions with real data, when the opportunity arises. The Columbus module provides such an opportunity, as it has been in orbit for over 10 years and additionally has a

large surface area of over 40 m². The plan and preparation for the Columbus impact survey is presented in "Measuring impact craters on the ISS Columbus module" (Putzar et al, 2018). The data are gathered by a video camera to scan the surface of the Columbus module for impact craters. This footage is still being analyzed. Final crater counts and analysis is ongoing. In this work, two different debris models, Master2009 (Flegel et al., 2011) and Ordem2k (Liou et al., 2002)) and one meteoroid model from Grün et al. (1985) were considered for the theoretical flux predictions. All of these are integrated in the ESABASE2/D (Miller, 2017) software. With this tool, geometric and non-geometric debris/meteoroid-analyses can be performed. The non-geometrical analysis uses a flat plate with user specified

orientation, while the geometrical analysis uses a fully 3D model, including shadowing effects from other spacecraft parts. Exemplary flux-predictions (geometric and non-geometric) will be shown in a later section of this paper.



Figure 2: Columbus module of the ISS with robot arm.
Image credit: DLR

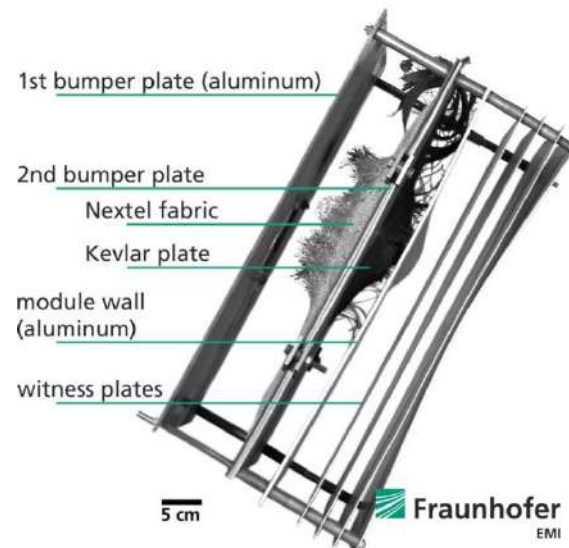


Figure 3: Shielding of the Columbus module. Image credit: Fraunhofer EMI

2 Columbus module shielding

At first, we give a quick overview of the current shielding implemented in the cylindrical section of the Columbus module (Destefanis et al, 1999). Rather than having one thick wall, the shielding consists of multiple layers of different materials. The first bumper plate is made from 2.5 mm thick Aluminum 6061 T6. It is sufficient to block small or slow particles; its main purpose, however, is to break up larger, more dangerous particles into small fragments, dispersing the impact energy onto a larger surface area. Behind the outer bumper, a second bumper is located, consisting of four layers of Nextel 312-AF62 and a 6 mm thick Kevlar 192-812/epoxy plate. Its purpose is to stop/slow down the fragments. The final layer of the shield is the module wall, which is made from 4.8 mm thick Aluminum 2219 T851. The spacing between outer bumper and module wall is 130.4 mm, the spacing between inner bumper and module wall is 42 mm. The shield was built to withstand Aluminum spheres with a diameter of 15 mm (corresponding to a mass of 5 g) at a velocity of 7 km/s. This is also known as the ballistic limit of the shield. Figure 3 shows a photograph of a shield specimen after hypervelocity impact testing. The witness plates are used to monitor residual fragment energy in case of perforation. They are not present in the on-board configuration.

3 Conduction of the survey

The survey of the surface of the Columbus module was planned in close cooperation with the NASA robotics operation team. It was carried out in two parts, the first part on September 5, 2018 and the second part on September 21–22, 2018. For the first part the camera scanned the first row of panels and for the second part it scanned the 9–12th rows of panels. These rows are facing different directions, which can be described by different zenith angles from 0° (space-direction) to 90° (ram-direction). Fluxes from meteoroids and space debris have different directional dependencies.



Figure 4: survey of the Columbus module. Image credit: ESA/NASA

Space debris impact mainly from within a plane parallel to the Earth's surface leading to maximum fluxes at the sides and forward-facing surfaces of a spacecraft in Earth orbit. Meteoroids impact from all directions, except from the part of space shadowed by Earth. By comparing fluxes on surfaces with different orientations, impacts from natural meteoroids and human-made debris can be distinguished to some extent. Theoretically, the camera

should be placed as close to the surface as possible, so that even small craters can be identified correctly, however due to equipment-security concerns, the camera was normally placed at 5 ft distance from the surface. Exceptions to this were the third panel of the first row and the second panel of the tenth row, which were studied from only 2 ft distance. The camera was placed nearly perpendicular to the surface for the survey.

4 Flux predictions

In this section some exemplary results for the meteoroid/debris flux will be presented. The ESABASE2/Debris tool was used to create a model of the Columbus-module and for the flux-calculations. The minimum particle diameter was chosen as 0.1 mm. For the 3D-results, meteoroid and debris fluxes are shown separately. The spacecraft is moving along the x-axis, in the positive direction. The unit of the flux is the number of impacts per square meter per year. Areas with a high impact count are colored in red, while low impact areas are colored in green and blue. Interestingly, the maximum values for flux occur at different zenith angles for meteoroid and debris models. For the meteoroid model the maximum occurs at a $\sim 45^\circ$ zenith angle and for the debris model the maximum flux is at $\sim 90^\circ$ zenith angle (which corresponds to the ram-direction). This can be explained by considering the different sources of the debris and meteoroid particles. While meteoroids are coming in from outer space, all the debris originates from human made hardware. Debris objects that can hit the ISS are mainly in nearly circular orbits, with similar altitudes as the ISS.

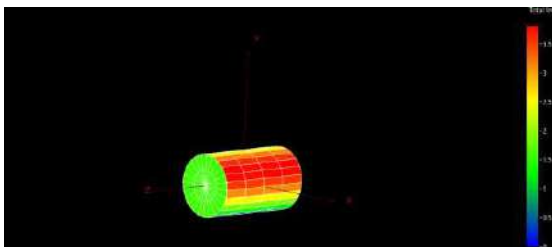


Figure 5: 3D-results for the meteoroid flux (Grün-model) for particles larger than 0.1 mm using ESABASE2/Debris. The flight direction is denoted by the x-vector. Image Credit: Maximilian Klaß, University of Oldenburg

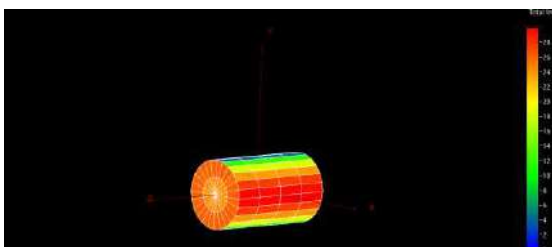


Figure 6: 3D-results for the debris flux (Master2009-model) for particles larger than 0.1 mm using ESABASE2/DEBRIS. The flight direction is denoted by

the x-vector. Image Credit: Maximilian Klaß, University of Oldenburg

The ESABASE2/Debris tool also allows calculations for simple generic geometries. For these, only a square plate in orbit is considered, for which the surface area, as well as the azimuth and zenith angle can be specified (one can also select it to be “randomly tumbling”). In the following figure, the different results for the particle flux (y-axis) for three different models are presented (Grün, Master2009 and Ordem2k), as function of the particle size (x-axis). The flux value is cumulative. The azimuth angle is selected to be 0° and the zenith angle is 90° (ram-direction). The surface area of the plate is chosen as 1 m^2 . The last figure shows the number of craters on the plate in relation to the crater diameter. The craters were assumed to be hemispherical. The craters were calculated using the thick-plate equation (assuming a hemi-spherical crater shape) as implemented in the ESABASE2/Debris tool (Miller, 2017).

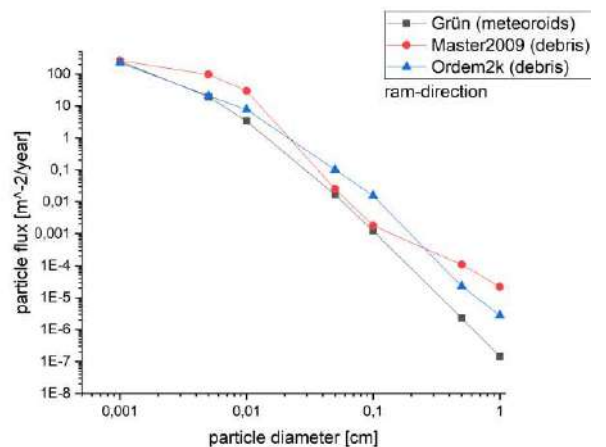


Figure 7: Particle flux for different debris/meteoroid models, using the non-geometrical analysis. Given are cumulative fluxes / m^2/year onto a flat plate facing in ram-direction.

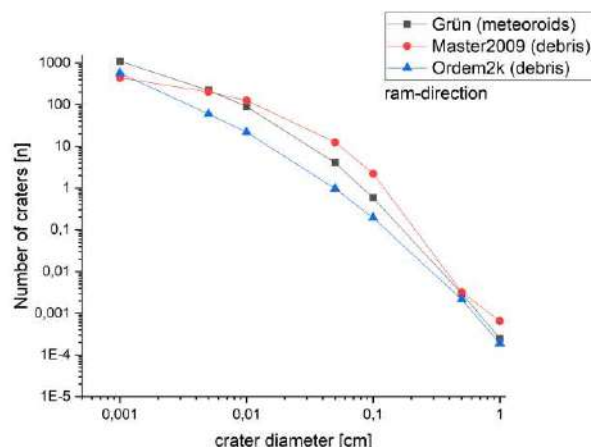


Figure 8: Number of craters for different debris/meteoroid models, using the non-geometrical analysis. Given is the cumulative number of craters/year on a flat plate facing ram direction having a surface area of 1 m^2 .

5 Summary and outlook

After 10 years in space a video survey of the Columbus module was conducted to analyze impact craters. Craters larger than 1-2 mm in size are visible on the video. The analysis of the video footage is still ongoing. In this paper first flux predictions from several meteoroid and space debris models are presented. More theoretical predictions will be made, by using different debris/meteoroid-models and different damage/crater size equations. Other analyses of the impact survey are performed at the TU Munich and the Fraunhofer Ernst-Mach Institut. The results of both the theoretical predictions and the analysis of the camera footage will be compared and consolidated. Once this is completed, it could lead to a validation or update of the existing flux models and ultimately to possible re-evaluation of the shielding necessary for different types of space missions.

References

1. Destefanis, R., Faraud, M. , Trucchi, M.: “Columbus debris shielding experiments and ballistic limit curves”, International Journal of Impact Engineering, Vol. 23, p. 181, 1999, doi: 10.1016/S0734-743X(99)00071-8
2. Flegel, S., Gelhaus, J., Möckel, M., Wiedemann, C. , Krag, H., Klinkrad, H., Vörsmann, P.: Master-2009 Software User Manual. Braunschweig: TU Braunschweig, Institute of Aerospace Systems, 2011. -RFQ No 21705/08/D/HK
3. Grün, E., Zook, H.A., Fechtig, H., Giese, R.H.: “Collisional Balance of the Meteoritic Complex”, Icarus, Vol. 62, p.244, 1985.
4. Liou, J.-C., Matney, M.J., Anz-Meador, P.D., Kessler, D., Jansen, M., Theall, J.R.: “The New NASA Orbital Debris Engineering Model ORDEM2000”, NASA/TP-2002-210780, May 2002
5. Miller, A., ESABASE2/Debris Release 10.0, Technical Description, Ref. R077-231rep_01_07_Debris_Technical Description, 2017
6. Putzar, R., Gulde, M., Sabath, D., Fiedler, H., Drolshagen, G., Braukhane, A., Horstmann, A., Wiedemann, C., Schimmerohn, M., Schäfer, F.: “Measuring impact craters on the ISS Columbus module”, Ref.: IAC-18, A6,3,5, x43898, IAC, Bremen, Oct. 2018

De-biasing of meteor radiant distributions obtained by the Canary Island Long-Baseline Observatory (CILBO)

Athleen Rietze¹, Detlef Koschny^{2,3}, Gerhard Drolshagen¹, Björn Poppe¹

¹Universitätssternwarte Oldenburg, Carl von Ossietzky University of Oldenburg, Ammerländer Heerstraße 114-118, D-26129 Oldenburg, Germany

Athleen.Selma.Rietze@uni-oldenburg.de

Gerhard.Drolshagen@uni-oldenburg.de

Bjoern.Poppe@uni-oldenburg.de

²European Space Agency, ESA/ESTEC, Keplerlaan 1, NL-2201 AZ Noordwijk, The Netherlands

Detlef.Koschny@esa.int

³Chair of Astronautics, Technical University Munich, Boltzmannstrasse 15, D-85748 Garching, Germany

The Canary Island Long-Baseline Observatory (CILBO) is a double-station camera setup for meteor observations. It is an automated system consisting of two stations with image-intensified video cameras. While one station is located on La Palma and the other camera on Tenerife, they both point at the same position in the atmosphere at an altitude of 100 km. With this overlap of the two observation volumes which is covered by both stations it is possible to track meteors and to analyse their trajectory. The data available for an analysis was collected by CILBO from December 2011 until January 2018. This work presents the relative number of sporadic meteors depending on their velocity and mass. Also, the method of de-biasing the data by comparing it to a velocity model for every velocity bin in every mass bin is explained. This paper refers to a model based on radar and in-situ observations for the 100 km altitude (ECSS, 2008). The consequent results of the de-biased meteor radiant distribution are shown.

1 Introduction

This paper describes a de-biasing method of sporadic meteor radiant distributions. This method was used to correct a dataset obtained by a double-station camera setup on the Canary Islands, called CILBO (Canary Island Long-Baseline Observatory). This system has been operating regularly since its installation by ESA's Meteor Research Group in 2011/2012 (Koschny et al., 2013). CILBO consists of two automated stations with image-intensified video cameras. One station is located on La Palma (ICC9) and the other camera on Tenerife (ICC7). Both intensified CCD cameras monitor the same volume of the atmosphere at an altitude of 100 km (Koschny et al., 2014). This way both cameras are able to detect a meteor which was observed in the overlap of the fields of view. The simultaneous meteor detections allow the calculation of the velocity and the trajectory of the meteor. The setup of the CILBO system is shown in Figure 1 (Drolshagen et al., 2014).

With the software MetRec (Meteor Recognizer) it is possible to automatically detect and analyse meteors (Molau, 1998). For further analysis the meteor detection is performed on the single station data by using the software MetRec. The orbits were computed by MOTS (Meteor Orbit and Trajectory determination Software). This software uses data obtained with the software MetRec. This way MOTS can compute the trajectory and also the orbital parameters of a meteor. For a more detailed description of this application see Koschny & Diaz del Rio (2002).

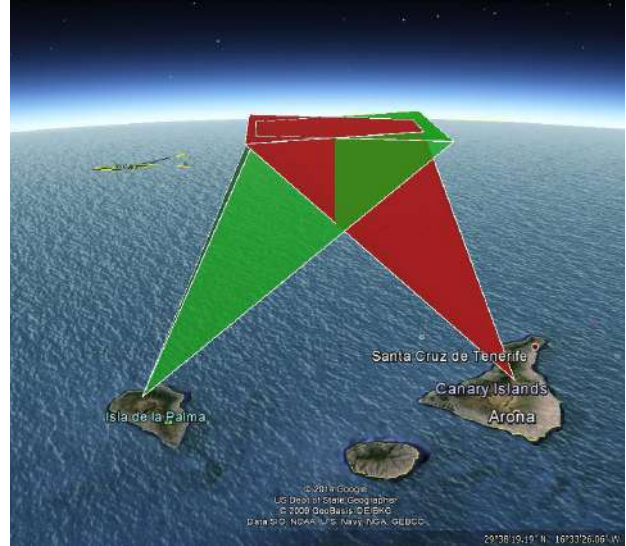


Figure 1— Sketch of the CILBO double station camera setup generated with Google Earth showing the fields of view of camera ICC7 (Tenerife, right island) and camera ICC9 (La Palma, left island) and the resulting overlapping volume (Drolshagen et al., 2014).

The velocity distribution of the detected meteors obtained by the CILBO system was compared by Drolshagen et al. (2014) to a model velocity distribution as given by the Space Environment Standard of the European Cooperation for Space Standardization (ECSS, 2008). This model is based on radar and in-situ observations. Drolshagen et al. (2014) noticed a heavy bias of the velocity distribution towards large and fast meteoroids. This is ascribed to a certain kinetic energy which meteoroids need to have to form a visible meteor trail. It was discovered that the velocity distribution of larger

meteoroids fits this model, which confirms the mentioned

bias.

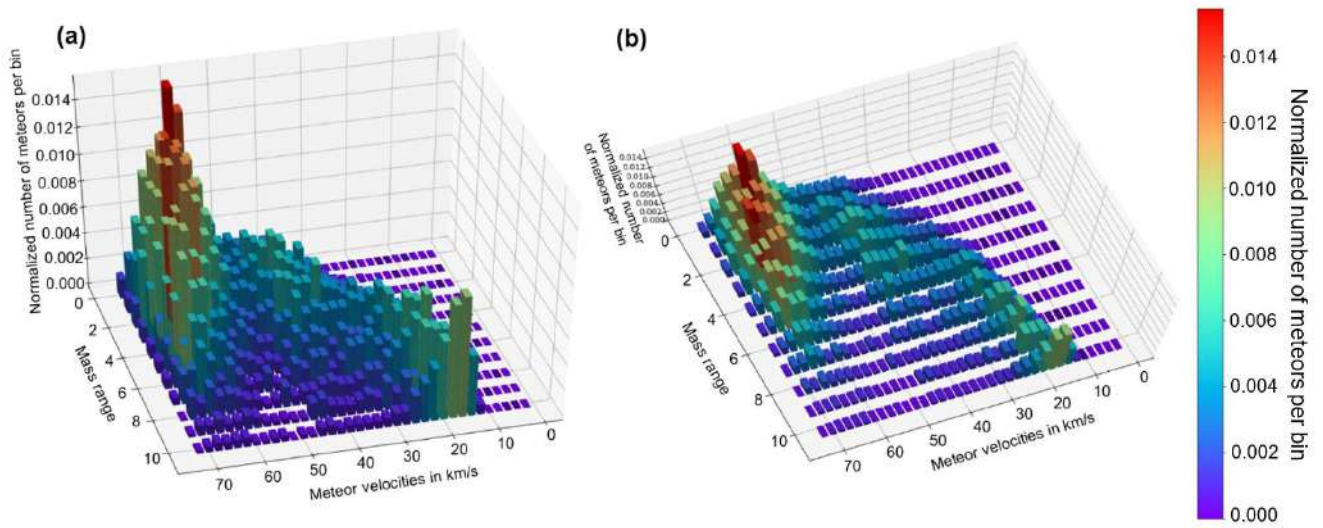


Figure 2 – (a, b) Different views on a three-dimensional graph of the relative number of sporadic meteors as a function of their mass and velocity

All simultaneously observed meteors are separated into shower meteors and sporadics by using MetRec and a D-criterion. The D-Criterion is a measure on how well the orbit fits a shower source (Rudawska et al., 2012). Meteors which cannot be assigned to a known meteoroid stream are called sporadics. So far six apparent sources of sporadic activity have been discovered. These sources describe radiant concentrations which are named northern and southern apex, northern and southern toroidal, helion and antihelion (Campbell-Brown, 2008). The so-called apex effect refers to the phenomenon that the meteoroids reach the atmosphere of the Earth with a relatively small velocity with respect to the Earth at the beginning of the night. However, in the early morning hours the meteoroids that reach Earth's atmosphere have a greater velocity with respect to the Earth.

The mass of each detected meteor was computed by using the luminous efficiency determined by Weryk and Brown (2013). Thereafter, the velocity distribution of sporadic meteors depending on their mass is examined (see *Figure 2*). In this paper the velocity distribution is compared to the model in order to calculate de-biasing factors as a function of the mass and the velocity of each detected meteor. We use the software MOTS to compute meteor radiants. These are converted into ecliptic latitude and ecliptic longitude. Then the respective de-biasing factors are applied to the data. The resulting de-biased radiant density distribution of sporadic meteors is presented and analyzed.

The de-biasing method described in this paper aims to show that the so far observed structures of sporadic activity in radiant density distributions only exist due to observational bias.

2 The CILBO velocity distribution

In the analyzed data obtained by CILBO during December 2011 and January 2018 there were 11934

simultaneously observed meteoroids assigned to sporadics by MetRec.

The sporadic meteoroids are sorted in fixed mass bins and velocity bins of 2 km/s. The mass intervals are chosen so that every mass bin consists of a significant number of observed sporadics. These mass ranges are listed in *Table 1*. The relative number of sporadic meteors depending on their mass and velocity is shown in the *Figures 2a* and *2b*. These are two different views on a three-dimensional graph. There are two populations visible. The slow and heavy meteors are detected very well. Also, the fast meteors are basically always detected. But *Figure 2* also shows that there should be a lot more meteors detected but these meteoroids are not visible for the CILBO camera system. This is due to the fact that their kinetic energy is too low to generate enough light. Hence these meteoroids cannot form a meteor trail bright enough so that it becomes detectable by the doublestation meteor camera system on the Canary Islands. A detailed explanation for these two populations is not yet available.

*Table 1 – Legend of the mass ranges utilized to present the sporadic meteors in *Figure 2**

Mass range in kg	
0	1.48e-8 – 9.69e-8
1	9.69e-8 – 1.45e-7
2	1.45e-7 – 2.18e-7
3	2.18e-7 – 3.26e-7
4	3.26e-7 – 4.89e-7
5	4.89e-7 – 7.33e-7
6	7.33e-7 – 1.10e-6
7	1.10e-6 – 1.65e-6
8	1.65e-6 – 2.47e-6
9	2.47e-6 – 3.69e-6
10	3.69e-6 – 1.90e-2

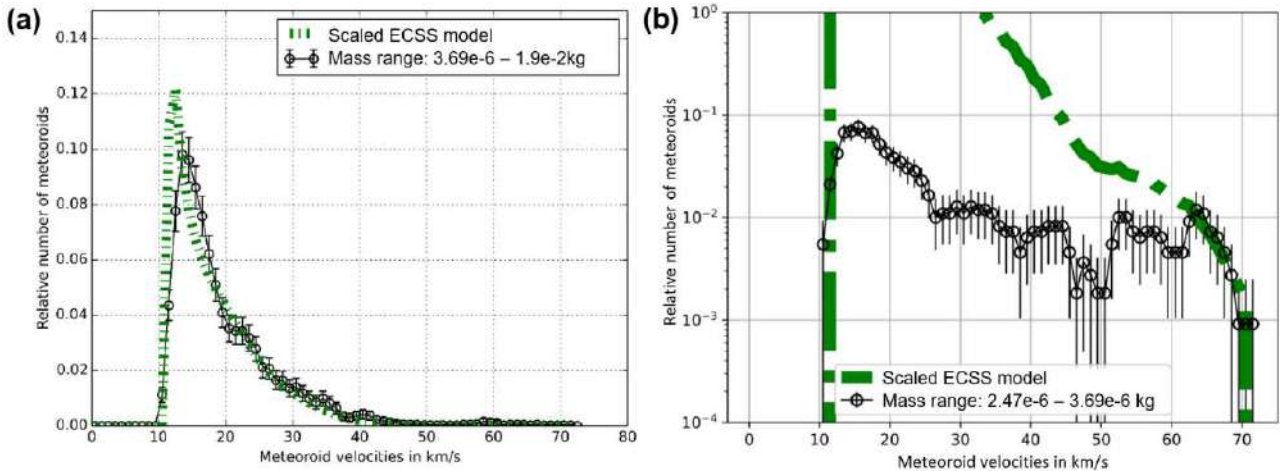


Figure 3 – Comparison of the normalized sporadic velocity distribution for two different exemplary mass ranges ((a) $3.69 \cdot 10^{-6} \text{ kg}$ to $1.9 \cdot 10^{-2} \text{ kg}$, (b) $2.47 \cdot 10^{-6} \text{ kg}$ to $3.69 \cdot 10^{-6} \text{ kg}$) of the CILBO data (black, dotted line) with the normalized model velocity distribution for 100 km altitude (green, dashed line)

3 Method of de-biasing meteor observational data

The ECSS distribution

The analysis of the data observed by CILBO showed that the data is heavily biased. Therefore, a correction for the observed meteors in the smaller mass ranges is necessary. Previous work by Kretschmer et al. (2015) and Koschny et al. (2017) shows that the model velocity distribution described by the Space Environment Standard of the European Cooperation for Space Standardization (ECSS, 2008) approximates the velocity distribution obtained by CILBO for large meteoroids. This ECSS standard includes the velocity distribution at 1 AU in free space for the sporadic meteoroid flux. These values were determined by A.D. Taylor. The data obtained by the Harvard Radio Meteor Project (HRMP) during 1968 and 1969 was used (Taylor, 1995). This model consists of the initial velocity distribution for meteoroids in free space, hence the amount of meteoroids observed for certain velocities in 1 km/s bins form this distribution. For an application of this standard in other altitudes the standard includes a procedure for recalculating the distribution. This is necessary due to the change of velocities near Earth because of the gravitation of the Earth. For further analyses the computation of the distribution at an altitude of 100 km is done (Drolshagen et al., 2014). It is presumed that the ECSS model describes for all mass ranges the true meteoroid distribution in near Earth space accurately. Thus, the ECSS distribution is utilized as a reference model for the de-biasing method.

Velocity distribution for different mass bins

The CILBO velocity distribution is compared to the mass independent Space Environment Standard of the ECSS recalculated for 100 km altitude. Every velocity distribution for every certain mass range is analysed individually. The relative number of meteoroids is plotted dependent on the meteoroid velocities in km/s for every certain mass range. The green dashed line describes the normalized ECSS distribution.

This way it becomes visible in Figure 3a that the normalized velocity distribution of the heavier meteoroids fits the model quite nicely. This implies that the heavier meteoroids can be detected by the utilized cameras nearly completely. For smaller mass ranges this is not the case. Figure 3b shows the normalized CILBO velocity distribution for a smaller mass range (black, dotted line) in comparison to the normalized reference model. The normalized velocity distribution by CILBO differs largely for smaller mass ranges from the mass independent ECSS model. This behaviour is already discovered by Drolshagen et al. (2014) and verified by Kretschmer et al. (2015) and Koschny et al. (2017). The reason for this behaviour is the already mentioned bias of the CILBO data towards high velocities and bigger masses of meteoroids. When fast meteoroids enter Earth's atmosphere they are more likely to be detected. This characteristic is caused by their higher kinetic energy. As a consequence, a higher kinetic energy of a meteoroid leads to a greater probability to form a brighter ionization trail. This results in a more probable detection of fast and large meteoroids. In contrast to these categories of meteoroids, a large number of faint meteors cannot be discovered by the utilized camera setup. Typically, lower velocities of meteoroids with respect to the Earth lead to fainter meteors. For further analysis the normalized CILBO distribution is fitted for each mass bin to the ECSS distribution on the left since faster meteoroids are more likely to be detected. Also, for the highest velocities the velocity distribution is assumed to be correctly distributed. This way the slope of the normalized distribution obtained by CILBO fits the slope of the normalized model at high velocities (Kretschmer et al., 2015). This is done for each mass interval. It can be seen in Figure 3b that the differences between the two distributions become bigger below a certain velocity. This implies that for a meteor to become visible for the detection system it has to have a minimum velocity.

De-biasing factors as a function of mass bins and velocity bins

In order to describe the amount of meteors that cannot be seen by the CILBO setup, an investigation of the

differences between the normalized CILBO velocity distributions and the reference model is necessary. This method leads to several factors as a function of mass and velocity. These factors are called de-biasing factors in the further analysis (Koschny et al., 2017). Kretschmer et al. (2015) already calculated the de-biasing factors for every mass bin. For this analysis the de-biasing factors are also calculated for every velocity bin of 2 km/s in every mass bin. The hereby determined factors are describing the amount of the meteoroids that enter Earth's atmosphere but cannot be detected by the cameras on the Canary Islands. This means that the de-biasing factor for the largest masses of meteoroids and also the highest velocities should be equal to 1. This is based on the fact that the model and the observed velocity distribution should match for those greater masses and velocities.

4 Radiant density distribution

The meteor radiants as computed by MOTS are converted from right ascension and declination into an ecliptic coordinate system, with the direction of the Earth's movement (the apex) in the center. In order to plot the radiant density distribution, the program HEALPix provided by Jet Propulsion Laboratory (NASA) is used. HEALPix stands for Hierarchical Equal Area isoLatitude Pixelization of a Sphere. By using this pixelization a subdivision of a spherical surface is produced with the effect that every pixel covers the same amount of the surface area (Górski et al. 2005).

The total number of pixels in the map n_{pix} can be derived by using (1) and (2), where n_{side} is the number of pixels per side and i_{res} is the resolution index.

$$n_{side} = 2^{i_{res}} \quad (1)$$

$$n_{pix} = 12 \cdot n_{side}^2 \quad (2)$$

Figure 4 shows the still biased radiant density distribution obtained by 7536 sporadic meteors. They were observed by the CILBO cameras between 2011 and 2018. These meteors were assigned to sporadics using the method of the D-criterion. It is visible that there is a higher concentration of radiants in the middle of the map. This structure is called apex source. The apex direction is the direction of the movement of the Earth in our Solar System. Furthermore, the toroidal sources are recognisable. Also, it is visible in *Figure 4* and *Figure 5* that the apex is shifted to the right. This is due to the way we use the application HEALPix.

Then the de-biasing factors are applied to the data and a de-biased radiant density distribution is computed (*Figure 5*).

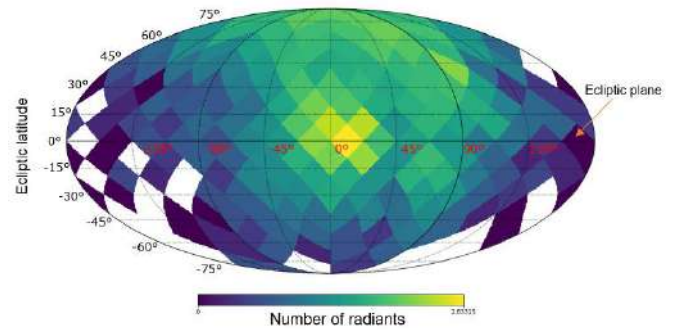


Figure 4– Biased radiant density distribution, NSIDE=4, labelled values (in red, on ecliptic plane) clarify the distance from apex

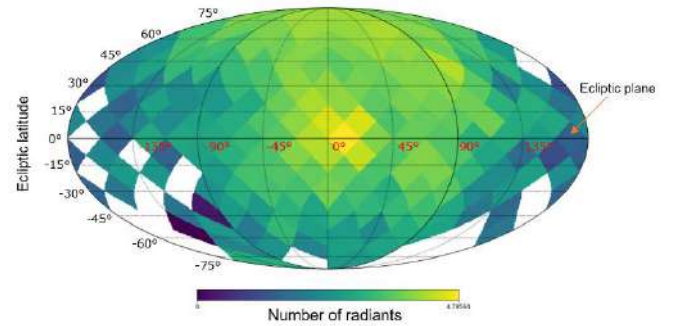


Figure 5 – De-biased radiant density distribution, NSIDE=4, labelled values on the horizontal axis (in red, on ecliptic plane) clarify the distance from apex

Figure 5 represents the de-biased radiant density distribution also obtained by 7536 sporadic meteors. By comparison of *Figure 4* and *Figure 5* it can be seen that a peak of radiants in the middle of the map is still discernible. It should be emphasised that the apex and the toroidal sources are a little less clear to recognize after the de-biasing. The structures seem to be blurred. But overall, they are still observable in *Figure 5*.

5 Conclusion

In this paper a method for de-biasing the meteor radiant density distribution was derived by analysing the data obtained by the CILBO double-station camera setup in the time period between December 2011 and January 2018. The explained de-biasing method is based on the CILBO velocity distribution in certain mass ranges and also on the reference model by the ECSS Space Environment Standard.

The apparent sources of sporadic meteoroids as mentioned by Campbell-Brown (2008) which appear in radiant density distributions are partly still visible. This implies that the de-biasing method works well but needs to be improved further.

To assign the simultaneously detected meteors to shower meteors and sporadics the software MetRec and the method of the D-criterion was used. From the data it is apparent that while using the D-criterion only a part of the actual shower meteors was assigned accordingly. It could be possible that the association of the meteors using MetRec works better. Thus, the methods to

distinguish sporadic and shower meteors should be investigated further.

References

- Campbell-Brown M.D. (2008). "High resolution radiant distribution and orbits of sporadic radar meteoroids". *Icarus*, **196**, pages 144-163.
- Drolshagen E., Ott T., Koschny D., Drolshagen G. and Poppe B. (2014). "Meteor velocity distribution from CILBO double station video camera data". In Rault J.-L. and Roggemans P., editors, *Proceedings of the International Meteor Conference*, Giron, France, 18-21 September 2014. IMO, pages 16-22.
- ECSS (2008). European Cooperation for Space Standardization, Space Engineering, Space Environment, ECSS-E-ST-10-04C. Noordwijk, Netherlands: ESA Requirements and Standards Division.
- Górski K.M., Hivon E., Banday A.J., Wandelt B.D., Hansen F.K., Reinecke M. and Bartelmann M. (2005). "HEALPix: A Framework for High-Resolution Discretization and fast Analysis of Data Distributed on the Sphere". *The Astrophysical Journal*, **622**, pages 759-771.
- Koschny D. and Diaz del Rio J. (2002). "Meteor Orbit and Trajectory Software (MOTS) – Determining the Position of a Meteor with Respect to the Earth Using Data Collected with the Software MetRec". *WGN, the Journal of the IMO* 30:4, pages 87-101.
- Koschny D., Bettonvil F., Licandro J., van der Luijt C., Mc Auliffe J., Smit H., Svendhem H., de Wit F., Witasse O. and Zender J. (2013). "A double-station meteor camera setup in the Canary Islands – CILBO". *Geoscientific Instrumentation Methods and Data Systems*, **2**, pages 339-348.
- Koschny D., Mc Auliffe J., Drolshagen E., Bettonvil F., Licandro J., van der Luijt C., Ott T., Smit H., Svendhem H., Witasse O. and Zender J. (2014). "CILBO – Lessons learned from a double-station meteor camera setup in the Canary Islands". *Proceedings of the International Meteor Conference*, Giron, France, 18-21 September 2014. IMO, pages 10-15.
- Koschny D., Drolshagen E., Droshagen S., Kretschmer J., Ott T., Drolshagen G. and Poppe B. (2017). "Flux densities of meteoroids derived from optical double-station observations". *Planetary and Space Science*, **143**, pages 230-237.
- Kretschmer J., Drolshagen S., Koschny D., Drolshagen G. and Poppe B. (2015). "De-biasing CILBO meteor observational data to mass fluxes". In Rault J.-L. and Roggemans P., editors, *Proceedings of the International Meteor Conference*, Mistelbach, Austria, 27-30 August 2015. IMO, pages 209-213.
- Molau S. (1998). "The Meteor Detection Software MetRec". *Meteoroids*, Astron. Inst., Slovak Acad. Sci., Bratislava, Slovakia. Pages 131-134.
- Rudawska R., Vaubaillon J. and Atreya P. (2012). "Association of individual meteors with their parent bodies". *ESO 2012. Astronomy & Astrophysics*, **541**, A2, pages 1-5.
- Taylor A.D. (1995). "The Harvard Radio Meteor Project Meteor Velocity Distribution Reappraised". *Icarus*, **116**, pages 154-158.
- Weryk R.J. and Brown P.G. (2013). "Simultaneous radar and video meteors-II: Photometry and ionization". *Planetary and Space Science*, **81**, pages 32-47.

How to test whether the magnitude distribution of the meteors is exponential

Janko Richter¹

¹ Lindenstr 28A, 12555 Berlin, Germany
janko@richtej.de

Very often it is assumed that the magnitude distribution of the meteors is exponentially distributed. Under these conditions, the ZHR and the population index are estimated from visual observations. But is the observed magnitude distribution really exponential? Is there any way to verify that, even if the perception probabilities are not known? This article will show how stochastic methods can be used to easily perform these checks. We will clearly see from the visual observations of two meteor showers that it cannot usually be assumed that the magnitude distribution of the meteors is exponential.

Then, the visual probability density distribution of meteor magnitudes is

$$\frac{dp}{dm} = \frac{1}{F(s)} f(m) e^{-sm}. \quad (3)$$

Using the shifting property of Laplace transform, we get the well known equation to compute the ZHR:

$$ZHR = c r^{m_{lim}} \frac{n}{t_{eff}}. \quad (4)$$

In addition, we also obtain an important relationship between the mean value of meteor magnitudes and the population index:

$$\bar{m} = \frac{-F'(s)}{F(s)}. \quad (5)$$

Finally, we get an important conclusion about the mean meteor magnitudes with which we will define our stochastic tests.

Lemma 2.1. *If two observations each have the same average meteor magnitude, then both observations have the same population index.*

This does not mean, however, that if two observations have the same average meteor magnitude, that the magnitude distribution of the meteors is exponential or that the magnitude distributions are equal. The equality of the two mean values results only from the assumptions made above. But with regard to that, the next statement is interesting.

Lemma 2.2. *If the mean meteor magnitude is the same for all limiting magnitudes, then the magnitude distribution of the meteors is exponential.*

Proof. In general terms, the mean value z results from

$$z(a) := \frac{\int_0^\infty m f(m) g(m-a) dm}{\int_0^\infty f(m) g(m-a) dm} = \frac{y_1(a)}{y_0(a)}, \quad (6)$$

1 Introduction

When evaluating the visual observations, it is often assumed that the magnitude distribution of the meteors is exponential and that all observers have similar perception probabilities (Rendtel & Arlt, 2011, p. 123–125). Based on these assumptions, ZHR and r-value are estimated. However, it is quite possible that the assumptions regarding the exponential magnitude distribution do not apply (Richter, 2018, p. 34–38).

With a stochastic test it is possible to show whether the assumptions are met. If the stochastic test rejects the assumption about the perception probabilities and in particular the exponential magnitude distribution, then no population index can be estimated. Similarly, it would even not be possible to estimate a ZHR on the basis of the estimated population index.

In this article we will see that the formulation of such a test is quiet easy and also there is no need of exact values of the perception probabilities.

2 The visual magnitude distribution

First we define m as the magnitude difference of a meteor to the limiting magnitude, where m is always larger than 0.0. Now, we can ask questions like "How likely is it that the magnitude of a meteor is greater than 2.0?"

We now assume the exponential probability density distribution of meteor magnitudes m :

$$\frac{dp}{dm} = \begin{cases} s e^{-sm} & m \geq 0 \\ 0 & m < 0 \end{cases}, \quad (1)$$

where p is the probability and s is the natural logarithm of the population index r .

With $f(m)$ as the perception probability function, we can use the Laplace transform to simplify the equations:

$$F(s) = \mathcal{L}\{f\}(s) = \int_0^\infty f(m) e^{-sm} dm. \quad (2)$$

where $g(m)$ is the function to be determined that has been shifted by the value a . We now examine how the mean value changes if a is minimally changed by da . So that the mean value itself does not change, we determine that

$$\frac{dy_0}{da} = \frac{dy_1}{da}. \quad (7)$$

Let

$$G(a) := \int_0^\infty g(m - a) dm. \quad (8)$$

If we apply the second mean value theorem for definite integrals on Equation 6 we get

$$y_0(a) = F_0(a) G(a) \text{ and} \quad (9)$$

$$y_1(a) = F_1(a) G(a). \quad (10)$$

By derivation of the last two equations we obtain

$$\frac{dy_0}{da} = F'_0(a) G(a) + F_0(a) G'(a) \quad (11)$$

$$\frac{dy_1}{da} = F'_1(a) G(a) + F_1(a) G'(a) \quad (12)$$

and finally because of Equation 7 we get

$$0 = (F'_1(a) - F'_0(a)) G(a) + (F_1(a) - F_0(a)) G'(a). \quad (13)$$

By solving the differential Equation 13 for $G(a)$ we find out that $G(a)$ and concluding from it also $g(m - a)$ is an exponential function as the only non-trivial solution.

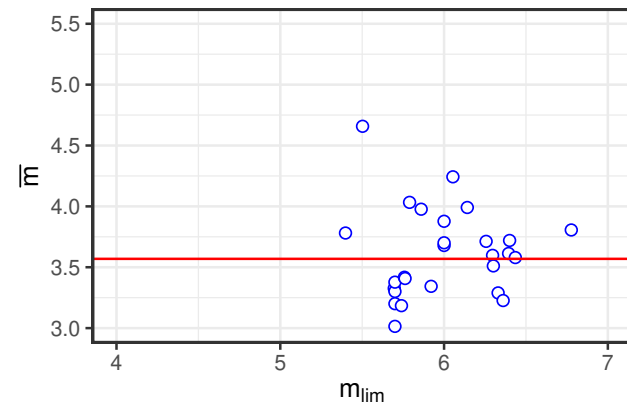


Figure 1 – Average magnitude of the meteors in relation to the limiting magnitude, based on the data of example 1 (Leonids). Each point has 1030 meteors. The red line marks the expected result.

4 Results

We now look at two examples of visual observations, which are briefly described in Table 1. The purpose is to show that the average meteor magnitude is independent from the limiting magnitude.

	Example 1	Example 2
Shower	LEO	PER
Year	1999	2015
Solarlong	235.5 – 235.6	138.5 – 141.5
Total of meteors	30903	28674
Total of observers	65	315

Table 1 – Statistics about the example observations.

Figure 1 shows that there is likely to be no dependence of the average meteor magnitude on the limiting magnitude. An analysis of a sample of 1000 meteors showed that both Fisher's test and the Chi-squared test confirm the null hypothesis 3.1. So we were not able to refute the null hypothesis here. But this is no proof for the validity of the null hypothesis.

It is worth mentioning that we get similar results from observations of the Leonid shower in other years in the same solar longitude range.

Observations from the second example give us a different result. Figure 2 shows very clearly that there is a correlation between the average meteor magnitude and the limiting magnitude. With other words: The average meteor magnitude and the limiting magnitude are stochastically dependent. This is confirmed by Fisher's test as well as the Chi-square test with a sample of 1000 meteors. This refutes the null hypothesis 3.1.

It is noticeable in Figure 2 that the differences in the average meteor magnitude are very significant. We can estimate that an observer with a limiting magnitude of 6.3 observes an average meteor magnitude higher by one magnitude than an observer with a limiting magnitude of 5.0.

Figure 3 shows the same data in a different representation. It is obvious that the temporal appearance of the

3 The statistical hypothesis test

The null hypothesis in a statistical hypothesis test is the assumption or assertion that we actually want to refute or reject. In our case, the null hypothesis is:

Hypothesis 3.1. *The magnitude distribution of the meteors is exponential and all observers have the same perception probabilities.*

With these assumptions and the relationships derived from them, we expect that the average meteor magnitude does not depend on the limiting magnitude. In detail we get from Lemma 2.1:

Lemma 3.2. *If several observations with different limiting magnitudes have different average magnitude values at the same time, we have to reject the null hypothesis 3.1.*

There are several statistical hypothesis tests to test the null hypothesis. The Pearson chi-square test, Fisher's exact test and Student's t-test are examples of algorithms to perform the test. It would be beyond the scope of this article to go into this in more detail. However, there is a large amount of literature on how to apply these tests. We will see from the following examples that a visualization can also provide useful results.

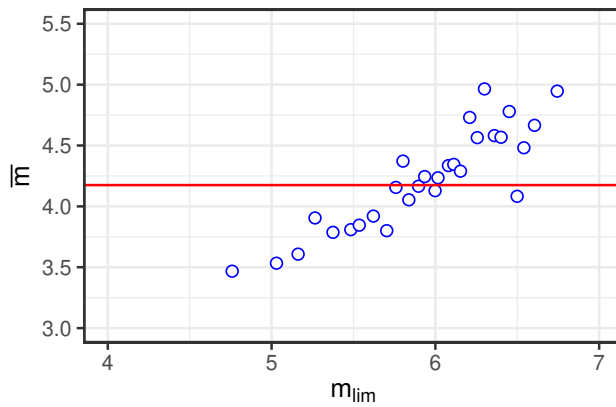


Figure 2 – Average magnitude of the meteors in relation to the limiting magnitude, based on the data of example 2 (Perseids). Each point has 956 meteors. The red line marks the expected result.

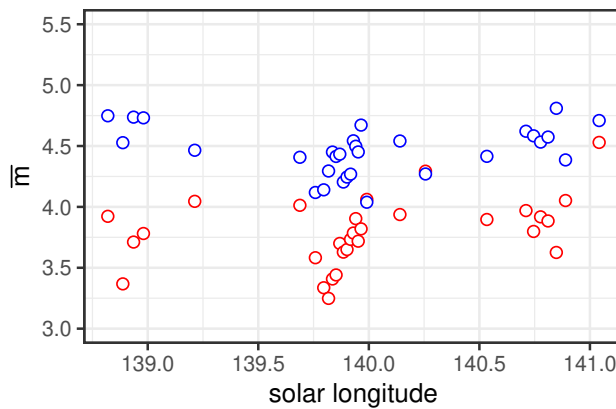


Figure 3 – Average magnitude of the meteors in relation to the solar longitude, based on the data of example 2 (Perseids). Each point has 478 meteors. Red dots are meteors observed at a lower limiting magnitude, blue dots at a higher limiting magnitude.

meteors has no influence on the current result. Meteors observed at a lower limiting magnitude have a different average meteor magnitude than meteors observed at a higher limiting magnitude. We get two different population indices at the same time. But that's a contradiction to Lemma 2.1.

It is also interesting here that we obtain similar results from observations of the Perseid shower in other years in the same solar longitude range.

5 Discussion

We have made two assumptions in our null hypothesis 3.1. One assumption refers to the distribution of meteor magnitudes and the other to the perception probabilities. It is difficult to assume that the detection probabilities depend on the observed meteor stream. So we can rule out that the perception probabilities are the cause of the different results in our two examples. It remains to be concluded that the magnitude distributions of meteors in both examples differ from each other. We can therefore assume from the test results in the second

example that this meteor magnitude distribution is not exponential.

6 Conclusion

We can conclude that, in general, we should not assume that the meteor magnitudes are exponentially distributed in the observable visual range. As a consequence of these results, only under the assumption of the exponential magnitude distribution we can estimate the ZHR with Equation 4. If this condition is not met, Equation 4 must not be used. Otherwise the results based on this would not be very meaningful. Also an estimate of the population index is no longer appropriate under these conditions.

It is therefore particularly important to use stochastic tests. Otherwise, it is to be expected that the results are not correct.

7 Future work

In order to be able to calculate a ZHR in the future, it is essential to obtain more information about the magnitude distribution of the meteors. In particular, a review of the published theoretical model (Richter, 2018) based on observation results would be important.

A further task is also to generalize Equation 4 in order to be able to estimate a ZHR if the assumption about exponential magnitude distribution of the meteors does not apply. This could possibly also be based on empirical results.

Regardless of these results, in the future it will always be a task in meteor science to apply stochastic tests and other stochastic tools whenever possible in order to check assumptions before conclusions are made from the observation results.

Acknowledgments

The author would like to thank all the observers whose observations made these results possible.

References

- Rendtel J. and Arlt R., editors (2011). *Handbook for Meteor Observers*. Third edition. IMO.
- Richter J. (2018). “About the mass and magnitude distributions of meteor showers”. *WGN, Journal of the International Meteor Organization*, **46**.

3414-2018: A Perseid fireball with exceptional light effects

Peter C. Slansky¹

¹ University for Television and Film Munich, Department II Technology
slansky@mnet-online.de

This talk presented the essence of a detailed article of the author, together with co-observer Bernd Gaehrken, in WGN journal (Slansky and Gaehrken, 2018). Additionally, the results of two camera (Slansky, 2019) tests (Slansky and Gaehrken, 2019) by the author were presented.

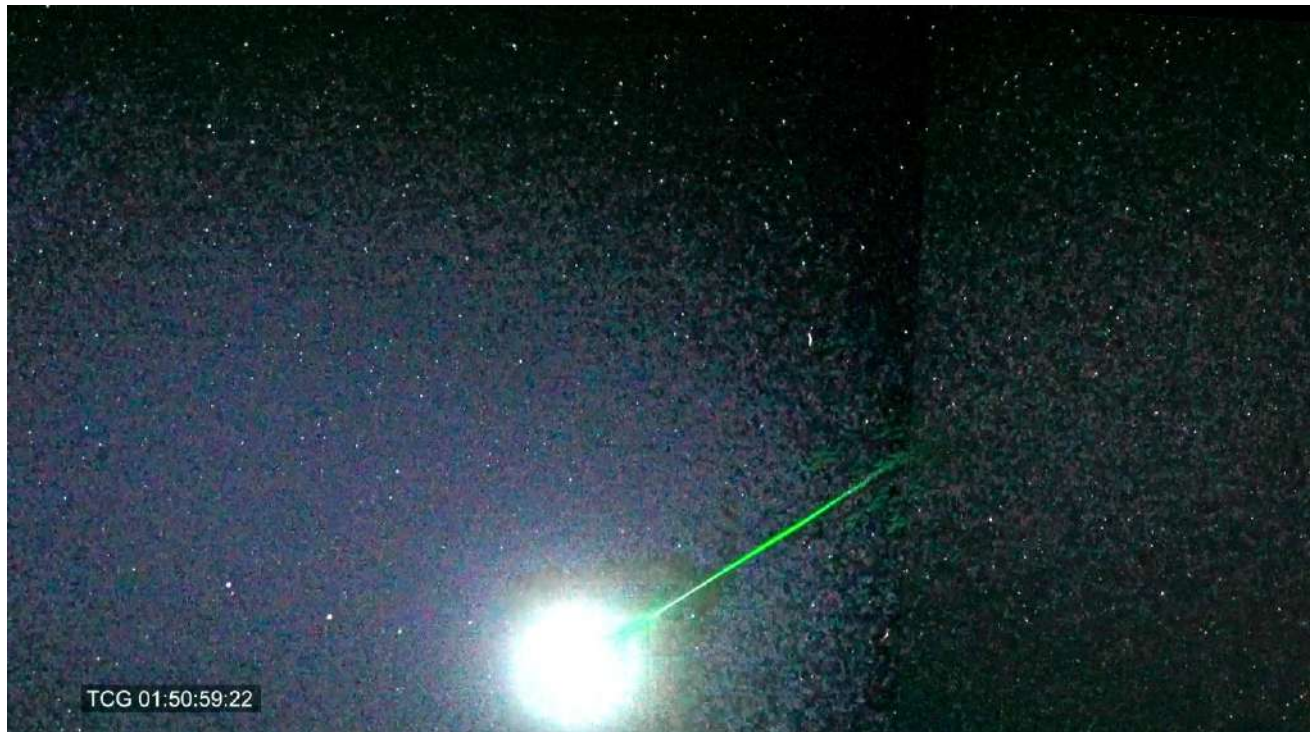


Figure 1: Composite image of two single video frames of the terminal flash. Right is camera 1, left camera 2. The bright star slightly right from the image center is Polaris. It has “wings” due to lens artifacts. The embedded time code (“TCG”) indicates UT in hours:minutes:seconds:frames. Note the widespread bluish sky glow. The original video in full HD resolution (40 MB) can be found at: http://slansky.userweb.mwn.de/bereiche/astronomie/meteore/bilder/bolid_13-08-2018_03-51_fhd.mp4.

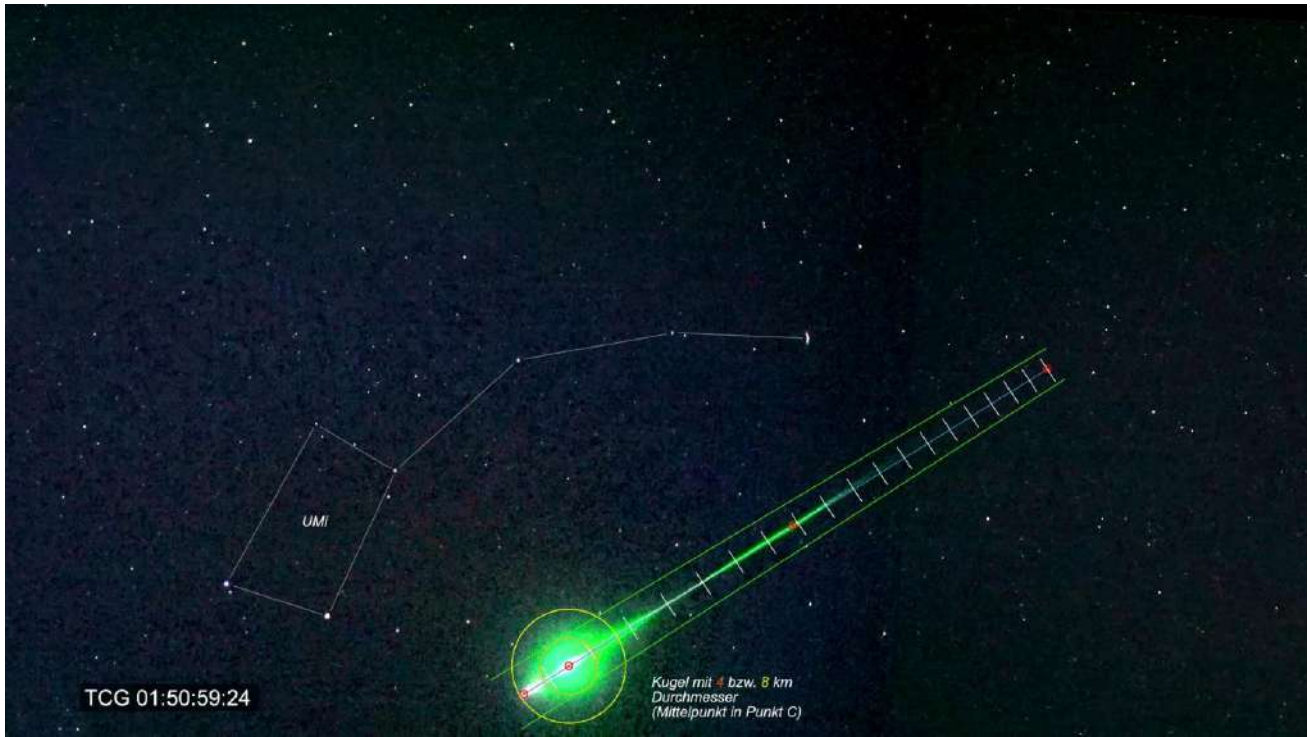


Figure 2: Two frames after the terminal flash. Every line rectangular to the trajectory marks one video frame ($= 40$ ms). Note the strong green afterglow with a diameter up to 8 km.

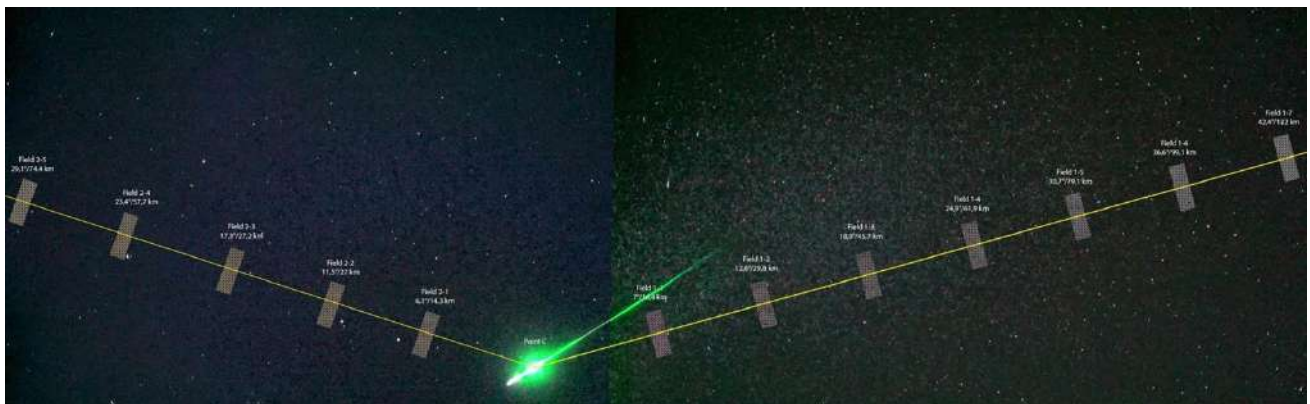


Figure 3: Measurement fields for the bluish sky glow; right: camera 1, left: camera 2. In order to reduce the influence of the apparent image noise each field is 40×160 pixels wide, with the code values averaged.

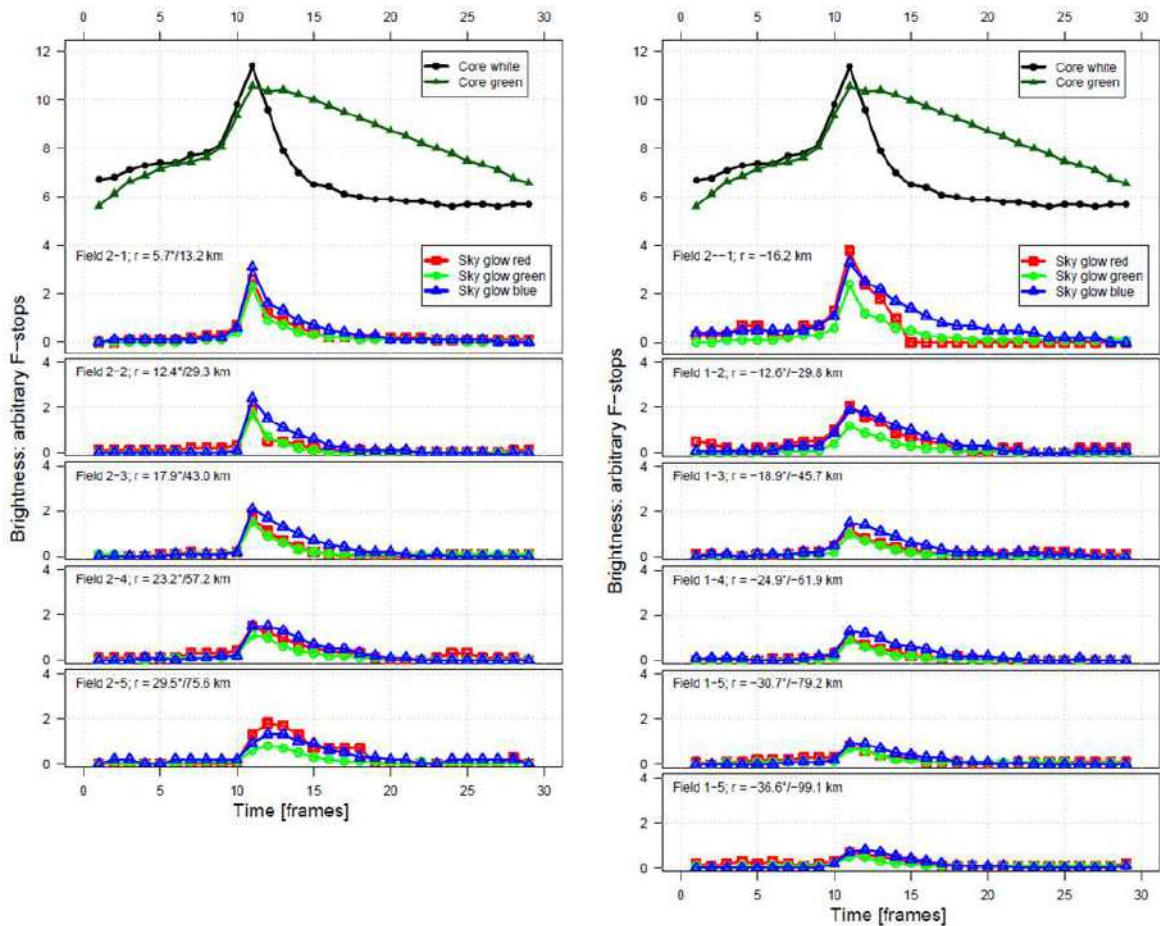


Figure 4: Photometric curves of the bluish sky glow indicated in the measurement fields according to Figure 3.

1 Introduction

This summary of the IMC 2019 presentation is not intended to repeat the whole content of the author's article, together with co-observer Bernd Gaehrken, in WGN journal (Slansky and Gaehrken, 2018).

Perseid fireball 3414-2018 fell on August 13th 2019, 01:51 UT over Ingolstadt, Germany. It was observed by the author from Geigersau/ Bavaria with two Sony α7S cameras at ISO 409 000 in video mode at 25 fps and $t = 1/25$ s equipped with two Canon FD 1.4/50mm lenses at $F = 1.4$. It also occurred on a photo of Juergen Michelberger and Reinhardt Wurzel taken from Horní Vltavice/ Czechia. From these two observations Juergen Michelberger calculated the trajectory.

2 Light effects of the 3414-2018 fireball

The exceptional light effects of 3414-2018 include a terminal flash with a strong green afterglow and a long-lasting persistent train. The results of a camera test ruled out that the appearance of the terminal flash was simply an artefact of overexposure ("blooming"): Images were presented that were made with identical camera-lens-settings to compare a point shaped light source with an areal light source. This test revealed that the terminal flash is an areal light source, with an unknown brightness profile. According to the measurement, the terminal flash and the green afterglow had a diameter of about 8 km

covering a volume of about 268 km³. The author has never heard about such dimensions of a terminal flash and cannot present any explanation.

Even more surprisingly, the terminal flash was accompanied/followed by a widespread persisting bluish sky glow that did neither follow the brightness development of the white meteor wake and terminal flash nor that of the green train and green afterglow. The author presented a measurement of the opto-electronical conversion function OECF of the Sony α7S by which a photometry of the sky glow was made in arbitrary F-stops. The sky glow lasted for more than 9 video frames (= 360 ms). It occurred in the same way in both cameras with the terminal flash inside the field of view of camera 2 but outside of the field of view of camera 1. It was detected up to a distance of 122 km from the point of the terminal flash, covering a volume of more than 4.3 million km³. Its bluish color stayed stable and was not affected by the drastic change in color from the white terminal flash to the green afterglow. Also, this widespread persisting bluish sky glow was completely new to the author.

3 Interpretation

Yes, observation of 3414-2018 was a "lucky strike" with the fireball flying exactly through the – comparably narrow – fields of view of both of the two cameras. Entry height of nearly 160 km was quite high. But it has to be taken into account that this camera is very light sensitive

so that the meteor was detected much earlier in the video than in the photo from the other observation site. At that time the radiant was very high, so the trajectory was very steep. As a consequence, the meteoroid reached the denser parts of the atmosphere quite quickly and expired in a terminal flash at 82.8 km altitude.

As an amateur in meteor observation the author does not speculate about the physical nature of the exceptional light effects of 3414-2018. Based on his profession he can rule out that they go back to camera/lens artefacts. Among scientists the following explanations are discussed:

- Proton-induced electric charge and magnetic fields (Šiljić et al., 2018).
- UV-radiation (Jenniskens, 2004).
- X-rays (Smirnov, 2015).

4 Conclusion

In analogy to the anthropic principle, the video observation of 3414-2014 can be seen as an example of the “camtropic principle”: these light effects could have been recorded only

- in color,
- at 25 fps (or more),
- at F=1.4 and ISO 409 000 (or more),
- in full HD resolution (or more),
- by two stations (or more).

Further meteor observation with this observation technology is expected to be highly valuable.

Acknowledgement

The author thanks Bernd Gaehrken for his support with the observation and analysis, Juergen Michelberger for calculating the trajectory and Reinhard Wurzel for his support of the analysis and for his valuable information about earth's atmosphere.

References

- Slansky, Peter C., Gaehrken, Bernd (2019): “3414-2018: A Perseid fireball showing exceptional light effects, observed by video, photo and radio”. *WGN, journal of the IMO*, 47:3, 79–92.
- Slansky, Peter C. (2016): “Meteor Film Recording with Digital Film Cameras with large CMOS Sensors”. *WGN, journal of the IMO*, 44:6, 190–197.
- Slansky, Peter C. (2019): “Opto-electronical conversion function of the Sony α7S with standard gamma”: http://slansky.userweb.mwn.de/bereiche/astonomie/aufnahmetechniken/bilder/oecf_sony-a7s.pdf.
- Slansky, Peter C., Gaehrken, Bernd (2019): “Camera test of the Sony α7S with a Canon FD 1.4/50 mm lens about blooming of overexposed highlights in regard of the video observation of fireball 3414-2018”: http://slansky.userweb.mwn.de/bereiche/astonomie/aufnahmetechniken/bilder/camera-test_sony-a7s_3414_2018.pdf.
- Šiljić A., Lunić F., Teklić J., and Vinković D. (2018): “Proton-induced halo formation in charged meteors”. *MNRAS*, 481, 2858–2870.
- Jenniskens P. (2004): “Meteor storms as a window on the delivery of extraterrestrial organic matter to the early Earth”. In Norris, R. P. and Stoothman, F. H., editors, *Bioastronomy 2002*, volume 213. IAU 281–288.
- Smirnov V. A. (2015): “About the nature of meteor flares”. In *Odessa Astronomical Publications*, 28, 58.

Results of the Polish Fireball Network in 2018

Mariusz Wiśniewski^{1,2}, Przemysław Żoładek¹, Arkadiusz Olech^{1,3}, Arkadiusz Raj¹,
 Zbigniew Tyminski^{1,4}, Maciej Maciejewski¹, Karol Fietkiewicz¹,
 Maciej Myszkiewicz¹, Marcin P. Gawroński^{1,5}, Tomasz Suchodolski^{1,6},
 Marcin Stolarz¹, Mariusz Gozdalski¹

¹ Polish Fireball Network, Comets and Meteors Workshop, ul. Bartycka 18, 00-716 Warsaw, Poland

brahi@op.pl, mazziek@gmail.com, parmo.pfn@gmail.com, ma.gozdalski@gmail.com,
 spammer.m@gmail.com, marcin.stolarz@gmail.com, krzysiek-pol20@o2.pl

² Central Office of Measures, ul. Elektoralna 2, 00-139 Warsaw, Poland

marand.w@gmail.com

³ Nicolaus Copernicus Astronomical Center, ul. Bartycka 18, 00-716 Warsaw, Poland

a.olech@camk.edu.pl

⁴ National Centre of Nuclear Research RC POLATOM, Soltan 7, Otwock-Świerk, Poland

zbyszek.tyminski@gmail.com

⁵ Faculty of Physics, Astronomy and Informatics, Nicolaus Copernicus University, Grudziądzka 5, 87-100 Toruń,
 Poland

motylek@astro.uni.torun.pl

⁶ Space Research Centre, Polish Academy of Sciences, ul. Bartycka 18A, 00-716 Warszawa, Poland

tomasz.suchodolski@ptma.pl

The Polish Fireball Network (PFN) is a project to regularly monitor the sky over Poland in order to detect bright fireballs. During 15 years of PFN operation 570,968 meteor events were recorded. In 2018 the PFN consisted of 40 continuously active stations with 68 sensitive analogue video cameras and high resolution digital cameras that recorded 82,247 meteor events. Using the PFN data from 2018 and the UFOOrbit software 15,296 trajectories and orbits were calculated.

1 Introduction

Since 2004, Polish Fireball Network (PFN) is patrolling the skies over Poland. Most of PFN observers are amateurs, members of Comets and Meteors Workshop and perform observations from their homes. Some stations are located in astronomical clubs and schools. In 2018 the network consisted of 40 continuously working stations (see Figure 1), with 68 sensitive CCTV video and digital cameras (Olech et al., 2006, Wiśniewski et al., 2017).

2 Cameras of PFN

The cameras of the PFN were able to cover the whole sky above Poland but the south-eastern Poland was particularly well covered because the majority of cameras are located in that area (see Figure 2). In most stations we use low cost sensitive CCTV analog video cameras equipped with lenses with $65.6 \times 49.2^\circ$ field of view. Currently there are 36 cameras of this type. We use MetRec (Molau, 1999) and UFOCapture (SonotaCo, 2005) software for meteor detection. UFOAnalyzer software is used for astrometric reduction of video recordings.

Part of the stations was equipped with 16 high sensitive Mintron 12v6 cameras with fast lenses. This cameras detected up to 4 times more meteors than low cost

cameras. Due to higher sensitivity and smaller fields of view we can record large number of fainter meteors.

Setups with digital cameras are based on sensitive DMK 33GX236. These cameras have resolution of 1920x1200 pixels and lenses with focal length of 2.4 mm which give 130x80 deg field of view. Comparison of low cost setup, sensitive setup and new digital HD setup is presented in Table 1.

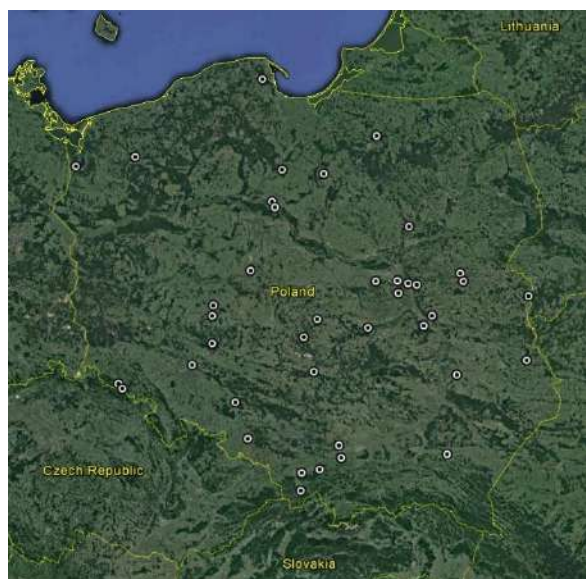


Figure 1 – Active stations of Polish Fireball Network in 2018

Table 1 – Types of camera working in PFN.

Parameter	Low cost setup	Sensitive setup	HD digital setup
Camera type	Tayama C3102-01A1	Mintron 12v6	DMK 33GX 236
Image resolution	480 x 576 pixels Interlaced	768 x 576 pixels Interlaced	1920 x 1200 pixels Progressive
Time resolution	25/50 fps 8 bit	25/50 fps 8 bit	50/25 fps 8/12 bit
Lens	1.2/4 mm	0.8/6 mm - 0.8/12 mm	1.2/2.4 mm
FOV	66x50 degrees	<66x50 degrees	130x80 deg
Pixel size	5' / pixel	<5' / pixel	4' / pixel

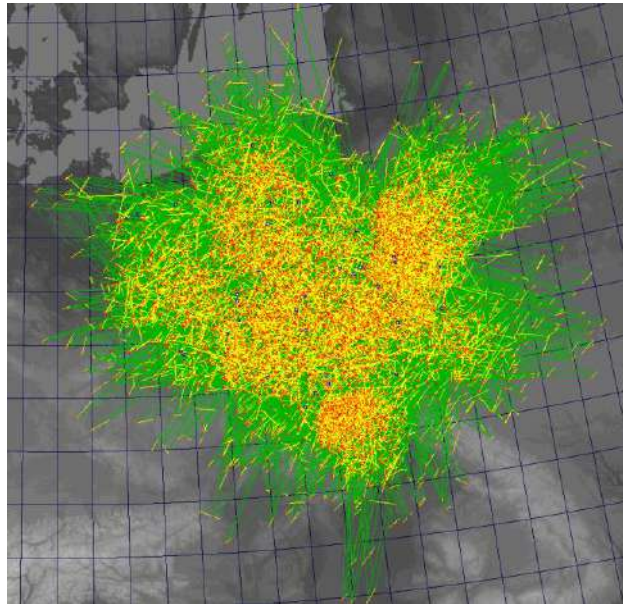


Figure 2 – Calculated trajectories of meteoroids in 2018

Detections from all PFN cameras are automatically transmitted via internet to central server where double station events are detected, analysed and then trajectory and orbit are determined. All calculations are checked by manual inspection.

3 Results of PFN in 2018

In 2018 PFN cameras recorded 83,095 single events. The collected data was preliminary analyzed using UFOOrbit software. The calculations were performed in a fully automatic way. The quality of the final results was controlled by UFOOrbit multiple parameter settings. Detailed information about the limiting parameters can be found in the software documentation (SonotaCo, 2009). The results with high uncertainty were rejected and the criterion was based on the set of the limit values.

We create also the PyFN software for trajectory and orbit calculation. PyFN (Żoładek, 2012) utilize the Celpeha method (Ceplecha, 1987).

Using this data 15,296 trajectories and orbits were calculated. Detailed numbers of detected and calculated meteors is presented in Table 2. In 2018, we maintained a similar number of detections as in the previous year. The reason for this may be a small amount of changes in the

equipment used by PFN. The year 2016 should therefore be considered unique due to the good weather during the Quadrantids, Perseids and Geminids peaks. The table contains preliminary numbers of registered meteors for 2004-2010. These data are re-analyzed to improve their quality using new data analysis algorithms.

Table 2 – Results of 15 years of PFN observations.

Year	Detections	Orbits
2004	4877	226
2005	11089	661
2006	15766	1310
2007	11914	547
2008	17740	1535
2009	15040	1251
2010	12814	903
2011	24099	3430
2012	28471	4186
2013	36347	6114
2014	46936	7351
2015	79083	13528
2016	100389	19087
2017	83095	14586
2018	82247	15296
TOTAL	570968	90160

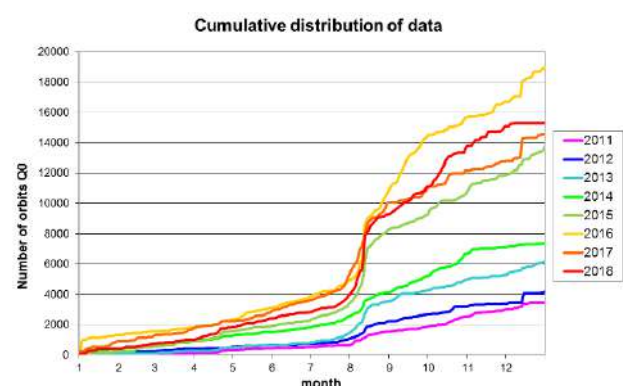


Figure 3 – Cumulative distribution of multistation detections in 2011-2018

Table 3 – Stations and observers of Polish Fireball Network.

ID	Name	Observer	Equipment
PFN01	Ostrowik	Maciej Myszkiewicz	PAVO1
PFN03	Złotokłos	Karol Fietkiewicz	PAVO3
PFN06	Kraków	Maciej Kwinta	PAVO6, PAVO7, PAV79 MDC14
PFN13	Toruń	Tomasz Fajfer	PAV14
PFN19	Kobiernice	Mariusz Szlagor	PAVO8
PFN20	Urzędów	Mariusz Gozdalski	PAV25, PAV26, PAV38, PAV99
PFN24	Gniewowo	Krzesztof Polakowski	PAV40, MDC09
PFN30	Wrocław	Mateusz Dmitrzak	PAVO1, PAVO2
PFN32	Chełm	Maciej Maciejewski	PAV35, PAV36, PAV43, PAV60, MDC09
PFN37	Nowe Miasto Lubawskie	Janusz Laskowski	PAV41
PFN38	Podgórzyn	Tomasz Krzyżanowski	PAV44, PAV49, PAV50, MDC15
PFN39	Rosocha	Andrzej Dobrychłop	PAV42
PFN40	Otwock	Zbigniew Tymiński	PAVO1, PAVO9, PAV52
PFN41	Twardogóra	Henryk Krygiel	PAV45, PAV53
PFN43	Siedlce	Maciej Myszkiewicz	PAV27, PAV61, PAV67, MDC07
PFN45	Łańcut	Łukasz Woźniak	PAV37
PFN46	Grabniak	Tomasz Łojek	PAV57, MDC06
PFN47	Jeziorko	Tomasz Lewandowski	PAV13, PAV62, PAV63, PAV65
PFN48	Rzeszów	Marcin Bęben	PAV59, PAV64, PAV77, MDC03
PFN49	Helenów	Paweł Woźniak	PAV23
PFN51	Zelów	Jarosław Twardowski	PAV22
PFN52	Stary Sielc	Marcin Stolarz	PAV66, PAV75, MDC04, MDC12
PFN53	Belęcin	Michał Kałużyński	PAV68
PFN54	Lęgowo	Grzegorz Tisler	PAV69
PFN55	Ursynów	Przemysław Żołądek	MDC01, MDC02
PFN56	Kolbuszowa	Cezary Wierucki	PAV71
PFN57	Krotoszyn	Tomasz Suchodolski	PAV70
PFN58	Opole	Filip Kucharski	PAV72
PFN59	Drawsko Pomorskie	Mirek Krasnowski	MDC10
PFN60	Bystra	Piotr Nowak	PAV74, PAV80
PFN61	Piwnice	Marcin Gawroński	PAV10, PIWO1
PFN62	Szczecin	Zbyszek Laskowski	MDC05
PFN63	Starowa Góra	Arek Raj	MDC11, MDC20, MDC26
PFN64	Grudziądz	Sebastian Soberski	MDC18
PFN65	Wadowice	Mariusz Szlagor	MDC13
PFN67	Nieznaszyn	Walburga Węgrzyk	PAV78, PAVO2
PFN69	Lampówko	Jacek Kapcia	PAV69
PFN70	Kodeń	Piotr Onyszczuk	PAV67
PFN71	Radomsko	Hubert Dróżdż	PAVO1
PFN72	Koźmin Wielkopolski	Krzesztof Polak	PAVO1, PAVO2
PFN73	Chrzanów Mały	Paweł Zaręba	PAVO1, PAVO2, PAVO3
PFN74	Brwinów	Paweł Zaręba	PAVO1, PAVO2
PFN75	Karpacz	Tomasz Krzyżanowski	PAV81
PFN76	Kozińce	Artur Jaśkiewicz	PAVO1

Using data from 2018, we checked how the number of recorded meteors is distributed for individual cameras. We found that each of the three camera groups are clearly separated (see Figure 3). Digital cameras record fewer meteors than low cost cameras. Detection numbers for individual cameras in both groups are similar and stay in the range of 400-1200 for digital and 1200-2400 for low-cost cameras. The amount of detections for sensitive analog cameras varies significantly from 2,400 up to 6,000 for best camera in 2018. The effectiveness of sensitive cameras strongly depends on the conditions in which they observe and the skills of the observer in the selection of detection parameters.

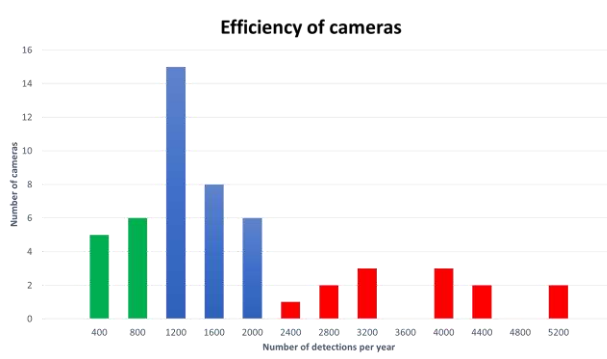


Figure 3 – Efficiency of the systems: green – digital cameras; blue – low cost analog cameras; red – sensitive analog cameras.

Acknowledgement

We would like to thank to all station owners, operators and observers for long term and precise work for Polish Fireball Network (see Table 3).

References

- Ceplecha Z., (1987), "Geometric, dynamic, orbital and photometric data on meteoroids from photographic fireball networks", *Bulletin of the Astronomical Institutes of Czechoslovakia*, July 1987, 38:222–234,
- Molau S., (1999), "The meteor detection software MetRec". W. J. Baggaley and V. Porubcan, editors, *Meteoroids 1998*, pages 131–+
- Olech A., Żoładek P., Wiśniewski M., Kransowski M., Kwinta M., Fajfer T., Fietkiewicz K., Dorosz D., Kowalski Ł., Olejnik J., Mularczyk K., Złoczewski K., (2006), "Polish Fireball Network", *Proceedings of the International Meteor Conference*, Oostmalle, Belgium, 15-18 September, 2005, IMO pp. 53-62
- SonotaCo (2009), "UFCaptureV2 Users Manual".
<http://sonotaco.com/soft/UFO2/help/english/index.html>
- M. Wiśniewski, P. Żoładek, A. Olech, Z. Tyminski, M. Maciejewski, K. Fietkiewicz, R. Rudawska, M. Gozdalski, M. P. Gawroński, T. Suchodolski, M. Myszkiewicz, M. Stolarz, K. Polakowski (2017), "Current status of Polish Fireball Network", *Planetary and Space Science*, Volume 143, p. 12-20.
- Żoładek P., (2012), "PyFN - multipurpose meteor software", *Proceedings of the International Meteor Conference*, Sibiu, Romania, 15-18 September, 2011, IMO pp. 53-55

Beta Taurids Video Campaign

Przemysław Żoładek², Arkadiusz Olech^{1,2}, Mariusz Wiśniewski^{2,3}, Marcin Bęben², Hubert Dróżdż², Marcin Gawroński^{2,4}, Karol Fietkiewicz², Artur Jaśkiewicz², Miroslaw Krasnowski², Henryk Krygiel², Tomasz Krzyżanowski², Maciej Kwinta², Janusz Laskowski², Zbigniew Laskowski², Tomasz Łojek², Maciej Maciejewski², Maciej Myszkiewicz², Piotr Nowak², Piotr Onyszczuk², Krzysztof Polak², Krzysztof Polakowski², Arkadiusz Raj², Andrzej Skoczewski², Mariusz Szlagor², Zbigniew Tymiński^{2,6}, Jarosław Twardowski², Walburga Węgrzyk², Paweł Zaręba²

¹ Nicolaus Copernicus Astronomical Center, Polish Academy of Sciences, ul. Bartycka 18,
00-716 Warszawa, Poland

olech@camk.edu.pl

² Comets and Meteors Workshop, ul. Bartycka 18,
00-716 Warszawa, Poland

brahi@op.pl

³ Central Office of Measures, ul. Elektoralna 2, 00-139 Warszawa, Poland
marand.w@gmail.com

⁴ Toruń Centre for Astronomy, Faculty of Physics, Astronomy and Applied Informatics,
N. Copernicus University, ul. Grudziądzka 5, 87-100 Toruń, Poland
motylek@astro.uni.torun.pl

⁵ Narodowe Centrum Badań Jądrowych, Ośrodek Radioizotopów POLATOM, ul. Sołtana 7,
05-400 Otwock, Poland
zbyszek.tyminski@gmail.com

This is a brief description of the daylight Taurids campaign conducted by Polish Fireball Network from June 20, 2019 to July 15, 2019. Multiple cameras have been converted to daylight operation using IR or neutral density filters. Daylight activity of the Taurids was not observed, one daylight fireball of unknown origin has been detected on June 30, 2019. The only double station meteor belonging to Taurids complex was a Zeta Perseid observed on the brightening sky just before the sunrise.

1 Introduction

The Taurids are a low inclination meteoroid streams evolutionary connected with 2P/Encke comet. Some authors suggest that history of the stream is more complicated and that the Taurids may be connected with older and much larger object disintegrated in the past (Asher et al., 1993, Babadzhanyan et al., 2008). Taurids are separated into two branches - northern and southern. Both branches intersects Earth orbit twice a year. The autumn encounter is well known to the night sky observers. Northern branch forms the Northern Taurids meteor shower (NTA), southern branch - Southern Taurids (STA) with wide and flat maximum in October and November. There is also daytime encounter which may be observed mostly using radio methods. Beta Taurids are active from the beginning of June to the first half of July with a maximum close to June 28. The second daytime shower is a Zeta Perseids shower which peaks about two weeks before the Beta Taurids. Taurids are not a very active meteor shower. It's typical ZHR is about 5 at maximum, however a comparatively big number of bright meteors is observed every year. There is a significant activity enhancement observed in some particular years connected with very bright fireballs occurrence (Asher 1991, Asher et al., 1993). For such years (known also as swarm years) there is a close encounter with a part of the stream involved in 7:2 res-

onance with Jupiter. The best nighttime encounters have been predicted for 2005 and 2015 while the daytime encounter looks to be especially promising in 2019. The 2005 and 2015 returns were spectacular. Numerous fireballs reached magnitude higher than -8 magnitude, some with magnitudes above -15 magnitude. (Olech et al. 2017). Such bright fireballs could be easily observable on the daytime sky using dedicated equipment; the observing campaign has been prepared for 2019 Beta Taurids daylight encounter.

2 Preparations

Initial plans considered purchase of specialized equipment - allsky cameras with low sensitivity but high resolution sensors. Connected with special filters such equipment should be suitable for daylight fireball detections. Finally, only a limited variant has been realised with usage of existing PFN detectors. Such cameras should be prepared for daylight observations. The analog cameras have been switched to low gain, for digital cameras also the exposure time was adjusted to optimal daylight values. Some significant detection rate improvement should be possible with filters mounted in the front of objective lens. Properly chosen filter will improve the fireball to background signal ratio. A simple analysis has been performed for this purpose. Spec-

trum of the various high-pass filters has been checked against the spectrum of daylight sky and spectrum of one of the recently observed Taurid fireballs (Matlovič et al. 2017). The best signal to background ratio has been obtained for IR720 highpass filter. Such filter efficiently reduce the daylight sky while the light produced by fireball is reduced with lesser efficiency, mostly due to presence of strong oxygen line which is passed by the filter. Signal to background ratio (converted to magnitudes) for various filters has been summarized in the table below.

Table 1 – Fireball brightness vs background brightness for various filters. D - loss of background light, F - loss of fireball light, Diff - difference. All intensities converted to magnitude scale. Negative difference for yellow filter means that this filter is not suitable for daylight detections. Calculated gain for orange filter is negligible, also the red filter is not so useful. Calculated gain for IR720 high-pass filter is however significant.

Filter	D	F	Diff
Baader Yellow	0.2	0.27	-0.07
Baader Orange	0.87	0.76	0.11
Baader Red	1.54	1.38	0.16
Hoya 720	3.3	1.92	1.38

Meanwhile, the daylight fireball occurred over northern Poland on 2019 02 08 14:35:55 UT. This fireball has been detected by two car recorders and was later found on PFN camera located at Lamkówko close to Olsztyn. This camera was operated with MetRec software, the sky was covered by thin layer of semitransparent clouds. The fireball is clearly visible on the image presented below. This detection has proven that daylight detections are possible even with simple analog cameras switched to operation during daylight hours.

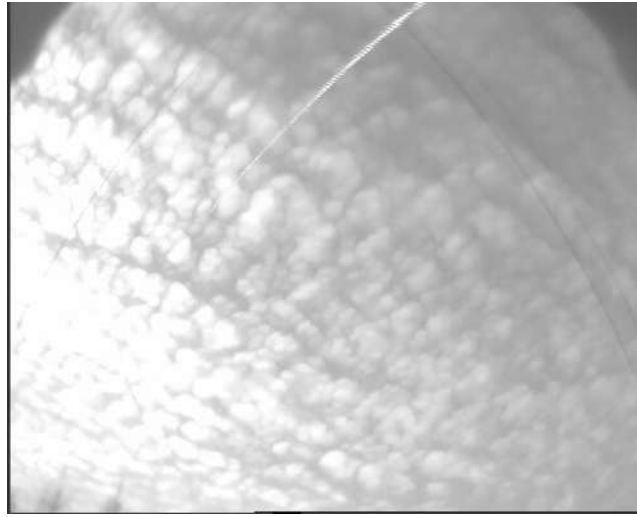


Figure 1 – Daylight fireball recorded by PFN69 Lamkówko station, 2019-02-08 14:35:55 UT

A list of stations and cameras prepared for daylight observations is presented in the table below. Two stations were equiped with IR720 filters, most of other cameras were equiped with neutral density (ND16, ND4) filters. For all digital cameras gain and exposure time has been adjusted. From June 20 to July 15 all mentioned cameras were switched to daylight observations.

Table 2 – List of cameras switched to daylight observations between 2019-06-20 and 2019-07-15

Station	Camera	Observer	Filter	Type
PFN06	MDC14	Maciej Kwińska	ND16	DigitalHD
PFN29	MDC13	Mariusz Szlagor	IR720	DigitalHD
PFN32	MDC08	Maciej Maciejewski	ND16	DigitalHD
PFN32	PAV43,35	Maciej Maciejewski	ND16	PAL
PFN32	PAV36,60	Maciej Maciejewski	ND16	PAL
PFN38	MDC15	Tomasz Krzyżanowski	IR720	DigitalHD
PFN40	PAVO9,3	Zbigniew Tyminski	ND4	PAL
PFN41	PAV45,53	Henryk Krygiel	ND16	PAL
PFN50	MDC24	Andrzej Skoczewski	none	DigitalHD
PFN62	MDC05	Zbigniew Laskowski	none	DigitalHD
PFN63	MDC26	Arkadiusz Raj	ND4	DigitalHD
PFN67	PAVO2,78	Walburga Węgrzyk	ND4	PAL
PFN73	PAVO1,2,3	Paweł Zaręba	ND16	PAL
Warszawa	PAVO3	Karol Fietkiewicz	none	PAL

3 Observations and results

During the observing campaign weather was good with only few cloudy days. All cameras made thousands of false detections. Most of detections were caused by birds, insects and planes flying at various altitudes. Few detections were similar to meteors (straight line patch, proper angular speed, point light source) and required more detailed examination. Obviously software and hardware used for observations were sufficient for detecting bright objects moving on the bright sky. Limiting magnitude for detections should be at least -10 magnitude.



Figure 2 – Typical false detections caused by birds and insects, PFN38 Podgórzyn, DMK33GX174 with IR720 filter

There is one daylight fireball captured by temporary station in Warsaw, on 2019-06-30 14:31:56 UT. The fireball appeared over northern horizon and unfortunately was not detected by other stations. After photographic calibration of the video frame the back prologation of observed patch has been verified. This fireball was probably a member of helion sporadic source but not a member of Taurid stream. With almost complete lack of daylight fireball detections we decided to examine all PFN data recorded at the end of every night during the campaign period. From few dozens of meteors recorded after 1:00 UT only few bear some resemblance to Taurids. After trajectory and orbital calculations only one Taurid stream member has been recognized. This meteor appeared on 2019-06-30 01:23:11

UT and was barely visible on the brightening sky. Meteor was captured by digital camera located at PFN50 Brzozówka and two analog cameras from Rzeszów and Kraków. The trajectory was located over southern Poland between Kraków and Tarnów. The initial velocity was typical for Taurid stream ($V_{inf}=31.7$ km/s), the radiant was located only 7 degrees over horizon, few degrees north of the Beta Tauri, in the Auriga constellation. Trajectory parameters and orbital elements are presented in the tables below. Orbital elements have been calculated using PyFN software (Żoładek, 2011) and independently using Meteor Toolkit (Dmitriev et al, 2018). Orbital elements differ significantly from these known for 7:2 resonance stream expected this year ($D' > 0.05$ when compared to 2015TX24 object). Comparison with the IAU MDC shower list shows that detected meteor belongs to another branch of the stream called Zeta Perseids (172 ZPE).

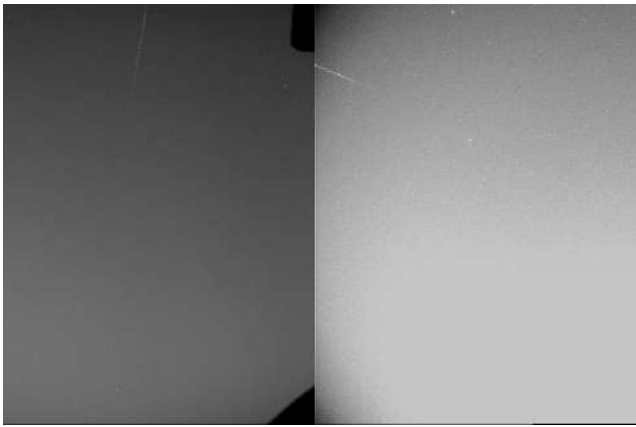


Figure 3 – The only one Taurids complex member detected - 2019-06-30, 01:23:11 UT, PFN48 Rzeszow (left), PFN06 Krakow (right)

Table 3 – Atmospheric trajectory data, meteor 2019-06-30 01:23:11 UT

Parameter	Beginning	Terminal
Velocity [km/s]	31.7 ± 0.1	31.5 ± 0.1
Height [km]	93.3 ± 0.6	87.8 ± 0.1
Longitude [deg]	21.340 ± 0.004	20.872 ± 0.001
Latitude [deg]	49.977 ± 0.002	49.7065 ± 0.0006
Slope [deg]	7.0 ± 0.8	6.6 ± 0.8

Table 4 – Orbital elements calculated with PyFN (left column) and Meteor Toolkit (right column), meteor 2019-06-30 01:23:11 UT

Parameter	PyFN	Meteor Toolkit
a	2.05	1.97
e	0.8512 ± 0.071	0.8434 ± 0.057
i	7.56 ± 0.41	7.35 ± 1.04
q	0.3061 ± 0.005	0.3088 ± 0.077
ω	58.52 ± 0.93	58.67 ± 0.7
Ω	97.74 ± 0.00015	97.78 ± 0.005
Period [y]	2.93	2.77

2019 and July 15, 2019. Equipment used was able to detect fireballs brighter than -10 magnitude on the daylight sky. Daylight activity of the stream was not observed. Only one daylight fireball was observed but it was not a member of Beta Taurids or Zeta Perseids. The only member of Taurids complex was a Zeta Perseid bright meteor observed on June 30 at dawn. The campaign was an interesting test for daylight detections capability of the video meteor software like MetRec and FreeTure.

Acknowledgements

This work was supported by authors themselves.

References

- Asher D. J. (1991). *The Taurid Meteoroid Complex*. PhD thesis, Oxford Univ. (England).
- Asher D. J., Clube S. V. M., and Steel D. I. (1993). “Asteroids in the Taurid Complex”. *MNRAS*, **264**, 93.
- Babadzhanov P. B., Williams I. P., and Kokhirova G. I. (2008). “Near-Earth Objects in the Taurid complex”. *MNRAS*, **386:3**, 1436–1442.
- Dmitriev V., Lupovka V., and Gritsevich M. (2018). “Meteor Toolkit — Free Distributable Open-Source Software for Determination and Analysis of Meteoroid Orbits”. In *81st Annual Meeting of the Meteoritical Society*, volume 81, page 6210.
- Matlovič P., Tóth J., Rudawska R., and Kornoš L. (2017). “Spectra and physical properties of Taurid meteoroids”. *Planetary and Space Science*, **143**, 104–115.
- Olech A., Żoładek P., Wiśniewski M., Tymiński Z., Stolarz M., Bęben M., Dorosz D., Fajfer T., Fietkiewicz K., Gawroński M., Gozdalski M., Kałużny M., Krasnowski M., Krygiel H., Krzyżanowski T., Kwinta M., Lojek T., Maciejewski M., Miernicki S., Myszkiewicz M., Nowak P., Polak K., Polakowski K., Laskowski J., Szlagor M., Tissler G., Suchodolski T., Węgrzyk W., Woźniak P., and Zaręba P. (2017). “Enhanced activity of the Southern Taurids in 2005 and 2015”. *MNRAS*, **469:2**, 2077–2088.
- Żoładek P. (2012). “PyFN - multipurpose meteor software”. In *Proceedings of the International Meteor Conference, 30th IMC, Sibiu, Romania, 2011*. pages 53–55.

4 Summary

Polish Fireball Network conducted a video campaign devoted to daylight fireball detection between June 20,

AMOS and interesting fireballs

Juraj Tóth, Pavol Matlovič, Leonard Kornoš, Pavol Zigo, Dušan Kalmančok, Jaroslav Šimon, Jiří Šilha, Jozef Világi, Martin Baláz, and Peter Vereš

Dept. of Astronomy, Physics of the Earth and Meteorology, Faculty of Mathematics, Physics and Informatics, Comenius University in Bratislava, Slovak Republic
toth@fmph.uniba.sk

AMOS (All-sky Meteor Orbit System) is an image-intensified all-sky video meteor system originally developed for the Slovak Video Meteor Network in 2007 at the Astronomical and Geophysical Observatory in Modra (AGO) of the Comenius University. Currently, five stations are operational in Slovakia and two on Canary Islands since March 2015. A pair of AMOS cameras was installed in Chile in March 2016 to monitor the meteor activity on the southern sky. Another pair of AMOS cameras was installed in September 2018 on Hawaiian Islands, atop of Haleakala and Mauna Kea. I will present some interesting fireballs observed by AMOS systems.

1 Introduction

AMOS (All-sky Meteor Orbit System) is an intensified all-sky meteor video system originally developed for the Slovak Video Meteor Network in 2007 at the Astronomical and Geophysical Observatory (AGO) Modra, Comenius University (Tóth et al., 2011, Zigo et al., 2013). Currently, four stations are in operation in Slovakia and two cameras were installed on the Canary Islands in March 2015 (Tóth et al., 2015). Pair of AMOS cameras was installed in Chile in March 2016 (Tóth et al., 2016) for the permanent meteor activity monitoring of the southern sky. The AMOS cameras were continuously updated from the first prototype in 2007. Currently, digital cameras DMK with resolution of 1600 x 1200 pixels and 20 fps are used, which corresponds to the field of view 180° x 140° and limiting sensitivity comparable to human eye (+5.5 mag for stellar objects, +4 mag for meteors and other moving targets). Also, the aluminum outer shell was upgraded with light, rain, temperature and humidity sensors to operate cameras fully autonomously at distant locations. AMOS cameras are operated

continuously throughout the whole year to monitor meteor activity even during the full Moon phase. A single AMOS station usually detects 10.000 – 20.000 meteors per year. Depending on weather conditions and distance among stations (Slovakia average 90 km, Canary Islands 147 km, Chile 83 km, Hawaii 127 km), simultaneous detections are on the level of 30 - 40 %. We are working on new detection software AMOS with KVANT company and meteor trajectory and orbits program MT based on Ceplecha et al., (1987), Borovička et al., (1995) and Kornoš et al., (2017) algorithms. Also, each site of the network is equipped with spectral camera AMOS-Spec or AMOS-SpecHR.

2 Future plans

Currently, we are developing AMOS cameras with collaborators in Australia and Namibia/South Africa (Figure 1, blue crosses). The aim is to develop a global network for 24 hour continuous monitoring of the influx of relatively faint meteors and characterization of weak meteor showers (Rudawska et al., 2015).

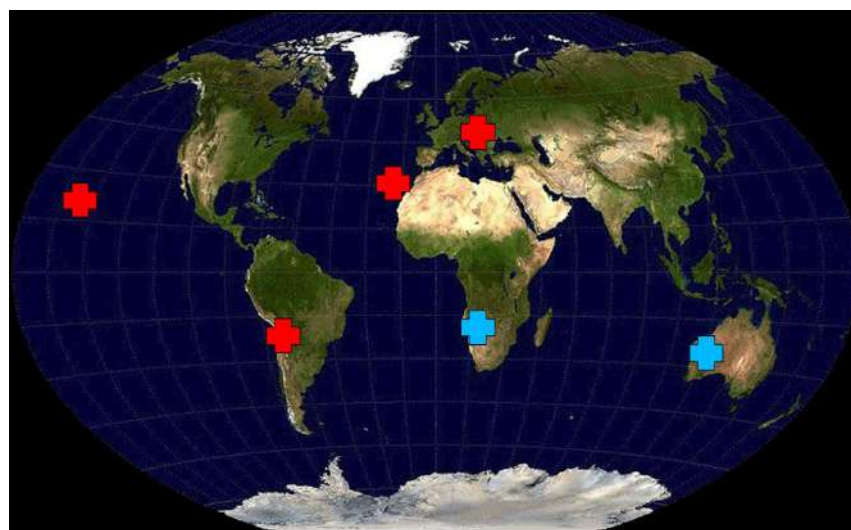


Figure 1 – Current state of the AMOS system global network. In red, operating stations in Slovakia (4 stations), Canary Islands (2 stations), Chile (2 stations) and Hawaii. In blue, planned expansion of the network to Australia and Namibia/South Africa.

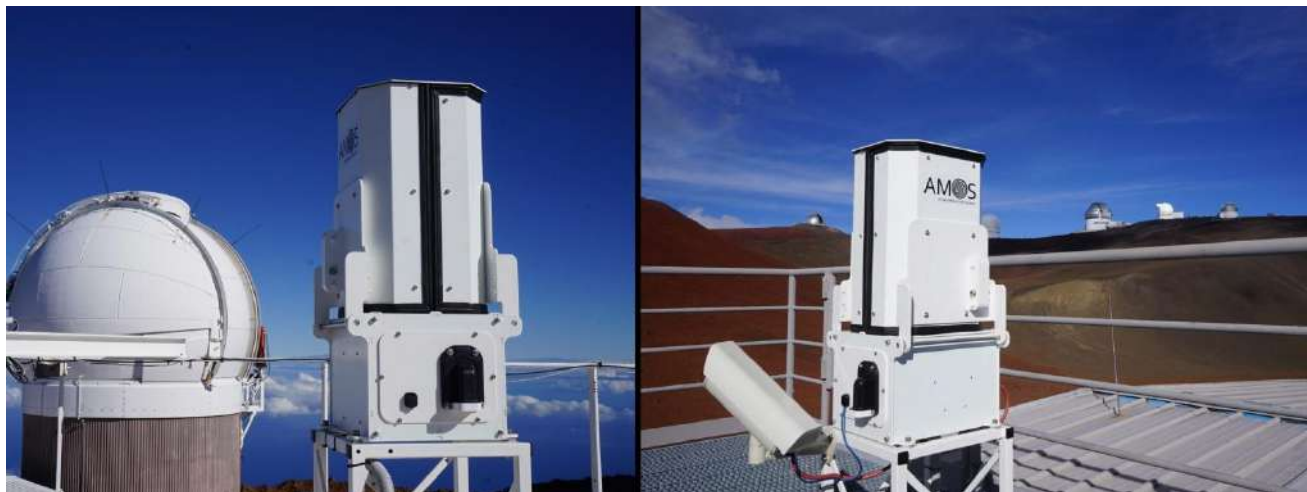


Figure 2 – AMOS system installations on Haleakala Observatory (left) and on Maunakea Observatory (right) with spectral camera.

3 Interesting fireballs

During our regular observations in each location, including all clear nights with moonlight too, we have observed dozens of fireballs. Some of them are already partly analysed (fireball of June 29, 2019 from Canary I.), where future publications are awaited. One recent example, AMOS system on Canary Islands observed (Figure 3) the bright fireball with absolute magnitude about -11 which lasted about 8s (October 1, 2019 00:02:47 UT). The fireball was a member of October Ursidae meteor shower (333 OCU), even though it was observed about 2 weeks earlier than the expected peak of OCU shower. However, the radiant position ($\text{RA}=145.3^\circ$, $\text{DEC}=64.7^\circ$) and orbit fit very well. The trajectory was shallow, north-west of La Palma island with beginning height 117 km and ending height 80 km (Figure 4).

4 Conclusion

The AMOS system is mainly dedicated to observe medium bright meteors up to +4 magnitude. Due to the all-sky coverage, it is able to cover very bright and long lasting events with some limitation in photometry.

Acknowledgement

This work was supported by grant APVV-16-0148 and VEGA 1/0596/18 and by operation of AMOS cameras by colleagues from AGO Modra. Many thanks to IAC staff and Alain Maury in SpaceObs and to Silvia Lisoni in Paniri Caur Chile. We are thankful for installation and maintenance of AMOS of Haleakala and Maunakea Observatory, University of Hawaii, Smithsonian Millimeter Array, namely M. Maberry, D. O'Gara, V. Kyselyov, S. Redford, S. Ho and Robert Jedicke. <https://fmph.uniba.sk/daa>

References

Borovička J., Spurný P., Keclíková J. (1995). "A new positional astrometric method for all-sky

cameras". *Astron. Astrophys. Suppl. Ser.*, 112, 173–178.

Ceplecha Z. (1987). "Geometric, dynamic, orbital and photometric data on meteoroids from photographic fireball networks". *Bull. Astron. Inst. Czechosl.*, **38**, 222–234.

Kornoš L., Ďuriš, F., Tóth, J. (2017). "AMOS orbit software, EDMOND database". In, *Proceedings of the International Meteor Conference*, Petnica, Serbia, 21-24 September 2017. IMO, xx-xx

Rudawska, R., Matlovič, P., Tóth, J., Kornoš, L. (2015). "Independent identification of meteor showers in EDMOND database". *Planetary and Space Science*, **118**, 38–47.

Tóth J., Kornoš L., Vereš, P., Šilha, J., Kalmančok, D., Zigo, P., Világi, J. (2011). "All-Sky Video Orbits of Lyrids 2009". *Publ. Astron. Soc. J.*, 63, 331.

Tóth, J., Zigo, P., Kalmančok, D., Šimon, J.; Kornoš, L.; Világi, J.; Rudawska, R.; Serra-Ricart, M.; Perez, J. C.; Licandro, J. (2015). "5 months of AMOS on the Canary Islands". In Gyssens, M.; Roggemans, P., editors, *Proceedings of the International Meteor Conference*, Mistelbach, Austria, 27-30 August 2015. IMO, 63-65.

Tóth, J., Kaniansky, S. (2016)." Expedition Atacama - project AMOS in Chile". In *Proceedings of the International Meteor Conference 2016*, Egmond, 295–296.

Zigo P., Tóth J., Kalmančok, D. (2013). "All-Sky Meteor Orbit System (AMOS)". In Gyssens, M.; Roggemans, P., editors, *Proceedings of the International Meteor Conference*, La Palma, Canary Islands, Spain, 20-23 September 2012. IMO, 18–20.

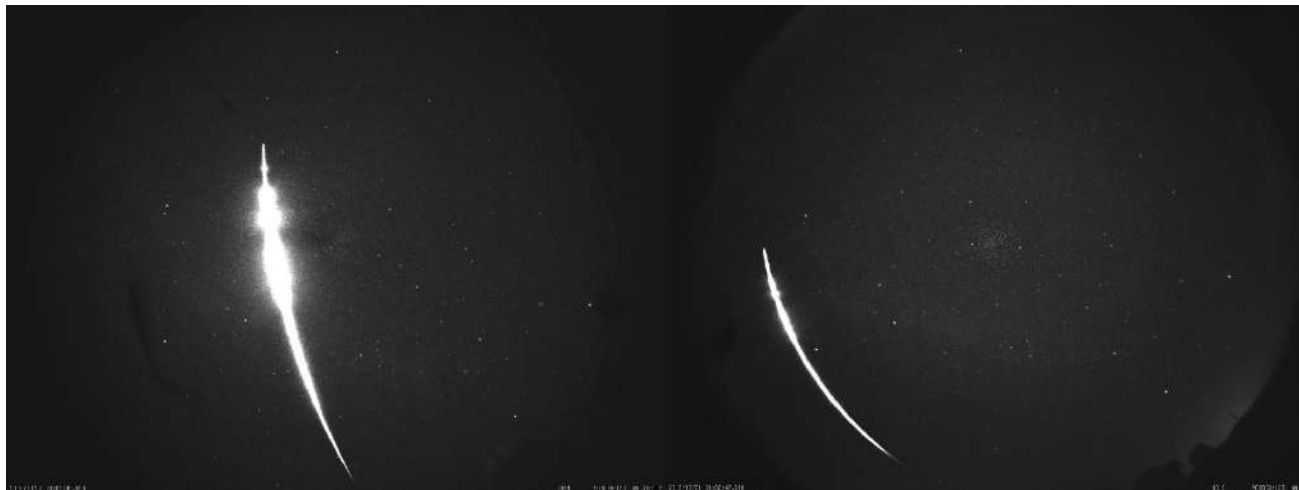


Figure 3 – Fireball of October Ursid meteor shower observed by AMOS system on Roche de Los Muchachos Observatory, La Palma (left) and on Teide Observatory, Tenerife (right) on October 1, 2019 at 00:02:47 UT.

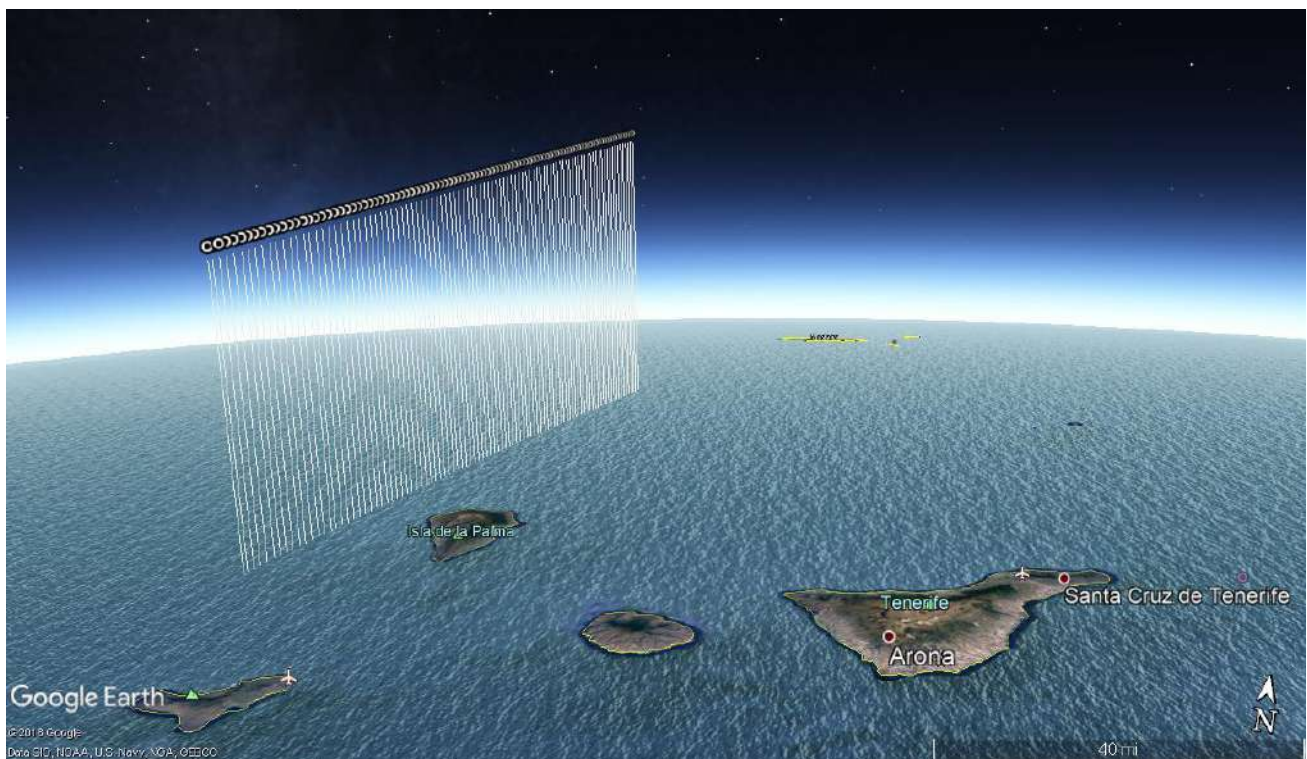


Figure 4 – The trajectory of the fireball of October 1, 2019 over Canary Islands.

A little tour across the wonderful realm of meteor radiometry

Jean-Louis Rault^{1,2}, François Colas¹

¹ IMCCE, Observatoire de Paris, France

² IMO Radio Commission, Hove, Belgium

Jean-Louis.Rault@obspm.fr

This paper describes the path strewn with pitfalls encountered during the development of a large dynamic range and very fast radiometer designed to precisely observe the meteor light curves. A small series production of a finalized version of the current prototype should accompany some video cameras from the FRIPON network.

1 Introduction

The development of a high speed and large dynamic range meteor radiometer was decided for the following main reasons:

- It would be interesting to search for potential correlations between the intriguing oscillations detected by the FRIPON radio network (Rault et al., 2017) appearing sometimes superimposed on the classical smooth meteor head echoes Doppler shifts curves (Figure 1).
- The FRIPON program (Colas et al., 2015) is in need of more accurate and detailed meteor light curves measurements than those obtained with its video cameras network (12 bits & 30 fps devices).

Because the present radiometer prototype is still in an active development phase, this paper is aiming more to give some hints and tricks about the design of the system, and to share the experience gained during the preliminary field tests, rather than to give a detailed and reproducible description of the equipment.

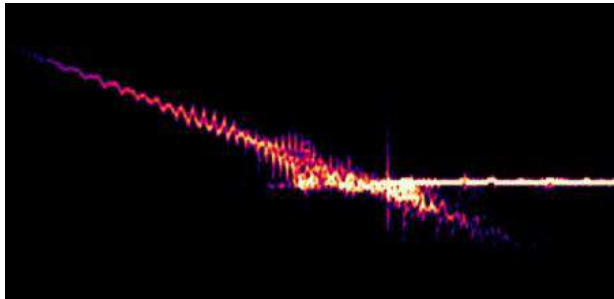


Figure 1 – Example of some intriguing pulsations observed on a head echo Doppler shift curve

2 System design

State of the art in terms of simple PIN diodes meteor radiometers

Vida et al. (2015) first proposed a low cost single PIN photodiode meteor radiometer, fitted with a 7.7 mm^2 active surface sensor, whose sensitivity was rather low.

Then, Segon et al. (2018) obtained encouraging results on bright meteors with a similar system, but equipped with 9 PIN photodiodes, increasing the surface of the light sensor to 67.5 mm^2 . At last, Buchan et al. (2018) proposed a large dynamic range radiometer using a single large surface light sensor (100 mm^2), and a non linear amplification chain allowing a huge dynamic range. Their prototype is still under development, and no meteor detections have yet been reported. The bandwidth offered by these 3 systems is a few hundred Hz.

Requirements specification for the present radiometer

The main requirements were as follows:

- High dynamic range (> 12 bits ADC analog to digital converter), with magnitudes brighter than -10 , which is the FRIPON cameras present limit.
- Large bandwidth (several kHz, compared to the 15 Hz limit for the FRIPON cameras running at 30 frames per second).
- Fisheye type sensor FOV (field of view).
- PIN silicon photodiodes sensors technology, to avoid photomultiplier tube systems complexity.
- Off-the-shelf recording and data processing software.
- Accurate data time stamping, to allow fine correlations between video cameras and radiometer data.
- Associated PC using Windows 7 or 10 as operating system (but Linux compatible for further development).
- Reasonable cost.

Main technological choices

A configuration using 16 cheap BPW34 photodiodes was chosen, giving a total 120 mm^2 light sensor surface.

Figures 2 and 3 show the relative spectral sensitivity curve and the field of view of such sensors.

At the beginning of the project, it was envisaged to install the 16 sensors on a portion of sphere, in order to create a kind of fly eye allowing a good optical sensitivity at low

elevations. This idea was abandoned quickly because in Western Europe the light pollution radiated by cities during night time is too often annoying. Installing the light sensors on a flat surface as shown on Figure 4 was finally a good choice, as confirmed during the field tests.

The photodiodes are used in the "current mode" instead of "photovoltaic mode" because it allows wider bandwidths. Transimpedance amplifiers are used to convert the diodes output currents into voltages (Johnson, 2004). The bandwidth limitation due to the parasitic capacitance of each photodiode is mitigated by the choice of 4 transimpedance amplifiers connected to batches of 4 photodiodes wired in parallel, as shown in Figure 5.

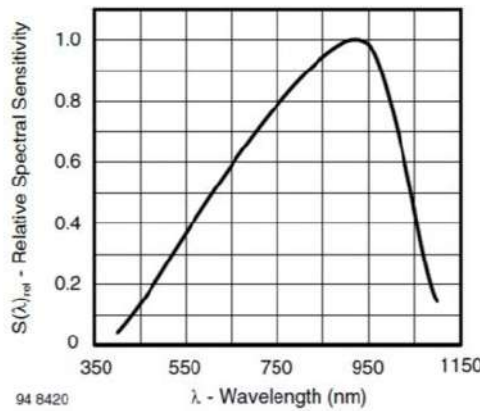


Figure 2 – Relative spectral sensitivity vs wavelength of the BPW34 photodiode

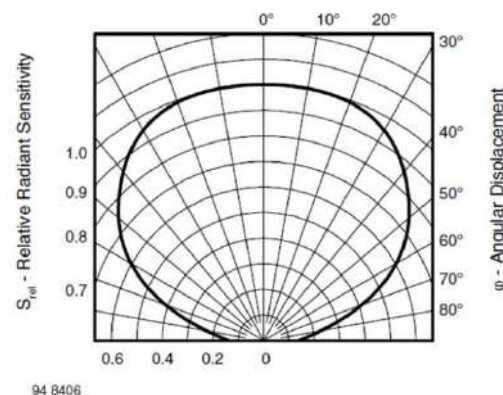


Figure 3 – Relative radiant sensitivity vs angular displacement of the BPW34 photodiode



Figure 4 – Matrix of 4x4 BPW34 photodiodes

The outputs of the transimpedance amplifiers are summed by an operational amplifier.

A TL072 JFET type of operational amplifier was selected because of its large bandwidth, its high linearity, its low noise and its low price.

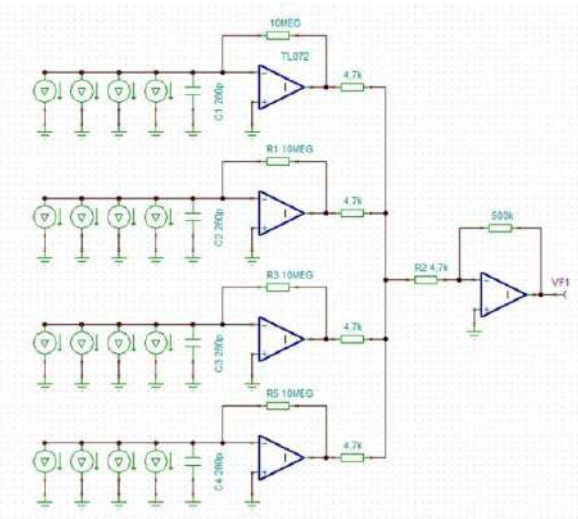


Figure 5 – Simplified diagram of the analog part of the radiometer

The bandwidth of the entire analog chain (including the photodiodes) was evaluated by means of TINA-Ti v9, a Texas Instruments simulation tool. After carefully adjusting the value of the feedback capacitors installed on each transimpedance amplifier, the bandwidth @ -3 dB goes from 0 to 20 kHz, as shown in Figure 6.

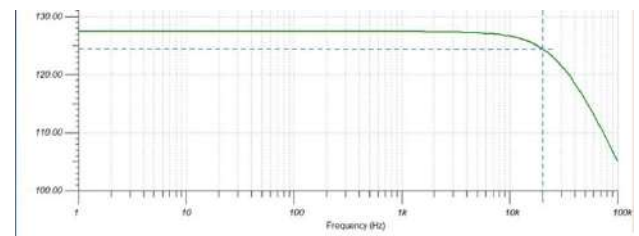


Figure 6 – Bandwidth of the analog chain computed by the TINA-Ti v9 simulation tool

A DI-1120 (from DATAQ Instruments) 4 channels / 180 kilo samples per second data acquisition system with a

resolution of 14 bits was selected for the present prototype. It is connected to the computer via an USB link.



Figure 7 – "Low noise" configuration

Two main configurations were tested for this prototype of radiometer:

- A very low noise configuration, using the photodiodes and the analog amplification chain only, embedded in a tea box (Figure 7).
- An "all in one" configuration, including the photodiodes, the analog amplification chain, the analog to digital converter, a USB to RJ45 Ethernet converter and a DC/DC 5V / + and -12V switching power supply embedded in a ruggedized steel box (Figure 8).

The ADC is used in a "two channels" mode, each channel being sampled at 40 kHz. The first channel is connected to a GPS output delivering accurate 1 PPS (pulse per second) for a precise data time stamping purpose. The second channel is used to record the light curves observed by the photometer.

The second version of the device (called "all in one") is easier to use in the field, because there is only one single Ethernet cable connecting the outdoors device to the indoors computer. However, as already mentioned by Segon et al. (2018) and by Buchan et al. (2018), the radiation of electromagnetic interferences by the digital part to the analog chain of the system creates internal noises on the very weak light curves. So the first configuration, although it requires two separate cables (one for the desired light curves signals, another one for the + and -12 V power supply), is preferable to avoid any interferences radiated by the digital parts of the photometer.



Figure 8 – "All in one" configuration

The light curves analog data are converted by the DATAQ ADC into digital data that are recorded on a hard disk or an SD memory card in a manufacturer's proprietary WDH format. These WDH format files can be replayed and analyzed thanks to the WINDAQ Browser software suite offered by DATAQ. However, to improve the quality of the observed meteor light curves, the WDH files can be easily translated into classical WAV files for further data processing. It is then possible to perform filtering and signal to noise improvement functions thanks to various well known off-the-shelf audio processing software programs such as Audacity, Adobe Audition or Izotope RX7.

3 Preliminary observation results

Several observations campaigns during different meteor showers have been performed to date in various locations, such as Observatoire du Pic du Midi, Observatoire de Haute-Provence, but also at home (in a high urban light pollution area) and in a remote alpine chalet located in a remote valley of the Jura Mountains (providing an excellent dark sky location).

Tentative taxonomy of some night time phenomena

The most significant initial finding was that observing the night skies in Western Europe with a sensitive and high speed photometer produces a large quantity of anthropic artefacts. Airplanes navigation and green LIDAR flashes (Figure 9), distant wind turbines flashes reflected by high altitude fluctuating clouds (Figure 10), flashes from groomers preparing the ski slopes of a distant ski station (Figure 11), etc. are very common as soon the Sun goes down ...

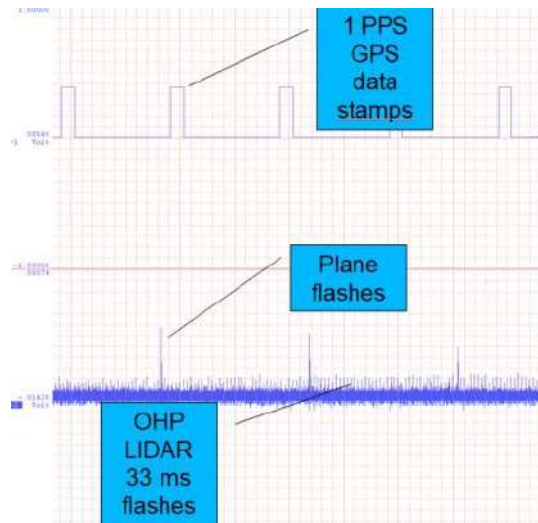


Figure 9 – Airplanes navigation flashes and green light LIDAR as seen at Observatoire de Haute-Provence

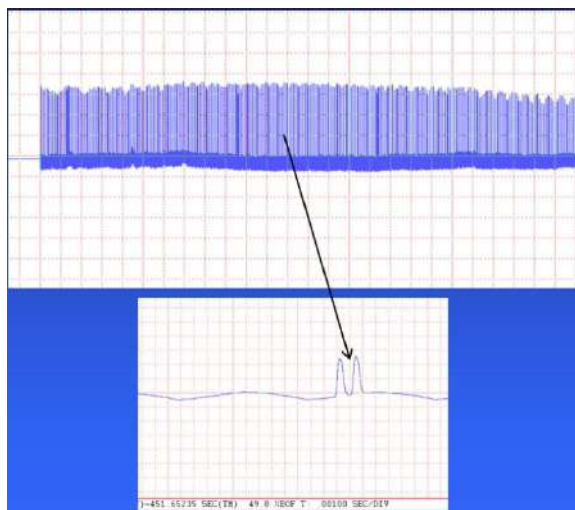


Figure 10 – Distant wind turbines red flashes (below the horizon) as detected by reflection on some passing clouds

Natural artefacts such as the Moon light (Figure 12) and distant lightning (Figure 13) are also very frequent.

All these false alarms can be easily identified, but the signature of some distant car headlights or of pedestrians walking by night with a headlamp can be confused with a meteor light curve signature.

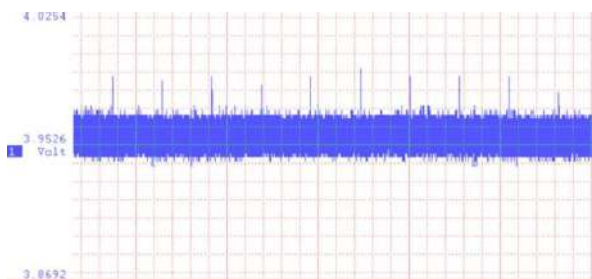


Figure 11 – Snow groomers at work in the La Mongie ski resort



Figure 12 – Example of Moon light (mag -12.2) modulated by passing clouds

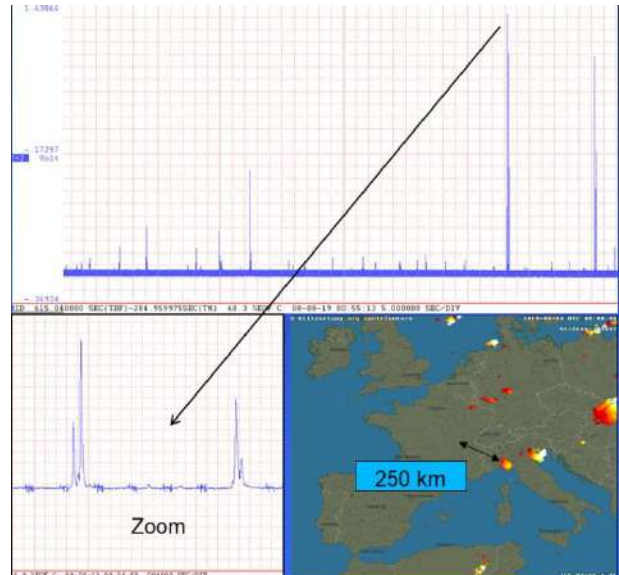


Figure 13 – Distant lightning over Italy detected in Jura Mountains at a distance of 250 km

The conclusion is that such a photometer must be used in conjunction with the data given by a meteor cameras network, allowing to sort reliably the real meteor light curves and the interferences.

Improving the signal to noise ratio of the meteor recorded light curves

Various filters have been successfully tested on the data records to improve the faint meteor light curves signal to noise ratio. Power grid parasitic lines at 50 Hz and their harmonic frequencies at 100 Hz, 150 Hz etc. radiated by the LED and the sodium street lights can be minimized by using a comb filter as shown on Figure 14. Figure 15 shows such a meteor light curve before and after applying the comb filter processing.

The quality of some light curves polluted by complex stationary noises can be enhanced (Figure 16) by using a spectral de-noising function: a copy of the stationary noise (with no meteor light curve) is first analysed by the audio processing software, and then removed from the record containing the meteor light curve.

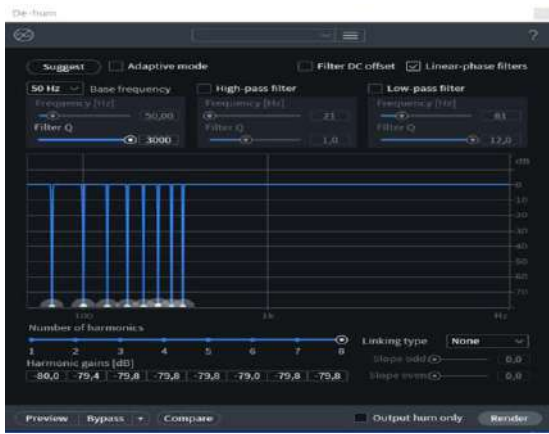


Figure 14 – Adjustable comb filter offered by the RX7 audio processing software

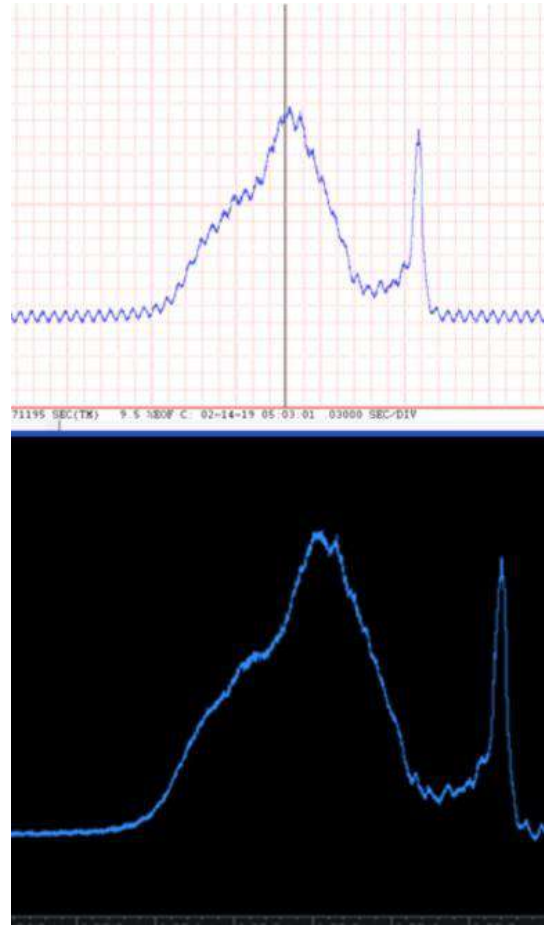


Figure 15 – Upper curve: raw signal of a meteor light curve. Lower curve: useful signal cleaned by the comb filter

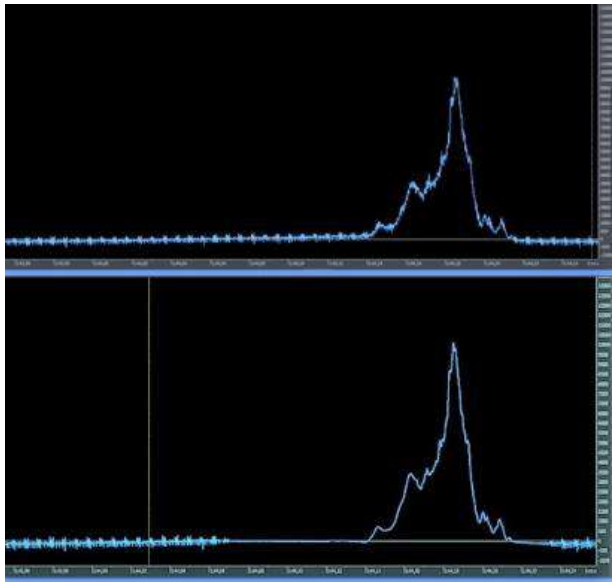


Figure 16 – Upper curve: raw signal of a meteor light curve polluted by a complex stationary noise. Lower curve: useful signal cleaned by the de-noising function of the RX7 audio processing software

4 Discussion

The present radiometer is still in development, mainly to improve as much as possible the signal to noise ratio on the low intensity meteor lights curves. The main improvement track that is still being explored is to find the most effective isolation between the analog and digital parts of the system. In the "low noise" configuration, a transmission of the signals to the indoors ADC via a shielded differential line instead of a coaxial cable is considered.

5 Conclusion

The present little tour across the wonderful realm of meteor radiometry clearly shows that the road is long and full of obstacles when aiming at good quality light curves observations. The natural and anthropic false alarms and the internal noises created by the digital components radiating spurious noises into the high gain analog chain of the radiometer forces the user to follow different tactics. In summary:

- During the development phase of a photometer, separate or shield appropriately the analog and the digital parts of the equipment, and use low noise power supplies such as batteries (no switching mode DC converters, etc.).
- During the observation campaigns, choose a location that is protected as well as possible from any light pollution such as cities lights, roads, farms, etc.
- During the phase of data reduction, always use some data obtained by a meteor cameras network, to correlate the presence of a real meteor with the potential light curve detected by the radiometer. Be cautious when using digital

processing such as filtering (high pass, low pass, notch filters), or spectral de-noise functions. These functions have to be carefully adjusted to decrease the interferences without distorting the useful signals, i.e. the desired real meteor light curves.

Acknowledgement

Many thanks to Denis Vida (Vida et al., 2015), Renato Turcinov (Segon et al., 2018), Hadrien Devillepoix (Buchan et al., 2018) and David Darson (Ecole Normale Supérieure, Paris, France) for our fruitful dialogues about the art of meteor radiometry.

References

- Buchan R.G., Howie R.M., Paxman J. and Devillepoix H.A.R.. (2018). “Developing a Cost-Effective Radiometer for Fireball Light Curves” in Rudawska R., Rendtel J., Powell C., Lundsford R., Verbeeck C. and Knöfel A., editors, *Proceedings of the International Meteor Conference*, Pezinok-Modra, Slovakia, 30 August – 2 September 2018, pages 123–126.
- Colas F., B. Zanda, J. Vaubaillon, S. Bouley, C. Marmo, Y. Audureau, M.K. Kwon, J.-L. Rault, S. Caminade, P. Vernazza, J. Gattaccea, M. Birlan, L. Maquet, A. Egal, M. Rotaru, C. Birnbaum, F. Cochard and O. Thizy . (2015). “French fireball network FRIPON” in Rault J.-L. and Roggemans P., editors, *Proceedings of the International Meteor Conference*, Mistelbach, Austria, 27–30 August 2015, pages 37–39.
- Johnson M., (2004). Photodetection and Measurement. Maximizing performance in optical systems McGraw-Hill, editor.
- Rault J.-L. (2017). “Fine-scale observations of the Doppler frequency shifts affecting meteor head radio echoes” In Gyssens M. and Rault J.-L., editors, *Proceedings of the International Meteor Conference*, Petnica, Serbia, 21–24 September 2017. IMO, pages 103–106.
- Segon D., Vida D., Butković M., Malaric M. and Turčinov R. (2018). “First simultaneous radiometric and video observations of fireballs using a low-cost radiometer”. *WGN, Journal of the IMO*, 46:2, 62–70.
- Vida D., Turčinov R., Šegon D. and Siladi E. (2015) “Low cost meteor radiometer in Rault J.-L. and Roggemans P., editors, *Proceedings of the International Meteor Conference*, Mistelbach, Austria, 27–30 August 2015, pages 180–184.

FRIPON Network internal structure

Adrien Malgoyre Adrien¹, François Colas²

¹OSU Pythéas, CNRS, Université dAix-Marseille, 13007 Marseille, France
adrien.malgoyre@osupytheas.fr

²Institut de Mécanique Céleste et de Calcul des Ephémérides (IMCCE), Observatoire de Paris, 75014 Paris, France
francois.colas@obspm.fr

We present an overview of our internal scripts and software used in the Fripon network after a few years of improvement. As we're a pooled IT Service and because we are engaged in other science project, our goal was to increase the level of automation for this long time survey. Now it is almost done! Through a few simplified diagrams we present the data recovery chain as well as the associated open-source software that allows us to magnify this network of observation easily. The goal of the presentation is to show how FRIPON works and how it can be extended over Europe.

Optimizing the scientific output of satellite formation for a stereoscopic meteor observation

Jona Petri¹, Julia Zink and Sabine Klinkner¹

¹ Institute of Space Systems, Pfaffenwaldring 29, 70569 Stuttgart, Germany
petri@irs.uni-stuttgart.de and klinkner@irs.uni-stuttgart.de

The Institute of Space Systems (IRS) and Technische Universität Berlin are planning a joint mission to observe meteors and dust particles using two small satellites of approximately 30 kg each in low Earth orbit. The mission consists of a formation of two identical satellites observing the same area for the stereoscopic observation of meteors, eventually allowing the calculation of the corresponding meteoroid trajectory. The payload comprises a miniature dust sensor and a camera system for meteor observation. The constellation of the satellite formation, i.e. inter-satellite distance, orientation, orbit, etc., fundamentally influences the potential output of a meteor event observation. This paper focuses on the optimization of the formation parameters with the already selected camera system. Furthermore, requirements for the satellite system were derived. This is done by using several simulations written in Python as well as evaluating data from a ground based meteor observation system. This allows the optimization of the scientific output of the mission.

1 Introduction to FACIS mission

The joint two year mission FACIS (Formation for Analysis of Cosmic particleS) between the IRS (Institute of Space Systems) and Technische Universität Berlin is dedicated to observe meteors using a camera system and measure dust particles using a dust sensor. The mission consists of two 30 kg satellites, allowing a stereoscopic meteor observation. Detailed information about the FACIS mission can be found in (Hufgard et al., 2018). In a previous paper, the camera selection using a simulation was described (Petri et al., 2019). Furthermore the selected camera was tested inside a thermal-vacuum chamber. In this paper the scientific output of the formation is optimized by analysing the influence of different mission parameters. The paper is divided into two parts: First, the expected meteor detection rates for different parameters are calculated by adapting the SWARMS simulation (Bouquet et al., 2014). In the second part, the simulation is validated by analysing data from ground based meteor observations with CILBO (Koschny et al., 2013). The data is also used to derive requirements for the camera system.

2 Simulation of meteor detection rates

The SWARMS simulation was originally developed by Bouquet A. et al. They kindly made their Python code available for us to use and adapt. The simulation is originally used to calculate the expected meteor detection rates of a single orbiting camera system. The simulation takes into account various mission parameters such as the satellite orbit, camera limiting magnitude and field of view as well as satellite tilt angle. We adapted this simulation in order to simulate the detection rates for a formation of two satellites. The changes are described in the following. We call the adapted version SWARMSv2 in order to differentiate between the work

done by Bouquet A. et al. and ours. Besides SWARMS, we also used an ASTOS scenario to calculate the observation time for the formation, depending on the orbit and satellite distance.

2.1 Adaptation and simulation settings

This paper focuses on the simulations results, therefore only a short list of adaptations and modifications to the SWARMS simulation is given:

- Addition of a second satellite .
- Calculation of detection rates for one satellite or formation of two satellites.
- Implementation of rectangular FOV (field of view).
- Addition of lateral meteor trajectory angle β .
- Calculation of meteor magnitude.
- Option to simulate ACS (Attitude Control System) error.
- Implementation of different meteor mass distribution models.
- Option to change meteor speed.
- Option to use ECSS¹ speed distribution.
- Calculation of limiting magnitude using sensitivity script (Petri et al., 2019).
- Calculation of optimal satellite distance to maximize the covered area.
- Export data and plots of results and formation geometry.
- Implementation of more plots of satellite formation and results.
- Option to simulate different parameters in a loop.

The settings used for the following simulations were derived from the CILBO data (see second part of this paper) as shown in Table 1. The main focus of the sim-

¹European Cooperation for Space Standardization, see (European Cooperation for Space Standardization Space Engineering, 2008)

Table 1 – Simulation parameters for SWARMSv2 simulations

Parameter	Values
Parameter changed for each simulation	
Orbit altitude	High: 565 km, Low: 300 km
Focal length, F#	Wide FOV: 12.7 mm, 1.4, Narrow FOV: 35 mm, 1.9
Models	Gruen, Halliday
Mass range Gruen	Low: 0.01 g to 10 000 g High: 0.1 g to 10 000 g
Mass range Halliday	0.01 g to 30 000 g
Parameter constant for each simulation	
Tilt angle	0, 5, 10, 15, 20, 25, 30, 35, 40 and 42 deg
Camera	<i>GenieNano M1920</i>
Number of observations	2
Obser. time Gruen	40 h
Obser. time Halliday	674 h ($\times 2$ for low orbit)
Meteor angle γ mean	-62.65 deg
Meteor angle γ sigma	22.48 deg
Meteor angle β mean	90 deg
Meteor angle β sigma	20 deg
Speed distribution	From ECSS standard
Number of frames for detection	3
Reference lim. magnitude	3.18 (from SensorSensitivity script)
Exposure time	$\frac{1}{6}$ s

ulations is to evaluate the effect of different orbits, tilt angles and FOVs on meteor detection rates. These rates depend on various parameters (see Table 1). The parameters are not independent and influence each other. Therefore, it is difficult to evaluate the effect of a single parameter. We choose to evaluate each parameter by plotting the meteor detection rates against the satellite tilt angle. The tilt angle indicates the area covered by both satellites, a higher tilt angle results in a larger observation area. In order to maximize the overlapping area of the two FOVs, the distance between the satellites must be adjusted depending on the satellite tilt angle. Therefore, the ideal distance is calculated and then used for each tilt angle respectively. The calculation is done by using basic geometry and depends on the orbit altitude, FOV and tilt angle. By that, it is ensured that always the maximum possible overlapping area is used for the simulation, which in turn maximizes the meteor detection rates. The combination of the satellite tilt and distance into basically one parameter allows to evaluate the effect of different parameters depending on the satellite tilt without minding the satellites distance.

2.2 Simulation results and discussion

Before presenting the simulation results, it is important to mention the limitations and assumptions made for the simulation. First, it is assumed that both satellites are in the same orbit, tilted towards each other by the same angle and using the same camera system.

Furthermore, the sensitivity of the camera is assumed to be constant over the whole field of view. However, this assumption is not valid, since loss of sensitivity was observed in ground based systems (Albin et al., 2017). This has to be taken into account when estimating the expected number of meteors. Finally, only meteors detected by both satellites are used to calculate the detection rates.

The limitations of the simulation are the following: The calculated meteor rates are based on models and do not take into account meteor showers. This means the rates are only an estimation and are used to evaluate the relative effect of mission parameters. Furthermore, the simulation uses the brightness of a meteor to determine a possible detection, but does not state the signal-to-noise ratio of an image. This means, a detection may not be useful due to the poor image quality. Thus, compared to the simulations, detection rates are smaller in reality.

2.2.1 Effect of orbit altitude and operation time

In general, the greater the covered area, the higher the meteor detection rates. Thus a higher orbit results in a greater coverage and detection rates, as seen in Figure 1. The number of detected meteors fluctuates due

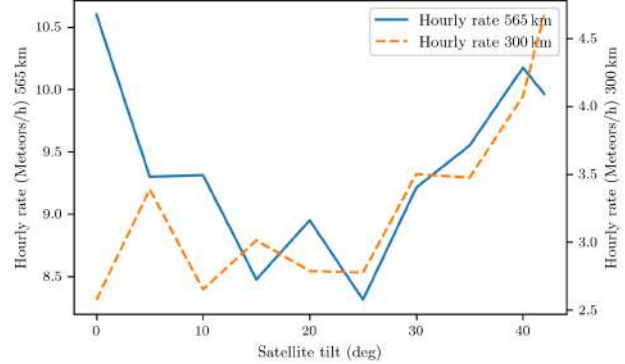


Figure 1 – Hourly rate for 565 km and 300 km orbits using the 12 mm lens and the Gruen model with a minimal meteoroid mass of 0.1 g

to random assignment of meteor properties.

While a higher orbit increases the coverage and thus the detection rate, the orbit altitude also influences the operation time. The operation time is the time during which both satellites are in eclipse. The operation time is also influenced by the orbit type and satellite distance. A higher orbit decreases the eclipse time. Therefore, it was analysed whether the greater coverage or the longer operating time has a larger impact on the detections. Furthermore, the satellites distance also influences the operation time and was taken into account as well. The analysis was done by determining the total operation time for each scenario with ASTOS and then calculating the number of detected events during the mission using the hourly detection rates from

SWARMS. As a result, the greater coverage of a higher orbit compensates for the shorter operation time. The orbit type (different LTAN (Local time of ascending node)) has little influence on the overall detections. The satellite distance is influenced by setting the tilt angle which is analysed further in the next section.

2.2.2 Effect of tilt angle

The greater the tilt angle, the greater the covered area and thus the number of meteors inside the FOV. However, the area increases faster than the number of events detected. This is due to the greater distance to meteors at the edge of the FOV, which limits the detectability of low mass, and therefore faint, meteors. As a result, the hourly rate decreases first with an increasing tilt angle. Furthermore, Figure 2 shows that the increase in

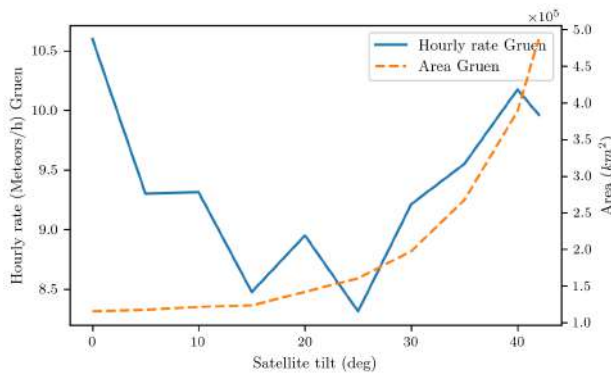


Figure 2 – Hourly rate and covered area for a 565 km orbit

area is low at the beginning, only with a larger tilt angle the area increases significantly. This is the case for tilt angles greater than 20 deg. That explains why the hourly rate decreases first with tilt angle (due to greater distance) and then increases due to greater coverage. A useful tilt angle must therefore be greater than 20 deg. The same effect is observed in (Bouquet et al., 2014, Fig. 9). The maximum usable angle is reached when the edge of the FOV hits the horizon.

2.2.3 Effect of meteor mass distribution and tilt angle

In Figure 3 the hourly rates using the Halliday (Halliday et al., 1996) and Gruen (Grün et al., 1985) model are plotted against the tilt angle. In general, the Halliday model generates less lightweight meteoroids and more heavier meteoroids. In contrast, the Gruen model generates more meteors in total, especially towards lower meteoroid masses. In the simulations, the lower masses are set to 0.1 g (Halliday and Gruen) and 0.01g (Gruen). The mass does not only have a huge effect on the absolute number of meteors detected, but also affects the relation between tilt angle and detection rate: The Halliday model and the Gruen model ($m > 0.1$ g) show first a decrease and then an increase in the hourly rate, but those changes are small. In contrast, when using the Gruen model ($m > 0.01$ g), the hourly rate decreases

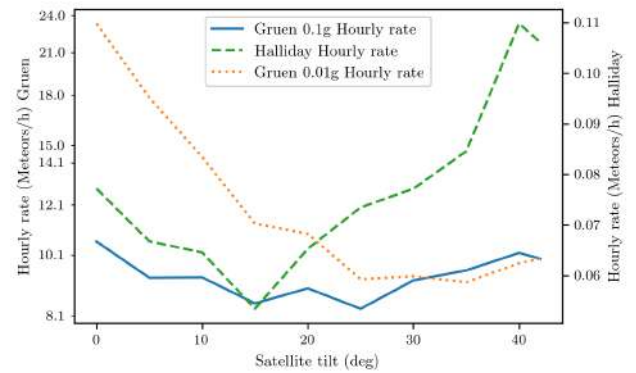


Figure 3 – Hourly rate for a 565 km orbit and different mass distribution models and settings.

with the tilt angle, despite a greater coverage. Furthermore, a lower minimum mass results in a higher hourly rate, due to more fainter meteors being generated. Those faint meteors together with the geometry of the formation lead to the decrease of the hourly rate with greater tilt angle. Before explaining this effect, the geometry of the formation needs to be explained: The tilt angle is set by the user. Depending on this angle, the distance of the two satellites is determined to maximize the covered area. The greater the tilt angle, the greater the distance between both satellites. The covered surface area increases with tilt angle, therefore the number of meteors inside the FOV increases. But the area increases faster than the number of detected meteors, because faint (and therefore lightweight) meteors far away from the camera can not be detected. This is due to the reduction of apparent brightness from the greater distance to the meteor. If only heavier meteors are simulated (which is also the case when using the Halliday model), this effect is negligible. But for small meteor masses and greater tilt angle, this effect becomes significant. For a great tilt angle, the meteors close to the camera on the first satellite are far away from the camera on the second satellite and vice versa. Therefore, small meteors can only be detected by one camera (see Figure 4 for a visual representation). For a small tilt angle, the distance to the meteors is in the same order of magnitude for both satellites. As a result the hourly rate decreases with increasing tilt angle, due to the greater distance to meteors for one satellite. This effect is stronger in higher orbits. A higher tilt angle is beneficial for the observation of bright meteors, due to the increased area. For faint meteors a smaller tilt angle is more suitable.

2.2.4 Various effects and results

The simulation also allows to examine the effect of satellite movement and the lateral meteor angle β . Both influence the projection of the meteor on the sensor, thus the apparent angular velocity of the meteor as seen from the sensor is changed. The angular velocity, besides the (apparent) brightness of a meteor, has a huge influence on the detectability of a meteor: The higher the angular velocity, the lower the probability of detection. This

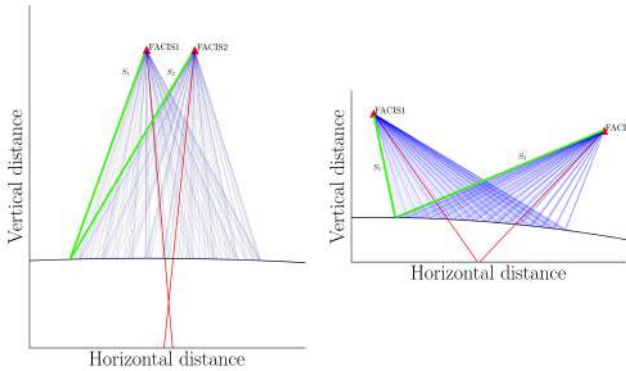


Figure 4 – Geometry for a tilt angle of 5 deg (left) and 30 deg (right). Left: The distance to meteors is in the same order of magnitude for both satellites, even for meteors at the edge of the FOV ($S_2 \approx S_1$). Right: The distance from a meteor at the edge of the FOV to satellite one is significantly shorter than to satellite two ($S_2 >> S_1$).

is because the signal is spread over several pixels with a short dwell time. The angular velocity is affected by the satellite movement, by the direction the meteors arrive, as well as their speed. Thus, all factors must be analysed to determine their influence. As can be seen in

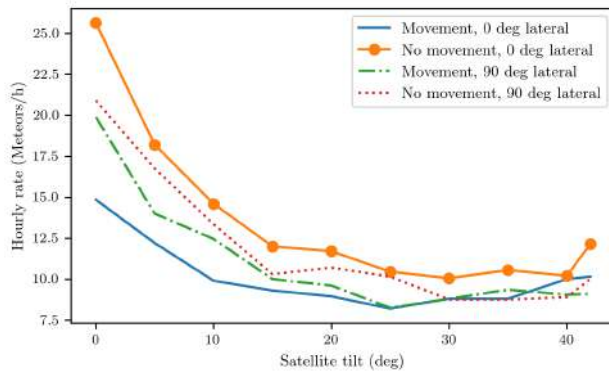


Figure 5 – Hourly rate for 565 km orbit and the Gruen model with a minimal mass of 0.01 g. The ECSS speed distribution is used with β between 0° and 90° and movement of the satellite (not) taken into account

Figure 5, the overall shape of the curves is similar. If the satellite movement is taken into account, the hourly rate decreases as well. A greater lateral angle also results in a decreased hourly rate. Both is due to the greater angular velocity. Thus, it is important to choose realistic values for the speed and angular distribution.

The effect of the size of the FOV is straightforward: A wider FOV covers a greater area and therefore increases the hourly rate. Beside this obvious effect, the FOV also influences the scientific output of the instrument: A wide FOV should be chosen, if the meteor flux should be determined. In this case, a huge covered area is desirable. For the determination of the meteor trajectory, a narrower FOV results in a greater angular resolution and therefore preciser determination of speed and meteor trajectory.

When conducting simulations, the simulation time and

grid size must be carefully set: If the simulation time is too low, not enough meteors are generated and the hourly rate is unrealistic. In contrast, a long simulation time results in long simulation runs. Furthermore, when selecting the grid size, the FOV size must be considered: A narrower FOV requires smaller grid size in order to determine the covered area correctly. Since meteors are created at grid intersection points, a coarse grid results in less meteors detected, because not enough points occur inside the FOV.

2.2.5 Summary of SWARMSv2 simulation

For a single satellite observing meteors, different missions have already been analysed, e. g. (Bouquet et al., 2014) and (Oberst et al., 2011). The main results from these analysis are that the greater the coverage the higher the resulting hourly rate. However, a mission comprised of two satellites is more complex and differs from a single satellite mission: While a greater coverage is also desirable, attention must be paid if the increased coverage is achieved by tilting the satellites, because tilting the satellites means also increasing the distance between the satellites to increase the overlapping area. This results in a large distance to the meteor for at least one satellite. As a consequence, the detection rate decreases. Furthermore, the FOV must be chosen carefully, in order to compromise between higher coverage and precise speed determination. More analyses are necessary to evaluate the influence of the speed determination precision and satellite distance on the trajectory calculation.

3 Evaluation of CILBO data

The knowledge of the satellite attitude is necessary to determine the meteor position and thus calculate the trajectory. Any error in measuring the attitude has an influence on the trajectory accuracy. In order to set up requirements for the satellite bus, this influence must be quantified. Therefore we analysed data from the CILBO observatory. CILBO is a ground based meteor observatory in Tenerife (Koschny et al., 2013), dedicated to the stereoscopic observation of meteors. The two stations are located about 100 km apart from each other and equipped with intensified CCD cameras. Thanks to T. Albin, we were able to use the database of cleaned meteor observations, in order to analyse the influence of satellite attitude knowledge accuracy on the trajectory determination. Furthermore, we use the data to derive reasonable meteor properties for the SWARMSv2 simulation. The database contains 12 045 meteors, simultaneously observed between January 2013 and August 2015 from the two stations. The meteors are observed with at least four frames, the trajectory determination deviation is less than 500 m and the altitude is at least 80 km. For more details on the database see (Albin et al., 2015) and (Albin et al., 2017).

3.1 Approach and scope

The database contains different parameters. The following ones were used on this analysis: The measurement accuracy of the meteor position determined on the sensor of each camera stated in arcminutes ('). Furthermore, the velocity of the meteor, given in km s^{-1} , is used. Finally, the accuracy of the calculated trajectory is given in m. This accuracy states how well the trajectory fits to the meteor positions. The fitting error is treated as an error in the trajectory. All data points are derived from several images. Therefore, for each parameter mentioned before, actually four values exist in the database: The mean value, the standard deviation, the median value and the absolute deviation of the median value. For this analysis only the median and mean values are used.

3.2 Satellite attitude accuracy

The goal is to determine the influence of the accuracy of the meteor position determination on the final accuracy of the trajectory. It is expected that a higher inaccuracy of the meteor position results in a higher inaccuracy of the meteor trajectory. For the later derivation of requirements for the satellite attitude determination accuracy, it is assumed that the inaccuracy of the meteor position is solely a result of the inaccuracy of the satellite attitude determination. In order to evaluate only the influence of the meteor position error, the evaluation is done for meteors with the same properties (velocity and magnitude). The meteors are separated into velocity ranges from 10 km s^{-1} to 45 km s^{-1} in 5 km s^{-1} steps. The magnitude is between -1 and 3 for all meteors. A separation into magnitude bins would result in an insufficient amount of meteors in each bin. The meteors within each velocity range are then categorized into a meteor position accuracy bin. The bins range from $0.01'$ to $0.06'$ while each bin is $0.002'$ wide. For each meteor position accuracy bin the median/mean trajectory accuracy is calculated from all meteors inside this bin. The resulting diagram for a velocity range is shown in Figure 6. Assuming a sufficient amount of meteors, the

Table 2 – Trajectory errors calculated from slope camera 1 median values velocity range 15 km s^{-1} to 20 km s^{-1} for different satellite attitude knowledge errors

Attitude knowledge accuracy (')	Trajectory error min (m)	Trajectory error max (m)
0.08	82	157
0.1	102	197
0.12	123	236
0.13	133	256
0.15	154	295
0.17	174	335
0.18	185	354
0.2	205	394
0.22	226	433
0.23	236	453
0.25	257	492
0.27	277	532
0.28	288	552
0.3	308	591
0.32	329	630

the data points. The slope of this line is determined for each velocity range and camera. Besides of the slope, the standard deviation for each line is calculated and given in absolute and relative values. Generally, the median values can be fitted more accurate than the mean values, therefore only the median values are considered. The best fit using the median values could be achieved for camera 1. For this reason, the maximum and minimum slopes calculated for this camera are used. The minimal slope of $1029 \text{ m}'$ is calculated for the velocity range 15 km s^{-1} to 20 km s^{-1} (see red line in left diagram in Figure 6). The maximum slope value is $1972 \text{ m}'$ for the velocity range 30 km s^{-1} to 35 km s^{-1} . Those values are used for the calculation of the relation between attitude knowledge accuracy and trajectory error. As mentioned before, it is assumed that the meteor position error results solely from the attitude knowledge error. The formula to calculate the trajectory error is:

$$\text{Traj. error(m)} = \text{attitude accura.(')} \times \text{slope(m')}\quad (1)$$

The results are summarized in Table 2. A typical attitude knowledge accuracy of $7''$, results in a trajectory error between 120 m and 230 m . This is an estimation of the trajectory error resulting from the inaccurate determination of the satellite attitude. Additional errors, like the determination of the photometric centre of a meteor, will further degrade the trajectory accuracy.

3.3 Meteor properties

As mentioned in the first part of this paper (see Section 2), the meteor properties must be carefully set in the simulation in order to get realistic results. The CILBO database contains sporadic and shower meteors observed over the course of more than one year. By analysing the meteor properties and their distribution, not only the simulation is improved, but also camera

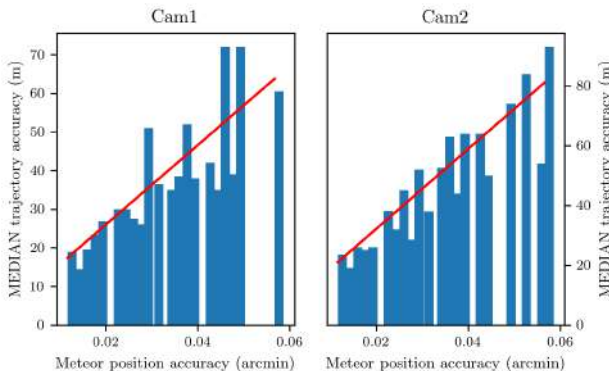


Figure 6 – The median meteor position accuracy for a velocity range of 15 km s^{-1} to 20 km s^{-1} and the fitted line shown with a red line.

relationship between meteor position accuracy and trajectory seems linear. Therefore, a line is fitted through

requirements can be derived. Therefore, the meteor velocity, the angle between camera boresight/zenith and meteor radiant, the distance (camera to meteor) and the magnitude are analysed. This is done by creating histograms of the corresponding property, calculating the mean value, standard deviation as well as minimum and maximum value. If the distribution is Gaussian, which is the case for the angle, distance and magnitude, those values can be directly used in the simulations (see Table 3). This is because in the simulations the meteor properties are assumed to be Gaussian and specified with their mean value and standard deviation. The non Gaussian distributions are further analysed.

The distance distribution is Gaussian if the distance to the meteors at their maximum magnitude is used (see Figure 7). In this case, the mean value is shifted to higher values than the expected 100 km. The mean distance to the meteor is not Gaussian distributed, but has a mean value of about 101 km. Nevertheless, a value of 101 km can be used in the simulations for the meteor distance.

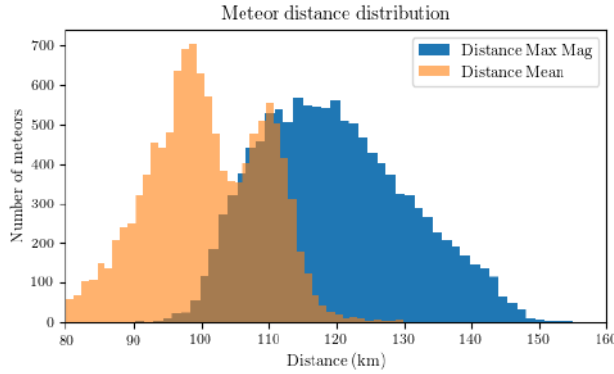


Figure 7 – CILBO meteor angle distribution

The velocity distribution was already analysed (Drolshagen et al., 2014). The speed distribution for one shower may be Gaussian, however this is not true for the overall speed distribution. Therefore, we decided to use the speed distribution according to the ECSS standard (European Cooperation for Space Standardization Space Engineering, 2008).

The magnitude distribution, shown in Figure 8, is used to derive the required limiting magnitude for the camera system. Therefore, the calculated apparent magnitude in the CILBO database is converted into an apparent magnitude as seen from the satellite. This magnitude is reduced due to two effects: The higher distance to the meteor and the angular velocity. The first apparent magnitude distribution in Figure 8 takes only the first effect into account, the second one both effects. The reduction of magnitude due to angular velocity is calculated from the formula in (Kingery & Blaauw, 2017). All variables can be taken from the CILBO database, except the FWHM (Full Width Half Maximum). This value is estimated with 3 px from a CILBO meteor image shown in (Koschny et al., 2013). As can be seen in the distribution diagram (Figure 8), the angular velocity has only a small effect. The mean magnitude for

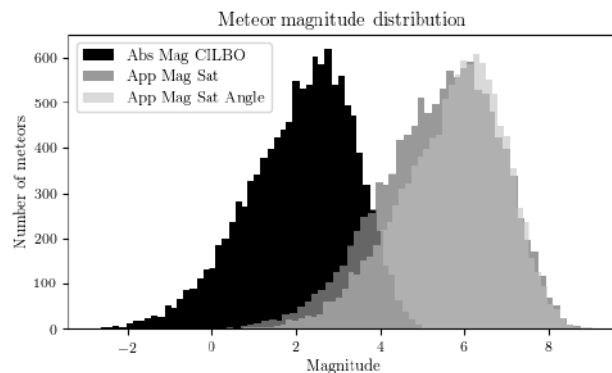


Figure 8 – CILBO meteor magnitude distribution: The apparent magnitude for the CILBO system is shown (left). Two distributions show the magnitude as seen from the satellite, taking into account only the reduction due to distance and the reduction due to distance (App Mag Sat) as well as angular velocity (App Mag Sat Angle).

Table 3 – Mean meteor properties from CILBO data. The mean, maximum, minimum value as well as standard deviations are calculated.

Property	Mean	Std. dev.	Max	Min
Apparent Magnitude Satellite	5.42	1.38	8.95	0.01
Absolute Magnitude	2.1	1.27	5.29	-2.79
Angle bore-sight (°)	63	22.26	122.95	3.29
Angle zenith (°)	44	17.62	1.63	88.94
Velocity (km s^{-1})	40.3	16.7	90	10.2
Distance max mag (km)	120	10.99	167.34	90.17
Distance altitude (km)	101	8.5	129.95	80.08

this distribution is 5.7, the peak value is 6.22. The apparent magnitude distribution for the CILBO system has a mean value of 3.17 and a peak value of 3.2. The peak value indicates the limiting magnitude. Therefore, the camera needs to have a meteor limiting magnitude of greater than 6.22 in order to have a similar performance as CILBO. According to our simulations, the camera can observe meteors up to magnitude 2.82 from a 565 km orbit when using the mean meteor properties stated in Table 3. The stellar limiting magnitude is about 5.75. This means that our camera system would observe all meteors that CILBO observed if placed on the ground. However, taking into account the higher distance for the orbital observations, the system would not observe all meteors CILBO did. However, due to the greater coverage, it is expected that more meteors could be observed.

4 Conclusion

We simulated a formation of two satellites using the modified SWARMS simulation. The parameters of the formation have a huge influence on the scientific output and the effect differs from a single satellite mission. The tilt angle has a huge influence on which and how many meteors can be observed. A greater tilt angle increases coverage, which benefits measurements of bright meteors, but at the same time decreases the capability to observe faint meteors. The selection of the FOV size is a trade-off between accuracy of speed determination and coverage. The orbit altitude has a significant influence on the coverage, thus a high orbit should be chosen. The coverage has a huge influence on the detection rates. A higher coverage results in higher detection rates, except if the higher coverage is achieved by tilting the camera. In this case, the distance to faint meteors increases and therefore the detection rate decreases. However, at a certain tilt angle the effect of greater coverage dominates and detection rates increase again. For the FACIS mission the highest possible orbit (565 km) should be used, with a tilt angle of at least 25 deg, which results in a distance of 614 km. The chosen lens has a FOV of 48 deg \times 31 deg, which is a suitable compromise of coverage and angular resolution (160 000 km² and about 0.05 deg / px).

Furthermore, we were able to evaluate the effect of satellite attitude accuracy knowledge on the trajectory determination using the CILBO data. With an attitude knowledge error of 7'', the error should be less than 250 m. The CILBO database was further used to compare the selected camera with the CILBO system and derive realistic meteor properties to aid the SWARMS simulation.

All in all the influence of different parameters could be analysed, which enables us to further develop an observation concept. Future work includes further investigation of the attitude error on the trajectory calculation and developing a detailed observation concept.

Acknowledgements

We would like to thank the SWARMS authors for making their simulation code available to us, furthermore we thank Thomas Albin for providing us the CILBO database and giving valuable feedback on our evaluation.

References

- Albin T., Koschny D., Molau S., Srama R., and Poppe B. (2015). "Influence of the pointing direction and detector sensitivity variations on the detection rate of a double station meteor camera". In *International Meteor Conference Mistelbach, Austria*. pages 226–232.
- Albin T., Koschny D., Molau S., Srama R., and Poppe B. (2017). "Analysis of the technical biases of meteor video cameras used in the CILBO system".
- Bouquet A., Baratoux D., Vaubaillon J., Gritsevich M. I., Mimoun D., Mousis O., and Bouley S. (2014). "Simulation of the capabilities of an orbiter for monitoring the entry of interplanetary matter into the terrestrial atmosphere". *Planetary and Space Science*, **103**, 238–249.
- Drolshagen E., Ott T., Koschny D., Drolshagen G., and Poppe B. (2014). "Meteor velocity distribution from CILBO double station video camera data". In *Proceedings of the International Meteor Conference*, edited by: Rault, J.-L. and Roggemans, P., IMO, volume 1622. page 1821.
- European Cooperation for Space Standardization Space Engineering (2008). "Space Environment ECSS-E-ST-10-04C".
- Grün E., Zook H., Fechtig H., and Giese R. (1985). "Collisional balance of the meteoritic complex". *Icarus*, **62:2**, 244–272.
- Halliday I., Griffin A. A., and Blackwell A. T. (1996). "Detailed data for 259 fireballs from the canadian camera network and inferences concerning the influx of large meteoroids". *Meteoritics & Planetary Science*, **31:2**, 185–217.
- Hufgard F., Lengowski M., Barschke M. F., Harmansa N., Klinkner S., and Brieß K. (2018). "Preliminary study of an academic micro-satellite formation mission for meteoroid trajectories determination and dust mass flow measurement". In *presented at the Small Satellites Systems and Services Symposium*.
- Kingery A. and Blaauw R. (2017). "Determination of the meteor limiting magnitude". *Planetary and Space Science*, **143**, 67–70.
- Koschny D., Bettonvil F., Licandro J., Mc Auliffe J., Smit H., Svedhem H., de Wit F., Witasse O., Zender J., et al. (2013). "A double-station meteor camera set-up in the Canary Islands—CILBO". *Geoscientific Instrumentation, Methods and Data Systems*, **2:2**, 339–348.
- Oberst J., Flohrer J., Elgner S., Maue T., Margonis A., Schrödter R., Tost W., Buhl M., Ehrich J., Christou A., et al. (2011). "The smart panoramic optical sensor head (sposh)—a camera for observations of transient luminous events on planetary night sides". *Planetary and Space Science*, **59:1**, 1–9.
- Petri J., Schmidt A., Zink J., and Klinkner S. (2019). "Design and test of a cots based imaging system for stereoscopic meteor observations". In *Proceedings of IAA Smallsat conference*.

Investigation of meteor properties using a numerical simulation

Martin Baláž¹, Juraj Tóth¹, and Peter Vereš^{1,2}

¹ Comenius University in Bratislava, Mlynská dolina, 84248 Bratislava, Slovakia
 martin.balaz@fmph.uniba.sk

² Minor Planet Center, Harvard-Smithsonian Center for Astrophysics, Cambridge, MA 02138, United States

We present new capabilities of the meteor simulation toolkit ASMODEUS. We used the numerical simulation to visualise how varying the initial properties of meteoroid particles affects the properties of corresponding meteors. Unlike in simulations of meteor showers, where properties of meteoroids are sampled from predefined distributions and meteor data sets are evaluated statistically, in this method meteoroid properties are varied in a systematic way. Most parameters remain constant, while one or more attributes (such as initial particle mass, entry angle or material properties) are assigned evenly spaced values from defined intervals, either on linear or logarithmic scale.

Possible applications of the method include investigation of beginning and terminal heights, luminosity profiles, effects of diurnal or annual variation of upper atmospheric density and many more. Comparison of the output of the simulation to observational data for single meteors also makes validation of theoretical models feasible, and enables us to develop better ablation and deceleration models.

thor's master thesis (Baláž, 2018). The program proved highly capable when used for simulation of meteor showers, with the resulting data used for debiasing of actual meteor observation datasets. For an in-depth description of the program and its mathematical and physical foundations please refer to (Baláž et al., prep.).

In order to investigate the effects of variation of input parameters (in our case properties of meteoroids) on the output (properties of the meteors), the simulation required a new method of generating the initial population. Multiple improvements to the visualisation subsystem were also made, along with restructuring and optimizing the code to allow for larger datasets.

2.1 Generating the meteoroids

In the original design of the simulation it was important to approximate the real distribution of particle masses, velocities and material properties of shower meteors, which effectively resulted in a Monte-Carlo generator. In this work we were more interested in purely synthetic cases, which required a markedly different approach.

At the deepest level of abstraction we are trying to isolate and possibly quantify the effect of variation of some property of the meteoroid on the observed meteor. This naturally translates to holding values of most parameters constant, while slowly varying one (eventually two) parameters. The resulting population thus comprises a set of meteoroids with mostly identical properties, differing only in one of their parameters, e. g. mass, density, entry angle or position above the Earth's surface.

Naturally, some of these properties are related: for instance, the radius of the particle is determined by its

1 Introduction

The differential equations describing the motion and ablation of a meteoroid are non-linear. Most models of meteor flight also include quantities that have to be determined empirically, such as density of the atmosphere or heat of ablation of meteoroid material. Therefore, except for the most basic models (Beech, 2009), finding a closed-form expression for dependence between input and output is not possible. Numerical simulations remain the only effective means of investigation of these models. Multiple such computer programs have been developed, such as MeteorSim (Gural, 2002).

In this submission we tried to use such simulation program to isolate the effect of changes to initial properties of meteoroids to resulting meteors. It should be noted that we mainly attempted to show the capabilities of this method and the simulation used, rather than to perform detailed analyses of the outputs. However, even from these relatively simple plots we may observe and learn something about the expected behaviour of meteoroids during their atmospheric entry.

The simulation could also be employed to improve models of meteor dynamics and ablation. By confronting its outputs with observations of real meteors it should be possible to devise models that are in better agreement with reality.

2 Overview

We used Asmodeus, a multi-purpose meteor simulation toolset originally developed as a part of the first au-

mass and density. Hence it was necessary to decide which parameters should be considered fundamental and which should be thought of as derived. The set of irreducible properties contains

- initial particle mass,
- density of the material,
- coefficient of heat transfer,
- specific enthalpy of vaporisation,
- drag coefficient,
- shape factor,
- position vector in the Earth-Centred, Earth-Fixed reference frame, specified in terms of geographic latitude, geographic longitude and elevation above the surface,
- velocity vector at initial position in the Earth-Centred Inertial reference frame, which is specified in terms of declination, right ascension and speed.

Any of these properties may be automatically varied within some pre-defined interval. Logarithmic spacing within the interval should be used if the range is too wide.

To further simplify calculations, we mostly worked with a single observer located at the North Pole and always used the same time. Declination and right ascension of the radiant can then be directly related to the particle's velocity vector without complex transformations, allowing for easier interpretation of the output.

2.2 Visualisation

For visualisation we used the `matplotlib` library. Each dataset was plotted on a scatter plot, effectively displaying up to four independent properties at the same time:

- *horizontal* and *vertical* position code the examined properties,
- the *colour* of the dot represents the varied input parameter, enabling the viewer to follow one selected particle,
- the *size* of the dot conveys some measure of the size of the meteoroid, such as its mass or absolute magnitude.

All presented charts are scatter-plots of all frames. Only properties that do not depend on the position of the observer are shown. However, the simulation is readily capable of showing these properties – for instance, plotting the observed altitude against apparent brightness

is possible as well. Visualisations that show dependence on observed positions in the sky can also be plotted on a polar graph, representing the whole hemispherical sky as seen by a ground-based observer. The frame where absolute brightness of the meteor is maximal is always emphasised.

3 Simulations

In the simulations we used the same set of default values of parameters, as shown in Table 1. All parameters could be overridden as required on a case-by-case basis. Material properties were taken from (Baláž, 2018), where we modelled the Perseid meteor shower. The position of the radiant was set to the North Pole while the time was set to approximate the vernal equinox ($\lambda_\odot \approx 0$).

The simulation was run with a constant-step Runge–Kutta integrator with 1000 steps per second. A meteoroid was considered to be completely vaporised when its mass decreased below 10^{-12} kg, at which point the run was aborted and the program proceeded to the next meteoroid.

3.1 Variable entry angle

The first presented case is a simple study of variable entry angle of meteoroids. Initial properties from table 1 were used, except for declination, which was varied between 10° and 90° with logarithmic spacing. 30 particles were simulated.

Naturally, we should expect that particles entering on steeper trajectories penetrate deeper into the atmosphere, as shown in 1. Consequently, they will encounter denser layers earlier and thus will ablate much faster. Since kinetic energy of all meteoroids is equal and in each case must be completely dissipated by the time the meteoroid loses all its mass, we should also expect their peak brightness to be much higher. The meteors are plotted again with absolute magnitude versus time in Figure 2.

3.2 Variable particle mass

Another interesting case is shown in changing the initial mass of the particle. The mass was varied between 10^{-9} to 10^{-3} kg. To cover the interval with sufficient resolution logarithmic spacing was used.

In Figure 3 we see the effect of increasing mass on the elevation and absolute magnitude of the meteor at the moment of maximal absolute brightness. In this model, a tiny Perseid with initial mass of 1 µg produces a hard-to-detect meteor of magnitude $+11^m$ while a 1-ton boulder results in a spectacular -19^m fireball. In reality, more massive particles would invariably undergo fragmentation, which would result in substantial changes to their light curves as well. The overall shape of the curve is nevertheless almost the same in all cases.

group	property	symbol	value
size	initial mass	m_0	0.001 kg
	density	ρ	625 kg m ⁻³
	heat transfer coefficient	Λ	1
material	specific enthalpy of vaporisation	Q	6 MJ kg ⁻¹
	drag coefficient	Γ	0.5
shape	shape factor	A	1.21
	geographic latitude	ϕ	90°
position	geographic longitude	λ	0°
	elevation	h	150 000 m
velocity	declination	δ	90°
	right ascension	α	0°
	speed	v	59 000 m s ⁻¹
time	initial time	t_0	2019-03-20 21:58:00 UTC

Table 1 – Default values of meteoroid properties used in all studied cases

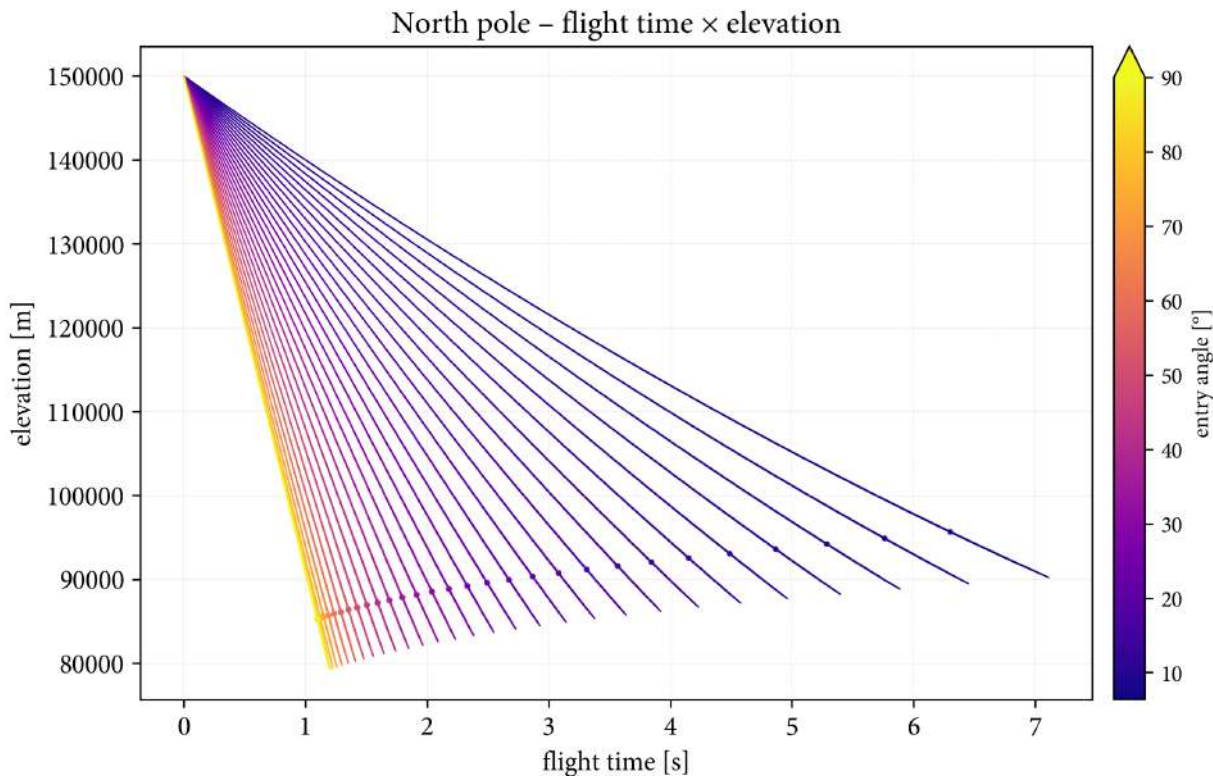


Figure 1 – The dependence between elevation and time. As expected, meteoroids entering on steep trajectories penetrate much deeper into the atmosphere, losing less speed than those on shallow trajectories.

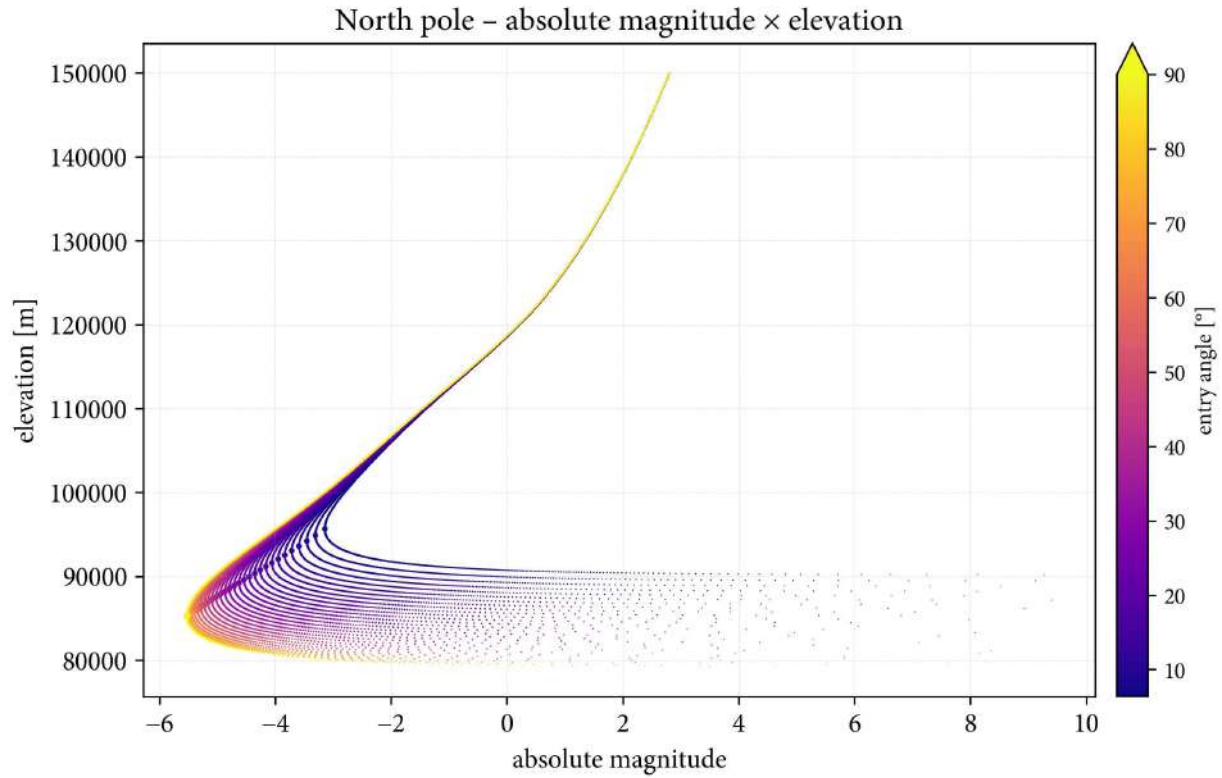


Figure 2 – The same data set with absolute magnitude plotted against elevation. As anticipated, meteoroids on steeper trajectories produce brighter meteors, with difference between 90° and 10° being slightly over two magnitudes. Note the characteristic nose-shaped profile and the change of slope occurring near height of 125 km. This closely copies the rapid increase in rate of change of atmospheric density in the MSIS-E-90 model (Community Coordinated Modeling Center, 1990).

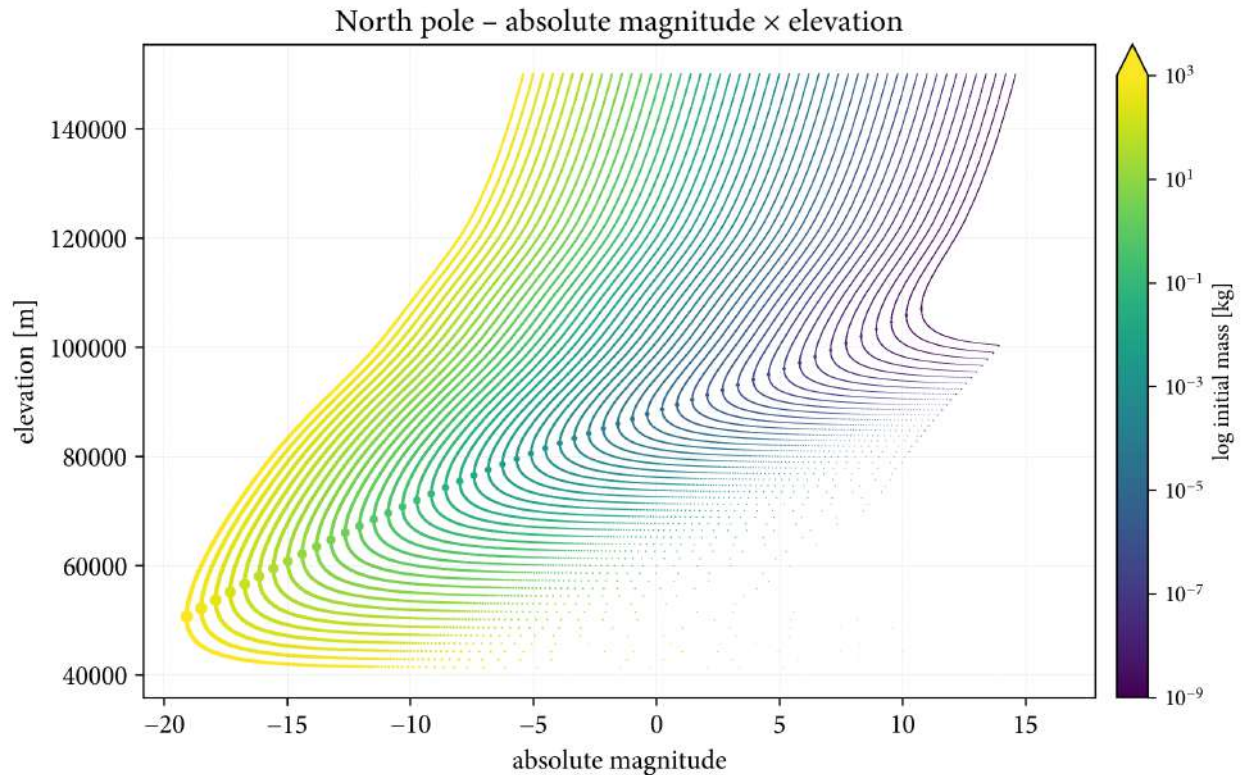


Figure 3 – Elevation against absolute magnitude plotted for the variable-mass Perseids. The generic “nose” shaped profile and the change in the ablation regime near 125 km are well visible again.

The same dataset is revisited in Figure 4, where the horizontal axis is changed to display the fraction of the meteoroid mass that has not yet ablated. All meteoroids attain maximum luminous power at approximately one fourth to one third of their original mass.

However, the observed behaviour is apparently not linearly dependent on the initial mass. A minimum is reached for particles with initial mass of approximately 10^{-7} kg, which attain maximal brightness only after losing about 75 % of their mass; and a maximum for particles with initial mass of about 0.03 kg. Very massive particles ($m \geq 100$ kg) penetrate much deeper and ablate rapidly in lower layers of the atmosphere. The exponential increase of atmospheric density dominates the slight decrease in velocity due to drag here.

Repeated simulations with different values of material constants or entry geometry confirm that maximal luminous power is attained when a meteoroid has lost approximately two thirds of its original mass due to ablation. This value is approximately correct for all realistic parameter combinations, regardless of particle mass, entry angle or density. A significant deviation could only be observed when highly exotic values of Q or Λ were used. However, such numbers are well beyond the interval where this simple physical model can be expected to give meaningful answers, and thus were not explored further.

3.3 Variable density

In the last case we investigated the effect of variable density. Again, we used values of properties corresponding to a simplified model of the Perseids, with density varied in an unrealistically wide interval of 200 kg m^{-3} to 20.000 kg m^{-3} . This could represent an entire range of natural materials from extremely porous clumps of dust of cometary origin to lumps of heavy metals (forgoing the necessary changes to other material properties). All other material properties were held constant.

Since initial mass is constant as well, the radii of the particles are also different. We plotted similar graphs as in the previous case, the plot of elevation against absolute magnitude (Figure 5) and of elevation against fraction of initial mass (Figure 6). The expected trend is that since denser particles are smaller in diameter, they are subject to less aerodynamic drag and subsequently should penetrate deeper into the atmosphere.

In Figure 5 it is possible to identify the same “nose” shaped profiles. In this case the absolute magnitude is almost independent of input parameters, with maximum brightness of approximately -5^m . The shape of the curve stays roughly constant in the entire plotted range, however, for denser meteors the entire curve is shifted downwards, with maximum brightness attained at heights from 90 to 75 kilometres. This is in agreement with our expectations.

In the second plot (Figure 6) we see a roughly linear increase in mass fraction at maximum brightness, rang-

ing from approximately 0.27 for particles at the lower end of the spectrum, compared to about 0.34 for the densest particles. The general rule is thus observed in this case as well.

4 Conclusion and future research

The simulation proved capable of simulating the atmospheric entry of meteoroids and visualising the properties of resulting meteors in a comprehensible way. We have shown that it is possible to isolate the effects of slight changes to the input and investigate their influence on the output. Many of the observed effects, such as more massive particles reaching lower heights before being destroyed, can also be easily explained intuitively. However, it should be noted that even this relatively simple model displays very complex behaviour of its output when the input parameters are changed. While actual meteors are even more complex and variable, with such a simulation it is nevertheless possible to investigate the behaviour of meteoroids during their atmospheric entry and quantify the effect of variation of their initial properties.

It would certainly be beneficial to further refine the assumptions of the model, most importantly the expression for light emission. The currently used equations do not consider the heat capacity of the meteoroid, which is especially important for bodies entering with lower speeds, or very small particles which experience significant pre-heating in the upper layers of the atmosphere.

Incorporating fragmentation into the model could greatly improve the scientific value of the results. However, while fragmentation of actual meteors when observed with photometers or cameras is well understood, further research is necessary to enable us to develop a suitably precise model for virtual particles.

Many more possible areas of research can be considered. More simulations of meteor showers and statistical analyses of the observed populations can be performed, such as verification of relationships between mass and population indices. This should not be too strongly dependent on the used equations of motion and ablation, and the obtained results could be readily confronted with real observations.

Verification of multiple previously obtained results in different sub-fields of meteor astronomy is also possible. One example is finding the optimal direction for observation with a narrow-field camera when the position of the radiant is known (Molau, 2018). The Monte-Carlo method could provide even more precise results, accounting for observation bias or other effects that are hard to express analytically, with minimal modification to the simulation toolset. Eventually even the underlying physical model could be changed in an attempt to find the best match to observational data.

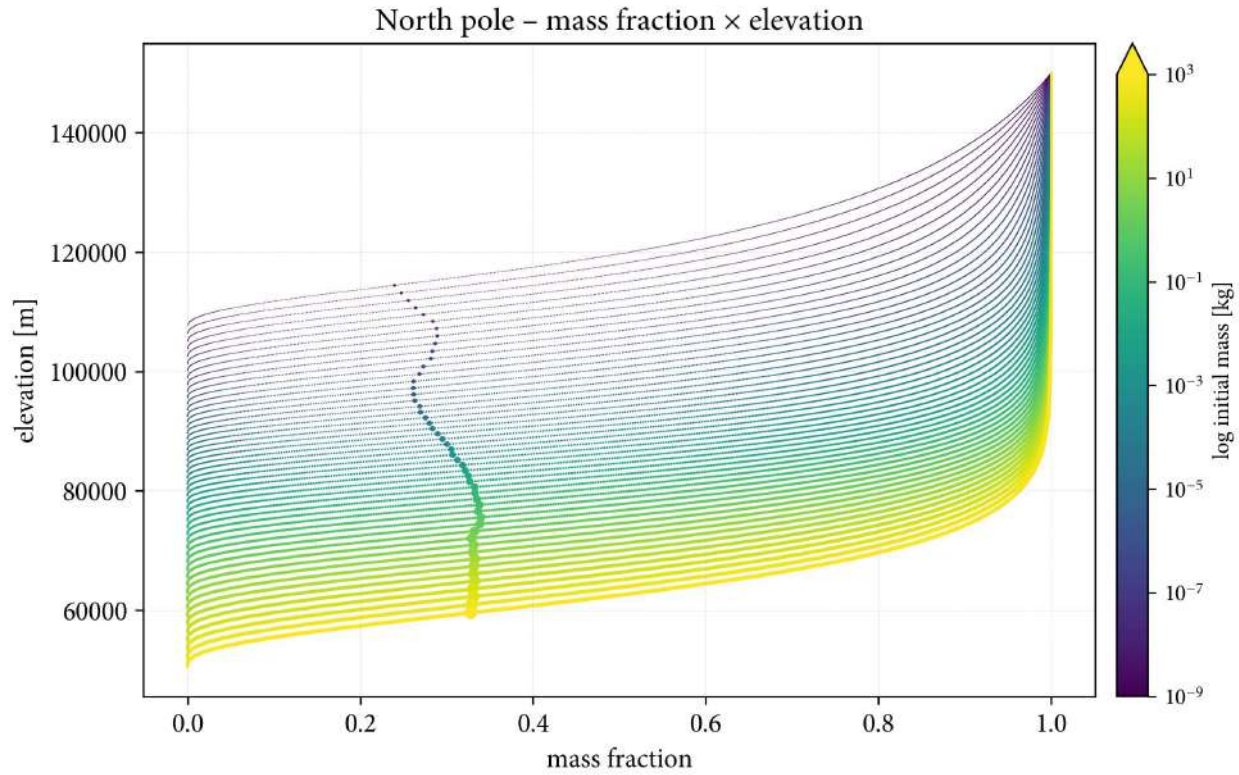


Figure 4 – Scatter plot of elevation against mass fraction. All meteors start at the right side of the chart (mass fraction = 1) and end at the left side (mass fraction = 0). There is a slight tendency for meteoroids with higher initial masses to attain maximum brightness earlier during ablation, but the dependence is far from linear.

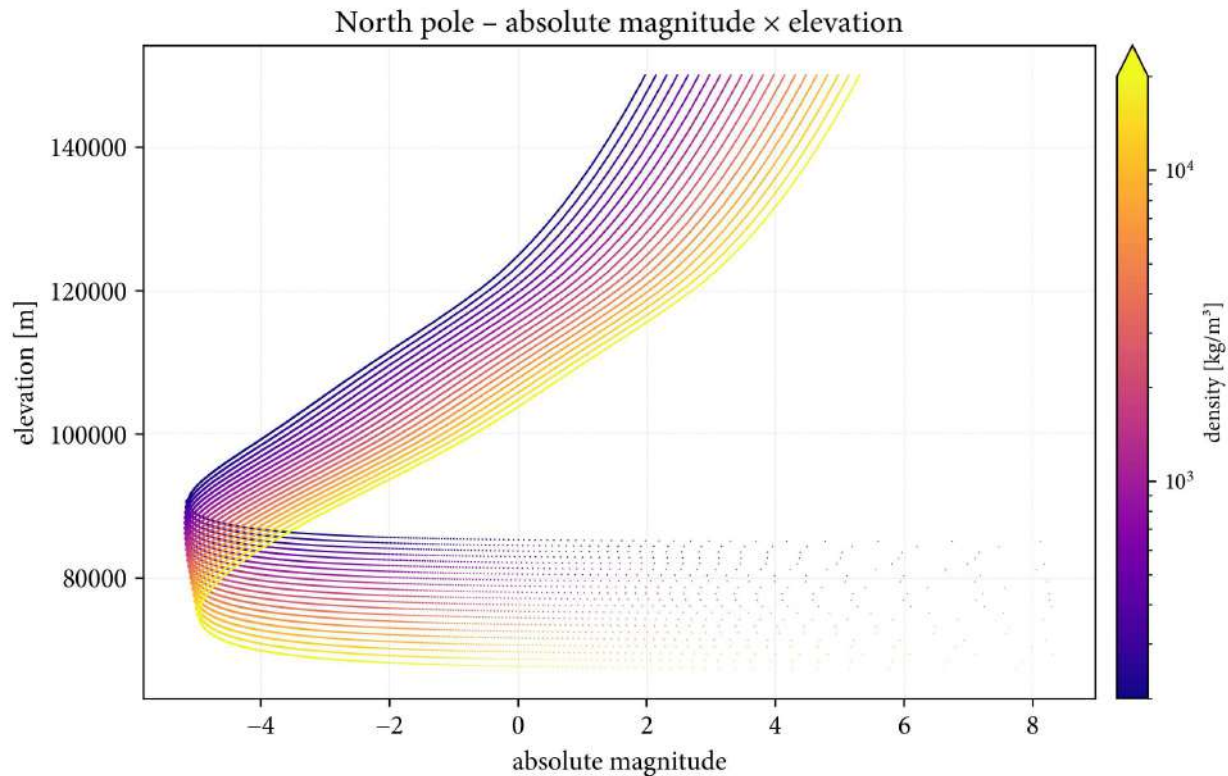


Figure 5 – Elevation against absolute magnitude plotted for the variable-density Perseids with constant particle mass of 1 g. The shape of the light curve and maximum brightness are almost equal in all cases, but there is a visible shift to lower terminal heights for denser particles.

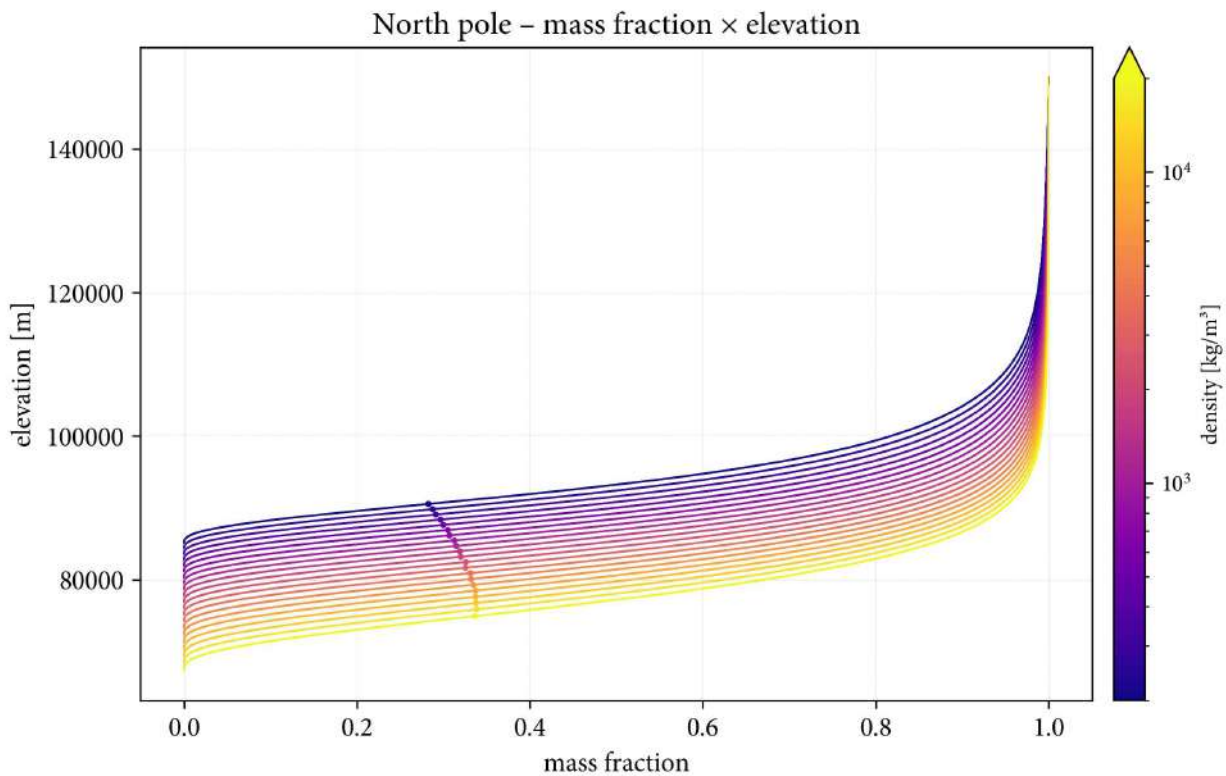


Figure 6 – A plot of elevation against mass fraction. The “one-third-rule” is observed again, with a slight shift to higher fractions for denser particles. The trend is approximately linear, but levels off at density about 6000 kg m^{-3} .

5 Acknowledgements

This work was supported by the Comenius University grant G-19-056-00, grant APVV-16-0148, VEGA 01/0596/18 and by the special scholarship awarded by Comenius University (March 2019).

References

Baláž M. (2018). “Determination of total meteoroid flux in millimetre to metre size range”. Master’s thesis, Comenius University in Bratislava, Bratislava, Slovakia.

Baláž M., Tóth J., Jedicke R., and Vereš P. (in prep.). “ASMODEUS meteor simulation toolset”. *Planetary and Space Science*.

Beech M. (2009). “On the shape of meteor light curves, and a fully analytic solution to the equations of meteoroid ablation”. *Monthly Notices of the Royal Astronomical Society*, **397:4**, 2081–2086.

Community Coordinated Modeling Center (1990). “MSIS-E-90 atmosphere model”.

Gural P. (2002). “Meteor observation simulation tool”. In *Proceedings of the International Meteor Conference 2001, Cerkno, Slovenia*. pages 29–35.

Molau S. (2018). “The perfect observing direction”. In *Proceedings of the International Meteor Conference*.

The bridge of spies

Peter C. Slansky¹

¹ University for Television and Film Munich, Department II Technology

slansky@mnet-online.de

Instead of a presentation this was a fragmented stand-up narration about a place of history nearby the IMC 2019's excursion destination: the Glienicker Brücke that became famous as "The bridge of spies".

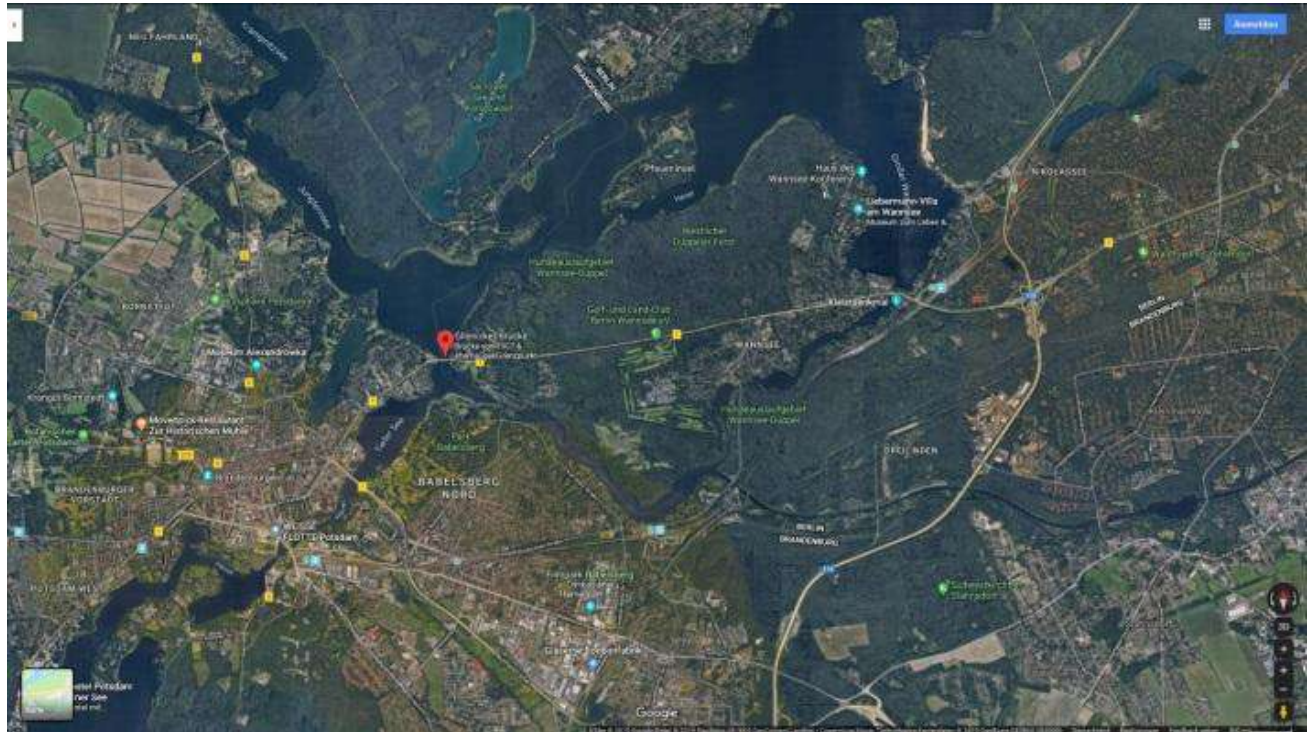


Figure 1: The Glienicker Brücke, displayed by Google Maps today. On the right bank is the State of Berlin, on the left bank the State of Brandenburg. The Institute for Astrophysics, destination of the IMC 2019 excursion, is 4 km south-southwest. The UFA film studios are 4 km southeast, the southern curve of the AVUS race track was 8 km east-northeast.

1 Introduction

The Glienicker Brücke was built in 1907. It connects the south-western part of Part of Berlin with Brandenburg. In the era of the Cold War it was used three times to exchange captured spies and dissidents between the NATO and the Soviet Union. Many movies referred to this very special place at the border between the two blocks of the Cold War, including 'The Bridge of Spies' from 2015 with Tom Hanks as a leading actor, directed by Steven Spielberg.

2 Narration

It is less known that this bridge had also been the place where three men from the German Democratic Republic (DDR) managed to break through the border to the Federal Republic of Germany. Completing the absurdity of the cold war, "the West" was on the east bank of the bridge and "the East" on its west bank. On 10th of October 1989 many others followed these three men, as the bridge was officially opened for traffic after 28 years...

Even less known is the fact that at the end of the Second World War in late April 1945 this bridge had been the last escape for the soldiers of the German Wehrmacht to be captured by the US Army instead of the Soviet Army. Among them was the father of the author, aged 20. His last stand had been the banked curve of the AVUS, the fastest car racing track of the world of that time. Today the former curve is vanishing between the trees of the Grunewald.

Very close to the Glienicker Brücke are the famous UFA film studios, birthplace of the classic German movies. Only a hundred meters north the first German film school had been established in the 1950s, the Film University Babelsberg. In its early years it was situated in a line of Gründerzeit-Villas at the Griebnitzsee, just 1.5 km west-southwest from the bridge. During the Potsdam conference 1945 Stalin and Marshall Schukow had stayed here. From there it was only 200 m north to Western Berlin – across the lake. There was a tale that one night a film student managed to escape swimming to West-Berlin without using the bridge – but using a fake swan over his diving mask.

Eight kilometers to the northeast, in the Grunewald forest, there is another hidden place of history: the remains of the southern curve of the AVUS, the world's fastest motor racing track of that time. Here the Mercedes Silberpfeils and the Auto Unions had hunted for speed records in the 1930s. The southern curve was built as a banked curve. In the last days of the Second World War it served as the last stand of a platoon of the German Wehrmacht. In late April 1945 they escaped from here, crossing the Glienicker Brücke, to reach the river Elbe to be caught by the American Army instead of the Soviet Army – among them the father of the narrator.

Peace and international collaboration – as we do in the IMO – are not self-evident...

Daytime fireball capturing

Felix Bettonvil^{1, 2, 3}

¹ Leiden Observatory, Leiden University, Leiden, The Netherlands

bettonvil@strw.leidenuniv.nl

² NOVA Optical Infrared Instrumentation Group, Dwingeloo, The Netherlands

bettonvil@astron.nl

³ KNVWS Meteor Section

Traditionally, fireball patrol cameras are constructed to capture fireballs during night time. Fireballs nonetheless – and in particular meteorite dropping ones – do not only appear at night time: there are various examples of great fireballs that did appear at twilight or even daytime. In an attempt to have also daytime coverage I will present some recent test work on a panoramic surveillance cam.

1 Introduction

Fireball patrol cameras are commonly designed to capture fireballs during night time. Due to the presence of stars that act as reference points this is great for obtaining high accuracy, but fireballs – and in particular meteorite dropping ones – do not only appear at night time: there are various examples of great fireballs that did appear at twilight or even daytime.

Three bright fireballs over the Netherlands in the past 1.5 year appeared during twilight or day time (i.e. Broek in Waterland meteorite, January 11, 2017, 17:09 CET; Daylight fireball June 28, 2019, 21:30 CEST, with sonic boom and 564 visual IMO reports; Daylight fireball September 12, 2019, 14:50 CEST, over Germany, 583 IMO reports, detected by CNEOS¹).

Although daylight fireballs are clearly noticed by the general public, the amount and quality of pictures and videos is typically rather limited, at least in the Netherlands: no dedicated meteor camera exists to capture fireballs during daytime².

In this paper I describe an idea, as well as first experiences with a possible solution for daylight fireball imaging: a panoramic surveillance cam.

2 Daylight captures

In the rare cases that daylight – or twilight fireballs are captured within The Netherlands with photo or video, this is mostly done with low resolution dash cams, often mounted in moving vehicles, or with security cams. Obtaining proper reference images (best with stars) turns out to be difficult or not possible at all, resulting in low quality trajectories and lots of work.

3 Surveillance cams

Nowadays the surveillance camera market offers so-called forensic surveillance cameras, high-resolution cameras equipped with fisheye lenses, which make me think whether this is something for our field. Table 1 illustrates the typical specifications of these cameras.

Table 1 – Forensic surveillance camera specifications

Specifications
10 Mpxl or more
180+ deg Field of view
10+ frames per second
Auto exposure setting
Motion detection software
Including Ethernet connection, NTP, webserver
Weather proof, robust

¹ <https://cneos.jpl.nasa.gov/fireballs/>

² It should be noted that there are also a few FRIPON stations (Colas, 2019) in The Netherlands, and soon also an All-sky 6 (Hankey, 2019), in principle capable of taking daytime images, but not (yet) routinely used, as well as a proposal was done by me to extend the widely used DSLR-based All-sky cameras into twilight (Bettonvil, 2019).

Typical brand names are Dahua, Vivotek, Hikvision, Axis.

4 Specifications

The camera that we selected for our test is the Axis M3058 PLVE Forensic panoramic network camera (Figure 1). Specifications of this camera are given in Table 2. Cameras from the other vendors have very similar specifications – although not identical, are similar priced, and vary mostly in the provided software.

The selected camera measures circa 15 cm in diameter and is approx. 8 cm tall.



Figure 1 – Axis M3058 PLVE Forensic panoramic network camera as used in the test

Table 2 – Specifications of Axis M3058 PLVE Forensic panoramic network camera

Table Head	Column Head
# pixels	12 Mpx
resolution	3.6 arcmin / pxl
projection	Equi-solid-angle projection, circular image
Exposure range	0,04 ms – 2s
fps	up to 30 fps
protection	IP66
Digital I/O	yes
Local storage	Yes, SD card

5 Review

In the remainder of this paper I will evaluate the camera.

Build quality

The build quality of the camera is very good. The housing is made of a sturdy die-cast aluminum, apparently vandal-proof, which is also used as a heat-sink for the electronics

inside. Everything inside and outside looks high quality.

Ease of use

It is extremely easy to use the camera. Once powered (via the Ethernet cable: it works with PoE – Power over Ethernet), the camera can be accessed via a web-browser, by typing in its IP address. I tested the camera both on a Windows 10 and Mac IOS/Safari and both work. Although Axis offers video surveillance software (handy if you use more than one camera), I did do all tests via the built-in webserver and web-browser.

Motion Detection

All surveillance camera vendors offer motion detection software to detect motion in the image after which a sequence of images can be stored, an alarm initiated and/or an email send. I experienced that this software is very advanced: it is able to detect human beings, it is very good in detecting faces, hands, etc., and very effective in rejecting all others, from animals, car lights, moving branches of trees, etc. In other words: on fireballs the built-in software will not trigger.

One should be able to program own detection algorithms on a separate computer, analyzing the video stream, if one would like so, however.

Optical quality

The camera is sold as a forensic cam. This allows the user to zoom in into the digital image, and thus very good image quality is expected. The on-board software also offers dewarping, in which the live typical fisheye-distorted image is stretched into a regular undistorted formatted crops, but which we do not use. The fisheye lens has a focal length of 1.3 mm and is F/2.

First test images show the fisheye-typical chromatic aberration near the horizon (Figure 2, left). There is also some weak ghost visible, resulting in a double, vertical displaced image, although much weaker in intensity. With the dome (Figure 2, right), the ghosts are more clearly visible, being brighter in intensity.

Night time exposures (Figure 3, see also next Section), shows the same behavior. At large zenith angle (low elevation) we see that the stars are not symmetric anymore but start to be elongated and appear double at high zenith angles ($h < 30$ deg); see also Figure 4. At small zenith angles the stars look crisp and symmetric.



Figure 2 – Crops of a regular daylight image near the horizon; (left) without protecting dome; (right) with dome.

Exposure range

The camera can automatically adjust its exposure. Designed for daytime use (or night time with IR), it is however able to increase its exposure time to up to 2 seconds, enough to capture stars up to magnitude 4 at dark skies. This is a very nice characteristic as it enables taking reference images for astrometry during night time.

The camera has also the option to use WDR (Wide Dynamic Range), being a dynamic white balance which can vary over the field of view. This way both dark regions in the image (e.g. trees at the horizon) and bright regions (e.g. the blue sky) can be imaged so that local contrast is optimal and not over- or underexposure occurs. This results in great images, ensures that we more easily see fireballs at the daylight blue sky, but makes photometry harder of even impossible.

6 Tests

Astrometry

In order to evaluate how accurately a fireball trajectory can be determined, astrometry was done on a single night time exposure (without dome). For this a standard astrometry model was applied, based on a linear 6-variable plate

constant model with fisheye distortion projection function, and using a least-square-fit as well as iterative derivation of the plate center.

The fisheye lens turns out to be of equi-solid-angle projection type.

Based on 23 reference stars, a plate fit error of 1.2 arcmin was achieved, equal to one third of a camera pixel, rather typical for all-sky work. We conclude that the mediocre image quality at larger zenith angles does not affect the astrometry: apparently finding the center of gravity of each star is still accurate.

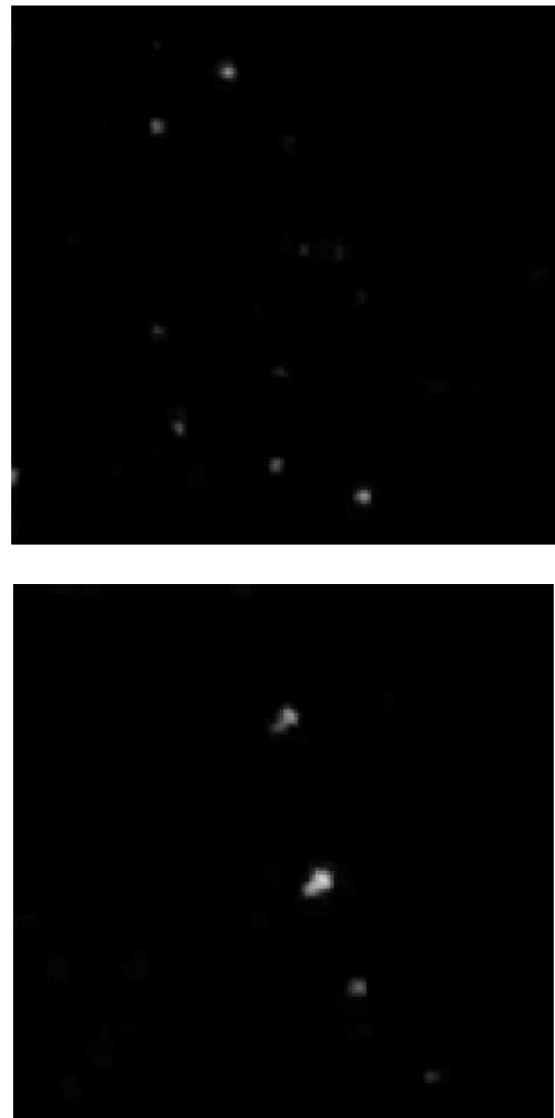


Figure 3 – Two close ups of stars in a night time exposure; (top) center field of view; (bottom) $h = \sim 30$ deg.

Data stream

Due to the large CMOS chip and high frame rate, the data stream is expected to be very high. In the highest quality, indeed data volume can reach a TeraByte per 24 hours.

Surveillance camera manufacturers have however created a suite of compression techniques to reduce the size of the data stream, both in the spatial and time domain, and the software offers many parameters to choose an optimal one for your particular application.

The Axis cameras offers two stream formats: MotionJPEG, and H.264, both packed as .mkv file.



Figure 4 – Close up of an area near the edge of the field of view: city lights on the horizon.

Figure 5 gives as an example two close ups of an image detail, in MotionJPEG (25 Gb/hr), and H.264 (0.4 Gb/ hour). The first looks noisier and the detail slightly more crispy, but not much.

The memory can be set up as a cyclic buffer memory, overwriting the data if the storage is full. With a large SD card, 24 hours capturing in high quality is possible, which in principle removes the need for live auto-detection (motion detection).



Figure 5 – Two close ups of an image detail in MotionJPEG format (25 Gb/hr), and H.264 (0.4 Gb/ hour).

Jitter

For determination of the velocity the temporal stability of the capture rate is important. I did not perform tests (yet), but expect to be small (milli-sec range), also based on information by Axis, and of no concern for our work.

Service

As Axis is worldwide company, I contacted them to report the issue with the moderate image quality. Their service is impressive, with prompt feedback and exchange on detailed data and analysis, and involving experts. It resulted in an immediate shipment of the camera to their repair center in Hungary for examination. They decided to replace the entire camera, but unfortunately, the new camera was not much better in quality, and Axis responded that the remaining error is typical for these type of cameras.

7 Conclusions

Pros:

- the camera has a high spatial resolution, and high frame rate, well suited for fireball detection,
- weather proof and very robust,
- installation is very easy,
- can take images day and night, and sensitive enough to capture stars, allowing proper astrometry which can be used for daytime fireballs,
- astrometry is very acceptable, despite the aberrations of the lens.

Cons:

- 8 bit only,
- when WDR (dynamic white balance) is used (preferred for optimal contrast), proper photometry is expected to be impossible,
- the offered motion detection is useless, as it is not able to detect fireballs (software is too advanced; fireballs are neglected). But because the camera can store the videos for 24 hours, this is not

- seen as problematic. Desktop tools could be developed to do real-time detection,
- I expected a higher optical quality.

The camera is not extremely cheap, but its price range is similar to a FRIPON and Allsky6 camera (~1k EUR).

Finally, I conclude that this is a good camera for daytime fireball detection, and I recommend the camera for use.

References

- Bettonvil F. (2019). "Extending all-sky photography into twilight". In R. Rudawska, J. Rendtel, C. Powell, R. Lunsford, C. Verbeeck, A. Knöfel, editors, *Proceedings of the International Meteor Conference*, Pezinok-Modra, Slovakia, 30 August – 2 September, 2018, IMO, not published.
- Colas F. (2019). "FRIPON first results after 3 years of observations". In U. Pajer, J. Rendtel, M. Gyssens, C. Verbeeck, editors, *Proceedings of the International Meteor Conference*, Bollmansruh, Germany, 3-6 October 2019. IMO, these proceedings.
- Hankey M. (2019). "The All Sky 6 and Video Meteor Program of the AMS Ltd.". In U. Pajer, J. Rendtel, M. Gyssens, C. Verbeeck, editors, *Proceedings of the International Meteor Conference*, Bollmansruh, Germany, 3-6 October 2019. IMO, these proceedings.

The Daylight Fireball of September 12, 2019

Sirko Molau¹, Jörg Strunk¹, Mike Hankey², Laura Kranich¹, Carsten Jonas¹, Felix Bettonvil³, Dieter Heinlein¹, Andre Knöfel¹, Andreas Möller¹ and Wolfgang Hamburg¹

¹Arbeitskreis Meteore e.V, Germany

sirko@molau.de, j-strunk@gmx.de, laura@lk-photo-film.de, carsten.jonas@jonas-medizintechnik.de, dieter-heinlein@t-online.de, aknoefel@minorplanets.de, andrmoel@gmail.com, w.h@mburg.org

²American Meteor Society, USA

mike.hankey@gmail.com

³KNVWS Werkgroep Meteoren, Netherlands

bettonvil@strw.leidenuniv.nl

On September 12, 2019, at 12:50 UT, a daylight fireball was observed over northern Germany, which probably resulted in a meteorite fall at the Danish/German border near Flensburg. It was recorded by AMS21, one of our AllSky6 fireball cameras in Germany. This paper summarized the state of analysis as of early October 2019.

1 Introduction

On September 12, at 12:50 UT, a daylight fireball occurred over northern Germany. Within hours, more than hundred sightings have been reported via the AMS/IMO fireball report form¹. First analyses indicated an impact point for possible meteorite(s) in the North Sea. Two weeks later the number of visual reports had grown to over 500, which makes it one of the best observed events ever (Figure 1).

2 Video Observations

At daytime, all (?) current fireball networks are inactive because the cameras are too sensitive for daylight and/or there are too many false detections under daytime conditions. Due to the quick alert, it was possible to save and manually check the video footage of the three German AllSky6 cameras (Figure 2), anyway:

- AMS16 at Ketzür was down at daytime due to thermal problems,
- AMS21 at Herford was heavily overcast,
- AMS22 at Lindenberg was also clouded out.

However, it was in fact not totally overcast at Herford, but we could indeed find traces of the fireball in a small cloud gap (Figure 3). It became the second daylight fireball ever recorded with an AllSky6 system.

3 Trajectory Calculations

We computed the entry plane of the meteoroid from the AMS21 video (Figure 4), which matched to the trajectory obtained by extending the meteoroid trail observed by US military sensors (CNEOS²).



Figure 1 – Visual observers of the daylight fireball.



Figure 2 – Currently active AllSAky6 stations in Germany.



Figure 3 – The fireball as recorded by AMS21 at Herford.

¹ https://fireball.amsmeteors.org/members/imo_view/event/2019/4385

² <https://cneos.jpl.nasa.gov/fireballs/>

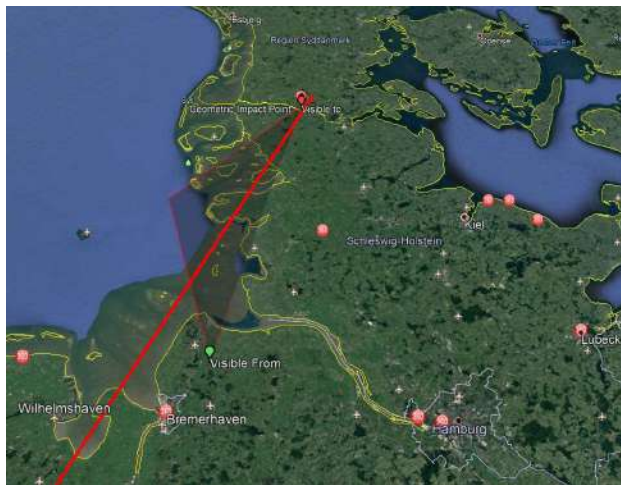


Figure 4 – Meteoroid plane determined from AMS21 data, and trajectory obtained by CNEOS.



Figure 5 – The fireball recorded by a surveillance camera at a shipyard in Marknesse / NL.



Figure 6 – The fireball recorded by the action cam of a kite surfer.

Thanks to our video it became evident, that the impact area was not over the North Sea, but close to the Danish/German border near Flensburg. It turned out, that visual reports collected within two hours after the event were more accurate than the sum of all reports received in the first few days.

Information on the spectacular fireball was quickly shared via the AKM Meteor Forum and IMO Homepage³. Further recordings were obtained by chance, e.g. from surveillance camera at shipyard Marknesse in the Netherlands (Figure 5) and from the action cam of a kite surfer (Figure 6) at the North Sea.

Based on the CNEOS data, the meteoroid was characterized as follows:

- initial size: ~2 m,
- energy: 0.48 kt TNT,
- initial velocity: 18.5 km/s,
- initial mass: ~12 t (at $\rho=3 \text{ g/cm}^3$).

Given these data, a meteorite fall was most likely.

4 Strewn Field Calculations

Jim Goodall published a number of bulletins placing the strewn field north-west of Flensburg (Figure 7). Our own calculations (from Mike, Andreas, Felix) placed the strewn field a little more to the south-east. The area was not perfect, but reasonably well suited for meteorite searches.

5 Meteorites

Some of us (Laura, Carsten, Sirkko, Jörg) visited the strewn field once or several times in September, but did not find a meteorite.

Meteor Event Bulletin — Flensburg, Germany Version 2.2: September 21, 2019 04:53 UTC

Trajectory Data:		Strewn Field Prediction Data:	
Date/Time UTC	09/12/2019 12:49:48	Simulation Date/Time UTC	09/12/2019 12:49:48
Local Date/Time (+2.0)	09/12/2019 12:49:48 PM	Simulation Engineer	Jim Goodall
Reference Location	54.50°N 9.15°E	Trajectory Data Source	CNEOS*, Marchal v. Video, Holger Scheele Video, Jörg Strunk Video, Marknesse Video
Reference Altitude	42 km	Weather Data Source	IORA Weather Balloon Data
Estimated Energy/Mass	0.48 kt / 12000 kg	Simulation Type	Monte Carlo, Unknown Meteoroid
Bearing (Heading)	8.487° North	Simulation Data Count	204 scenarios / 500,334 fragments
Incidence Angle	66.15° from vertical	Strewn Field Prediction Notes: The colored squares shown on the map indicate the relative probability of meteorite finds, based on the estimated variation in the trajectory, weather data, meteorite density, and fragmentation. The color scale is normalized to this simulation only and not comparable to other simulations.	

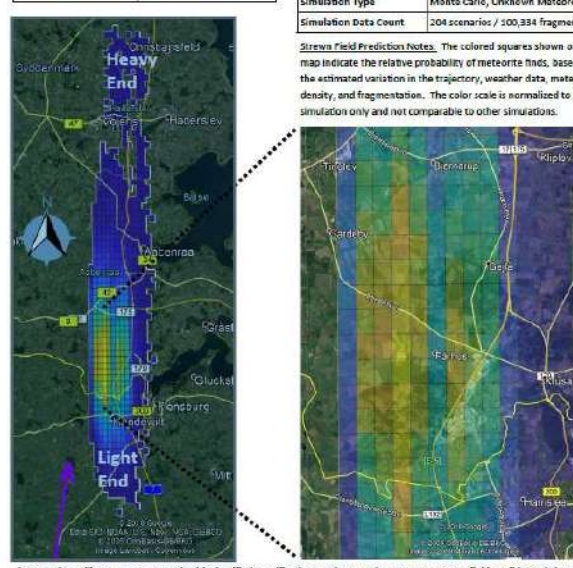


Figure 7 – One of the bulletins of Jim Goodall with strewn field calculations.



Figure 8 – Meteorite that was found in a backyard in southern Flensburg on the day after the fireball.

However, the International Meteor Organization³ (IMO) and the German Aerospace Center⁴ (DLR) were approached by a man from the Flensburg area who reported to have found a possible 26g meteorite in his backyard on September 13 (Figure 8). From visual inspection, the meteorite seemed to be genuine, but we only know for sure once the analysis is done.

The finder (Figure 9), who asked to stay anonymous for the moment, was visited by AKM members and could be convinced to let his find be analyzed by renowned meteorite specialists with dedicated equipment.

Analyses are still ongoing, but first results indicate an unusually low density of only $\rho=2.0 \text{ g/cm}^3$. The internal color was not typical for an ordinary chondrite, too. Later radio nuclide analysis of short-lived isotopes confirmed it to be a fresh meteorite, so it is almost certainly linked to the daylight fireball of September 12, 2019. Further results are expected soon and will be published elsewhere.



Figure 9 – The lucky finder of the meteorite and his wife.

6 Outlook

We are still trying to obtain proper calibration data from the Marknesse video and further recordings of the event with sufficiently precise astrometry to pin down the impact area and narrow the strewn field. Further searches by AKM members are planned for October 2019.

³ <https://www.imo.net>

⁴ <https://www.dlr.de>

ESA's activities on fireballs in Planetary Defence

Regina Rudawska¹, Juan Luis Cano³, Ramona Cennamo³, Luca Conversi³, Laura Faggioli³, Rüdiger Jehn², Detlef Koschny^{1,4}, Javier Martín Ávila³, Marco Micheli³, Toni Santana-Ros², Robert Luther⁵, Natalia Artemieva^{6,7}, Kai Wünnemann^{5,8}

¹ ESA/ESTEC, Noordwijk, The Netherlands

regina.rudawska@esa.int

² ESA/ESOC, Darmstadt, Germany

³ ESA/ESRIN, Frascati, Italy

⁴ TU Munich, Germany

⁵ Museum für Naturkunde Berlin - Leibniz Institute for Evolution and Biodiversity Science, Berlin, Germany

⁶ Planetary Science Institute, Tucson, USA

⁷ Institute for Dynamics of Geospheres, RAS, Russia

⁸ Freie Universität Berlin, Berlin, Germany

Since January 2009, the European Space Agency (ESA) has a 'Space Situational Awareness' programme, addressing, among other points, the topic of Planetary Defence. The Planetary Defence aims to ensure that we know about asteroids or comets potentially hitting our planet, and what to do about it. Among services provided via a technical portal at <http://neo.ssa.esa.int> a Fireball Information System (FIS) will be accessible in the near future. Once completed it will provide a comprehensive entry point to relevant information (time, location, brightness, images, videos, etc.) on observed fireballs events since 2010 having visual magnitude brighter than -10. Other Planetary Defence activities on fireballs are: The deployment of a space-based fireball camera, and the development of an impact effects simulation tool, based on an impact effects knowledge-base.

1 Introduction

For over 10 years now, the European Space Agency (ESA) is dealing with the topic of potentially Earth-threatening small bodies within its Space Situational Awareness programme. This programme – currently being re-branded to the 'Space Safety' programme – addresses three main points: threats coming from Space Weather (linked to e.g. the Sun's activity), threats from satellites or space debris, and Planetary Defense. The latter is defined as (...) *activities and actions to predict and mitigate a potential impact by an asteroid or comet on the Earth*¹.

Within its Planetary Defence activities, ESA is performing work in three separate areas:

- I. Observations of near-Earth objects (NEOs) – carried by ESA-owned telescopes, via contracts to other telescope operators, and by developing a dedicated NEO survey telescope, e.g. Flyeye telescope (Cibin & Chiarini, 2019).
- II. Data provision – by computing and providing different relevant services at its technical web portal <http://neo.ssa.esa.int>. Here, the core activity is to compute the orbits of all known NEOs 100 years into the future and check whether they could impact our planet. Those that could are

being ingested into 'Risk List'. Other services are e.g. a database of physical properties or a Fireball Information System (addressed later).

III. Mitigation – setting up interfaces with civil protection agencies to inform them about upcoming potential impacts and discuss mitigation measures. ESA is also discussing mitigation in international groups dealing with the asteroid impact threat, e.g. the International Asteroid Warning Network (IAWN) and the Space Mission Planning Advisory Group (SMPAG)². Moreover, ESA is proposing the HERA space mission to the binary asteroid Didymos to observe the asteroid system, asteroid properties, and the outcome of NASA's kinetic impactor technology demonstration mission DART (Double Asteroid Redirection Test) (Cheng et al., 2016).

2 Why Planetary Defence?

The official mandate of the Space Situational Awareness programme is

the protection of our planet, humanity, and assets in space and on Earth from dangers originating in space.

¹So defined in the Terms of Reference for the Space Mission Planning Advisory Group, <http://www.smpag.net/terms-of-reference-v0>

²For more information about these groups, see their relevant web pages: <http://www.iawn.net> and <http://www.smpag.net>, accordingly.

More concretely, the top-level goals of Planetary Defence are (...) *to be aware of natural objects in space. To predict possible impacts and their consequences and inform relevant parties. To prepare for risk mitigation, by technological developments and on the political level.*

The interest and activities of ESA depend on the size of the object. Asteroids as small as 1 m will already create a spectacular fireball, attracting lots of public attention. For example, the Flensburg fireball over Northern Germany on 13 September, 2019 kept one ESA staff busy for basically a whole day, just responding to press queries. In this case, it is important that the Agency is informed quickly and reliably, to provide correct information.

Stony objects larger than 10 m are expected to generate damage – see as an example the Chelyabinsk event. There, a roughly 20 m object entered the Earth’s atmosphere over the city of Chelyabinsk in Siberia. The generated shockwave shattered windows and garage doors, and created substantial damage. Roughly 1500 people were injured, mainly because they were watching the event behind glass windows. Had this object been discovered in advance, a simple warning to open windows and not stand behind them would have mitigated the damage substantially. That is exactly what the Planetary Defence activities are aiming for – discover these objects in time, and inform the civil protection agencies that would take appropriate measures.

According to agreements on an international level, starting at 50 m diameter, space agencies have to consider deflecting the object. This is discussed world-wide within the already mentioned Space Mission Planning Advisory Group, which consists of delegations of all major space agencies on this planet. As a space agency, ESA is not only studying different deflection techniques, but also proposing the space mission ‘Hera’. Hera is a small spacecraft which would observe the aftermath of a real deflection demonstration, executed by NASA. NASA plans to hit the smaller body of the binary system Didymos with a kinetic impactor spacecraft. Without explosives, just via momentum transfer, the velocity of the secondary body will be altered slightly. This can be observed by a change in the orbital period of the secondary body around the primary. To really understand the momentum transfer, information on the target properties, the generated impact crater, and the precise mass of the secondary body is important (Raducan et al., 2019). This can only be obtained with an observer spacecraft like Hera. A decision point in November 2019 will show whether ESA receives the budget for this mission.

3 Why fireballs?

For ESA’s Planetary Defence activities, fireball observations are relevant for two reasons. They cover the small size range (meters to tens of meters) of asteroids, for which less than 0.1% of the population is known. There is a large uncertainty in the actual flux density of

these objects (Boslough et al., 2015) which a detailed assessment of fireball observations could reduce.

A second motivation for ESA’s Planetary Defence office is the public attention – bright fireballs generate queries by the public, and ESA is often contacted by the press to comment on them. Thus, we have interest in knowing about them before being contacted by the press.

For these main reasons, ESA is funding some activities related to fireballs. More details for these activities are given in the following sections.

4 NEMO – the near-real time Earth atmospheric impact monitoring system

An object of 1 to 2 m in diameter is not expected to do any damage on the ground – but the resulting fireball would be so bright that it would be visible in daylight. The public and the press are becoming more and more aware of the fact that we are constantly being bombarded by these objects. A 1 m object is expected to enter the Earth’s atmosphere typically every few weeks. To ensure that ESA is aware of these objects, we are setting up the NEar real-time MOnitoring system (NEMO). NEMO is constantly monitoring social media and flags any reports about fireballs. It provides a computer interface visualising the events. It is being developed at the University of Oldenburg, Germany, and will be installed at ESA premises in January 2020. For more details, see another paper in these proceedings (Ott et al., 2019a).



Figure 1 – The Carancas impact crater with roughly 14 m in diameter. It was created by an exceptionally small asteroid of just above 1 m in size. From Kenkemann et al. (2009).

Note that there seems to be at least one event where a very small meteoroid, just a little above 1 m in size, hit the ground. This is the Carancas event, which happened in 2007 in Peru (Figure 1). However, this is really seen as an exception and therefore not considered here.

5 The impact effects knowledge base

For stony objects >15 m and iron objects >3m, we are expecting effects on the ground. Thanks to a contract

with the Museum für Naturkunde Berlin, Germany, we are setting up a knowledge base on impact effects. This knowledge base collects all known information on possible effects (e.g. shock waves in the atmosphere, or radiation of light) – both from real events (Kenkmann et al., 2009), and from simulations (Artemieva & Shuvalov, 2019). It collects these effects as a function of asteroid parameters like mass, velocity, entry angle and strength. Computer simulations can model the effect of an atmospheric entry quite well. However, the computation times for just one simulation can be in the order of days to weeks. In the case of an imminent impact we do not have that much time. This is where the knowledge base comes in. It will collect all known information. When a new threatening object is discovered, one can interpolate the effects from the knowledge base. In a follow-up contract to the ongoing setup of the knowledge base, an engineering-level software tool will be developed which allows these interpolations. The aim is to be able to estimate the effects to a reasonable accuracy within tens of seconds, rather than days or weeks.

6 The Fireball Information System and the European Network of fireball cameras

One of the mandates of ESA's Planetary Defence activities is to collect and provide information on fireballs brighter than -10 magnitudes. Since the formulation of this requirement over 10 years ago, a database to collect fireball events world-wide has been set up by the International Meteor Organisation (IMO)³ and the American Meteor Society (AMS)⁴ (Hankey, 2014). We have therefore shifted the focus of our work to provide complementary information. As part of the NEMO project, the University of Oldenburg is now regularly checking infrasound data from the International Monitoring System of the Comprehensive Nuclear Test-Ban Treaty Organisation (Ott et al., 2019b). These data can be used to estimate the energy release during a fireball event. They regularly post the results on the IMO and AMS web pages, e.g. (Ott & Drolshagen, 2019). We are using the Fireball Information System to ensure the long-term archiving of images and metadata of the German part of the European Network (EN) of fireball cameras. This is done via a contract with DLR Berlin, Germany. For more details, see Margonis et al. (2019) in these proceedings.

7 Predicting fireballs

On 06 October 2008, the Catalina asteroid sky survey discovered an object later designated 2008 TC3. It was found to hit Earth's atmosphere about 19 hours later,

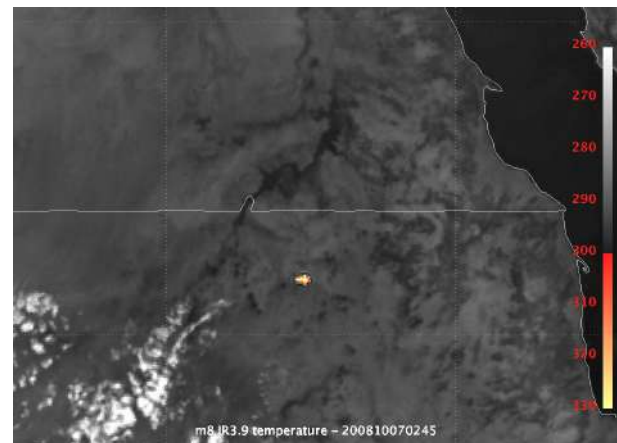


Figure 2 – The fireball caused by the entry of 2008 TC3 over Sudan. Image credit: Eumetsat.

over Sudan. With an estimated 7 m of size, it was small enough to not produce any damage. The fireball was observed by a weather satellite (Figure 2), and it was possible to recover meteorites on the ground (Jenniskens et al., 2009). This was not only scientifically relevant, but also demonstrated that we have the capability to predict such events.

Since then, three more predicted fireballs occurred. One went unnoticed in the South Pacific (2014 AA) on 01 January, 2014 (Farnocchia et al., 2016). It was only confirmed by looking at infrasound data records after the fact. Another asteroid, 2018 LA, was discovered only a few hours before it generated a nice fireball over Africa on 02 June, 2018 (Farnocchia et al., 2018). It was about 2 to 4 m in size. The fireball was recorded by several surveillance cameras. 2019 MO was also discovered only a few hours before it entered the Earth's atmosphere – over the Caribbean Sea without causing any damage (Ott & Drolshagen, 2019). It was confirmed in data from an Earth-observing satellite.

Predicting fireballs is very useful for scientific purposes. Given enough warning time, camera systems and spectrographs can be installed close to the event, to observe the fireball. Comparing these data to data obtained by remotely observing the asteroid when still in space will allow to compare the data sets. If meteorites are found, in-situ analyses of the object can be performed. Eventually, this will lead to us being able to better interpret the asteroid observational data.

8 Conclusions

Even though most fireball events do not cause any significant damage, ESA's Planetary Defence activities include several activities related to fireballs. Together with DLR Berlin, we are creating a long-term archive for the German data of the European Network (EN) of fireball cameras. Moreover, we are preparing a tool to quickly compute impact effects together with the Museum für Naturkunde Berlin, Germany. Furthermore, we are using our asteroid orbit predictions to predict fireballs. Last but not least, we are setting up an alert

³https://fireballs.imo.net/members/imo_view/browse_reports

⁴https://fireball.amsmeteors.org/members/imo_view/browse_reports

system which quickly informs us about fireball reports. To avoid being hampered by clouds, the best location for a fireball camera would be in space. The US is providing selected data from 'US Government Sensors' on the website of their Center for NEO Studies⁵. These are military sensors, and no information on their properties is available. In Europe we are therefore aiming at bringing a camera into space which would be dedicated to observe natural fireballs. Funding for the development of such an instrument is available and will begin in 2020. The main argument for enhancing the collection of fireball data is to better constrain the flux density in the size range of a few meters. For this, every amateur camera that contributes to the data set in a controlled way is useful.

References

- Artemieva N. and Shuvalov V. (2019). "Atmospheric shock waves after impacts of cosmic bodies up to 1000 m in diameter". *Meteoritics and Planetary Science*, **54**, 592–608.
- Boslough M., Brown P., and Harris A. (2015). "Updated population and risk assessment for airbursts from near-earth objects (NEOs)". *Proc. 2015 IEEE Aerospace Conference*.
- Cheng A. F., Michel P., Jutzi M., Rivkin A. S., Stickle A., Barnouin O., Ernst C., Atchison J., Pravec P., Richardson D. C., and AIDA Team (2016). "Asteroid Impact & Deflection Assessment mission: Kinetic impactor". *Planet. Space Sci.*, **121**, 27–35.
- Cibin L. and Chiarini M. (2019). "The Fly-Eye Telescope, a reality that will provide an effective solution for NEO". In Flohrer T., Jehn R., and Schmitz F., editors, *1st NEO and Debris Detection Conference*, volume 1.
- Farnocchia D., Chesley S. R., Brown P. G., and Chodas P. W. (2016). "The trajectory and atmospheric impact of asteroid 2014 AA". *Icarus*, **274**, 327–333.
- Farnocchia D., Christensen E., Gibbs A., Kowalski R., Denneau L., Heinze A., Brown P., Micheli M., and Chodas P. (2018). "The impact of small near-Earth asteroid 2018 LA". In *AAS/Division for Planetary Sciences Meeting Abstracts*, page 111.02.
- Hankey M. (2014). "American Meteor Society Fireball reporting system and mobile application". In Muinonen K., Penttilä A., Granvik M., Virkki A., Fedorets G., Wilkman O., and Kohout T., editors, *Asteroids, Comets, Meteors 2014*.
- Jenniskens P., Shaddad M. H., Numan D., Elsir S., Kudoda A. M., Zolensky M. E., Le L., Robinson G. A., Friedrich J. M., Rumble D., Steele A., Chesley S. R., Fitzsimmons A., Duddy S., Hsieh H. H., Ramsay G., Brown P. G., Edwards W. N., Tagliaferri E., Boslough M. B., Spalding R. E., Dantowitz R., Kozubal M., Pravec P., Borovicka J., Charvat Z., Vaubaillon J., Kuiper J., Albers J., Bishop J. L., Mancinelli R. L., Sandford S. A., Milam S. N., Nuevo M., and Worden S. P. (2009). "The impact and recovery of asteroid 2008 TC₃". *Nature*, **458**, 485–488.
- Kenkmann T., Artemieva N. A., Wuennemann K., Poelchau M. H., Elbeshausen D., and Prado H. N. d. (2009). "The Carancas meteorite impact crater, Peru: Geologic surveying and modeling of crater formation and atmospheric passage". *Meteoritics & Planetary Science*, **44**, 985–1000.
- Margonis A., Elgner S., Heinlein D., Koschny D., Rudawska R., Faggioli L., Mialle P., and Oberst J. (2019). "Provision of European Fireball Network Data". *These proceedings*.
- Ott T. and Drolshagen E. (2019). "Fireball over the Caribbean (South of Puerto Rico) detected before it entered!". <https://www.imo.net/fireball-over-the-caribbean-detected-before-it-entered/>. Accessed: 25.06.2019.
- Ott T., Drolshagen E., Koschny D., Drolshagen G., Pilger C., Mialle P., Vaubaillon J., and Poppe B. (2019a). "NEMO Vol. 3 - Status of the NEar real-time Monitoring system". *These proceedings*.
- Ott T., Drolshagen E., Koschny D., Mialle P., Pilger C., Vaubaillon J., Drolshagen G., and Poppe B. (2019b). "Combination of infrasound signals and complementary data for the analysis of bright fireballs". *Planetary and Space Science*, page 104715.
- Raducan S. D., Davison T. M., Luther R., and Collins G. S. (2019). "The role of asteroid strength, porosity and internal friction in impact momentum transfer". *Icarus*, **329**, 282–295.

⁵<https://cneos.jpl.nasa.gov/fireballs/>

Provision of European Fireball Network Data

Anastasios Margonis¹, Stephan Elgner², Dieter Heinlein³, Detlef Koschny^{4,5},
Regina Rudawska⁴, Laura Faggioli⁴, and Jürgen Oberst^{1,2}

¹ Institute of Geodesy and Geoinformation Science, Technische Universität Berlin, Germany
anastasios.margonis@tu-berlin.de

² Institute of Planetary Research, German Aerospace Center, Berlin, Germany
stephan.elgner@dlr.de and juergen.oberst@dlr.de

³ German Fireball Network, Augsburg, Germany
dieter.heinlein@t-online.de

⁴ ESA/ESTEC, European Space Agency, Noordwijk, The Netherlands
detlef.koschny@esa.int, regina.rudawska@esa.int and juergen.oberst@dlr.de

⁵ Lehrstuhl für Raumfahrttechnik, Technische Universität München, Germany
detlef.koschny@tum.de

The European Fireball Network (EN) has been continuously operating since the late 1960s, recording on average 30-40 fireballs every year. The overall objective of this work is to provide the data on these events recorded by the first generation camera stations of the EN to the European Space Agency (ESA) on a regularly basis. The collected metadata of all fireball events will be updated to meet the required import format and will be ingested into the Fireball Information System (FIS), managed by ESA. This also includes the delivery of the corresponding image data. Furthermore, a fast reporting service on fireball events is currently used with the digital all-sky camera located at German Aerospace Center (DLR) in Berlin-Adlershof. Plans to extend the network by installing new digital camera stations are currently under investigation. At least one additional automated camera system is planned to be installed in the vicinity of the first camera station for simultaneous observations of events, allowing the reduction of double-station fireball image data. Information about recorded and confirmed fireball events will be sent to ESA via e-mail in a predefined format.

1 Introduction

The *Space Situation Awareness* (SSA) program was introduced by ESA in 2008, with the goal of supporting Europe's independent utilisation of space through the provision of timely and accurate information and data regarding the space environment, and its hazards to infrastructure in orbit and on the ground.

Atmospheric entries of large meteoroids are frequently observed by casual eyewitnesses in the form of fireballs. To systematically study these events, multiple camera stations covering a large area are required, which will monitor the night sky routinely. The first networks dedicated on the observations of fireballs included those in Europe (Ceplecha & Rajchl, 1965), the United States (McCrosky et al., 1971) and Canada (Halliday et al., 1978). In Europe, optical observations began near Ondrejov Observatory in former Czechoslovakia in 1951 and by 1966 the camera network was extended covering large parts of southern Germany.

These same manually operated camera stations are still active today, although modern digital all-sky systems have replaced the early cameras located in the Czech Republic (Spurný et al., 2007). The operation of the analogue cameras is coordinated by German Aerospace Center (DLR) and currently involves 12 camera stations (Figure 1), including one in Luxembourg and one in France, covering approximately an area of ~ 1 Mio km^2

(Oberst et al., 1998). In the following sections we refer to the data acquired by the camera stations operated by DLR simply as EN data.

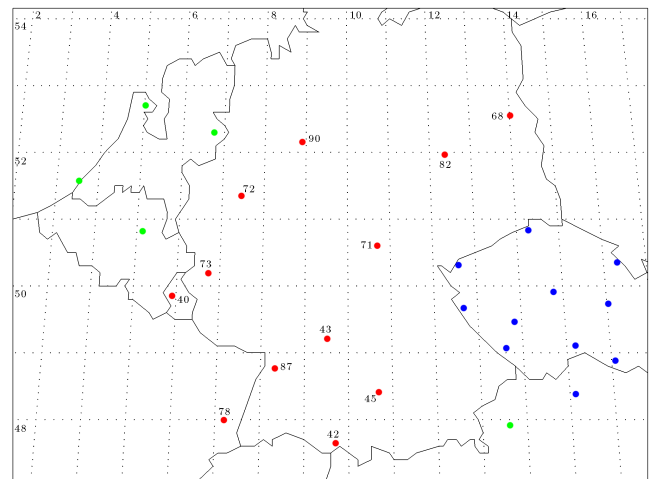


Figure 1 – Locations of all active all-sky camera stations (red numbered dots) of the EN camera network, operated by DLR.

2 Objectives

In past years, only a few exceptionally bright events were selected out of the acquired image dataset for further processing, since the procedure for reducing images obtained by film cameras is rather complex and time

consuming. As a result, a relative large number of fireball events have been not analysed yet. The main objective of this project is to provide formatted EN data to ESA in such a manner that the data remain exploitable in the future. Further objectives include the establishment of a real-time notification service for fireball events and the investigation of expansion strategies of the digital camera network.

Delivering metadata of fireball events to ESA

Under a previous contract a routine was written which converts fireball event metadata to .xml files for ingestion into the Fireball Information System (FIS). Following successful testing, the routine will be used to produce formatted EN data which will be delivered every three months to ESA. An extended metadata file format has been re-defined including the following information regarding:

- fireball event (e.g. date and time, country, etc.),
- observer (e.g. name, e-mail - optional),
- general observation (e.g. direction, brightness, speed, colour, etc.),
- meteoroid/meteorite (if applicable),
- event location (e.g. azimuth, elevation, etc.),
- camera system (e.g. pointing, focal length, etc.),
- orbital elements.

Providing real-time information on fireball events

Another goal of this project is to provide real-time information on fireball events. A bash script checks the operating computer every two minutes for new detections and automatically sends an e-mail to a mailing list providing basic information of the potential event (e.g. date and UTC time, direction, etc.). This script is used at the all-sky camera system located at DLR's Institute of Planetary Research in Berlin-Adlershof and is currently under testing. The planned installation of a second camera at the TUB will allow simultaneous observations of fireball events, removing efficiently false detections. Moreover, additional information of an event can be provided, once the reduction of double-station image data is performed using existing software (Margonis et al., 2018). Information about recorded and confirmed fireball events will be sent to ESA via e-mail in the agreed format. This format will be consistent with the one defined for the classical camera stations of the network.

We will study the possibilities of setting up additional automated camera stations to increase coverage of the monitored areas and chances of fireball detections in the case of sporadic cloud cover. Improvements are necessary regarding the form and the content of the notifications as well as the implementation of strategies to minimise false reports (e.g. clouds, airplanes etc.).

Archiving previous fireball data

Fireball data from previous years will be delivered at ESA (Fig. 2). The deliveries shall include complete data (metadata and images) from the years 2004-2019 and continue until 2021. The conversion and delivery of the data to ESA will be performed at DLR.

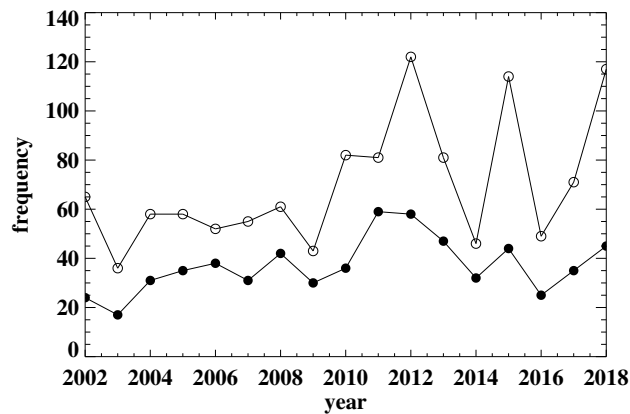


Figure 2 – Number of fireball events recorded by the EN cameras in the time period between 2002-2018 (filled circles). The number of images showing a fireball for each year are shown in open circles. The higher number of images compared to the number of events indicate that several events were recorded by more than one stations.

3 Summary and future work

During the last decades camera stations of the EN network have recorded several hundreds of fireball events observed from northern-central Europe. The images generated by the first generation all-sky cameras are of high geometric and radiometric quality allowing the accurate reconstruction of the atmospheric entry of a particle. This large dataset will be adequately archived and maintained in the FIS database, managed by ESA. Consequently, preceding data of fireball events will become available to the meteor community for study, further processing or/and reassessment of the recent results. Additionally, the expansion of the network and the replacement of the outdated analogue camera stations with modern digital camera systems will increase the efficiency of the fireball observations and provide a basic platform for real-time information of future events.

Acknowledgements

The authors would like to acknowledge all the operators of the EN camera stations for their valuable support. This work was funded by the European Space Agency under the contract number ITT A0/1-9020/17/DE/MRP.

References

- Ceplecha Z. and Rajchl J. (1965). "Programme of fireball photography in Czechoslovakia". *Bulletin of*

- the Astronomical Institutes of Czechoslovakia*, **16**, 15.
- Halliday I., Blackwell A. T., and Griffin A. A. (1978). “The Innisfree meteorite and the Canadian camera network”. *JRASC*, **72**, 15–39.
- Margonis A., Christou A., and Oberst J. (2018). “Observations of meteors in the Earth’s atmosphere: Reducing data from dedicated double-station wide-angle cameras”. *A&A*, **618**, A99.
- McCrosky R. E., Posen A., Schwartz G., and Shao C.-Y. (1971). “Lost City Meteorite Its Recovery and a Comparison with Other Fireballs”. *JGR*, **76**, 4090–4108.
- Oberst J., Molau S., Heinlein D., Gritzner C., Schindler M., Spurny P., Ceplecha Z., Rendtel J., and Betlem H. (1998). “The “European Fireball Network”: Current status and future prospects”. *Meteoritics and Planetary Science*, **33**.
- Spurný P., Borovička J., and Shrbený L. (2007). “Automation of the Czech part of the European fireball network: equipment, methods and first results”. In Valsecchi G. B., Vokrouhlický D., and Milani A., editors, *Near Earth Objects, our Celestial Neighbors: Opportunity and Risk*, volume 236 of *IAU Symposium*. pages 121–130.

Evidence of shock metamorphism in Bursa L6 chondrite: Raman and infrared spectroscopic approach

Ozan Unsalan¹, Cisem Altunayar-Unsalan²

¹Ege University Science Faculty Physcis Department, 35100, Bornova, Izmir, Turkey
ozan.unsalan@ege.edu.tr

²Ege University Central Test and Analysis Laboratory Application and Research Center (EGE MATAL), 35100, Bornova, Izmir, Turkey

The main goal of this study is to identify mineralogical composition of Bursa L6 stony chondrite and investigate its shock stage by Raman and Fourier Transform Infrared spectroscopic techniques. Very well-known characteristic double band of olivine was detected at 820/852 cm⁻¹ in Raman spectrum and forsterite composition of Bursa L6 chondrite was derived to be 75%. Raman spectroscopic part of this study showed the presence of plagioclase feldspar pyroxene signals, ringwoodite (high-pressure polymorph of olivine), maskelynite and augite. From infrared spectroscopic data we obtained the existence of maskelynite. A detailed discussion was given on the possible shock stage of Bursa chondrite based on the band profiles in Raman spectrum; we suspect the pressures to be at least higher than 35 GPa.

Optimisation of double-station balloon flights for meteor observation

Jeremie Vaubaillon¹, Antoine Caillou², P. Deverchere³, Chloe Colomer¹, Danica Zilkova¹, Apostolos Christou⁴, Jacques Laskar¹, David Baratoux⁵, Marc Fouchard¹, Francois Colas¹, Lucie Maquet¹, Mirel Birlan¹, Sylvain Bouley⁶, Pierre Vernazza⁷, Benoit Carry⁸ and Pierre Beck⁹

¹ IMCCE, 77 Av Denfert Rochereau, 75014 Paris, France

Jeremie.Vaubaillon@obspm.fr and chloe.colomer@gmail.com and danizilkova@gmail.com and Jacques.Laskar@obspm.fr and Marc.Fouchard@obspm.fr and Francois.Colas@obspm.fr and Lucie.Maquet@obspm.fr and Mirel.Birlan@obspm.fr

² KYU-ACE, 2 Chemin des sources, Vayres-sur-Essonne, France

antoine.caillou@kyu-aero.com

³ ScotopicLabs

philippe@scotopiclabs.com

⁴ Armagh Observatory, College Hill, Armagh, N-Ireland, UK

Apostolos.Christou@Armagh.ac.uk

⁵ Geosciences Environnement Toulouse (GET), UMR5563, 31400, Toulouse, France

david.baratoux@gmail.com

⁶ GEOPS, IDES, UPSud, Orsay, France

sylvain.bouley@gmail.com

⁷ LAM, 38, rue Frdric Joliot-Curie, 13388 Marseille cedex 13, France

pierre.vernazza@gmail.com

⁸ Universit Cte d'Azur, Observatoire de la Cte d'Azur, CNRS, Laboratoire Lagrange, Nice, France

benoit.carry@oca.eu

⁹ IPAG, 414, rue de la piscine, 38041 Grenoble, Cedex 09, France

pierre.beck@obs.ujf-grenoble.fr

The “Meteor Automated Light Balloon Experimental Camera” (MALBEC) project aims at the observation of meteor from stratospheric altitude. The advantage is mainly to guarantee the success of an observation run of a meteor shower, even in presence of clouds. In order to fully exploit the scientific potential of a meteor observation (e.g. derive the internal structure and origin via the measure of tensile strength and orbit), double-station setup is required. The consequence for MALBEC is the necessity of stabilisation and we show that a 3-axis stabilisation is necessary. In addition, the two stations must be separated by a distance ranging from $\sim 40 - 110$ km, and the cameras must point towards the same portion of atmosphere. We show that under usual circumstances, double station stratospheric observation is possible since the distance and the azimuth between the two balloons (experiencing different atmospheric conditions) varies in small proportions. Under usual slow wind conditions, the distance between the stations varies by a few kilometres and the elevation of the azimuth and elevation of the cameras needed to observe the same portion of atmosphere varies by a few degrees only.

1 Introduction

The observation of meteors has been widely expanded in the last decade thanks to the democratisation of electronic devices as well as tools to process the data (Colas et al., 2016; SonotaCo, 2009; Jenniskens et al., 2011; Hankey & Perlerin, 2014). Some scientific goals of such observations and the means to achieve them are summed up in Table 1. Many of those goals require double-station observations and measurements. Unfortunately, any observation campaign might be ruined by clouds, or impaired by the presence of the Moon

(because of light diffusion raising the limiting magnitude). In order to get rid of these obstacles, stratospheric flights embarking a video camera were conducted in the past (Moser et al., 2013; Sánchez de Miguel et al., 2016; Koukal et al., 2016). However all these endeavours included single station observations.

The “Meteor Automated Light Balloon Experimental Camera” (MALBEC) project aims to observe meteors from two stratospheric platforms. In this paper, we present the feasibility of such observations.

Table 1 – Several Scientific goals of meteor observations and means to achieve them.

Goal	Mean	Requirement
ZHR, flux, SFD	count	Wide FOV camera
meteoroid property	tensile strength	3D-trajectory (double station), light curve
origin, parent	orbit	3D-trajectory and velocity (double station)
age	orbits dispersion	3D-trajectories and velocities (double station)

2 Constraints related to stratospheric double station observations

In general, in order to provide scientifically useful results, double station observations should comply with the following constraints:

- The distance between the two stations must be (roughly) in the range of 40-120 km.
- Ideally, the meteor path should be perpendicular to the segment defined by the two stations. The angle between the meteor path and the two stations must be (roughly) between 40 and 140 deg (Gural, 2012).
- The two stations must point at the same portion of atmosphere.

In the case of stratospheric observations, these constraints translate into the necessity to

- stabilise the gondola,
- ensure that the distance between the stations stays within the desired range for the duration of the observation run.

The MALBEC gondola is carried by a latex Helium-inflated balloon similar to those used for daily atmospheric probing purpose. The constraints imposed by aviation regulation are the following: total mass less than 4 kg and density less than 13 g/cm³.

3 Stabilisation of the MALBEC nacelle

The MALBEC project effectively began in August 2017 thanks to a grant provided by CNES, the French Space agency. The first two flights were not stabilised and were intended to test the feasibility of electronic correct function in stratospheric environment, as well as observations of the sky with a scientific camera (brand: Basler, type: "Ace 2000 165um"). In Dec 2017 a 1-axis stabilisation was tested, showing that stabilisation is feasible. However the pitch and yaw were still changing fast. In May 2018, a modified gondola with aerodynamic shape was tested in order to improve the 1-axis stabilisation, but it became clear that 3-axis stabilisation is needed. In Feb and May 2019, a 3-axis stabilised gondola using three brushless motors (Figure 1) was tested and provided satisfactory results: the pointing direction of the camera did not change by more than

0.5 deg and no vibration higher than 1 Hz was measured. However, a slow drift of the azimuth was noticed during the 2 hours flight, and this must be tackled in future versions of the nacelle.



Figure 1 – The 3-axis stabilised MALBEC gondola in 2019.

4 Prediction of the MALBEC nacelle trajectory

In order to demonstrate the feasibility of stratospheric double station meteor observation, it is mandatory to check the relative distance between the two stations, as well as the variation of their relative azimuth and elevation. The distance must stay in the range 40 - 110 km for the duration of the observation. The azimuth and elevation of the cameras should ensure that the same portion of the atmosphere at 100 km (typical altitude of meteors) is covered by the two fields of view. In order to ensure that the distance between the two stations is kept within the appropriate range for the duration of the flight (40 - 110 km), we developed a tool to simulate

the flight and predict the trajectory of the MALBEC nacelle. Initially, a full physical model of the balloon was developed (Zilkova & Vaubaillon, 2019), but too many unknown parameters resulted in a large difference between the predicted trajectory and the real one. We now use a simpler (engineering) model considering:

- Constant ascending velocity ranging from 5.0 to 6.5 ms^{-1} .
- Equivalent sphere radius for free fall phase of 0.65 m.
- Wind velocity as a function of longitude, latitude and altitude are taken from the ARPEGE model¹ provided by MeteoFrance.
- Topography data are used to evaluate the altitude of the nacelle with respect to the ground at each step of the computation. The program is stopped whenever the nacelle hits the ground. Data with 25 m step were provided by Institut Géographique National (IGN).

The remaining unknown parameter is mainly the altitude of explosion of the latex balloon, ranging from 25000 to 35000 m. This translates into a difference of simulated versus real landing position ranging from 2 to 15 km under usual low velocity tropospheric and stratospheric winds (Figure 2 and Figure 4).

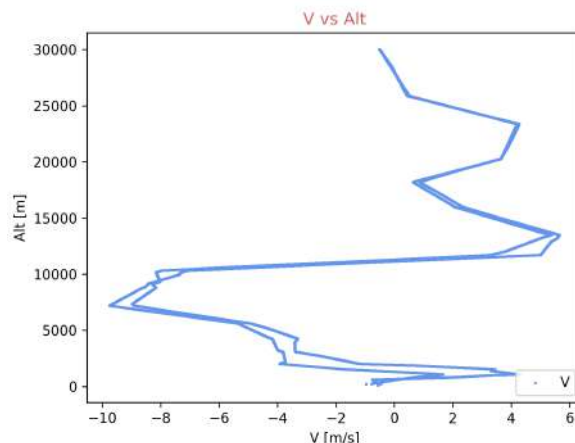


Figure 2 – Typical slow wind meridional velocity as a function of altitude during a MALBEC flight. The two curves correspond to the ascending and descending phase of the flight.

The simulation of a double stratospheric MALBEC station shows that for the ascending phase of the flight (corresponding to the observation phase):

- The two trajectories have similar shapes, even if the ascending velocity differs by 1 ms^{-1} and the time of launch differs by two minutes (Figure 3).
- The distance between the nacelles varies by a few km only (Figure 4).

- The azimuth and elevation needed for the stations to point towards each other varies by a few degrees only (Figures 5 and 6).

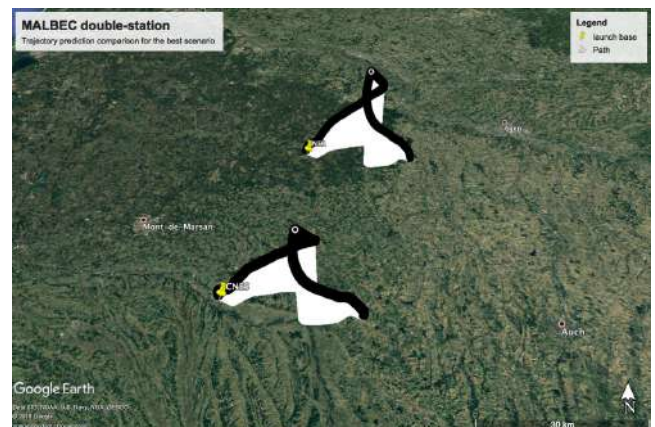


Figure 3 – 3D-prediction of the trajectory of two MALBEC gondolas for double station stratospheric observation of meteors.

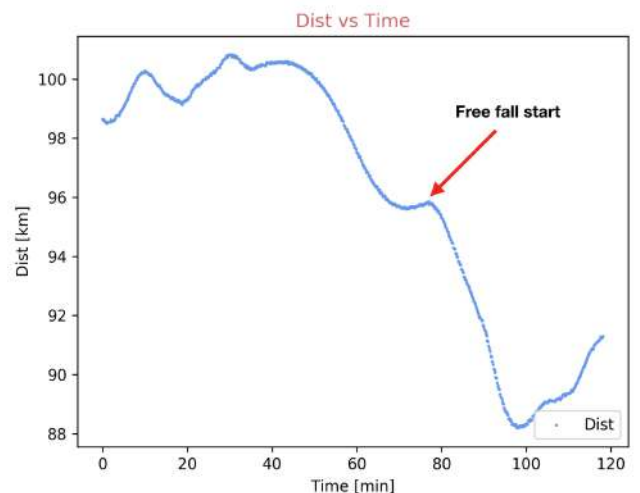


Figure 4 – Distance between MALBEC gondola 1 and gondola 2, as a function of time during the double-station simulated flight. Free fall of gondola 2 starts at around 80 min.

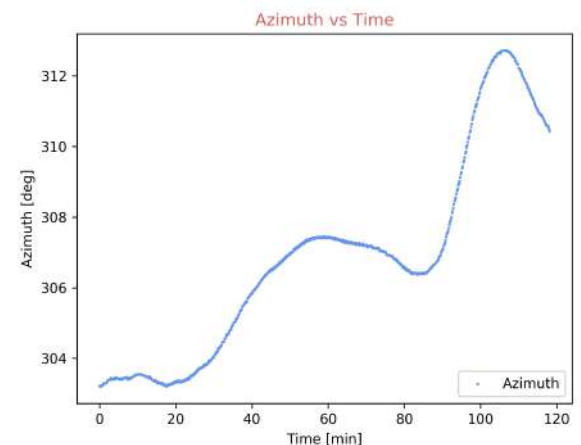


Figure 5 – Azimuth of MALBEC nacelle 2 as seen from nacelle 1, as a function of time. Free fall starts at around 80 min.

¹available at <https://donneespubliques.meteofrance.fr/>

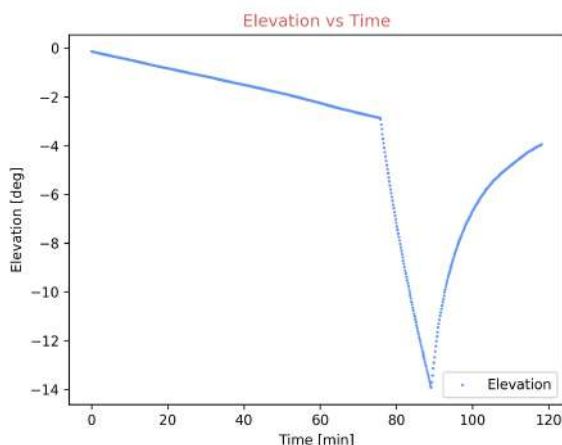


Figure 6 – Difference of elevation angle between the two simulated MALBEC cameras. The elevation angle is the angle needed for a camera to point at the same portion of atmosphere as the other camera. The difference between the two elevation angles results from the varying distance of the two gondolas. Free fall starts at around 80 min, resulting in a decrease of the difference of elevation.

5 Conclusion

Double stratospheric station meteor observation is feasible under usual slow atmospheric wind conditions with the developed stabilised MALBEC gondola. Future work includes an improvement of the stabilisation in order to compensate for a slow drift of the azimuth of the camera. In addition efforts will focus on solving electromagnetic incompatibility preventing the onboard GPS to fix.

Acknowledgements and disclaimer

The MALBEC project is supported by CNES, INSU, PNP and Observatoire de Paris. Wind data were provided by MeteoFrance under a research licence. Topography data were provided by IGN under a research licence. We are grateful to Dr. Francisco Ocaa Gonzlez for fruitful discussions during the International Meteor Conference 2018, Pezinok-Modra, Slovakia.

References

- Colas F., Zanda B., Bouley S., Vaubaillon J., Marmo C., Audureau Y., Kwon M. K., Rault J. L., Vernazza P., Gattacceca J., Caminade S., Birlan M., Maquet L., Egal A., Rotaru M., Jorda L., Birnbaum C., Blanpain C., Malgoyre A., Lecubin J., Cellino A., Gardiol D., Di Martino M., Nitschelm C., Camargo J., Valenzuela M., Ferrière L., Popescu M., and Loizeau D. (2016). “FRIPON network status”. In Roggemans A. and Roggemans P., editors, *International Meteor Conference Egmond, the Netherlands, 2-5 June 2016*. page 55.
- Gural P. S. (2012). “A new method of meteor trajectory determination applied to multiple unsynchronized video cameras”. *Meteoritics and Planetary Science*.

Hankey M. and Perlerin V. (2014). “AMS fireball program, community website, mobile app, and all-sky camera”. In Gyssens M., Roggemans P., and Zoladek P., editors, *Proceedings of the International Meteor Conference, Poznan, Poland, 22-25 August 2013*. page 120.

Jenniskens P., Gural P. S., Dynneson L., Grigsby B. J., Newman K. E., Borden M., Koop M., and Holman D. (2011). “CAMS: Cameras for Allsky Meteor Surveillance to establish minor meteor showers”. *Icarus*, **216**, 40–61.

Koukal J., Srba J., Lenža L., Kapuš J., Erdziak J., and Slošiar R. (2016). “STRATO 02/2015 - The Perseids 2015 stratospheric balloon mission”. *WGN, Journal of the International Meteor Organization*, **44:1**, 12–15.

Moser D. E., Suggs R. M., Cooke W. J., and Blaauw R. (2013). “The 2012 Lyrids from non-traditional observing platforms”. In Gyssens M. and Roggemans P., editors, *Proceedings of the International Meteor Conference, 31st IMC, La Palma, Canary Islands, Spain, 2012*. pages 146–149.

Sánchez de Miguel A., Ocaña F., Tapia Ayuga C. E., Madiedo J. M., Zamorano J., Izquierdo J., Gómez Sánchez-Tirado M. A., Ortúñoz F., Mayo D., Raya R., Conde A., and León P. (2016). “The 2016 Quadrantids Balloon-Borne Mission Over Spain: Full HD and Colour Videorecording”. In *Lunar and Planetary Science Conference*. page 2637.

SonotaCo (2009). “A meteor shower catalog based on video observations in 2007-2008”. *WGN, Journal of IMO*, **37**, 55–62.

Zilkova D. and Vaubaillon J. (2019). “Estimating the flight path of a stratospheric balloon for meteor observations”. In *Meteoroids 2019 conference, poster # 17*.

Polarization of the night sky in Chile 2019

Bernd Gährken¹

¹ bgaehrken@web.de

Chile has some of the best astronomical locations on Earth. In 2019 there was a solar eclipse in Chile which attracted many observers. As solar eclipses always occur at New Moon, there was an opportunity to enjoy the dark sky. The nights were used to take some images with a polarization filter to study the glow of the night sky.

1 Introduction

The Olbers paradox shows the resulting contradiction in the prediction of a bright night sky and its actual dark appearance. Heinrich Wilhelm Olbers formulated this problem in 1823. It concerns world models that correspond to the perfect cosmological principle. In an infinitely extended universe with a uniform distribution of stars over long distances. Under these conditions, the light of a star would have reached the earth from every direction and the sky would appear at least as bright as the surface of the stars after a long time. The problem resolved itself as man realized that the Universe is unlimited but not infinite and expands.

2 Observations

In 2019 we visited the Paranal in Chile after the solar eclipse. The Paranal considered one of the darkest locations in the world – even here the night sky is not totally dark, between the stars still some light from the sky can be recognized. Why is the sky not really dark? There are three possible solutions:

- light comes from outside the solar system (galactic cirrus)
- light comes from inside the solar system (zodiacal light)
- light comes from earth (airglow: recombination-effects in the upper atmosphere)

The zodiacal light is simply to identify on pictures (Figures 1 and 2). But the question is: What is the light outside the zodiacal band and the band of the Milky way? Is it originating from the galaxy, from the solar system or from the earth? A possible solution to find an answer is the analysis of its polarization. Galactic cirrus and zodiacal light are reflections on dust and should be polarized.

- If the night-glow depends on galactic cirrus, the polarization should change with the position of the Milky Way.
- If the night-glow depends on zodiacal light, the polarization should change with the position of the sun

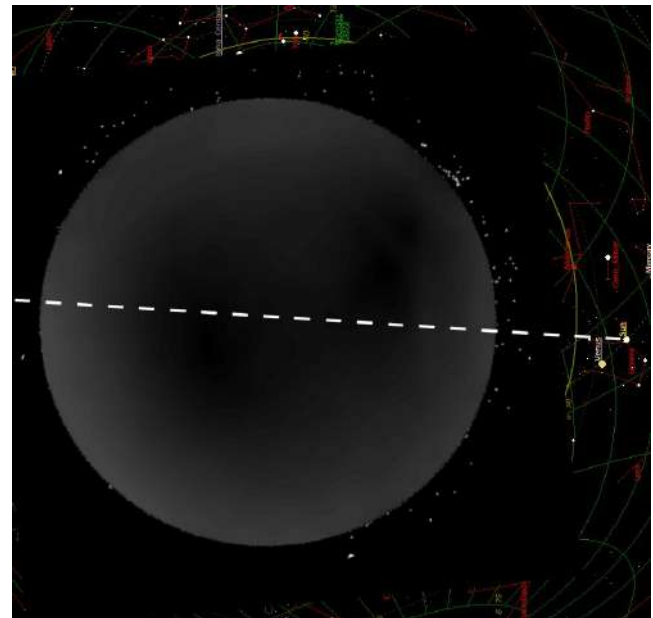


Figure 1 – Polarization after sunset (sun on right side).

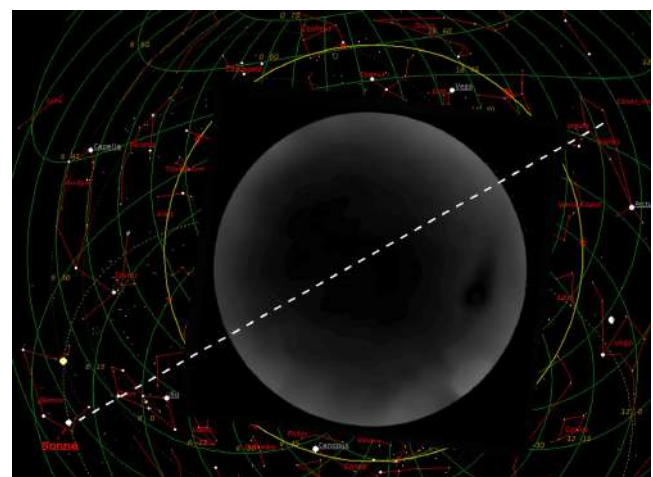


Figure 2 – Polarization in the morning sky (sun down left).

- If the night-glow depends on light coming from earth (airglow), the polarization should be independent during the night.

Our pictures show a polarization of the zodiacal light. This was expected (Leinhard, 1975), but also other parts of the sky are strongly polarized at longer exposure

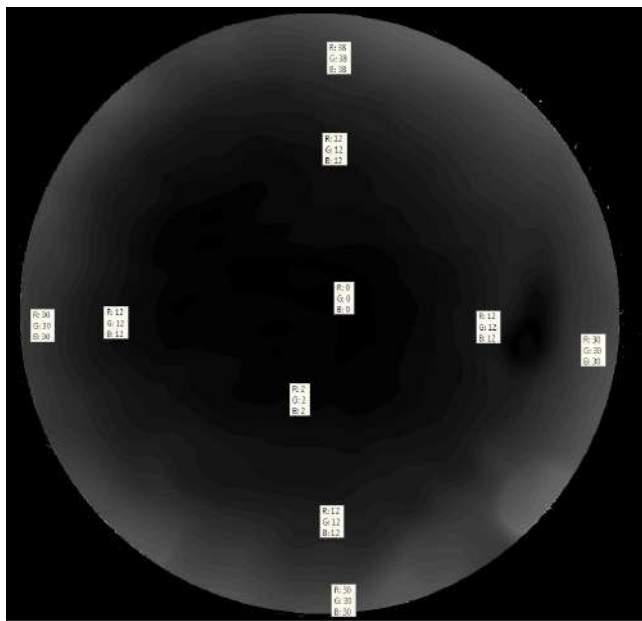


Figure 3 – Polarization degree of the night sky.

times (Figure 3). The relation of this polarization to the sun position was checked by combining the pictures with a planetarium program. During night there was no significant influence of the position of the sun and no influence of the position of the Milky Way.

The polarization is like a ring surrounding the horizon. Airglow seems to be the dominant factor for the polarization of the night sky. Near the horizon polarisation reaches up to 30%. Near the zenith it decreases to 0. At some measurements we had an elongated minimum or a double minimum. Possible explanations could be an inhomogeneous distribution of the airglow near the horizon or stray light from other sources.

References

- Leinhard C., 1975). “Zodiacal light – a measure of the interplanetary environment”.

The ESA Leonids 2002 expedition

Detlef Koschny, Roland Trautner, Joe Zender, André Knöfel, Jorge Diaz del Rio, and Rüdiger Jehn

`detlef.koschny@esa.int`

In the year 2002, ESA undertook an observing campaign in Southern Spain to observe the expected Leonid storm under good weather conditions. Two teams were set up, one close to the observatory of the Astronomical Institute of Granada, the other one in La Sagra, about 150 km away from the first location. Our observations encompassed measurements with optical video cameras with image intensifiers, and a ELF/ULF measurement system based on an experiment flown on the Cassini/Huygens mission. During an observing period of 3 nights, we could perform successful observations. Visual meteor counts contributed to the world-wide Zenithal Hourly Rate measurements collected by the International Meteor Organization. In this presentation, we introduce the instrumentation and recording equipment. Type and amount of available data is presented, and the scientific results are shown. We also give a short summary of the results from a video camera that was flown onboard a DC-8 airplane in a campaign organized by the SETI Institute. This presentation is a historical repeat of a presentation given one year after the campaign at the same location.

The full article can be found in the proceedings of the previous International Meteor Conference at Bollmannsruh (Koschny et al., 2004).

D. Koschny, R. Trautner, J. Zender, A. Knöfel, J. Diaz del Rio, and R. Jehn. (2004) "The ESA Leonid campaign 2002 to Spain". In C. Triglav-Čekada and C. Trayner, Eds., Proceedings of the International Meteor Conference, Bollmannsruh, Germany, September 19-23, 2003. IMO, pp. 70-77.

Conference summary

Felix Bettonvil^{1, 2, 3}

¹ Leiden Observatory, Leiden University, Leiden, The Netherlands

bettonvil@strw.leidenuniv.nl

² NOVA Optical Infrared Instrumentation Group, Dwingeloo, The Netherlands

bettonvil@astron.nl

³ KNVWS Meteor Section

Without doubt we can say that the 2019 IMC in Bollmannsruh was once again a great success. During the four days a plethora of topics was presented, covering the wide scope of meteor science well. Instrumental development, software tools, observational results, analysis, modelling as well as public awareness was discussed, on an exciting conference location and in a great atmosphere with participants of all ages, both amateur and professional. Great achievements have been in the realization of very large camera networks, the availability of handy software tools and cross fertilization between disciplines and areas of interest. Meteor science is clearly broadening, making it very exciting.

1 Introduction

At the last few IMCs it has become a kind of custom to end the conference with a summary talk. I'm a great fan of this, as it gives the opportunity to look back at the conference, sketch the overall status and as well gives a possibility to look forward, and feel very honored to have been asked to do this for the 2019 conference. My summary of course has a personal bias and in 15 minutes it has not been quite possible to present a comprehensive summary covering all topics, hence at the beginning of this paper I like to start with the disclaimer that my conclusions might be (very) biased, are incomplete and can (easily) be too black and white or wrong. Some topics and names will unavoidably be missing, but that does not mean at all they were below a certain level or not worth mentioning. Not at all, I just had to make choices.

If interested, I recommend to also have a look at the presentation slides, which project my summary in a more visual and therefore different way.

2 ‘Jury’

By having accepted the request to prepare this talk, I must say I enjoyed the conference this year also in a different way. Obviously there was no sense to prepare much in advance and I intended (and succeeded) to attend all talks,

made notes and tried from all details to build an overall picture. I must say this was a very enjoyable experience! The first statement I like to therefore make immediately is that IMC 2019 was a splendid conference, and if I was a jury member (Figure 1), I would give this IMC very high marks! The IMC is the annual conference of IMO, which as an international organization brings together individuals and (local) societies, supports their work and local initiatives. Not covered in presentations, but clearly an important aspect of such conferences is as organizer (read IMO) to be open minded, to listen to the needs, act as a platform, steer and assist. I saw this clearly happening. Fantastic.



Figure 1 – Conclusion of the jury panel about this IMC.

3 Meteors and beyond

What is so obvious nowadays is that meteors are not simply these *streaks-in-the-sky*, which we already count for ages do derive their rate and photograph to compute their orbits. We all

understand today that meteors are to be seen together with other research fields including meteoroids in space, asteroids, comets and meteorites, with links to atmospheric physics and geology too. Although they are each disciplines for themselves – some of them having their own research communities and conferences –, their fields do overlap, and we need them to built-up the complete understanding of what is happening with the smaller particles in our solar system (Figure 2). It makes the field extremely interesting.

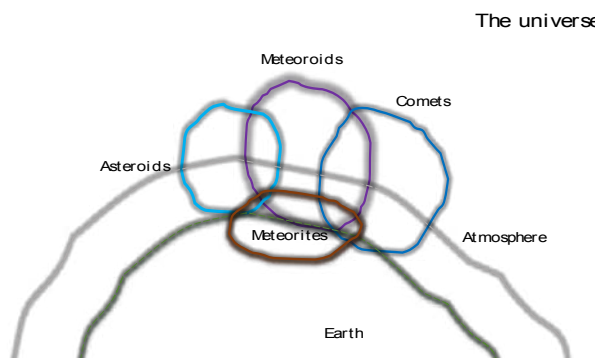


Figure 2 – Meteor science covers many topics.

4 LOC, SOC & GA

Organizing an IMC is a synonym for a lot of work. The *Local Organizing Committee* (LOC), being the group of enthusiasts that take care of all organization aspects, did a tremendous job. It became utterly clear what an important place Bollmannsruh has been, and still is, for the ‘Berlin’ meteor community. The LOC succeeded perfectly in creating a conference atmosphere as it should be at an IMC, which for me also expanded into the excursion: seeing the beautifully restored large refractor on the Telegrafenberg, the Einstein tower, and learning of the important work done on deriving the exact value of Earth’s gravity. A site with significant historical importance!

A couple of years back the IMC also named a *Scientific Organizing Committee* (SOC). It is definitely worth mentioning as these are the people which are not so visible, as they do their work mostly hidden and before the conference, but they do contribute in an equal manner to the success of the conference. They collect all presentations, ensure that a high-quality, broad

spectrum of topics is being covered. Thank you David Asher, Esther Drolshagen, Theresa Ott, Marc Gyssens, Jean-Louis Rault, Jürgen Rendtel, Juraj Tóth, and Jérémie Vaubaillon for your contributions here!

One certainly related topic is the handing-out of the awards for the best poster and nicest meteor photo. Making a good poster is an art in itself, as it is also the case of course for an oral presentation. I support having such poster and photo competition as it helps to raise your quality: you always can learn how to improve your own.

Though likely seen as the least exciting bit of the conference, and strictly spoken even not part of the conference, on the second evening of the conference, for members of IMO there is traditionally the annual General Assembly (GA). I believe it deserves some words here too as it is the place where suggestions for our future can be made, strategy discussed and eventually decisions made. Important!

5 Statistics

IMCs bring meteor people together, enable exchanging experiences, thoughts and ideas. As in many science areas, we can subdivide the area in specific topics, sub-fields and/or disciplines, in different flavours. Let’s us have a look in a selection of various disciplines (according to my own preference). I have grouped them into:

- Instrumentation
 - o the area of designing, building and operation of instruments
- Software tools
 - o all kind of computer software which we can use for our meteor work
- Observations and measurements
 - o the area of actual observations or measurements carried out, be it from the ground or space, or in a lab.
- Analysis
 - o the reduction of the observations/measurements, understanding what we have learned, e.g. computation of a ZHR, orbits, stream composition, etc.

- Modelling & theory
 - o the creation of theory, making of models, both analytical and simulated.
- Miscellaneous, history and public awareness
 - o all the leftover topics, historical aspects, and outreach activities.

All these fields I think are to be covered in order to obtain a ‘healthy’ science field, in some kind of equal proportion. You could link them to each other like a sort of chain ‘instruments – observations/measurements – analysis – models/theory’, which we can of course follow in both directions. (I explicitly did not mention ‘tools’ as they can be used everywhere in the ‘chain’).

To get an idea how this looks for our IMC we can count the number of presentations and group them per discipline. We do that both for 2003 and 2019, the two IMCs that were held in Bollmansruh (Figure 3).

As we can easily see in 2003 the majority of the talks dealt with observations, covering about half of all presentations. Second largest category was analysis.

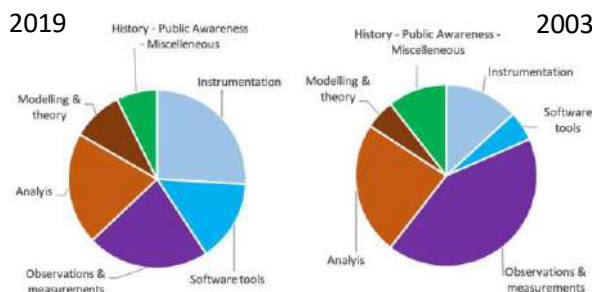


Figure 3 – Distribution of disciplines at the IMC in 2019 and 2003

In 2019 we see that the distribution has changed considerably and is more even. And that is how it should be I think!

It the next section I will go into some details of each discipline.

6 Disciplines

I Instrumentation

Instrumentation has always been a relatively large contributor for talks. Instruments are

obviously needed in our field and naturally advance with the ever-moving-forward technology. We saw talks on ground-based instruments (e.g. a radiometer by Rault), balloon (MALBEC, Vaubaillon) as well as space (e.g. optimization of the stereoscopic angle of meteor observation from space by Petri). I also always consider calibration efforts as part of the discipline of instrumentation, of which an example was nicely presented by Lamy on the calibration efforts and problems on BRAMS.

We also saw the success of building large operational networks; there were talks of FRIPON (Colas), hundreds of all-sky cameras over France and neighboring countries including a reduction pipeline and outreach activities, and the US based AllSky6 program with some stations also in Europe (Hankey). In my talk I made the joke of a large competition (Molau even compared them in a talk) about who will be first covering the entire world, but of course it’s ironic as in reality is that all have their own strength: redundancy is very welcome.

II Software tools

As described in Section 5, with ‘Software tools’ I refer to all tools that help us in doing our meteor work. (In a way I consider these also as ‘instruments’ as they help us being a tool to facilitate our observations, analysis and modelling. It is a ever-growing field.) Two facts I like to highlight: 1) More and more we follow the principles of ‘open source’ (e.g. Github), and 2) the constantly growing computer power providing new opportunities. Computers now can now be so powerful that they start to compete with humans which was nicely highlighted by Calders (Go AlphaGo vs. Lee Sedol in Go game), and the applying of neural networks also in our field (Calders, Gural), and enabling the handling of large data sets, and huge models.

I like to highlight too the revival of the IMO Video flux tool (Meteor flux reloaded, by Molau), which enables, next to the reknown *live ZHR graph*, the same for video observations. We saw here nonetheless also a weakness of the

always evolving technology together with the dependence on a small pool of experts, which we should try to avoid.

Baláž presented a simulation tool, named ASMODEUS, in which initial properties of meteoroids are used to compute the properties of observable corresponding meteors in a systematical manner. In my opinion his examples showed very well the power of the tool for understanding all kinds of meteor aspects (Figure 4). Highly recommended.

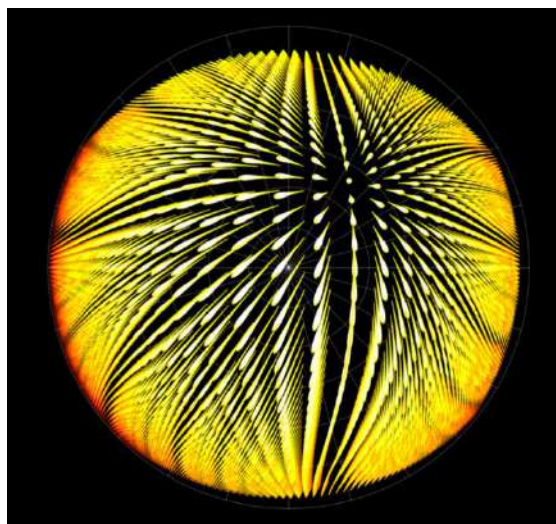


Figure 4 – Screen shot of an example of ASMODEUS output.

III Observations and measurements

Is the actual observing not the most satisfying aspect for many us? For sure it is true that for many the hobby started with observing a meteor shower, isn't it?

I have chosen to name this discipline 'observations and measurements' on purpose as I wanted to broaden the discipline to the retrieval of information in the widest sense, of which our so well-known visual observing is only one. There are nowadays quite a few other ways of retrieving information and of course the conference has been well filled with many great observation reports. I limit myself to some personal unusual highlights that I noted down and I think are remarkable: 1) daytime meteors, and in particular fireballs which are increasingly detected during daytime as well; or the search for meteorites, in desert areas with drones (Talafha), and the report by Molau on Daylight Fireball of September 12 over The Netherlands and Germany; and 2) lab measurements, for example the retrieval of

information by shooting lasers at meteorite samples (Ferus/Křívková).

I cannot withhold to also mention the talk by Gährken about taking wide field night time polarization photos to study polarization effects on airglow, and his successful attempts to explain what he saw. A nice combination of measurement and analysis!

IV Analysis

That brings us straight to the next discipline, that do we do with the observations? This is the field of 'Analysis' and forms the link between observations and our models and theory. This is the area of discoveries – which I enjoy a lot –, and of which we luckily had quite some contributions.

Slansky presented a terminal flash of a bright Perseid, and tried to explain, supported by lab experiments, what the cause could have been.

There were various talks on meteor distributions: fireball rates versus moon crater impacts based on their diameter/blast energy (Kersztri); on the amount of sporadics (Pfiffel); on the population index r (Richter) in which was advocated, based on stochastic methods, that it cannot always be assumed that the population index is exponential; clustering of Geminids (Koten), as well as impact flux predictions based on study of surface damage on the ISS (Klaß).

Marin-Yasela spoke about Comet 67P/C-G as visited by Rosetta and Philae in 2014-2016. We have learned that a huge amount of dust is enshrouding the comet resulting in 4 km wide nucleus. A single chunk was observed and followed.

Finally I like to highlight the talk by Rendtel on forecasts of some minor showers.

V Models and theory

Although less in total than the others, there were also presentations on theory and modelling. Modelling of several minor meteor showers resulted in identification of some new parent bodies (Hajduková). Lukashenko spoke on numerical simulation of the flow around meteor fragments, and I also found very

interesting the talk on the determination of mass of iron meteoroids (Čapek), based on (thermal) physics, and combining analytical and numerical modelling, and linking them to observations.

VI Historical aspects, public awareness, miscellaneous

In this last category I put all that was left, but surely wasn't the least attractive. The first is outreach and public awareness which is a very important aspect nowadays in every field of science. Astronomy has always been a quite appreciated subject, and this is certainly true for meteors, fireballs and meteorites. The IMO fireball form is a great example and does an excellent job. Updates on great initiatives were given by Ott & Drolshagen on NEMO (NEar real-time MOnitoring system) and I would also like to mention the Petnica School of meteor Astronomy in Serbia, which is such a unique initiative (Pavlović). Another nice initiative reported on was the German Nachtlichtbühne citizen science project focusing on an app for nightlight phenomena like light-pollution and meteors. Finally, there was a poster by Stenborg on the use of weather webcams on the web and automatic search in their data streams for fireballs, which I found a great idea.

The second category was on the historical aspect: Koschny reused an old Leonid campaign report from only 10 years ago. Although still fresh in our minds, it was so obvious how much did change in our world in ten years!

7 Some other points of view

As already mentioned, technology advances with a steadily increasing pace. There is almost no scientific area where there are no technology-freaks, which try to bend the latest technology towards an application for use in their fields. That is absolutely also the case in our meteor science. And although it is clear that many of us like to fiddle with instruments, we also need these.

But there is more: in particular the (video) networks grow with an impressive rate. The US Allsky 6 system, FRIPON in France and also

others like CAMS all use modern state-of-the-art equipment at the time of initiation, but to build up an entire network, operate it, maintain it and ensure that it provides a steady output stream, requires other skills than 'just' building a fancy camera system (which I find no less impressive). Enormous effort is put in these, and with success. I find this a remarkable achievement, very well done! It enables unlocking a whole new wealth of data, and it involves new and also young enthusiasts. This is also true in the radio field with BRAMS.

I was very happy to see that many participants not only reported on their 'own' expertise field, but also looked across the border. For understanding a certain aspect in a meteor shower, data from disciplines are combined or analysis simulations and observations compared. It is evident: there is more and more synergy and I think this is a very good sign.

I started to see more attention on QUALITY, by which I like to refer to the understanding of errors, accuracy, dependencies. How does accuracy influence our understanding, or what could we derive from data if a camera would, for example, be twice as good.

I was also delighted to again see many new faces at this IMC. It is encouraging to see that the field keeps being interesting (which it is!), and is also important for securing IMO's long-term future. With the help of Jürgen Rendtel I did some statistics on the age distribution of IMC participants. Let's have a look at Figure 5, which shows the age distribution in bins of 10 years. As one can see the major class is the one in the category of 41 to 50 years. Thereafter it slowly decreases. There is also a significant representation in the category of 21-30. Interestingly, the category 31-40 is the smallest. Could it be that this is the age that this group is too busy with starting careers, and kept busy with their children, but return later on? It seems not unrealistic – and indeed we see many participants that are coming for many, many years –, but it would be worth verifying with data from other years. If true there should not be a worry for the future ... good!

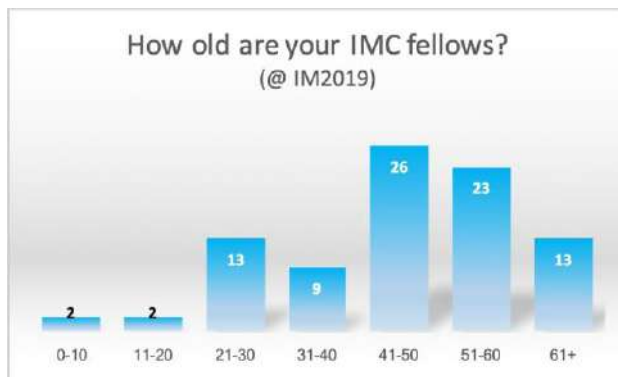


Figure 5 – Age of IMC participants in 2019.

8 Did we (I) miss anything?

I've already stated that it has been a great conference. But if you ask me what I missed and give me some time to think about it, I can come up with some ...

Visual work: it is our motor! It has been for many years the main observation method and main source of information. Certainly some of you know that I'm a big fan of continuing visual meteor work. IMO built up a large historical record, which is unique and without doubt very valuable. It is the *only* observing method which is stable over decades, and we should pursue with ingesting data in our databases. Despite the fact that it's maximal fun to witness an outburst or maximum yourself with your own eyes, there is the pull from all modern overwhelming observing techniques, but these evolve quickly and it is not easy to guarantee consistency over long time frames. We should constantly keep encouraging (new) observers to learn and exploit this field. Unfortunately, the number of visual work oriented talks is low already for a number of years.

(Shower) forecasts: An exciting topic is always to learn from our modelling specialists if increased activity can be expected in the next years or not.

Some great work is being done on spectroscopy (e.g. Ward's work), and this is certainly a growing field with I think great potential for amateurs. Generally, spectroscopy is a workhorse instrument in normal astronomy. I would love seeing even more presentations on this topic next year!

Workshops: this year we had none of them. Maybe we can consider continuing this tradition next year, for example one on the spectroscopy?

9 Amateurs vs. professionals

I could not withhold to also include a final comment on the relationship between amateurs and professionals. In essence the IMC is an amateur conference, being an annual convention, where members of IMO from all over the world meet and share experience. Meteor science is, however, a field where since long amateurs deliver 'scientifically' relevant information, as well has been and is a motivator for pupils **and** students to become scientists, and even astronomers: there is more than a single example where an amateur meteor observers became a meteor scientist. And the connection remains. In a way you can say that we are married to each other, a kind of interwoven when it comes to our interests. This is certainly unique in the world of astronomy. Although the goal for amateurs (hobby, fun) and professional (scientific understanding) do not have to be hundred percent the same I dare say that you can speak of a true family, which we easily can conclude from the amount of professional participants, and is becoming very obvious that IMC and *Meteoroids* are combined.

Let's make sure that this cross fertilization remains optimal, which we do currently really well, IMHO.

Thank you for all your work!

I hope to see you all next year again!

Python ablation and dark flight calculator

Dušan Bettonvil¹

¹ Utrecht, The Netherlands

d.bettonvil@gmail.com

I present a Python based dark flight and ablation calculator, based on classical analytical formulas.

1 Introduction

The last two years I participated in various meteorite search campaigns. None were successful in finding the meteorite. This gave me the idea to create a Python program to calculate the dark flight and ablation trajectory of meteors.

2 Atmosphere trajectory

The meteor trajectory in the atmosphere consists of two parts: ablation and dark flight.

Ablation

The friction of the air with the fireball surface produces a lot of energy. The energy is converted mostly into heat

and light. The heat causes the meteor to evaporate. The amount of friction depends on the air density, speed and shape of the fireball. Rounder meteors have a rounder shape factor. When the fireball shape is not known, a sphere would be used for the simulation.

Dark flight

When the meteor stops emitting light it enters the so-called dark flight. The speed of the meteorite at the beginning of the dark flight is typically 2-4 km/s. At these low speeds the meteor is influenced by wind, and due to the air drag the meteorite decelerates further to reach final ‘free fall’ velocities of 30 m/s (for small meteorites) (Ceplecha Z. 1966).

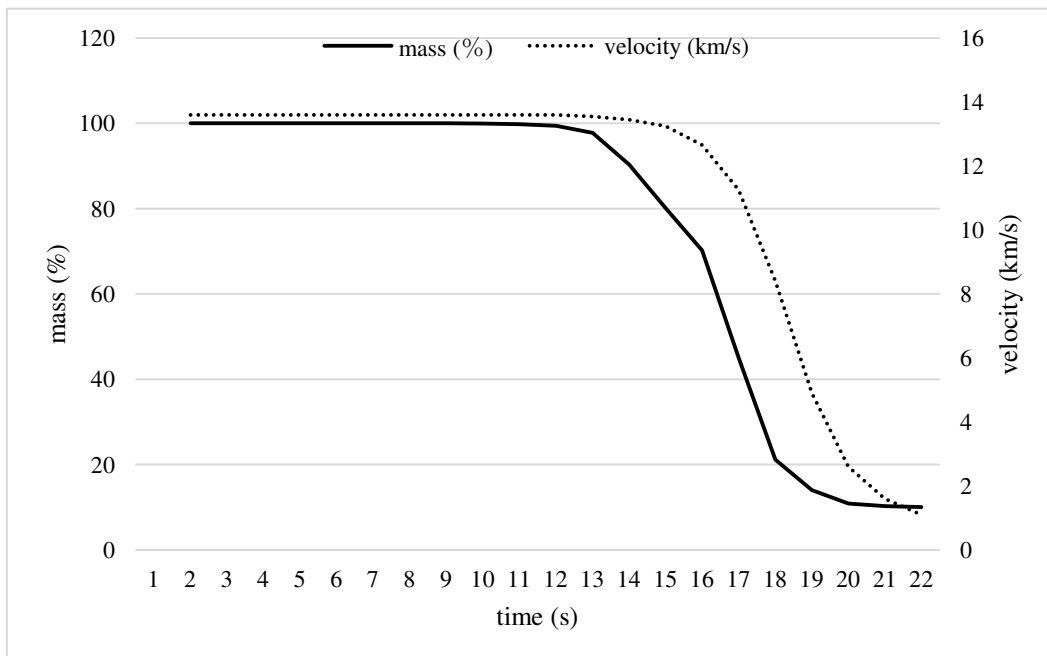


Figure 1 – meteor mass and speed loss curves mapped against time for a typical fireball.

3 Program

The program is written in Python and licensed open-source. The work in progress part of the program is available on Github¹.

Input

Figure 2 shows the input parameters the program takes for the calculation of both the ablation and dark flight parts.

Initial mass

Initial velocity

Material density

¹ <https://github.com/dudaPy/AblationCalculatorPy>

Zenith angle
Weather data
Luminous trajectory start point
Luminous trajectory end point
Luminous trajectory start height
Luminous trajectory end height
Optional:
Meteor fragments
Shape factor
Luminous efficiency
Drag coefficient
Heat transfer coefficient
Heat of ablation

The program reads these parameters from a file or directly as input variables to the Python function. The weather data is read from University of Wyoming Weather Web², optionally it can also be read from a csv file.

Calculation Loop

The program calculates the new parameters for the meteor every 0.001 seconds. The ablation loop exits once the deceleration drops below 100 m/s or the mass loss is minimal. The data of the meteor then gets passed on to the dark flight loop that then calculates the position and speed of the meteor till it hits the ground.

Output

The program outputs a table showing the height, mass, speed and location of the meteorite at the given time.

LUMINOUS TRAJECTORY					
TIME	HEIGHT	SPEED	DECCEL	MASS	VISUAL FRAGMENTS
(S)	(KM)	(KM/S)	(M/S/S)	(%)	MAG
1.50	139.2	13.6	0	100.0	5.3 vis 1
2.00	135.6	13.6	0	100.0	4.7 vis 1
2.50	132.0	13.6	0	100.0	4.1 vis 1
3.00	128.4	13.6	0	100.0	3.4 vis 1
3.50	124.8	13.6	0	100.0	2.8 vis 1
4.00	121.2	13.6	0	100.0	2.2 vis 1
...
19.50	21.6	2.5	1305	10.7	-6.8 vis ...
20.00	21.0	1.9	878	10.4	-5.6 vis 4
20.50	20.6	1.5	617	10.2	-4.5 vis 4
21.00	20.2	1.3	451	10.1	-3.6 vis 4
21.50	19.9	1.1	340	10.0	-2.8 vis 4
22.00	19.6	0.9	264	10.0	-2.1 vis 4

Figure 3 – Head and tail of ablation output in Python shell.

DARK FLIGHT	TIME	HEIGHT	Long.	Lat.	vel	vel_L	vel_h	vel_x	zenit_angle
(S)	(KM)	(deg)	(deg)	(km/s)	(m/s)	(m/s)	(m/s)	(deg)	
22.00	19.6	52.61350	6.03790	0.94	791.46	-504.69	0.00	57.48	
24.00	18.8	52.62253	6.02716	0.59	491.02	-329.02	0.57	56.18	
26.00	18.3	52.62854	6.02024	0.43	345.84	-248.78	2.21	54.27	
28.00	17.8	52.63302	6.01516	0.34	266.42	-208.93	2.89	51.90	
30.00	17.4	52.63655	6.01121	0.28	216.23	-187.62	3.18	49.06	
...
178.00	0.8	52.66212	5.99790	0.08	6.80	-74.89	0.65	5.21	
180.00	0.7	52.66234	5.99767	0.08	7.00	-74.37	0.63	5.40	
182.00	0.5	52.66257	5.99743	0.08	7.28	-73.83	0.55	5.65	
184.00	0.4	52.66281	5.99716	0.07	7.58	-73.27	0.34	5.91	
186.00	0.2	52.66301	5.99685	0.07	7.59	-72.73	-0.21	5.96	
188.00	0.1	52.66317	5.99654	0.07	7.15	-72.30	-0.82	5.68	

Figure 4 – Head and tail of dark flight output in Python shell.

4 Conclusion

The main parts of the python ablation and dark flight calculation program are done, but need a lot of cleaning up and program efficiency improvements. The output needs to be optimized by adding graphs, maps and cleaner tables for easier usage of the program.

Acknowledgement

Thanks to Felix Bettonvil for finding and collecting most of the formulas for this program.

References

Ceplecha Z. (1966). “Classification of meteor orbits”. *Bulletin of the Astronomical Institute of Czechoslovakia*, 17, 96. (Reference)

www.spaceacademy.net.au/watch/debris/metflite.htm

² <http://weather.uwyo.edu>

My first visual observation

Uroš Bettonvil¹

¹uros.bettonvil@gmail.com

This summer I did my first visual IMO observation.

1 Introduction

Before I did my first visual IMO observation, I was already observing meteors. But I was not counting them. I was just watching them. I slowly learned how it works. First I learned what magnitude means. At that time I just guessed which magnitude it is. Luckily I then I did not send the data to IMO.

2 Location

The observations were done in Debelo Brdo in Serbia, $\lambda=19^{\circ}41'13''$ E $\varphi=44^{\circ}09'30''$ N h=1033. Debelo Brdo is a mountain nearby Valjevo. Debelo Brdo was the place where I did my first visual observation. The first time that I was watching meteors was in 2014. I was 6 years old at the time. You can imagine that I was just looking at the sky. Each summer at Debelo Brdo there is a camp for observing meteors. At that camp there are around 30 people.

3 Observation

My method of noting the meteors is with a big paper roll. It's like toilet paper but the width is 1/3 of a toilet paper. When I see a meteor I note down for example 'P-1'. The 'P' means Perseid and the '-1' means that the magnitude is '-1'. I note sporadic like an 'S'. Each 5 minutes I mark the UT time. At the camp someone shouts regularly what the time is. And each time when you see that the sky has changed you count a star field. You note it just for example CEP23. 'CEP' means Cepheus and '23' means 23 stars in Cepheus. Each time when you note something, you flap the paper and go further.

4 Data

When I woke up the next day the first thing that I wanted to do is to fill out the form. The first time that I observed I saw 44 meteors. Table 1 shows my first observation.

Table 1-Magnitude distribution

	-2	-1	0	1	2	3	4	5	6	Tot
showers										
per	1			8	5	6	8	1		29
spor					1	7	3	3	1	15

I was always fast with finishing my forms because I never saw more than 50 meteors. My highest limit magnitude was 6.2.

Pictures

Figure 1 shows a picture of a field in Debelo Brdo.



Figure 1 – Debelo Brdo, field

Figure 2 shows a picture from the dining table in Debelo Brdo with all the observers.



Figure 2 – Dining table

Figure 3 shows the mountain house in Debelo Brdo.



Figure 3 – Mountain house

Comparison of radio meteor observations during the period from 1. to 17. August 2019

Dolinsky Peter¹, Necas Aales², Karlovsky Jan³

¹Slovak Central Observatory, Komarnanska 137, 947 01 Hurbanovo, Slovak Republic
peter.dolinsky@suh.sk

²Slovak University of Technology in Bratislava, Faculty of Materials Science and Technology in Trnava, Institute of Integrated Safety, Ulica Jana Bottu 2781/25, 917 24 Trnava, Slovak Republic
ales.necas@stuba.sk

³M. R. Stefanik Observatory and Planetarium, Sladkovicova 41, 920 01 Hlohovec, Slovak Republic
jan.karlovsky@gmail.com

During the period from August 1 to 17, 2019, we performed radio meteor observations from three different stations (Iza, Hurbanovo, Vrbove). The main aim was to compare detecting systems and differences between them in sensitivity and interferences. The period around maximum of Perseids was chosen to obtain higher detected hour rates of echoes. The main study was held at a frequency of 143.05 MHz, but 50 MHz apparatus was used too. Correlation coefficient and linear dependences between detected rates was determined. These values were from R=0.7 to R=0.9 at different data sets. Also, 143 MHz and 50 MHz rates were compared. We also estimated the Perseids maximum using 24-hour moving averages to circa 13.5 August 2019 UT. During the period from August 12 to 13 we used the data from the 4th station in Hlohovec to compare radio spectrums of strong echoes from these stations.

1 Introduction

Reflections of radio waves from meteor trails were recorded and registered at four stations (Hurbanovo, Iza, Vrbove, Hlohovec) during the Perseids activity. From these data sets we analyzed the period from 9 to 17 August 2019.

2 Description of the equipment

Stations Iza, Vrbove and Hlohovec operated at a frequency of 143.05 MHz, receiving signal from GRAVES (N47.35° E5.52°, France) transmitter. Hurbanovo station operated at a frequency of 143.05 (GRAVES) and 49.79 MHz receiving TV transmitter LVIV (N49.85° E24.04°, Ukraine).

Iza station (N47.75° E18.23°) was equipped with 9-element Yagi antenna (vertical polarization, elevation 0°, azimuth 270°), Yaesu VR-5000 receiver in CW mode and PC using HROFFT 1.0.0f.

Vrbove station (N48.62° E17.72°) was equipped with 9-element Yagi antenna (vertical polarization, elevation cca 5°, azimuth 270°), RTL SDR + sdrsharp and PC using HROFFT 1.0.0f.

Hlohovec station (N48.42° E17.81°) was equipped with GP antenna 1/4 + preamplifier 26 dB, RTL SDR + sdrsharp and PC using SpecLab software for recording echoes.

Hurbanovo station (N47.87° E18.19°) was equipped with 9-element Yagi antenna (vertical polarization, elevation cca 0°, azimuth 270°), RTL SDR + sdrsharp and PC using HROFFT 1.0.0f, and 4-elements Yagi antenna (horizontal polarization, elevation 0°, azimuth 60°). The

communication receiver ICOM-R75 was used to detect radio waves. It was tuned to the frequency of 49.73970 MHz with CW modulation. A computer with the Linux operating system and the program HROFFT 1.0.0f was used to register echoes.

3 Data processing

Data obtained by continuous registration from 1 August 2019 to 17 August 2019 were recorded (Figure 1). Due to disturbances and some technical accidents the main analyzed part was shortened to period from 9 to 17 August 2019. The 50 MHz registrations was affected by ionospheric Es reflections also. All data were recorded at level 10 dB and converted to RMOB format using software HROFFTtoRMOB. Hour rates between two stations can be described as linear function

$$Ny = a.Nx + b \quad (1)$$

Nx and Ny are hour rates recorded at station x and y, respectively.

Table 1 – parameters of regression

x	y	a	b	R
Iza	Hurbanovo	0.849	-1.418	0.862
Iza	Vrbove	1.129	5.486	0.850
Vrbove	Hurbanovo	0.620	-1.054	0.835
24-hour moving average (Iza + Hurbanovo + Vrbove)/3	24-hour moving average 143 MHz Hurbanovo 50 MHz	3.05	20.03	0.898

4 Conclusion

Based on the obtained data we determined coefficients between stations. They can be used to cover gaps in registrations caused by malfunction of equipment. We can estimate that almost all (approximately 70-80 %) recorded events are caused by the same meteors. Using 24-hour moving average we estimated maximum of Perseids activity to approximately 13.5 August ($L=140.2^\circ$) at 143 MHz and 14.0 August ($L=140.6^\circ$) at

50 MHz. 50 MHz registration is more affected by ionosphere and is thus less accurate. The registered hour rates depend strongly on geometry of transmitter-receiver-radiant thus maximum determined on basis of 24-averaging must be perceived as estimation, not as exact date. Anyway it agrees with ($L=140.36^\circ$) (Belkovich et al., 1995), and the difference of $DL=0.2^\circ$ from ($L=140.0^\circ$) (Rendtel, 2014) means a delay of circa 5 hours.

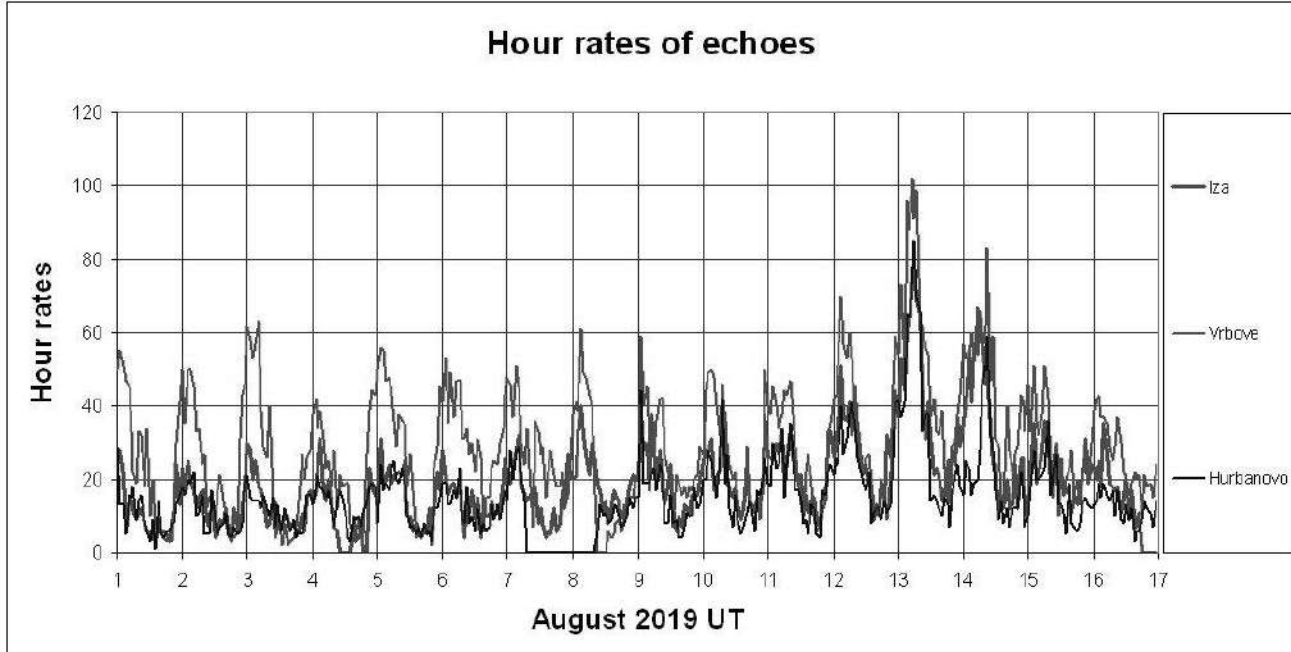


Figure 1 – Hour rates of detected meteor echoes.

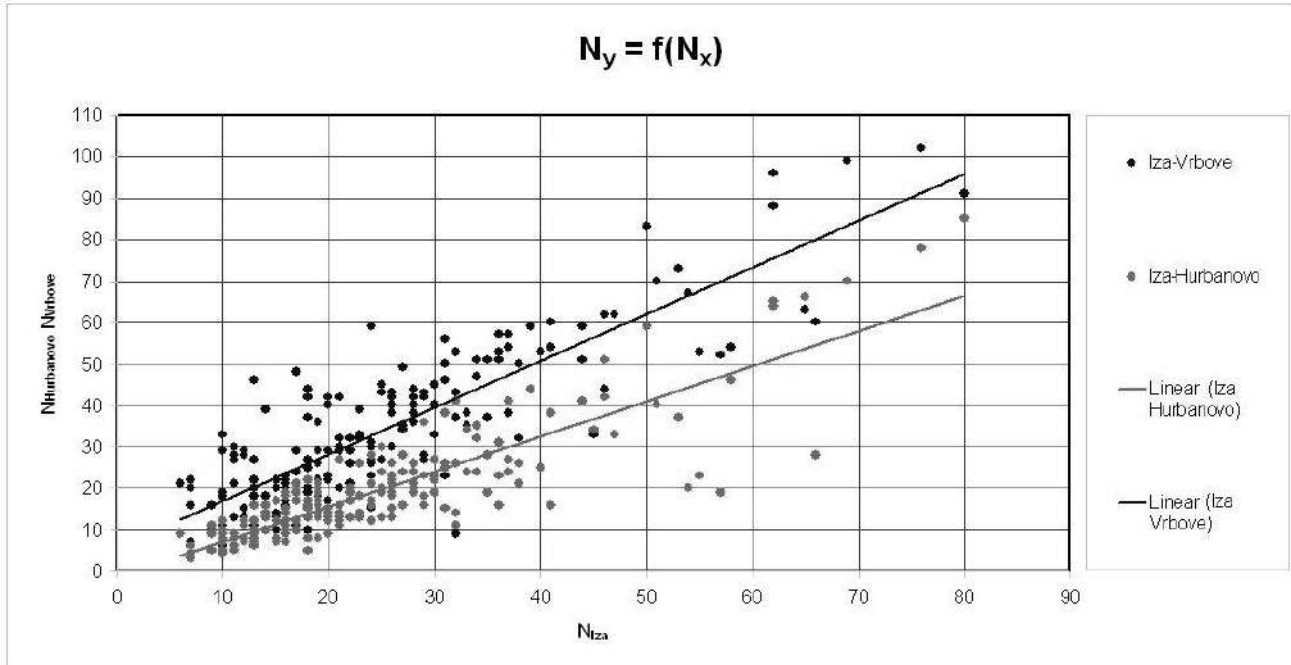


Figure 2 – Linear dependence of recorded number of echoes

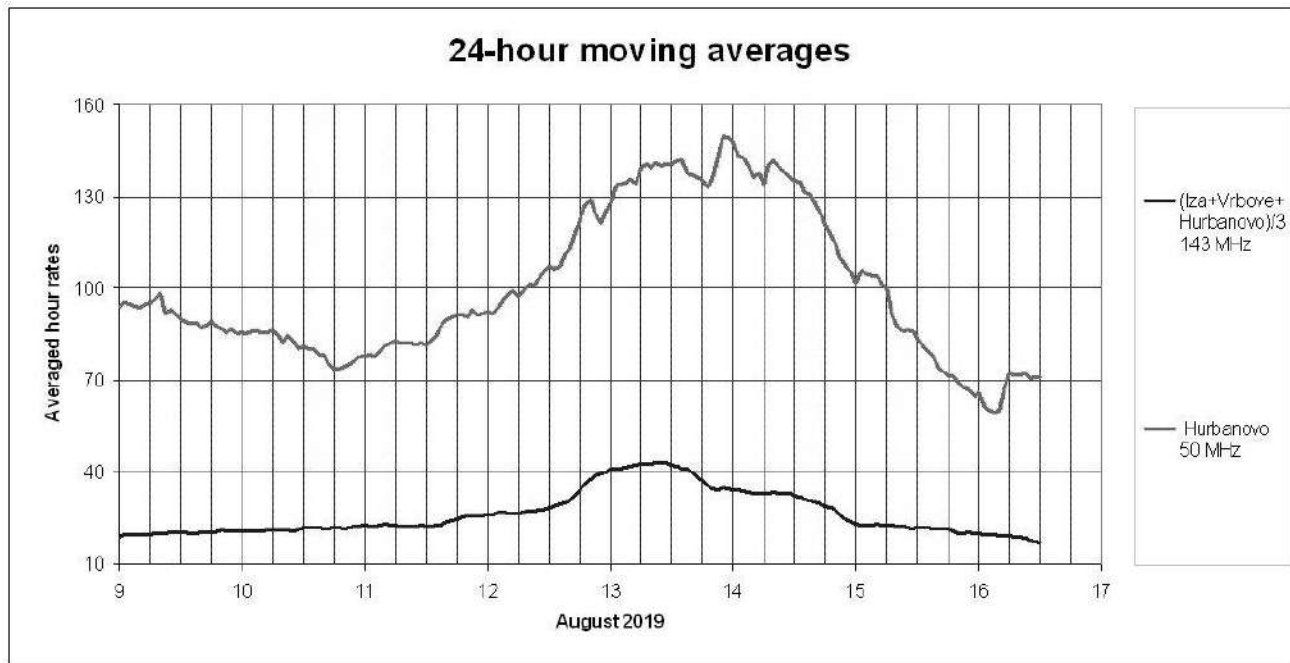


Figure 3 – 24-hour moving average of hour rates of echoes

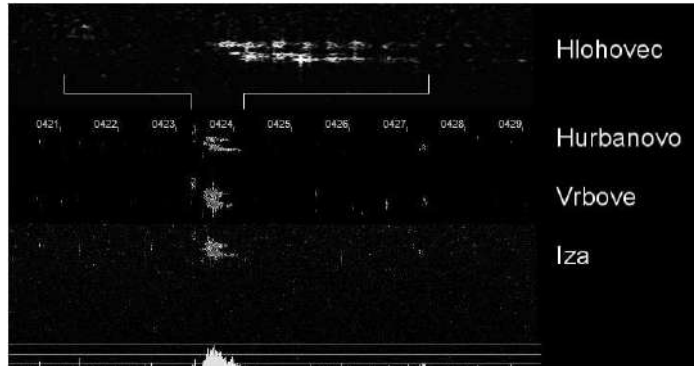


Figure 4 – Comparison of records of the selected echo by different stations. Hlohovec station has higher time resolution.

References

- Belkovich O., Grishchenyuk A., Ishmukhametova M., Levin S., Levina A., Martynenko V., Suleymanov N. and Yaremchuk V. (1995) "Structure of Perseids from visual observations". *Earth, Moon, and Planets*, **68**, 207-215.

Rendtel J. (2014). Meteor Shower Workbook 2014. IMO.

Deep learning applied to post-detection meteor classification

Pete Gural

Gural Software and Analysis LLC, Sterling, Virginia USA
pgural@gmail.com

Advanced machine learning techniques have been applied to automating the confirmation and classification of potential meteor tracks in CAMS video imagery. Deep learning performs remarkably well, surpassing human performance, and will likely supplant the need for human visual inspection and review of collected meteor imagery. Recurrent neural networks (RNNs) and convolutional neural networks (CNNs) have been applied to both meteor time series measurements and video meteor imagery, respectively. The CNN MeteorNet will be explored in the future as a potential upstream meteor detector.

The contents of this poster are fully described and detailed in a recently published paper by the author in the journal *Monthly Notices of the Royal Astronomical Society* (Gural, 2019). If one is unable to obtain the paper from the MNRAS site, you can request a PDF from the author at the indicated email address.

Gural, P.S., 2019. “Deep Learning Algorithms Applied to the Classification of VideovMeteor Detections”, *MNRAS* 489, 5109-5118

Application of high power lasers for a laboratory simulation of meteor plasma

Anna Křivková¹, Lukáš Petera¹, Martin Ferus¹

¹J. Heyrovsky Institute of Physical Chemistry, CAS

anna.krivkova@gmail.com

lukaspetera67855@seznam.cz

martinferus@email.cz

Interpretation of meteor plasma dynamics, its spectra and the dominant spectral features is currently mostly provided by mathematical modelling. Our results show that synthetic spectra calculation is not the only method for such in-depth study of meteor spectra. Laboratory experiments can help with qualitative and quantitative evaluation of the observational data and assignment of important spectral features in meteor emission spectra. Plasma induced by high power lasers provides very suitable experimental approach for such purely laboratory simulation of meteor plasma. Importantly, target experiments with ablation of various real specimens of meteorites help to understand behavior of meteor plasma under strictly controlled laboratory conditions. We show that at least extrapolation of parameters is better than only theoretical simulation. In our study, we provide description, evaluation of advantages and also limitations of this new experimental approach based on laser ablation of real meteorite samples using a wide range of laser sources: Terawatt-class large laser infrastructure PALS, high power Ti:Sa femtosecond laser, laboratory Nd:YAG, ArF excimer laser and large diode pumped solid state laser infrastructure HiLASE.

Numerical model of flight and scattering of meteor body fragments in the Earth's atmosphere

Vladislav Lukashenko¹, Fedor Maksimov¹

¹ Institute for Computer Aided Design of the Russian Academy of Sciences, 2nd Brestskaya Street 19/18, Moscow, Russia
lukashenko-vt@yandex.ru and f_a_maximov@mail.ru

A method is presented that allows to simulate a supersonic flight of several meteor body fragments in the Earth's atmosphere. First aerodynamic problem is solved by calculating the flow around meteor body fragments, then ballistic problem is solved by moving bodies according to the acting aerodynamic forces and their own velocities within short period of time, and the process is repeated. The method was tested on the problem of fragmentation of the meteor body into two identical circular cylinders that have been placed near each other on the line perpendicular to the flight direction. Obtained values for the velocities of the bodies are consistent with theoretical estimates.

1 Introduction

Meteor bodies are severely disrupted during their passage through Earth's atmosphere. As the result, one or more stages of fragmentation may occur during the flight of a meteoroid. During each fragmentation stage several fragments are formed that are initially located close to one another. At first these fragments move together as a group, however the differences in acting forces on each body should result in gradual change of the configuration of bodies over time: some fragments may get separated from the group, while others may continue to move together. The simulation of dynamics of such system of bodies must take into account the relative influence of the bodies on each other.

The studies concerning the dynamics of multiple bodies are often carried out by determining aerodynamic properties of the bodies at different relative positions (for example, see Marwege et al., 2018; Zhdan et al., 2005; Stulov et al., 1995). This approach works relatively well for small numbers of bodies but becomes inconvenient for big systems due to a large number of potential positions of the bodies and time-consuming calculations. An alternative idea is to solve aerodynamic and ballistic problems in parallel, referred as the adjoint problem (for example, see Barri, 2010). Aerodynamic properties of each body are determined based on the current configuration, then the coordinates and speeds of the bodies are changed according to the acting forces and moments. In this case, the aerodynamic problem is solved only for those states of the system that take place during the flight.

In papers of Lukashenko and Maksimov (2017; 2019a; 2019b) a method has been developed for solving the adjoint problem with the use of a grid system. This approach allows to calculate the flow field around the groups with potentially large number of bodies, and each body may have shape and size that differs from others. In order to test the method, a problem of separation of two identical circular cylinders was considered.

2 Methodology

The complete mathematical formulation of the adjoint problem and algorithm can be found in Lukashenko and Maksimov, 2017; 2019a. A uniform grid with rectangular cells is used to describe the external non-viscous flow field. A set of other smaller grids is used to simulate the flow near the surfaces of the bodies. These grids are connected with each corresponding body and have exponential concentration of coordinate lines to the surface (Figure 1). Thin-layer approximation to the Navier-Stokes equations is used to describe the flow on these grids (i.e. viscous flow is considered).

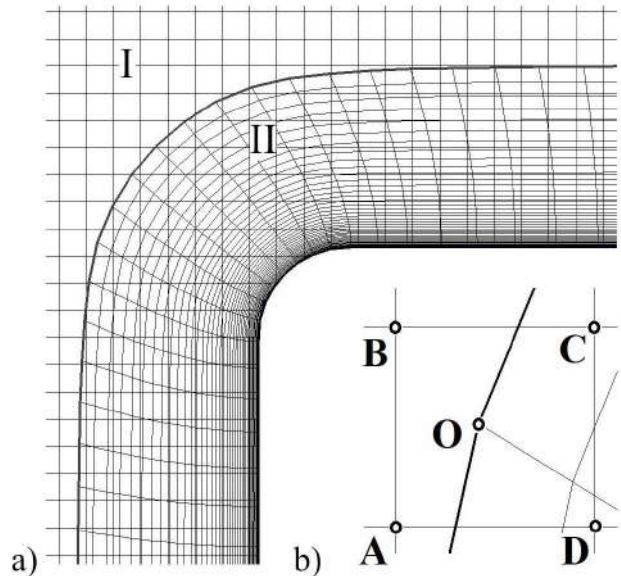


Figure 1 – Schematic representation of a set of grids that is built around a singular body (a) and the relative arrangement of nodes (b).

The uniform grid I and individual body grid II are built independently so their grid notes do not match (Figure 1a). An information exchange is established between the grids in order to tie them together. The

outer nodes of the grid II receive information about the flow parameters from the grid I. The inner nodes of the grid II give information about flow parameters to the grid I. The flow directly at the surface of the body is not considered on the grid I. If a node O is found within a grid cell ABCD and requires information from it (Figure 1b) then flow parameters for node O are calculated via lineal interpolation from the flow parameters of the nodes A, B, C, and D.

A two-step predictor-corrector method is used to calculate the flow field. The aerodynamic forces and moments acting on each body are calculated from the pressure distribution. A ballistic problem is solved at the next stage – the state of the whole system is recalculated after a small time interval. For two-dimensional plane problem the movement of each body is described by a system of equations:

$$\begin{aligned} X^{t+\Delta t} &= X^t + (V_x^t - V_{x,av}^t) \Delta t, \\ V_x^{t+\Delta t} &= V_x^t + \frac{F_x^t}{m} \Delta t, \\ Y^{t+\Delta t} &= Y^t + (V_y^t - V_{y,av}^t) \Delta t, \\ V_y^{t+\Delta t} &= V_y^t + \frac{F_y^t}{m} \Delta t, \end{aligned} \quad (1)$$

where t is current time; Δt – time step; (X, Y) – coordinates of the center of mass; $\vec{V} = (V_x, V_y)$ – body velocity vector; $\vec{V}_{av} = (V_{x,av}, V_{y,av})$ – average velocity vector of the whole system; $\vec{F} = (F_x, F_y)$ – vector of the acting forces; m – body mass.

In most cases the shape of meteor body (and its fragments) is not known so the bodies with a spherical shape are used in modelling. In reality there may be more complex forms, and the method allows to consider them. If the body has non-spherical shape then two additional equations are used to describe its rotation around the center of mass:

$$\begin{aligned} \alpha^{t+\Delta t} &= \alpha^t + \omega^t \Delta t, \\ \omega^{t+\Delta t} &= \omega^t + \frac{M_z^t}{I_{zz}} \Delta t \end{aligned} \quad (2)$$

where α is the angle of rotation; ω – angular velocity; M_z – pitching moment; I_{zz} – body's moment of inertia.

After recalculation of the system state is done, each body is moved together with its own grid to the distance that it should have passed. The flow field is recalculated over the given time interval Δt with a new position of the bodies. A new pressure distribution is calculated on the surfaces of the bodies. The whole process is repeated multiple times until calculations are completed.

3 Calculation of collisions

In order to model dynamics of a complex system of bodies it is also important to calculate collisions. If one body appears in the area behind another it will have

reduced resistance from the flow (Figure 2) and, as a result, it will catch up with the body flying ahead. A collision is bound to occur in this situation as was shown by Barri (2010).

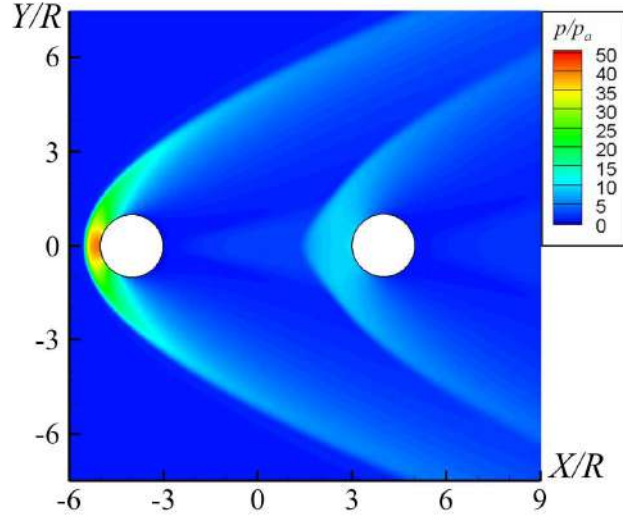


Figure 2 – Pressure distribution for a supersonic flight of two bodies that are located directly one after another. Mach number $M=6$.

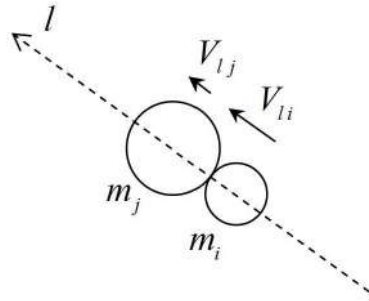


Figure 3 – Schematic representation of a collision between two different bodies.

The model of “billiard balls” is used. Fragments are considered to be rigid bodies with constant mass. If bodies are represented by circular cylinders then in two-dimensional plane problem the state of each individual body is fully described by coordinates of its center of mass (X, Y) , velocity vector $\vec{V} = (V_x, V_y)$ and body radius R . The body grids may cross with each other but their outer nodes should not cross the surface of the bodies. So collision of the bodies i and j happens upon the condition:

$$\sqrt{(X_i^t - X_j^t)^2 + (Y_i^t - Y_j^t)^2} < R_i + R_j + C,$$

where C is a constant that is chosen based on the size of body grids and the limit on the time step Δt .

If we draw a line between centers of mass of the bodies – line of impact \vec{l} (Figure 3) then changes of the projections of velocities on the line of impact are given by formulas:

$$\Delta V_i = \frac{(1+k)m_j(V_{lj} - V_{li})}{m_i + m_j},$$

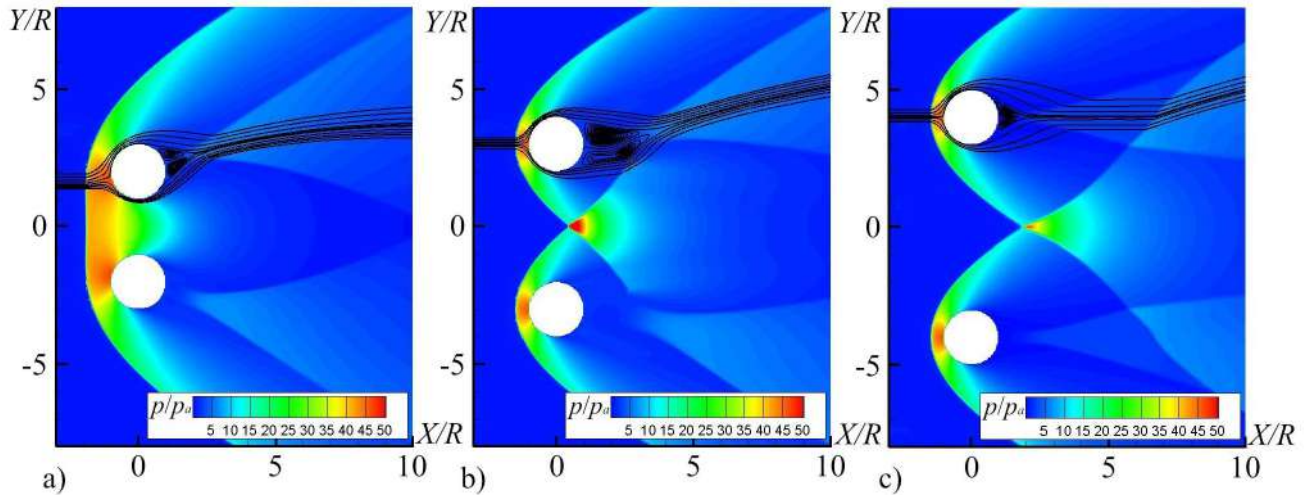


Figure 4 – Pressure distribution and streamlines for a supersonic separation of two bodies at a different distance d between them: (a) $d = 2$, (b) $d = 4$, (c) $d = 6$. Mach number $M=6$.

$$\Delta V_j = \frac{(1+k)m_i(V_{li} - V_{lj})}{m_i + m_j},$$

Shuvalov, 2001:

$$v_s = V \sqrt{\frac{\rho_a}{\rho_m} f(y_0)}, f(y_0) = \int_{d_0}^{d_m} c_y dy, \quad (3)$$

where k is the impact recovery coefficient. If $k = 1$ then there is no loss of kinetic energy and perfectly elastic collision of bodies occurs. If $0 < k < 1$ then some part of the kinetic energy is lost – inelastic collision occurs. If $k = 0$ then the velocities are averaged along the direction of impact \vec{l} similar to perfectly inelastic collision of the bodies.

It is important to note that each collision is calculated under the assumption that bodies collided with each other and fly apart over a different time step Δt^* . Generally $\Delta t^* > \Delta t$ so a larger time step should be made, however calculations for a collision of two bodies show that Δt^* and Δt are values of the same order (see Lukashenko and Maksimov, 2019b).

4 Testing and results

The method was used on the problem of separation of two identical circular cylinders. The size of used computation mesh was 1501x1501 with 50 cells across the unit of length. Three flow patterns can be distinguished for a supersonic flight of such bodies depending on the distance d between them:

- 1) collective flow with a combined head shock wave, interference creates a significant lateral force acting on the bodies (Figure 4a);
- 2) shock waves affect the flow of the bodies trail that leads to a decrease in flow resistance, there is no lateral force (Figure 4b);
- 3) isolated flow around bodies when there is large distance between them (Figure 4c).

These flow patterns can be observed for different values of the flight speed, however the distance, at which interference occurs, becomes shorter with the increase of the flight speed.

The separation velocity v_s for two identical bodies can be determined by the expression from Artemieva and

where V is initial flight speed, ρ_a – air density; ρ_m – density of meteor body fragment; d_0 – initial distance between bodies; d_m – distance at which aerodynamic interaction between bodies ceases to exist; c_y – coefficient of aerodynamic lift that is calculated from the lateral force F_y .

Calculations of dynamics were carried out for the problem of quasi-stationary separation of two iron bodies. The bodies were represented by circular cylinders with a weight of 1 kg, a radius $R = 0.027$ meters, and a width of $2R = 0.054$ meters. Atmospheric conditions were taken for the Earth's surface ($\rho_a = 1.293 \text{ kg/m}^3$). Initial speed of the bodies V and dimensionless distance d_0 between the bodies (distance divided by the radius of bodies R) were varied. The results of the calculated velocity of separation v_{sd} in comparison to theoretical estimate v_s given by the formula (3) are presented in Table 1.

Table 1 – Separation velocities of two cylindrical bodies.

Parameters	N1	N2	N3	N4
Initial speed V , m/s	1000	2000	1000	2000
Initial distance d_0	0.4	0.4	2.0	2.0
Theoretical v_s , m/s	9.1	15.5	6.6	9.0
Calculated v_{sd} , m/s	9.5	17.2	7.0	11.3

Obtained values for the separation velocity are consistent with theoretical estimates. However it is worth noting that formula (3) does not take rotation into account, and the calculations for rectangular cylinders with the use of full system of equations (1-2) show that additional lateral force may appear due to rotation (see Lukashenko and Maksimov, 2019a).

5 Conclusion

A method has been developed that allows to simulate dynamics of a supersonic flight of multiple bodies in the Earth's atmosphere. A system of grids is used to describe the external non-viscous flow field and the viscous flow near the surfaces of the bodies. The dynamics of the system is observed via iteration: at first aerodynamic problem is solved by calculation of the flow field, then ballistic problem is solved by moving bodies according to the acting aerodynamic forces and moments, and the process is repeated. The method allows to consider the flight of the bodies with non-spherical shape and calculate collisions of the bodies. The method was tested on the problem of fragmentation of iron meteoroid into two identical fragments near the Earth's surface. Obtained values for the separation velocities of the bodies were found to be consistent with theoretical estimates, that allows to conclude that method is reliable. The implementation of the method to model the dynamics of a group of meteoroid fragments will provide a scattering pattern of the fragments in the Earth's atmosphere and a set of possible trajectories.

mosphere". *Journal of Geophysical Research*, **106:E2**, 3297–3309.

6 References

Marwege A., Willems S., Gulhan A., Aftosmis M. J., and Stern E. C. (2018). "Superposition Method for Force Estimations on Bodies in Supersonic and Hypersonic Flows". *Journal of Spacecraft and Rockets*, **55:5**, 1166–1180.

Zhdan I. A., Stulove V. P., and Stulov P. V. (2005). "3D configurations of broken body fragments in a supersonic flow". *Doklady Physics*, **50:10**, 514–518.

Stulov V. P., Mirskii V. N., and Vislyi, A. I. (1995). *Fireball Aerodynamics*. Moscow: Nauka.

Barri N. G. (2010). "Dynamics of two spherical objects in supersonic flow". *Doklady Physics*, **55:10**, 516–518.

Lukashenko V. T. and Maksimov F. A. (2017). "Numerically simulated model of meteor body fragments distribution after destruction". *Engineering Journal: Science and Innovation*, **69:9**, 1–13.

Lukashenko V. T. and Maksimov F. A. (2019a). "Modeling the flight of meteoroid fragments with accounting for rotation". *Computer Research and Modeling*, **11:4**, 593–612.

Lukashenko V. T. and Maksimov F. A. (2019b). "Simulation of collisions between two identical meteoroid fragments arranged one behind the other". *Engineering Journal: Science and Innovation*, **90:6**, 1–14.

Barri N. G. (2010). "Meteoroid fragments dynamics: Collimation effect". *Solar System Research*, **44:1**, 55–59.

Artemieva N. A. and Shuvalov V. V. (2001). "Motion of a fragmented meteoroid through the planetary at-

Fireball Reporting in the context of the Citizen Science Project Nachtlicht-BÜHNE

Marius Hauenschild¹, Anastasios Margonis¹, Jürgen Oberst^{1,2}, Stephan Elgner², Joachim Flohrer², Friederike Klan³, Christopher Kyba⁴, and Helga Kuechly⁴

¹ Institute of Geodesy and Geoinformation Science, Planetary Geodesy, Technical University Berlin, Berlin, Germany

hauenschild@tu-berlin.de

² Institute of Planetary Research, Planetary Geodesy, German Aerospace Center (DLR), Berlin, Germany

³ Institute of Data Science, German Aerospace Center (DLR), Jena, Germany

⁴ Remote Sensing and Geoinformatics, GFZ Helmholtz Centre Potsdam, Potsdam, Germany

The Nachtlicht-BÜHNE is a citizen science project in the context of astronomy and space research regarding observations of the night sky. The goal is the development of reporting and data analysis tools, with which citizens collaborate with professional scientists from the communities. The project is focused on two pilot studies, on light pollution (DLR-DW/GFZ) and meteor science (DLR-DW/DLR-PF). Here, we report on our recent experiences and statistics of public meteor reporting.

1 Introduction

The European Fireball Network was built in the 1970s and consisted of 34 and more observation cameras with fish-eye lens or lens that photograph a curved mirror, which observe the night sky in Germany, Belgium, Luxemburg, Czech Republic and Austria (Oberst et al., 1998). Today there are 24 Cameras left. Citizens are also involved in the research. They can report a meteor or other night light phenomena by using a form or an e-mail on the website of Technical University Berlin or DLR. By using the information of both fireball detections, it is possible to confirm a phenomenon and classify it.

2 The purpose of fireball reporting

One of the problems with the exclusive use of camera detections is the limited availability. In order to obtain a good result, there must be no scattered light from the Moon and no twilight light. The weather must also provide ideal conditions. Due to these factors it is not possible to capture all fireballs. The messages of the citizens it is possible to determine the exact time, the possible fragmentation of the meteor, the change of the brightness, the color and the possible noise. The noise can indicate a meteorite fall, so that a search for it is worthwhile.

Time	21:34
Date	08/04/2019
Post Code	48599
Place	Gronau
Coordinates	52.18412 ; 7.028936
Line of Sight	north
Flight Direction	north to south
Duration of the Event	1-3 s
Brightness	mag - 16
Brightness Change	yes
Color	yellow, red, white
Color change	yes
Fragmentation	no
Afterglow	no
Sounds	yes
Comment
Image
Video
Name	Max Mustermann

Figure 1 - The fireball notification form (the values entered by the reporting person are fictional)

3 The meteor event on 12.09.2019

On 12.09.2019, we received an unusually high number of meteor reports associated with the daytime meteor event

over the North Sea on that day (14:50). There were 63 reports submitted using the form and 8 by e-mail. The map shows the positions of visual observers during the event, reporting from Germany (57). By means of fast cataloging of the acquired parameters it is possible to narrow down the area of the sighting after a short time.

With the help of an app we hope for a faster processing of the messages as well as a common standard of the form of messages, whereby the evaluation is facilitated. Likewise, the direction of flight could be determined by a visualization on the terminal of the user.

Eyewitness reports for the daytime meteor event over the North Sea on 12.09.2019 at 14:50 CEST

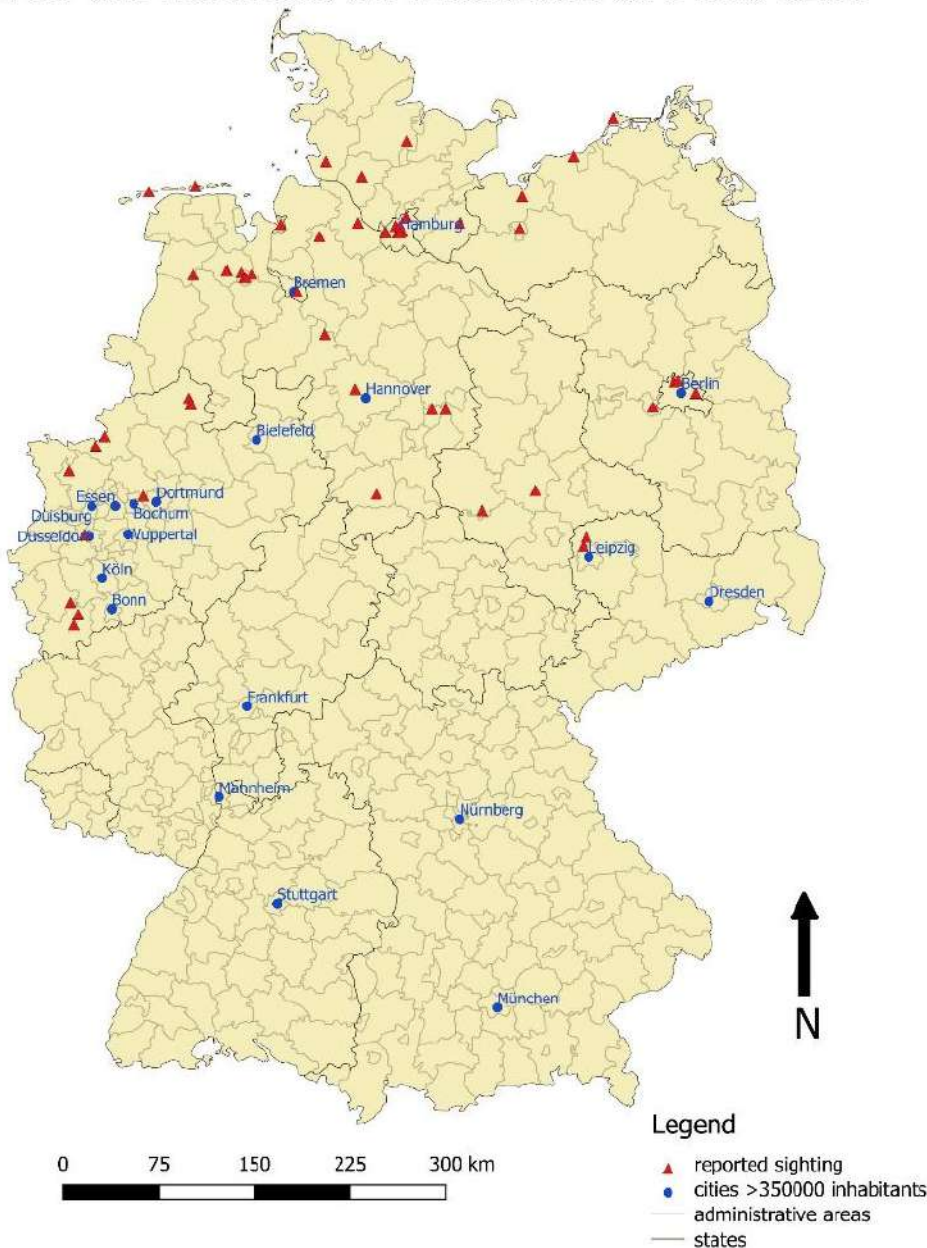


Figure 2 – Meteor event on 12.09.2019 in Germany

4 The introduction of the form

Prior to the introduction of the form sightings were reported only by email. The DLR webpage provides information on how to submit a report, however this guideline is optional. This sometimes leads to reports that cannot be evaluated. Since the introduction of the form, the answers in the questionnaire have been reduced to a

few options. The fields "flight direction" and "coordinates" can be freely filled by a user, while information on all other fields can be selected by a drop-down menu. For detailed description, a comment field is available. The main advantage of using a report form is that the data can be easily exported and used for further analysis. A message by e-mail is also still possible.

Figure 3 gives an indication of the increasing number of meteor reports since the introduction of the reporting form. The shorter duration of writing a message may increase the willingness of citizens to report. An app would probably increase this even further, as the smartphone can be used directly. Stronger networking between scientific institutes may also increase popularity of such an app. Moreover, information of a submitted event could be easier shared with all contributing users.

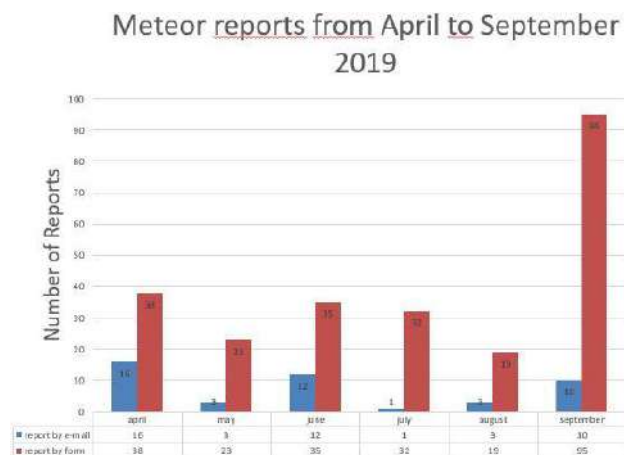


Figure 3 – Plot showing the number of meteor reports from April to September 2019 sent by mail and by form

5 Conclusions

Information regarding a fireball event can be acquired by reducing image data obtained by cameras of the European Fireball Network. This includes, for example, the determination of its trajectory and speed, and the estimation of its brightness. The combination of information derived from images obtained by cameras of the European Fireball Network and fireball reports of an event will facilitate the recovery of possible meteorites. A great advantage of using a dedicated smartphone application for reporting fireballs would be the standardised data that will be received for each event. Furthermore, it would be easier for the reporting person to describe the flight direction, colour and appearance of the phenomenon using example images or an integrated star map. Also, more citizens could be reached and receive information about the phenomenon promptly after an event. This could also increase the enthusiasm of the citizens for space.

References

- Oberst J., Molau S., Heinlein D., Gritzner C., Schindler M., Spurny P., Ceplecha Z., Rendtel J. and Betlem H. (1998) The „European Fireball Network“: Current status and future prospects. *Meteoritics & Planetary Science* **33**, 49-56

Automated determination of dust particle trajectories in the coma of comet 67P

J. Marin-Yaseli de la Parra¹, M. Kueppers¹ and the OSIRIS team²

¹ ESA European Space Astronomy Centre (ESAC), Camino bajo del Castillo s/n, Urb. Villafranca del Castillo, P.O. Box 78, 28691 Villanueva de la Cañada, Madrid, Spain

² Max-Planck-Institute for Solar System Research, Göttingen, Germany
jmarin@sciops.esa.int

We present the preliminary results and methods for an automated determination system of dust particles positions and trajectories in the near coma of comet 67P.

1 Introduction

This study is part of a PhD project and its objective is to understand the physical processes in the inner coma of the comet through measurements with the OSIRIS scientific camera system on Rosetta.

As a first exercise of the methods to be employed a set of images taken during the Rosetta operational phase will be analysed. Many thousand images of the dust coma were obtained by both dedicated sequences and serendipitous detections on frames acquired for different purposes. In many of those observing sequences, 100s of dust particles are identifiable in single images. Both the narrow angle camera (NAC) and wide angle camera (WAC) observed the same area through several (60–90) minutes. The focus of the study will be identify the individual dust particles. Of particular interest are the long trajectories that remain in the field of view during several minutes. The dust detected by OSIRIS can be divided into near-spacecraft dust with its apparent motion being dominated by spacecraft motion and near nucleus dust, moving radially away from the nucleus. In the latter case, the distance is known approximately and the size (with an assumed albedo and phase function) and velocity of the particles can be determined. In addition, the rotational light-curve of some particles is detectable in the images, providing additional information about spin period and shape.

Different data sets will be used to address the following scientific questions:

- Describe the evolution of the cometary dust population over the mission
- Search for changes both within an observing sequence and through the perihelion passage. The outcome will be used to evaluate if there is a preferred size range of dust particles as they leave the nucleus and if the their measured size distribution is primordial or the result of processes on the cometary nucleus and in the coma.
- Extract orbital parameters from individual dust particles to analyze the trend of the radiant trajectories, analyze if there are preferred regions of

dust emissions and contextualize with gas emissions and surface activities of the comet.

2 Methodology



Figure 1 – Test on individual particles to check the algorithm behaviour. The linear correlation between pixels movement and time demonstrates a correct characterization of the physical movement of the particles.

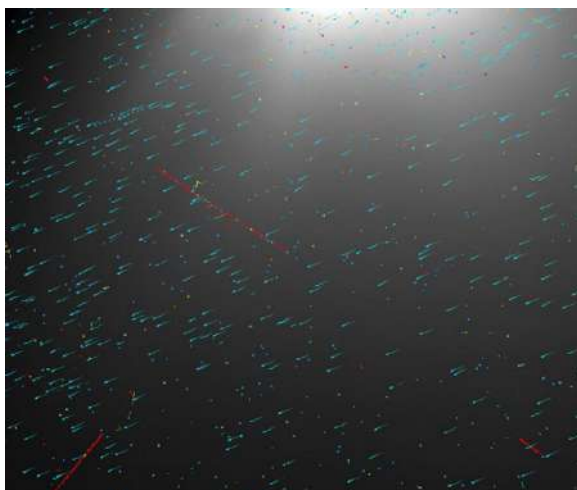


Figure 2 – Example of trajectories automated determined with a linear motion LAP tracker. The set of data contains 91 images over 1 hour and 28 minutes with different exposition times. The set is at a distance of 141 km from the target with phase angle of 70°. This sample was taken as a good exercise of degraded background with the coma visible on the top.

There are many software tools focused in the search of the perfect algorithm that traces particles from micro sizes to meter scales. The truth is that there is no such thing as a “one size fits all” tracking method. But it is common to divide the image analysis method in two different steps.

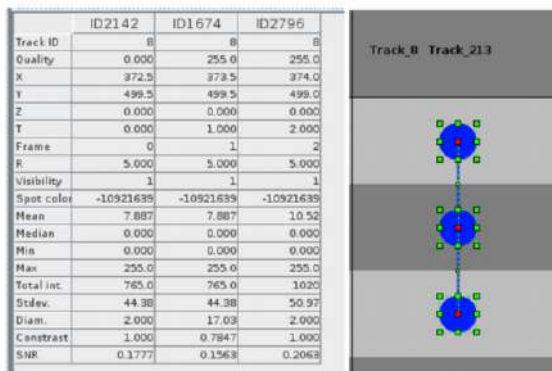


Figure 3 – Example of individual tracking characterization output.

The first one would include all technical conversions of the image to detect the particle itself (Figure 1). The output would be a spot extraction from background and their coordinates in every frame of the image sequence are characterized (Figure 2). When finding maxima algorithms are pretended to be used automatically, we found an aggregation of two scenes, when the particle is spherical either when velocities and distances make the particle elaborate a path in the frame. The second part of the methodology is based on the particle linking using other criteria. A simple nearest-neighbour method is the simplest approach to the problem. LAP framework proposed by Jaqaman or particle algorithms relying on Kalman filters to tackle linear motions are more elaborated algorithms and work well with certain trajectories.

Part of the software used for this method is a plugin called “Trackmate” contained in ImageJ open source software (Figure 3). Images were converted from PDS3 to bmp with Fairwood PDS Viewer. After that, the whole set of images was opened with ImageJ in 8 bit image. Different thresholds must be applied in order to compensate the different exposition times of the set of data. It is necessary to adjust the threshold to the images individually. An automated system will be applied in the future for this middle-step.

Acknowledgements

OSIRIS was built by a consortium of the Max-Planck-Institut für Sonnensystemforschung, Göttingen, Germany, CISAS University of Padova, Italy, the Laboratoire d’Astrophysique de Marseille, France, the Instituto de Astrofísica de Andalucía, CSIC, Granada, Spain, the Research and Scientific Support Department of the European Space Agency, Noordwijk, The Netherlands, the Instituto Nacional de Técnica Aeroespacial, Madrid, Spain, the Universidad Politécnica de Madrid, Spain, the Department of Physics and Astronomy of Uppsala University, Sweden, and the Institut für Datentechnik und Kommunikationsnetze der Technischen Universität Braunschweig, Germany. The support of the national funding agencies of Germany (DLR), France (CNES), Italy (ASI), Spain (MEC), Sweden (SNSB),

and the ESA Technical Directorate is gratefully acknowledged.

Elemental composition, mineralogy and orbital parameters of the Porangaba meteorite

Lukáš Petera¹, Libor Lenža¹, Jakub Koukal², Jakub Haloda³, Bára Drtinová, Dalibor Matýsek, Martin Ferus¹, and Svatopluk Civiš¹

¹J. Heyrovsky Institute of Physical Chemistry, CAS

lukaspetera67855@seznam.cz

libor.lenza@jh-inst.cas.cz

martinferus@email.cz

civis@jh-inst.cas.cz

²Valasske Mezirici Observatory

j.koukal@post.cz

³Institute of Geochemistry, Mineralogy and Mineral Resources, Faculty of Science, Charles University, Albertov
6, 12843 Prague 2, The Czech Republic
jakub.haloda@geology.cz

The main goal of this study was to provide data on the bulk elemental composition, mineralogy and possible origin of the fresh Porangaba meteorite, whose fall was observed approximately at 17:35 UT on January 9, 2015, in many areas of the state of São Paulo in Brazil. There are only about 30 meteorites with known major parameters, namely their elemental composition, mineralogy, and petrology, combined with knowledge of their trajectory in the Solar system. In this study, we provide a next case of such a body described in particular details: famous Porangaba meteorite. The surface of the meteorite was mapped by Scanning Electron Microscopy (SEM) and optical microscopy. The mineralogy and the bulk elemental compositions of the meteorite were studied using Energy-Dispersive and Wavelength-Dispersive X-ray Spectroscopy (EDS/WDS) together with Electron Back Scatter Diffraction (EBSD). The bulk elemental composition was also studied (for comparison) by several other techniques, namely Atomic Absorption Spectrometry (AAS), Inductively Coupled Plasma Mass Spectrometry (ICP-MS), Laser Ablation ICP MS (LA ICP-MS) and Calibration-Free Laser-Induced Breakdown Spectroscopy (CF-LIBS). Based on the very poor visual camera records of the Porangaba meteorite fall and using UFOOrbit software (SonotaCo, 2009), its orbit was tentatively calculated and possible candidates of source bodies in the Solar system were tentatively proposed. We also provide a laboratory simulation of meteor spectra emissions that can be used for at least qualitative comparing spectra from sporadic meteors with composition similar to Porangaba-like (L4 Ordinary Chondrite) bodies recorded by high-speed video-cameras equipped with simple grating spectrographs.

Geminids 2018

Jürgen Rendtel¹

¹ Leibniz-Institut für Astrophysik, An der Sternwarte 16, 14480 Potsdam, Germany
and International Meteor Organization, Eschenweg 16, 14476 Potsdam, Germany
jrendtel@web.de

A large number of visual data of the currently strongest annual meteor shower has been collected worldwide. Procedures to obtain a continuous activity profile are described. Despite the wide distribution of visual observers, a gap remains for Pacific longitudes. We show differences between ZHR profiles including (almost) all data and another based on a sample of selected data. To achieve an optimal temporal coverage and reliability of the ZHR, a composite profile with adapted selection parameters is needed. The Geminid peak ZHR of 150 ± 15 occurred on December 14 close to 14^h UT ($\lambda_{\odot} = 262^{\circ}2$ to $262^{\circ}3$). A deep “dip” was found in different data sets on December 14, 04^h UT ($\lambda_{\odot} = 261^{\circ}85$) when the ZHR dropped from above 100 to 70, followed by a steep increase towards the main peak.

1 Introduction

Due to the favourable radiant position, the Geminid meteor shower can essentially be observed from all latitudes. Especially, northern hemisphere observers can follow the activity during almost the entire night. This increases the possibility to compose a continuous data set. The largest interruption, however, occurs for the Pacific longitudes, i.e. after the end of North American observing window and the start of observing at Asian longitudes. Locations which could fill this gap are Hawaii and other Pacific islands and Alaska. In these regions we lack observers at the moment. Here we describe the attempt to close this gap as far as possible, and retaining reliable ZHR values for each section of the profile.

2 Visual Geminid data 2018



Figure 1 – Location of visual observers during the Geminid 2018 campaign. Note that not all observers which are marked here were also active in the maximum period.

In 2018 the conditions to observe the maximum period were favourable for visual observers. The Moon set before local midnight (first quarter only on December 15). In total, 64 observers distributed over almost all longitudes (Figure 1 submitted their data via the IMO web form to the Visual Meteor DataBase (VMDB) for this campaign (155 sessions). The covered period extends

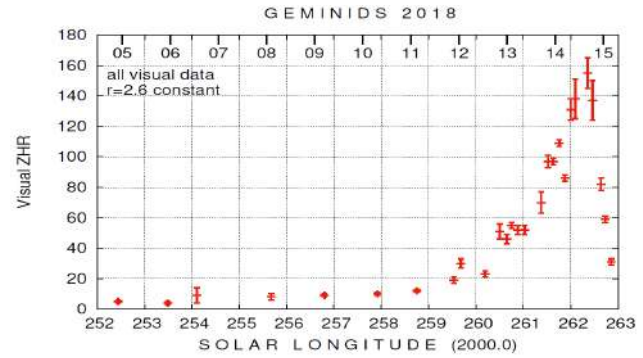


Figure 2 – Total ZHR profile of the Geminids 2018, using $r = 2.60$ for an overview. The tics of the dates given at the top refer to 00^hUT of the day.

from the activity start on December 4 to the end (due to moonlight interference) on December 16. Data from this period were splitted into 1398 intervals which comprise a grand total of 10,674 Geminids. The overall ZHR profile is shown in Figure 2. Next we concentrate on the peak period which covers the time between Dec 13, 19^hUT and Dec 15, 04^hUT. The sample consists of 7706 Geminids and 958 count intervals. Nevertheless, we find gaps in the series which we will investigate below. Before that, we check which other data can be used for comparison and calibration.

3 Other Geminid 2018 data

A similar data set is provided by the IMO Video Meteor Network. Using the fluxviewer (Molau, 2020), we obtain the flux density profile shown in Figure 3. This is a preliminary result and is based on the temporarily available data (as of October 2019). We can use this for comparison, but find that the profile lacks from the same gap as the visual data set.

Next, we find the continuous profile derived from radio forward scatter data worldwide by Hirofumi Sugimoto. The procedure to obtain a “radio ZHR” is described in

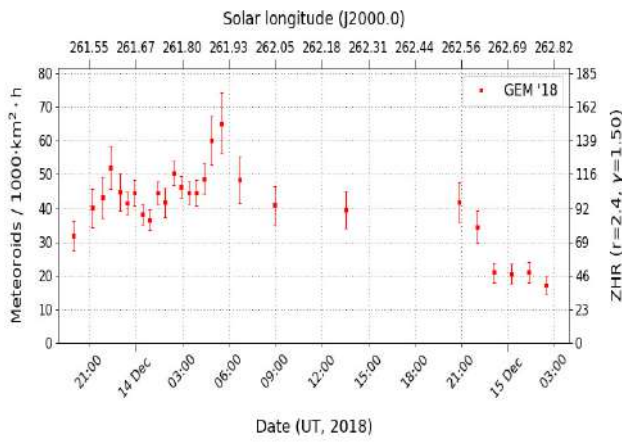


Figure 3 – Flux density profile of the Geminids 2018 in the period between December 13, 19^hUT and 15, 04^hUT as defined for the visual analysis. Here we use $r = 2.40$ and require at least 50 shower meteors per bin, achieving a temporal resolution of 15 minutes (source: <https://meteorflux.org/>).

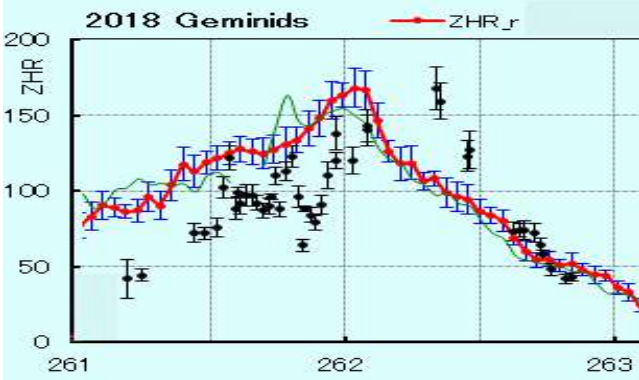


Figure 4 – Radio ZHR of the Geminids 2018 as derived by Sugimoto for the same period as in the other profiles (red curve). The black data points refer to visual ZHR from the IMO webpage (preliminary data). The dip at $\lambda_{\odot} = 261^{\circ}85$ found in the optical ZHR and flux density data which is discussed in section 5 does not occur in the radio data.

(Rendtel, Ogawa and Sugimoto, 2016). In Figure 4 we show only the same portion of the profile as for the optical data to allow to compare the two. The radio ZHR profile is obviously more skewed than the optical profiles, indicating the known mass segregation throughout the stream with the smaller meteoroids (fainter, radio meteors) occurring well before the brighter meteors (see, e.g. Rendtel, 2004). Therefore the radio ZHR is already at a high level when the optical data still record the ascend towards the maximum. The later descend of the radio ZHR is very steep, and the rates have considerably decreased when the optical data still suggest a reasonably high ZHR/flux density. So the radio data is less suited for a direct comparison of the values, but may help to find what happens in sections where the other series show gaps. The radio ZHR peaked definitely before the optical maximum occurred.

4 The Geminid maximum 2018

An analysis of visual observations of the Geminids 2018 has been published by Miskotte (2019), using partly the same data as this study but setting several selection criteria (limiting magnitude and others). Since we are mainly interested in a complete ZHR/flux density profile we (i) include all available data into the analysis, and (ii) applied the population index r for visual meteors in the magnitude interval $[-1; +5]$ as listed below which are adopted from Miskotte (2019):

λ_{\odot} range [°]	r
before 261.00	2.60
261.00 – 261.82	2.40
161.82 – 261.95	2.20
261.95 – 262.70	1.80
262.70 – 262.90	2.30
262.90 – end	2.60

Our first profile of the peak period (Figure 5) demonstrates the extension of the ranges with no observer coverage. Of course, we may vary the requirements for visual data to be included. For this visual ZHR profile the minimum number of Geminids per bin is set to 200. This is easily achieved as long as the number of observers is large enough, particularly at European and North American longitudes. We see that the Europe – America transition leaves no gap while the Pacific obviously lacks observers. The obvious “jump” of the ZHR from the latest European value to the first from America may be interpreted as an over-correction of the ZHR due to differing radiant elevations. If we look into the data in the VMDB, we find quite similar radiant elevations for reports from both sides of the Atlantic. This is partly due to the fact, that observers started only around or after moonset (roughly first quarter Moon). Further, the time difference between western Europe and eastern US is about 5–6 hours. The last “European” interval ended at 06^h50^m UT (Canaries; radiant elevation 43°), while the first “North American” interval started at 05^h55^m UT (Texas; radiant elevation 37°) – hence no radiant elevation jump and, moreover, one hour overlap. Hence the further ZHR increase should be no artefact due to observer bias or correction factors since also the observing conditions were quite similar on both ends.

Both the visual ZHR and the video flux density profiles in Figure 5 show identical variations. Among these are local minima (called short “dips” hereafter) at $\lambda_{\odot} = 261^{\circ}63$, at $261^{\circ}85$ and at $262^{\circ}62$ – or expressed as sub-peaks close to $261^{\circ}60$, at $262^{\circ}75$ and finally $262^{\circ}66$. This way we have an information about the reliability of details in the profiles we discuss later.

It seems that the selection criteria applied for Figure 5 are too restrictive for some periods. In the past, we have applied both a selection of “high quality data” versus the “including all data” for several major showers. The main advantage of the latter is the better coverage of the activity period which is the aim also in this study. The

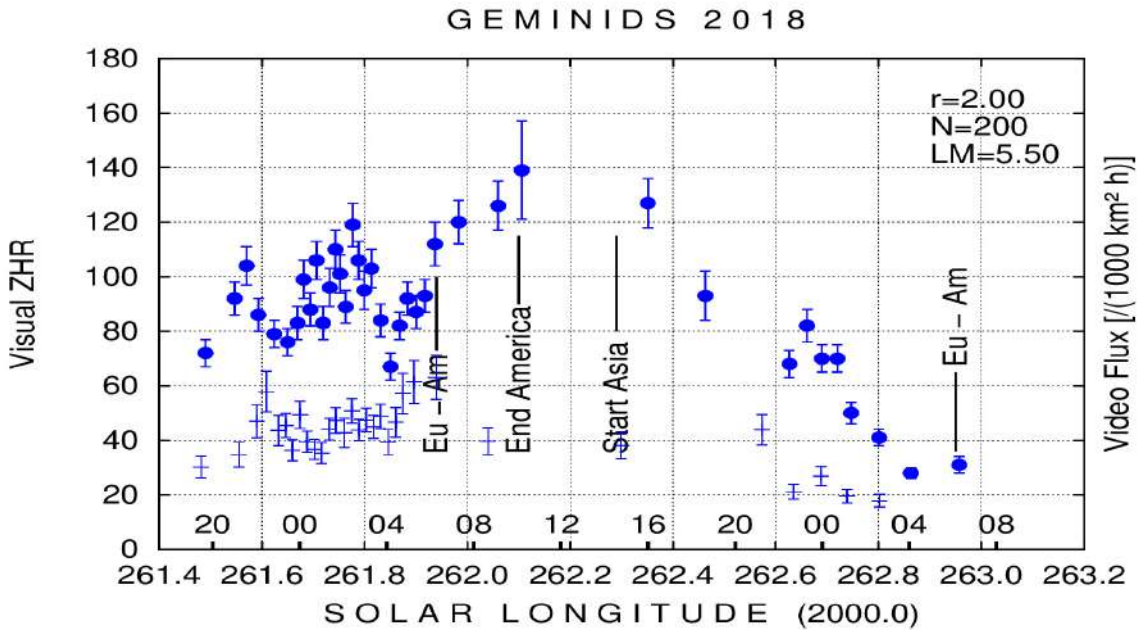


Figure 5 – Overview of the Geminid peak activity 2018 as observed visually (dots) and by video (crosses), setting $r = 2.00$ for the entire period. The time is given on the abscissa, starting December 13, 19^hUT and ending December 15, 12^hUT. For this first overview we used a constant $r = 2.00$ for both the visual and video data. The visual data have a minimum number of $N=200$ per bin and $LM \geq 5.50$ or better. The minimum number of video meteors is 60 per bin (using the temporary database). The gaps in the profiles are discussed in section 4.

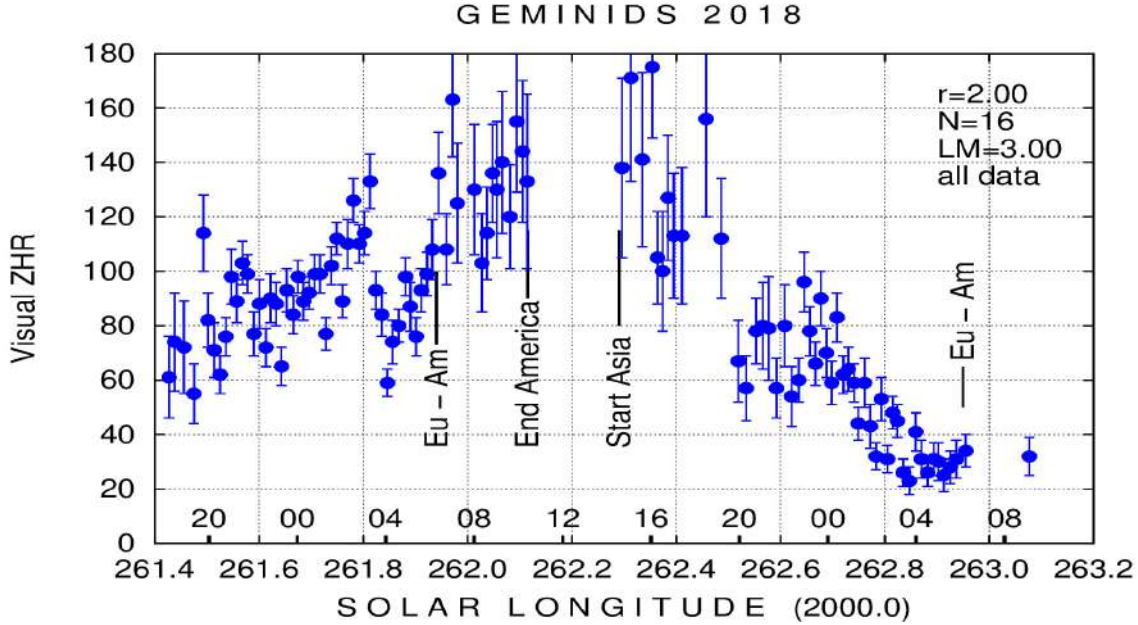


Figure 6 – Visual ZHR of the Geminid peak with $r = 2.00$ as in Figure 5 but requiring only 16 shower meteors per bin and allowing all data with LM from 3.0 onwards (“all data approach”).

result of the quite sloppy approach is shown in Figure 6, now “allowing everything”. This yields a huge “cloud” of data of very different weight. The difference in the two profiles shows the sections where extra adaption of the selection parameters is necessary. Especially, the rather large “Pacific gap” remains because the number of reports available from locations close to that gap is small. The uncertainty of the ZHR values as seen by the error bars becomes larger towards the edges.

Both general attempts to obtain a continuous profile are not satisfying. We eventually create a composite

profile as it has been utilised recently for the Perseids 2018 (Rendtel et al., 2018) and has been described by Veljković et al. (2019). This includes variations in the selection parameters which are summarised in Table 1.

Together with the information from the radio ZHR, we may conclude that the actual peak occurred for observers in the Pacific region on December 14 close to 14^h UT ($\lambda_{\odot} = 262^{\circ}.2$ to $262^{\circ}.3$). This confirms the long-term average position (Rendtel 2004; Rendtel 2014). The peak ZHR is in the range of 150–160, similar to the rates found in the previous years and thus confirm-

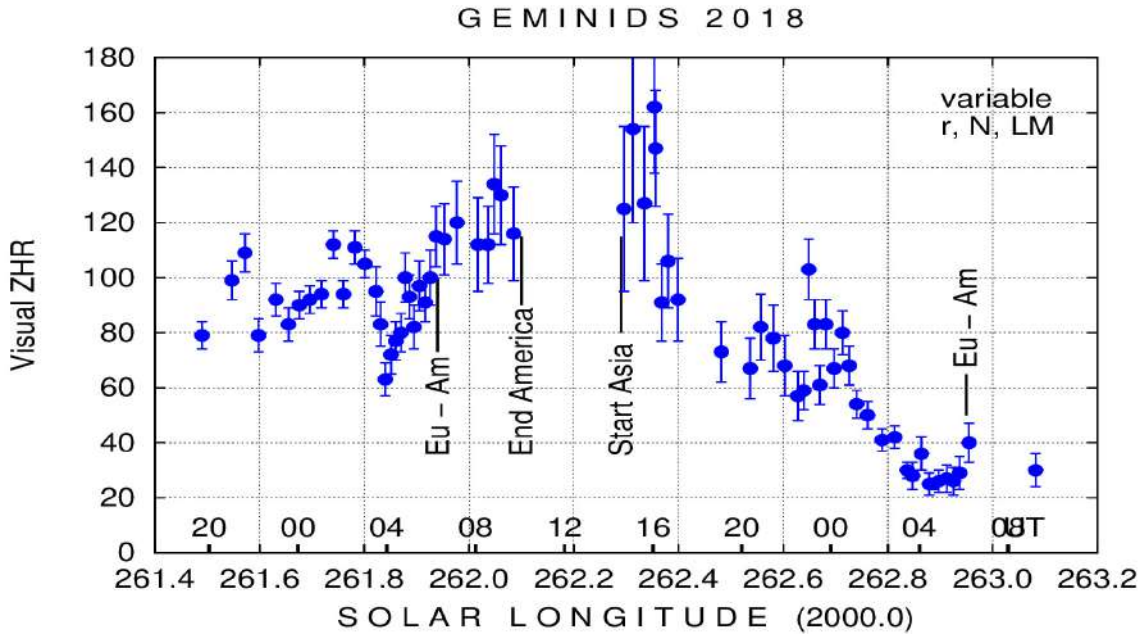


Figure 7 – Composite ZHR profile of the Geminid peak with the parameters listed in Table 1.

Table 1 – The final 2018 Geminid ZHR profile is composed of several sub-sets of the entire sample with different parameters to cover all possible sections and to achieve the optimum accuracy in each section. “Meteors” is the minimum number of meteors per bin; “interval length” is the minimum duration of an interval in minutes.

Date and period (UT)	r	Min LM	Meteors per bin	Interval length
Dec 13 18–03	2.40	5.50	200	30
Dec 14 03–05	2.20	5.50	100	10
Dec 14 05–07	2.00	5.00	60	15
Dec 14 07–13	1.80	5.00	40	15
Dec 14 13–16	1.80	3.00	16	15
Dec 14 16–24	1.80	4.50	36	15
Dec 15 00–04	2.30	5.50	100	15
Dec 15 04–05	2.30	5.50	30	15
Dec 15 05–10	2.60	4.50	20	15

ing the “high density Geminid phase” described by the modelling of Ryabova and the recent analyses (Ryabova and Rendtel, 2018).

Another rather striking feature occurs in the ascending branch of the ZHR and flux density curve. A preceding maximum is obvious in Figure 7. Perhaps it is better described as a deep dip in the ascend towards the actual peak. Many European observers indeed had the impression that after a good start the Earth moved into an “empty region” of the stream as it happened in the time with the highest radiant elevation. A ZHR decrease from 110 to 70 is striking as is the rapid increase to over 120 after that. The local minimum is centered at December 14, 04^hUT ($\lambda_{\odot} = 261.85^{\circ}$).

5 Discussion

The 2018 return of the Geminids confirmed the series of peaks with ZHRs of the order of 150 found during the last years. The peak is broad and has a FWHM of about 28 hours (December 13, 20^hUT until December 15, 00^hUT; $\lambda_{\odot} = 261.5^{\circ}$ to 262.7°). The peak cannot be determined accurately as it occurred in a gap caused by the uneven distribution of (optical, i.e. visual as well as video) observers over the longitudes. The center of the main peak profile is found to be at December 13 close to 14^h UT ($\lambda_{\odot} = 262.2^{\circ}$ to 262.3°) and thus at the position found from previous returns. The expected peak position for 2018 was December 14, 12^h30^mUT, i.e. $\lambda_{\odot} = 262.2^{\circ}$.

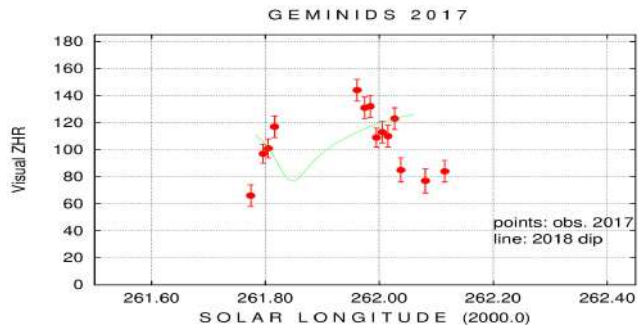


Figure 8 – Visual ZHR of the ascending branch of the Geminids in 2017 for the interval around the 2018 minimum ($\lambda_{\odot} = 261.85^{\circ}$). The thin line shows the ZHR data of the dip found in 2018.

The dip in the ZHR and flux density profiles is centered at December 14, 04^h UT ($\lambda_{\odot} = 261.85^{\circ}$). Such a local minimum was not detected in the previous return (Figure 8 for the Geminids of 2017). Sub-structures in the stream were also tried to find and to follow over longer periods (Rendtel, 2004), with limited success.

Since the Geminid stream is close to the Sun, is not

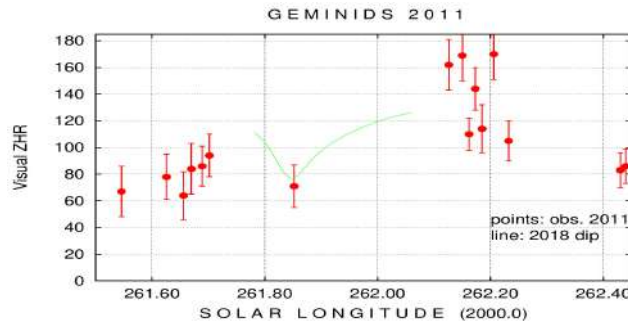


Figure 9 – Visual ZHR of the ascending branch of the Geminids in 2011 (about 5 orbital periods of the Geminids back) for the interval around the 2018 minimum ($\lambda_{\odot} = 261^{\circ}85$). The thin line shows the ZHR data of the dip found in 2018.

likely to find permanent structures like dust trails in long period streams. With an orbital period of just 1.43 years, any annual structure would require to extend over almost the entire orbit. If we assume particle concentrations of limited spatial extension, these would return only on some occasions and the probability should be higher to find encounters after 7 years. During this time the Geminid meteoroids have completed a little over 5 orbits. We looked into the VMBD data for 2011, just to test this possibility. The result is shown in Figure 9. There is only a single ZHR value at 09^h20^mUT ($\lambda_{\odot} = 261^{\circ}85$) which is lower than the neighbouring ZHRs. Nevertheless, the 2018 values plotted as a thin line in Figure 9 fit surprisingly well into the 2011 data. This incomplete profile can only be considered as a very weak hint at a returning feature after 7 years. The case gets more weight when looking at the 2004 ZHR – another 7 years back. Again, the actual position of the 2018 dip is less covered, but the profile inset fits surprisingly well here (Figure 10). The region in the stream has been investigated in some details recently (Rendtel, 2019). Nevertheless, it would be helpful if confirmed by other data sets and is a case for modelling the stream.

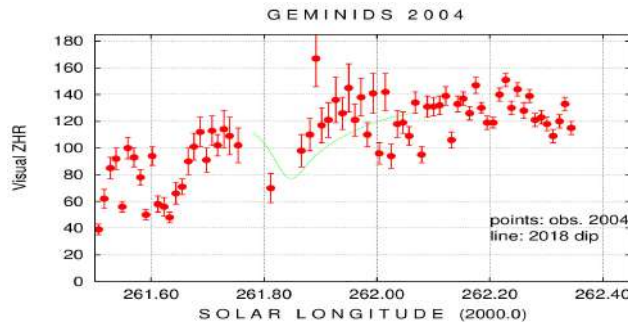


Figure 10 – Visual ZHR of the ascending branch of the Geminids in 2011 (another 5 orbital periods of the Geminids back) for the interval around the 2018 minimum ($\lambda_{\odot} = 261^{\circ}85$). The thin line shows the ZHR data of the dip found in 2018.

It is also noteworthy that the dip in 2018 is not seen in the radio ZHR graph (Figure 4). This hints at a remarkable depletion in the spatial number density of meteoroids causing optical meteors only.

6 Observers' note



Figure 11 – Composite image of bright Geminids of the 2018 maximum, taken with a Peleng fisheye lens $f = 8\text{mm}$ and a Canon EOS60Da. The individual exposures were 59 seconds, ISO set to 4000.

Finally, a personal note concerning the 2018 Geminids. I was lucky to spend time for a solar observing campaign at the Observatorio del Teide at Tenerife in December. The weather conditions were good (apart from an evening interval on December 13, just before the peak but with low radiant position). For the peak night, three Dutch observers (Carl Johannink, Koen Miskotte and Peter van Leuteren) joined me. All who have observed in a group know that experiencing high rates together contributes to the feeling of a great meteor shower maximum. Such observations also allow us to get feedback and a kind of calibration of everyone's data – these were the backbone of the currently applied observing and analysing procedures. A composite image of some bright Geminids is shown in Figure 11.

7 Conclusions

The Geminids reached their maximum in 2018 close to $\lambda_{\odot} = 262^{\circ}2$ to $262^{\circ}3$ with a peak ZHR of 150–160. The actual peak occurred in a period which is not covered by optical observations.

The strong dip on December 14, 04^h UT ($\lambda_{\odot} = 261^{\circ}85$) in visual ZHR and video flux density data is located in the ascending branch of the profile. While such a feature cannot be detected in the 2017 Geminids. There are hints at a similar dip in Geminid returns 7 and 14 years back (7 years are close to 5 orbital periods of the Geminid meteoroids). The dip requires confirmation by other data sets before it may be assumed that this is a region in the Geminid stream with lower spatial number density. Finally, the generally high level of activity (Ryabova and Rendtel, 2018) is confirmed by the present data.

Acknowledgements

Thanks to all observers who submitted their data to the IMO visual web page and to Sirko Molau for making the temporary video data available through the new fluxviewer webpage.

References

- Miskotte K. (2019). “The Geminids of 2018: an analysis of visual observations.” *eMeteorNews*, **4**, 207–212.
- Molau S. (2016). “MeteorFlux reloaded.” (U. Pajer, J. Rendtel, M. Gyssens, C. Verbeeck, eds.), *Proceedings IMC Bollmannsruh 2019*, 57–59.
- Rendtel J. (2004). “Evolution of the Geminids observed over 60 years”. *Earth, Moon and Planets*, **95**, 27–32.
- Rendtel J. (2014). “Meteor shower workbook”. IMO.
- Rendtel J. (2019). “On a possible recurring feature in the Geminid stream.” *WGN, Journal of the IMO*, **47**, 180–183.
- Rendtel J., Ogawa H., Sugimoto H. (2016). “Quadrantids 2016: observations of a short pre-maximum peak.” *WGN, Journal of the IMO*, **44**, 101–107.
- Rendtel J., Veljković K., Weiland T., Verbeeck C., Knöfel A. (2018). “Perseids 2018 – Analysis of Global Visual Data”. *WGN, Journal of the IMO*, **47**, 18–25.
- Ryabova G.O. and Rendtel J. (2018). “Increasing Geminid meteor shower activity.” *MNRAS*, **475**, L77–L80.
- Veljković K., Rendtel J., Verbeeck C., Weiland T., Knöfel A. (2019). “Tricks of the trade: global analysis of visual meteor shower observations using VMDB and MetFns – an example”. *Proceedings IMC Pezinok-Modra 2018* (R. Rudawska, J. Rendtel, C. Verbeeck, C. Powell, R. Lunsford, A. Knöfel, eds.), IMO, 2019.

Meteor candidate observations from automated weather camera sampling in VBA

Travis N. Stenborg¹

¹ The University of Sydney, NSW, 2006, Australia
tste6805@uni.sydney.edu.au

Automated sampling of webcam imaging is investigated as a means of meteor data collection. A sampling system was built with Visual Basic for Applications, the scripting language built into Microsoft's Office suite. Designed for use with an arbitrary set of target webcams, testing was performed with weather cameras on Australia's remote Norfolk Island, around the 2019 Perseid peak. Very probable meteor candidate imaging was secured, validating the viability of the data collection method. System source code has been made freely available.

1 Introduction

The goal of this work was to investigate the viability of automated webcam sampling for meteor data collection. Specifically, a system was envisaged that would perform unattended image downloads from an arbitrary number of user-specified public webcams. Additionally, an individually configurable sampling cadence would be used for each camera. If practical, it would allow observers to increase their observational coverage by collecting data from cameras distributed geographically, save money by using third party cameras, and save time by not requiring participation beyond program activation.

2 Methods

A webcam sampling system was built using Visual Basic for Applications (VBA). VBA was chosen as an implementation technology due to its ease of use (Hiestand, 2009), ubiquity and maturity (it's been part of Microsoft's Office suite since 1993, Getz and Gilbert 2006) and to leverage previous personal experience (e.g. Stenborg 2016).

The system manages webcams via a custom VBA class. Implementation included various functions within the broader set of Windows API functions, such as the base services, HTTP client library and URL moniker service. Downloaded files are given names containing a camera label and timestamp. For important sampling sessions, the system can be set to check for failed image downloads, symptomatic of internet connection loss, and sound an audible alert.

The Australian Bureau of Meteorology, with Airservices Australia, hosts weather cameras on Australia's remote Norfolk Island. Four publicly-accessible webcams¹, facing north, south, east and west, are situated at the international airport to provide visual confirmation of prevailing weather conditions. Each camera has a refresh rate of 120 s and provides sky coverage to an altitude of $\sim(34 - 35)^\circ$. Given the cameras' low light sensitivity

(capturing stars to at least apparent magnitude 5.98) and Norfolk Island's good dark sky conditions (contribution of total night sky brightness due to light pollution $< 1\%$, Falchi et al. 2016), the cameras were deemed capable of capturing visual meteors and thus selected as a test set.

An observational test run was conducted over five nights centred on the Perseid peak of 2019 (solar longitude $\lambda = 140^\circ$, Kronk 2014), with the system downloading $\sim 5\text{ MB}$ of images per hour, per camera, to capture meteors.

3 Results

Figure 1 shows an example meteor candidate, captured at 2019-Aug-13 15^h58^m04^s $\pm 2^s$ UTC, near the Perseid peak. Plotting the meteor's apparent path on gnomonic star maps (Znojil 1988) revealed no correspondence with a shower, Perseid or otherwise, even allowing for larger effective radiant diameters to accommodate plotting errors (as per, e.g. Rendtel and Arlt 2017).



Figure 1 – Capture of a candidate sporadic meteor (top right image quadrant) near the 2019 Perseid peak. This image was taken via automatic sampling of online images from a weather camera on Norfolk Island.

¹latitude $\approx -29.0388614^\circ$, longitude $\approx 167.9409638^\circ$

4 Discussion and Conclusion

The Perseids have a high ZHR (~ 100 , Kronk 2014), but bright time and poor southern hemisphere radiant visibility yielded no unambiguous Perseid detections. More limiting however, was camera imaging cadence. Weather cameras taking one image / 2 min are unlikely to capture meteors at a Perseid-like ZHR. Nonetheless, a strong sporadic candidate was captured, validating the data collection method at the proof-of-concept level.

System source code, embedded in an Excel workbook macro, has been uploaded to GitHub². The community is encouraged to leverage its easy configurability and apply it to a webcam set beyond the weather cameras used here. Observational campaigns will naturally be constrained by the limitations of any webcam set selected, but can supplement traditional meteor data collection methods.

Acknowledgements

Publicly-accessible infrastructure managed by the Australian government's Bureau of Meteorology and Airservices Australia was used for this research.

References

- Falchi F., Cinzano P., Duriscoe D., Kyba C. C. M., Elvidge C. D., Baugh K., Portnov B. A., Rybnikova N. A., and Furgoni R. (2016). “The new world atlas of artificial night sky brightness”. *Science Advances*, **2:6**, e1600377–e1600377.
- Getz K. and Gilbert M. (2006). *VBA Developer’s Handbook*. 2nd edition. Wiley, Alameda, CA.
- Hiestand J. W. (2009). *Numerical Methods with VBA Programming*. Jones & Bartlett Learning, Sudbury, MA.
- Kronk G. W. (2014). *Meteor Showers*. The Patrick Moore Practical Astronomy Series. 2nd edition. Springer-Verlag New York.
- Rendtel J. and Arlt R., editors (2017). *Handbook for Meteor Observers*. IMO.
- Stenborg T. N. (2016). *A New Population of Galactic Bulge Planetary Nebulas*. PhD thesis, Department of Physics and Astronomy, Macquarie University.
- Znojil V. (1988). “Gnomonický Atlas Brno 2000.0.”. *WGN, Journal of the IMO*, **16:4**, 137–140.

²<https://github.com/tstenborg/Webcam-Sampler>

Poster and photo contest

A nice tradition at the IMCs are the photo and poster contests. This year all participants had again the opportunity to submit posters and pictures before the conference. The only requirement was that the submitted work be one's own. During the coffee breaks and evenings all participants were able to view and discuss the works which were exhibited during the entire IMC.

This competition highlights the close connection between science and art. By observing meteors, scientific data can often be collected and beautiful and inspiring landscapes or environments can be captured at the same time.

1 Poster award

At the 2019 IMC there were a total of five posters instead of the usual three that received awards. There were two additional prizes awarded for two outstanding works by students. All posters can be found in the Proceedings:

Dušan Bettonvil submitted the poster “Python ablation and dark flight calculator” (page 164) and **Uroš Bettonvil** the poster with the title “My first visual observation” (page 166). Both were awarded with special prices.

The first place went to **Jürgen Rendtel** for his “Geminids 2018” poster (page 183).

Vladislav Lukashenko received the second price in this contest for the poster “Numerical model of flight and scattering of meteor body fragments in the Earth's atmosphere” (page 173).

Third in this contest was **Lukáš Petera** for the poster “Elemental composition, mineralogy and orbital parameters of the Porangaba meteorite” (page 182).

2 Photo award

The three winning images of the photo competition at this year's IMC are presented in the following.

The winner photo was taken by **Bar Westfried**. He submitted the picture “The ‘Martian’ observes Meteors”. The text that accompanied the photo in the contest is as follows: *The “Martian” is a statue on a hill next to our (the Meteor Division*

of the Israel Astronomy Association) observation site. That's not the statue's original name but a nickname the observers gave it. This photo was taken using a Nikon D850, with $f = 24 - 40\text{ mm}$, $f/2.8$ lens. Camera settings: 20 second exposure, $f/2.8$, ISO 6400.

The second place was awarded to **Felix Bettonvil** for the picture “Dutch skies, Dutch meadows, hunting for meteorites in the lowlands”. *the picture is an impression of a typical day of hunting for meteorites after a possible meteorite dropping in 2015 in Friesland in The Netherlands. For many days agricultural fields were explored, but unfortunately without a positive result. Instead glacial stones and remains of old pottery and smoking pipes were found, linking to the old fisherman tradition in that area, and an old, now disappeared, monastery. There might be a chance that the meteorite did not fall on land but in the nearby IJsselmeer instead.*

The third price was received by **Jürgen Rendtel** for his picture with the title “Taurid-decorated Orionid maximum”. His explanation of the photo: *October is a favourable time for meteor observers. There is considerable activity from several sources. The Orionid shower is one highlight of this month especially if one can observe it from a dark site at high altitude. The composite image shows four Orionids and a bright Taurid in the night of 2017 October 21–22, seen from the Observatorio del Teide at Tenerife, Canary Islands (elevation 2380 metres with two domes of solar telescopes in the foreground).*

Image taken with a Canon EOS 60Da using a $f = 8\text{ mm}$ Peleng fish eye lens, each one exposed 59 seconds. This way the star trails have a length of just $1/4$ deg, appear almost point-like and are close to visual impression.

We are looking forward to seeing more interesting and unusual images showing the wide variety of things we face when dealing with meteor astronomy at the next IMC – or also on the cover of the IMO Journal WGN.



Photo 1: The ‘Martian’ observes Meteors (Bar Westfried).



Photo 2: Dutch skies, Dutch meadows, hunting for meteorites in the lowlands (Felix Bettonvil).



Photo 3: Taurid-decorated Orionid maximum (Jürgen Rendtel).